



National Library  
of Canada

Acquisitions and  
Bibliographic Services Branch

395 Wellington Street  
Ottawa, Ontario  
K1A 0N4

Bibliothèque nationale  
du Canada

Direction des acquisitions et  
des services bibliographiques

395, rue Wellington  
Ottawa (Ontario)  
K1A 0N4

*Your file* *Voire référence*

*Our file* *Notre référence*

## NOTICE

The quality of this microform is heavily dependent upon the quality of the original thesis submitted for microfilming. Every effort has been made to ensure the highest quality of reproduction possible.

If pages are missing, contact the university which granted the degree.

Some pages may have indistinct print especially if the original pages were typed with a poor typewriter ribbon or if the university sent us an inferior photocopy.

Reproduction in full or in part of this microform is governed by the Canadian Copyright Act, R.S.C. 1970, c. C-30, and subsequent amendments.

## AVIS

La qualité de cette microforme dépend grandement de la qualité de la thèse soumise au microfilmage. Nous avons tout fait pour assurer une qualité supérieure de reproduction.

S'il manque des pages, veuillez communiquer avec l'université qui a conféré le grade.

La qualité d'impression de certaines pages peut laisser à désirer, surtout si les pages originales ont été dactylographiées à l'aide d'un ruban usé ou si l'université nous a fait parvenir une photocopie de qualité inférieure.

La reproduction, même partielle, de cette microforme est soumise à la Loi canadienne sur le droit d'auteur, SRC 1970, c. C-30, et ses amendements subséquents.

UNIVERSITY OF ALBERTA

A SPECTRAL STUDY OF EXCITATION PROCESSES  
IN A GLOW DISCHARGE

by

YUHUI ZHAO



A Thesis

Submitted to the Faculty of Graduate Studies and Research in Partial  
Fulfillment of the Requirement for the Degree of Doctor of Philosophy

DEPARTMENT OF CHEMISTRY

Edmonton, Alberta

Fall, 1995



National Library  
of Canada

Bibliothèque nationale  
du Canada

Acquisitions and  
Bibliographic Services Branch

Direction des acquisitions et  
des services bibliographiques

395 Wellington Street  
Ottawa, Ontario  
K1A 0N4

395, rue Wellington  
Ottawa (Ontario)  
K1A 0N4

*Your file* *Voire référence*

*Our file* *Notre référence*

THE AUTHOR HAS GRANTED AN IRREVOCABLE NON-EXCLUSIVE LICENCE ALLOWING THE NATIONAL LIBRARY OF CANADA TO REPRODUCE, LOAN, DISTRIBUTE OR SELL COPIES OF HIS/HER THESIS BY ANY MEANS AND IN ANY FORM OR FORMAT, MAKING THIS THESIS AVAILABLE TO INTERESTED PERSONS.

L'AUTEUR A ACCORDE UNE LICENCE IRREVOCABLE ET NON EXCLUSIVE PERMETTANT A LA BIBLIOTHEQUE NATIONALE DU CANADA DE REPRODUIRE, PRETER, DISTRIBUER OU VENDRE DES COPIES DE SA THESE DE QUELQUE MANIERE ET SOUS QUELQUE FORME QUE CE SOIT POUR METTRE DES EXEMPLAIRES DE CETTE THESE A LA DISPOSITION DES PERSONNE INTERESSEES.

THE AUTHOR RETAINS OWNERSHIP OF THE COPYRIGHT IN HIS/HER THESIS. NEITHER THE THESIS NOR SUBSTANTIAL EXTRACTS FROM IT MAY BE PRINTED OR OTHERWISE REPRODUCED WITHOUT HIS/HER PERMISSION.

L'AUTEUR CONSERVE LA PROPRIETE DU DROIT D'AUTEUR QUI PROTEGE SA THESE. NI LA THESE NI DES EXTRAITS SUBSTANTIELS DE CELLE-CI NE DOIVENT ETRE IMPRIMES OU AUTREMENT REPRODUITS SANS SON AUTORISATION.

ISBN 0-612-06317-8

Canada

UNIVERSITY OF ALBERTA  
LIBRARY RELEASE FORM

NAME OF AUTHOR: YUHUI ZHAO  
TITLE OF THESIS: A SPECTRAL STUDY OF EXCITATION  
PROCESSES IN A GLOW DISCHARGE  
DEGREE: Doctor of Philosophy.  
YEAR THIS DEGREE GRANTED: 1995

Permission is hereby granted to the University of Alberta Library to reproduce single copies of this thesis and to lend or sell such copies for private, scholarly, or scientific research purposes only.

The author reserves all other publication and other rights in association with the copyright in the thesis, and except as hereinbefore provided, neither the thesis nor any substantial portion thereof may be printed or otherwise reproduced in any material form whatever without the author's prior written permission.

.....*Jhao Yunhui*.....

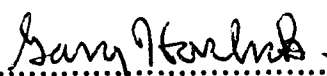
9632 - 75th Street  
Edmonton, Alberta  
Canada T6C 2H9

Date: *Oct. 3, 1995*  
.....

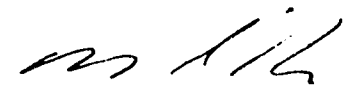
**UNIVERSITY OF ALBERTA**

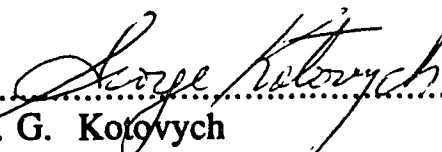
**FACULTY OF GRADUATE STUDIES AND RESEARCH**


The undersigned certify that they have read, and recommend to the Faculty of Graduate Studies and Research for acceptance, a thesis entitled **A SPECTRAL STUDY OF EXCITATION PROCESSES IN A GLOW DISCHARGE** submitted by Yuhui Zhao in partial fulfillment of the requirement for the Degree of Doctor of Philosophy


  
.....  
Dr. G. Horlick, Supervisor

  
.....  
Dr. F. F. Cantwell

  
.....  
Dr. N. J. Dovichi

  
.....  
Dr. G. Kotovych

  
.....  
Dr. J. Tulip

  
.....  
Dr. J. W. Carnahan, External Examiner

Date: *Sept. 28, 1995*

This thesis is dedicated to my parents,  
my wife and my daughter

## Abstract

Although the glow discharge has been used as a source in analytical atomic spectroscopy since the 1960's, the excitation of neutral and singly-ionized sample atoms in the glow discharge is not fully characterized or understood. The overall goal of this study is to detail the spectral character of emission from sample atoms in a glow discharge and to interpret the occurrence and relative intensities of certain spectral lines. The primary focus of the study is on the neutral atom and ion line emission of copper, zinc, silver and cadmium. It is shown that the character of the ultraviolet spectra of these elements is dominated by ion lines and that their relative intensities are highly dependent on the type of filler gas. Spectra for three filler gases (argon, neon, helium) were studied. The spectra were acquired using a Fourier transform spectrometer which greatly facilitated detailed spectral inter-comparisons. It was found that charge transfer and Penning processes involving the filler gas species, followed by stepwise de-excitation play significant roles in the ionization and excitation of analyte, thus setting the spectral character of ion line emission.

For neutral atom lines, however, the spectral patterns are similar for different filler gases. While using the same element and discharge gas, glow discharge emission spectra are strikingly different from that of the Inductively Coupled Plasma (ICP) which is the most studied and most familiar analytical plasma. The excitation of the neutral atoms in these two emission sources is thought to be very different. Due to the lack of local thermal equilibrium in the glow discharge, the excitation temperature concept can not explain the differences. Critical comparison of the spectral characteristics of these two sources indicates that ion-electron

recombination may be the major source of excited analyte atoms in the glow discharge as most of the neutral atom emission lines originate in transitions from high energy levels of the neutral atom. Stepwise de-excitation of these levels then contributes to emission from the lower levels of the atoms.



## **Acknowledgements**

I would like to express my sincere appreciation of Dr. Gary Horlick's immeasurable scientific guidance during my study in the University of Alberta. I also want to thank all the friends I have been with in this group for their friendship and help. I am also grateful to all the staff who work in the Department of Chemistry for their support and assistance. I enjoyed staying in this University and a lot of happy memories will be with me for the rest of my life.

My thanks also go to my wife Qiufeng Ge and my daughter Jinting for their understanding and support.

## TABLE OF CONTENTS

CHAPTER	PAGE
1. Introduction .....	1
1.1 Introduction .....	1
1.2 What is a glow discharge? .....	2
1.3 Some features of a glow discharge .....	5
1.3.1 Current-potential characteristics .....	5
1.3.2 Sputtering phenomenon .....	8
1.3.3 Light distribution in a glow discharge .....	8
1.4 The nature of a glow discharge .....	11
1.4.1 The cathode region .....	11
1.4.2 The negative glow .....	13
1.4.3 The Faraday dark space .....	15
1.4.4 The positive column .....	15
1.4.5 The anode regions .....	16
1.5 Applications .....	16
1.6 Problems in this area .....	19
1.7 The objective of the thesis .....	19
References .....	21
2. Instrumentation .....	24
2.1 Glow discharge devices .....	24
2.1.1 Planar cathode unit .....	24
2.1.2 Pin-type glow discharge .....	27
2.2 The spectrometers .....	27
2.2.1 The photodiode array system .....	27

CHAPTER	PAGE
2.2.2 Fourier transform spectrometer .....	30
References .....	37
3. Parameter studies -- Comments and measurements .....	38
3.1 Current - voltage - Pressure .....	38
3.2 Pre-burning .....	42
3.3 Cathodic sputtering .....	43
3.3.1 Description of cathodic sputtering .....	44
3.3.2 Some sputtering measurement .....	50
3.3.2.1 Differential sputtering .....	50
3.3.2.2 Sputtering rate measurement .....	51
3.4 Species number densities .....	53
3.4.1 Sputtered atoms .....	53
3.4.2 Metastables .....	56
3.4.3 Electrons .....	58
3.5 Spectrophysical parameters .....	59
3.5.1 Gas temperature .....	61
3.5.2 Electron temperature .....	61
3.5.3 Excitation temperature .....	63
3.5.4 Ionization temperature .....	64
3.6 Not all lines are created equally .....	65
3.6.1 The effect of filler gas - a mixed gas study .....	65
3.6.2 The effect of pressure and potential .....	68
3.6.3 Configuration .....	71
3.7 The excitation temperature paradox .....	73
References .....	85

CHAPTER	PAGE
4. A Spectral Study of Charge Transfer and Penning Processes in a Glow Discharge .....	88
4.1 Introduction .....	88
4.2 Experimental .....	91
4.3 Result and Discussion .....	93
4.3.1 Copper ion lines .....	95
4.3.2 Zinc ion lines .....	109
4.3.3 Silver ion lines .....	120
4.3.4 Cadmium ion lines .....	137
4.3.5 The iron spectra .....	149
4.4 The factors that influence charge transfer .....	156
4.5 Conclusion .....	158
References .....	161
5. Excitation and Emission Characteristics of Neutral Atoms in Glow Discharge - with Comparison to Inductively Coupled Plasmas .....	163
5.1 Introduction .....	163
5.2 Experimental .....	165
5.3 Results and Discussion .....	165
5.3.1 Overview of the brass visible spectra .....	165
5.3.2 Copper neutral atom lines - visible region .....	169
5.3.3 Copper neutral atom lines - UV region .....	181
5.3.4 Zinc neutral atom lines .....	197
5.3.5 Silver neutral atom lines .....	206
5.3.6 Cadmium neutral atom lines .....	215

CHAPTER	PAGE
5.3.7 Ion-electron recombination and the filler gas ion lines .....	221
5.3.8 Formation of ground state ions .....	231
5.4 Conclusions .....	232
References .....	234
6. Summary and Future Work .....	236
6.1 Summary of this study .....	236
6.2 Future work .....	244
Reference .....	244
Appendix .....	245

## LIST OF TABLES

TABLE	PAGE
3.1 Some fundamental parameters in glow discharges .....	60
3.2 Operating parameters for the temperature measurement .....	75
3.3 Iron lines used in the excitation temperature measurements ....	78
4.1. Parameter settings in the emission measurement .....	92
4.2. Metastable energy and ionization potential of Ar, Ne and He ...	96
4.3. Major AgII lines observed in the UV spectra .....	124
4.4. AgII lines in the 242 nm region .....	130
4.5. Ag II lines in the 213 nm region .....	133
4.6. AgII lines in the 224 and 228 nm spectral regions .....	136
4.7. AgII lines in the 268 nm region .....	139
4.8. Major Cd lines Observed in the UV spectra .....	143
4.9 Relative intensity of iron ion lines in glow discharge emission (UV) .....	152
5.1 Summary of copper atom lines in the visible spectral region (3d <sup>10</sup> upper states) .....	172
5.2 Summary of copper neutral atoms in the visible spectral region (3d <sup>9</sup> upper states) .....	177
5.3 Some characteristics of the GD and ICP lines noted in Fig. 5.11	184
5.4 Line data for Fig. 5.16 .....	193
5.5 Characteristics of lines highlighted in Fig. 5.19 .....	199
5.6 Visible region ZnI lines .....	203
5.7 Characteristics of AgI lines .....	211
5.8 Characteristics of the CdI lines .....	216
5.9 Argon lines noted in Fig. 5.34 .....	224
5.10 Ar lines noted in Fig. 5.35 .....	227

## LIST OF FIGURES

FIGURE	PAGE
1.1 A schematic diagram of a planar diode glow discharge .....	3
1.2 Potential-current feature of a gas discharge .....	7
1.3 Schematic description of the nature of a conventional glow discharge .....	9
1.4 Representation of some glow discharge related techniques .....	18
2.1 Schematic diagram of the Grimm-type glow discharge source	26
2.2 Schematic diagram of the pin-type glow discharge source .....	28
2.3 A spectrum obtained from the PDA system and plotted on an HP plotter .....	31
2.4 Block diagram of the FTS measurement system .....	32
2.5 An example of brass interferogram acquired with the FT system .....	33
2.6 Example spectra acquired with the FT system in different wavelength regions. (a) UV region with an R166 solar-blind PMT, (b) Visible region with a 1P21 PMT, (c) Near infrared region with a silicon photodiode detector. Sample: Brass. ....	35
3.1 Variation of the discharge current with applied potential (a) and filler gas pressure (b).....	40
3.2 Illustration of cathodic sputtering in a glow discharge. ....	46
3.3 A photograph showing the differential sputtering between cadmium (top) and aluminum (bottom) .....	52
3.4 Plot showing the mass loss of a brass sample vs. sputtering time 15 mA; 1200 V; Sputtering diameter: 7.0 mm .....	54
3.5 Plot showing the mass loss of a brass sample vs. sputtering time 55 mA; 1000 V; Sputtering diameter: 7.0 mm .....	55

FIGURE	PAGE
3.6	Variation of line intensities with helium content in the filler gas 67
3.7	Signal variation with applied voltage at constant 6.0 mA current 69
3.8	Signal variation with gas pressure at constant 6.0 mA current 70
3.9	A diagram showing the signal behavior when the current variation caused by increasing voltage (a) and by increasing pressure (b). ..... 72
3.10	Comparison of the brass spectra obtained from a pin-type (a) and a Grimm type (b) discharge devices. .... 74
3.11	Partial Fe UV spectra from glow discharge emission ..... 76
3.12	Partial visible spectrum from Fe-Ar glow discharge and the Boltzmann plot ..... 79
3.13	Partial UV spectrum from Fe-Ar glow discharge and the Boltzmann plot ..... 80
3.14	Partial Fe UV spectrum from the ICP and the Boltzmann plot 81
3.15	A section of Fe visible spectrum from ICP and the Boltzmann plot ..... 82
4.1	UV spectra of brass in three discharge gases: (a) argon, (b) neon and (c) helium. .... 94
4.2	A simplified energy diagram of Cu ion and the metastable and ionization potentials of the discharge gases ..... 97
4.3	A portion of brass spectra showing the relative intensities of the CuII lines in the vicinity of 248.579 nm. (a) Ar, (b) Ne, (c) He ..... 98
4.4	Expanded spectra region showing some of the CuII lines from the 5s to 4p transitions enhanced by Ne. (a) Ar, (b) Ne, (c) He 99



FIGURE	PAGE
4.5 A schemetic diagram illustrating the charge transfer from neon ions to copper atoms populating the 5s levels .....	101
4.6 A portion of spectra showing the extraordinary intensity of CuII 224.700 nm line in Ar. (a) Ar, (b) Ne, (c) He .....	102
4.7 A detailed diagram showing the availability of charge transfer in Ar-Cu discharge .....	103
4.8 A schemetic diagram illustrating the charge transfer from argon ions to copper atoms populating one of the 4p levels ...	105
4.9 A diagram showing the 4p to 4s transitions enhanced by charge transfer in Ne-Cu discharge .....	107
4.10 A portion of visible spectrum of brass in helium showing some 4f to 4d transition lines .....	108
4.11 Illustration of the population of CuII 6s, 4f levels by charge transfer and followed by stepwise de-excitation .....	110
4.12 A simplified energy diagram of Zn <sup>+</sup> with the metastable and ionization potentials of the discharge gases .....	112
4.13 A schemetic diagram illustrating a possible Penning process in He-Zn discharges .....	113
4.14 Relative intensity of ZnII 491.166 and 492.404 nm lines in different gases. (a) Ar, (b) Ne, (c) He .....	114
4.15 ZnII lines from 5d to 5p transitions populated by He <sup>+</sup> - Zn Charge transfer .....	116
4.16 Illustration of the 4f - 4d transitions enhanced by He <sup>+</sup> - Zn Charge transfer .....	117
4.17 ZnII lines in the vicinity of 206 nm region. (a) Ar, (b) Ne, (c) He .....	119

FIGURE	PAGE
4.18 A schemetic diagram illustrating the charge transfer from Ne <sup>+</sup> to Zn populating the Zn <sup>+</sup> 4d states followed by cascading .....	121
4.19 He <sup>+</sup> populating Zn <sup>+</sup> 5d level by charge transfer and enhancing the 4d-4p and 4p-4s transitions .....	122
4.20 Comparison of Ag UV spectra in argon and helium discharges. (a) argon, (b) helium .....	123
4.21 A simplified energy diagram of Ag ion and the metastable and ionization potentials of the discharge gases .....	125
4.22 A possible path of excitation of Ag <sup>+</sup> by Ar metastable atoms ..	127
4.23 A section of Ag <sup>+</sup> spectra in the 242 nm region showing the difference of line intensities in the two gases. (a) Ar, (b) He ...	129
4.24 Illustration of charge transfer between He <sup>+</sup> and Ag populating the 5d level and a cascading process .....	131
4.25 A portion of AgII spectra showing the lines from 5d - 5p transittions only appear in the He discharge. (a) Ar, (b) He .....	132
4.26 Some of the AgII lines in the vecinity of 224 nm generated from the 5d - 5p transitions. (a) Ar, (b) He .....	134
4.27 Expanded spectra showing AgII 227.532 and 227.743 nm lines only appear in the He discharge.(a) Ar, (b) He .....	135
4.28 Expanded spectra section in the vicinity of 268 nm showing the 6s -5p transition lines in He discharge. (a) Ar, (b) He .....	138
4.29 A path of He <sup>+</sup> - Ag charge transfer enhancing the 6s - 5p transitions .....	140
4.30 Comparison of Cd <sup>+</sup> spectra in Ar (a) and He (b) discharges ....	141
4.31 A simplified energy diagram of Cd ion and the metastable and ionization potentials of the discharge gases .....	144

FIGURE	PAGE
4.32 A possible mechanism populating the 6p excited states of Cd <sup>+</sup> and followed by stepwise de-excitations .....	146
4.33 The relative intensities of CdII 537.809 and 533.753 nm lines to the CdI 508.582 nm in Ar (a) and He (b) discharges .....	147
4.34 Charge transfer between He <sup>+</sup> and Cd and stepwise de-excitation	148
4.35 Expanded portion of Cd spectra showing the CdII 441.563 nm line in He discharge. (a) Ar, (b) He .....	150
4.36 A section of iron UV spectra in three discharge gases .....	151
4.37. A plot showing the relative intensity of some Fe ion lines altered by different gases in glow discharge .....	155
4.38 A diagram showing that charge transfer in Ne - Cu system favors the <sup>3</sup> D terms .....	159
5.1 Visible region spectra of brass in different discharge gases (a) Ar, (b) Ne and (c) He. ....	166
5.2. Comparison of brass visible spectra in argon based GD (a) and ICP (b). ....	168
5.3 Some CuI lines in argon glow discharge (a) 509.7- 528.8 nm and (b) 566.2 - 582.1 nm. ....	170
5.4 Energy level diagram ( or Grotrian diagram ) of CuI. Lines showing the major transitions observed in GD. ....	171
5.5 Detailed energy diagram illustrates transitions originated from 3d <sup>10</sup> nx configurations. ....	173
5.6 CuI lines generated from the transitions illustrated in Fig. 5.5	174
5.7 A portion of CuI spectra showing the diffusion lines from the auto-ionizing excited states .....	176
5.8 A CuI line generated from stepwise de-excitation .....	179

FIGURE	PAGE
5.9 A pair of CuI lines generated from the transitions $4d^9 4s 5s \rightarrow 4d^9 4s 4p \rightarrow 4d^9 4s^2$ .....	180
5.10 Comparison of brass ultraviolet spectra in argon based GD (a) and ICP (b). .....	182
5.11 A portion of brass spectra in the vicinity of 224.700 nm (a) GD and (b) ICP. ....	183
5.12. Relative intensities of two closely spaced CuI lines in GD (a) and ICP (b). .....	187
5.13 Energy levels involved in the transitions generating 219.958 and 219.975 nm CuI lines. ....	188
5.14 A portion of brass UV spectra from Ne (a) and He (b) discharges .....	190
5.15 Comparison of CuII and CuI line relative intensities between GD (a) and ICP (b) in the vicinity of 221 nm. ....	191
5.16 Comparison of CuII and CuI line relative intensities between GD (a) and ICP (b) in the vicinity of 217 nm. ....	192
5.17 Partial spectra showing the relative intensities of three lines in GD (a), (c), (e) and ICP (b), (d), (f). ....	195
5.18 Grotrian diagram showing the CuI transitions observed in ICP with the comparison to those in GD. ....	196
5.19 A portion of brass spectra showing the zinc lines in GD (a) and ICP (b) .....	198
5.20 Energy level diagram of ZnI. Lines show the major transitions observed in GD. ....	200
5.21 Zn I lines generated from 5s to 4p and 4d to 4p transitions ....	202
5.22 Zn I lines generated from 4d to 4p transitions observed in GD	204

FIGURE	PAGE
5.23 UV lines fall into the visible region because of aliasing .....	205
5.24 Lines from transitions $3d^{10}4s4d \rightarrow 3d^{10}4s4p$ (singlet) and $3d^{10}4s5d \rightarrow 3d^{10}4s4p$ (singlet) .....	207
5.25 Grotrian diagram showing the ZnI transitions observed in ICP with the comparison to those in GD. ....	208
5.26 Ag visible spectrum from a He based glow discharge .....	209
5.27 Scale expanded spectrum showing AgI lines from $5d \rightarrow 5p$ and $6d \rightarrow 5p$ transitions .....	210
5.28. Scale expanded spectrum showing AgI lines from $7s \rightarrow 5p$ transitions .....	213
5.29 Scale expanded spectrum showing AgI lines from $7d \rightarrow 5p$ and $6p \rightarrow 5s$ transitions .....	214
5.30 Cd visible spectrum from a He based glow discharge .....	217
5.31 CdI lines from transitions $5d(\text{triplet})$ to $5p$ (triplet) .....	218
5.32 Some CdI lines from transitions $5d(\text{triplet})$ to $5p$ (triplet) and $7s$ to $5p$ . ....	219
5.33 Some CdI lines from transitions $6d$ (triplet) to $5p$ (triplet) and $7d$ to $5p$ . ....	220
5.34 ArII lines observed in the visible region in glow discharge ...	223
5.35 Comparison of some Ar lines between GD (a) and ICP (b) .....	226
5.36 A portion of an Ar based GD-MS spectrum showing the existence of $Ar^{2+}$ ions .....	228
5.37 A portion of a spectrum obtained from a neon based GD .....	230
6.1 A schematic illustration of two Boltzmann plots .....	239
6.2 A plot used for calculating the $T_{Ne}$ and $T_{Ar}$ .....	242
6.3 Boltzmann plots for Fe-Ar discharge .....	243

## **Chapter 1. Introduction**

### **1.1 Introduction**

One of the most active areas in analytical chemistry is the search for new methods of multi-element analysis. This involves both improvement in existing methods and development of new methods. The inductively coupled plasma (ICP) has been one of the most powerful methods developed in the last two decades. With the full development and the realization of its limitations, there has been a search for new methods and a rediscovery of old ones. In the last two decades, one of the oldest techniques - glow discharge (GD) spectrometry has gained more and more popularity. The apparent simplicity, the capability of handling more than one kind of sample and the ability to act as a source of atomization, excitation and ionization for solid samples, have attracted a lot of interest in these devices. In particular the plane cathode glow discharge source introduced by Grimm [1] has been applied extensively as a source for analytical emission spectrometry. A wide variety of solid conducting samples as well as non-conducting powders have been analyzed and also, investigations on the fundamental aspects of this device have been published. Atomic absorption, atomic emission, atomic fluorescence and mass spectrometric techniques have all been coupled to glow discharge devices. In our laboratory, glow discharge devices have been successfully

interfaced to spectrometers that are concurrently used for ICP emission, ICP-MS and UV-VIS Fourier transform spectrometry.

## 1.2 What Is a Glow Discharge?

A glow discharge device is a spectrochemical source that is particularly applicable to the direct analysis of conductive solid materials and it is one of the earliest spectrochemical sources. It was first used in fundamental spectroscopic studies of atomic structure by Paschen in 1916 [2]. The simplest design of a glow discharge device [Fig. 1.1] consists of a low pressure (1-10 torr) rare gas discharge between an anode and a cathode which also usually is the sample or the sample host. It is initiated in a reduced pressure environment when the voltage applied between the two electrodes exceeds that necessary to cause breakdown of the rare gas, leading to the creation of electron-ion pairs. A glow discharge device can take many different forms. The most common devices include hollow cathode, Grimm type (hollow anode) and pin type configurations.

The glow discharge plasma is not as simple as it appears. It consists of the following components:

**Filler gas:** Usually an inert gas (Ar, Ne or He) is used and the most often used gas is argon because it is relatively heavy (vs. helium), cheap and has a low ionization potential. The gas exists in the following forms in the glow discharge plasma:

- ground state atoms: The majority of the gas atoms are in the ground state. The kinetic energy of these atoms is determined by the temperature, *i.e.* they are thermalized.

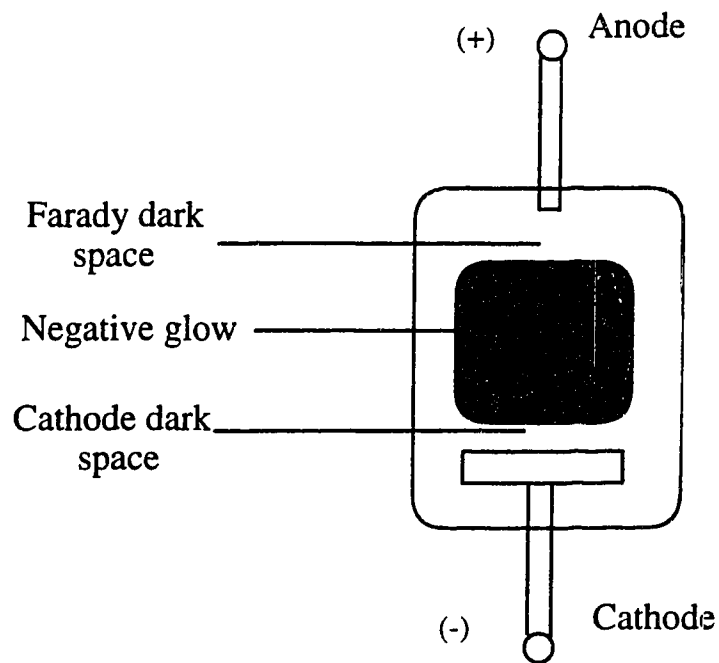


Fig. 1.1 A schematic diagram of a planar diode glow discharge.



- excited state atoms: Some atoms in the plasma are excited. Their formation may be caused by electron impact, collision with other species, Penning processes, dissociation, recombination etc.

- metastables: A very small fraction of the filler gas atoms are in the metastable state. Their formation may be caused by the electric field, collision with other species such as electron impact, Penning processes, recombination and cascading from higher levels;

- ground state ions: A small fraction of the carrier gas is ionized. Ions are formed by processes of collision with other species such as electron impact, Penning, dissociation, charge transfer etc.

- excited state ions : Among the gas ions a smaller fractions exists in the excited state. Excited ions may be formed by the collision of ground state ions with other species: such as electron impact, or dissociation from clusters, recombination with electrons by a multiple charged ion and charge transfer cascade from a higher excited level.

- multiple charged ions: These ions are mainly formed by electron impact. Multiple charged gas ions (up to six charges on an argon atom have been found in a glow discharge mass spectrometry study [3])almost certainly are produced by high energy electrons. In other words, some electrons penetrate into the negative glow and still have a few hundred electron volts of energy, and these electrons have enough kinetic energy to produce multi-charged ions.

- charged molecules or clusters: An ion and a neutral atom may combine by coulombic force to form a charged molecule. The formation of such may also be the result of a three body collision--two neutral atoms colliding with a high energy electron at the same time resulting in cluster formation.

**Electric field:** There is an electric field between the anode and the cathode when a discharge potential is applied. The direction of the field is towards the cathode surface. The non-uniformity of this field makes the plasma complicated. A strong electric field is located mainly in the region of the cathode dark space. The strength of this field linearly (almost) decreases from the edge of the cathode towards the negative glow region. This field may cause ionization of the carrier gas and the sputtered material. It is the main driving force for the bombarding ions which cause cathode sputtering. The ions formed by this field may not contribute very much to the ion population in the negative glow because most of the ions formed in the immediate cathode region are attracted back to the cathode. However, this field accelerates the electrons which are formed at the cathode surface or in the cathode dark space. The accelerated electrons can cause excitation and ionization of the carrier gas and the sputtered material in the negative glow and/or other parts of the glow discharge plasma. This is a major process sustaining the glow discharge.

**Electrons:** One of the major carriers of the discharge current is electrons. Electron energy range from near 0 to the value of the cathode potential (in electron volts) is possible. There may be three groups, i.e. thermal, secondary and primary electrons. Their energy distribution may not be Maxwellian.

### **1.3 Some Features of a Glow Discharge**

#### **1.3.1 Current-Potential Characteristics**

One observes a number of interesting phenomena when the current-density through a gas is increased.

At very low current density,  $10^{-14}$  to  $10^{-12}$  A/cm<sup>2</sup>, depending on the gap between the electrodes, a non-self-sustained discharge develops. Electron and ion production is due to external sources such as UV illumination of the cathode and cosmic rays [4]. When the current density is increased, more electrons and ions are produced by collisions between electrons and gas atoms in a multiplication process. Each accelerated electron generates a certain number of ions per path unit and a progressive increase in current density takes place.

At still increasing current density, gas breakdown occurs at about  $10^{-4}$  A/cm<sup>2</sup>. The ions and electrons perturb the electric field and the voltage drop across the GD decreases while the current increases. The discharge becomes visible with dark and light regions arranged in a characteristic manner as is discussed in the following section.

When the electric field is sufficient to ionize the gas without external input, a glow discharge has been established. When the current density is further increased, the voltage remains practically constant. The area of the cathode surface covered with the negative glow increases in proportion to the current. The voltage increases when the whole cathode is covered. A higher cathode fall is necessary to establish the larger electron emission. In this potential region, significant cathode sputtering takes place. The spectra show the characteristics of the cathode material. This is the region used in analytical spectrometry. The voltage reaches a maximum and decreases again when effects of cathode heating and gas heating become significant. For a cold cathode this maximum is appreciable; for a heated cathode it is only a small maximum. The overall potential current features are illustrated in Fig. 1.2 [4,5].

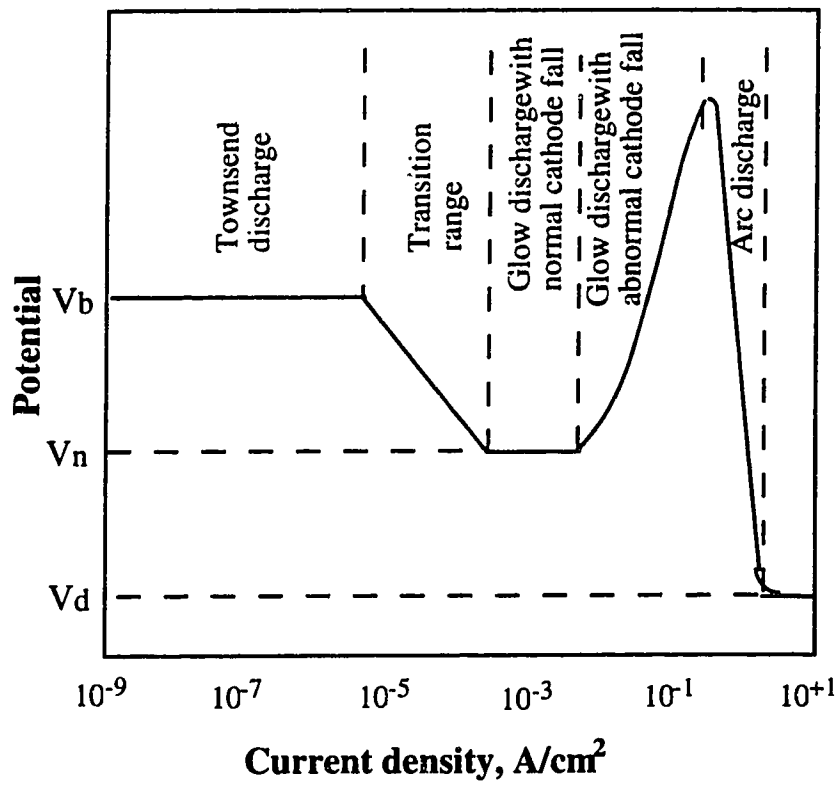


Fig. 1.2 Potential - current feature of a gas discharge.

### 1.3.2 Sputtering Phenomenon

Driven by the electrical field, most of the positive ions enter the cathode dark space will reach the cathode with a wide range of kinetic energy. The energy distribution is dependent on the values of the potential and the gas pressure [6]. A large number of positive ions with sufficient kinetic energy colliding onto the cathode surface will knock some material from the surface. This process is called cathodic sputtering. The efficiency of this process largely depends on the filler gas identity and the cathode material. The applied potential is another key factor affecting the degree of sputtering. The material sputtered from the cathode may be neutral atoms, ions or clusters. Ions sputtered from the cathode surface may be attracted back to the cathode as soon as they leave the surface. Neutral atoms and clusters have more chance of getting into the negative glow and the positive column. These particles may have some initial kinetic energy when they leave the cathode, but their movement into the negative glow and other regions of the discharge plasma is mainly by diffusion. Sufficient sputtering may generate a high number density of neutral atoms in the discharge plasma. By using a solid sample as the cathode, analyte is transported from the bulk sample to the plasma, and spectrometry studies can be carried out on the analyte. This forms the foundation for glow discharge atomic spectroscopy, and it will be discussed again in Chapter 3.

### 1.3.3 Light Distribution in a Glow Discharge

The actual distribution of the light in a glow discharge between the electrodes depends on the nature of the gas and operating conditions. As illustrated in Fig. 1.3 [7], the cathode itself is covered with a thin cathode glow, separated from the cathode by a thin dark layer less than 1 mm thick,

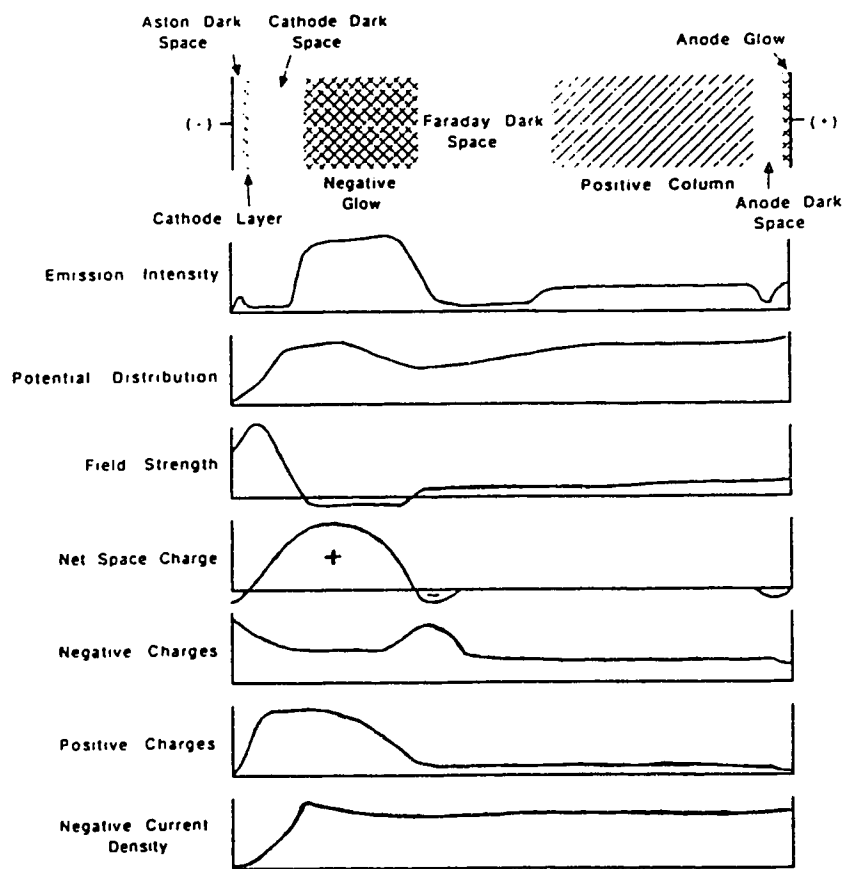


Fig. 1.3 Schematic description of the nature of a conventional glow discharge.

called the Aston Dark space. This glow is bounded on the other side by a much darker region called the Crookes or Hittorf Dark Space, most commonly known as Cathode Dark Space. For any given current the width of this space increases as the gas pressure is reduced [4,7]. Then follows another luminous region called the negative glow, bounded by an almost completely dark space, the Faraday Dark Space. Following the Faraday dark space, a uniform glow, fills the rest of the discharge chamber, reaching to the anode. This part of the discharge is known as the uniform positive column, or just positive column. It is also called as the discharge plasma. The luminosity is uniform when the discharging gas has high purity. Traces of impurities in the monatomic filler gas can produce alternative luminous bands.

The anode end of the positive column is some-times brighter and is called the anode glow, and this is separated from the anode itself by a narrow dark space called the anode dark space. In practice, a glow discharge can exist without a positive column, a Faraday dark space, and even a negative glow. It can never exist without a cathode dark space [8]. The length of the cathode dark space and the negative glow, in a given gas and at a given voltage, is dependent upon the gas pressure. The higher the pressure, the shorter these regions will be. The Faraday dark space and the positive column then occupy the remaining length up to the anode. When the inter-electrode distance is reduced but when the current is kept constant, all the above sections remain practically unaltered except for the positive column. This section is progressively reduced as the gap length is reduced, until it is eliminated altogether [4]. Such an arrangement would give a type of lamp producing a high proportion of neutral resonance lines

and ion lines. The dimensions of these zones depend on the pressure and nature of the gas, and on the discharge current.

## **1.4 The Nature of a Glow Discharge**

### **1.4.1 The Cathode Region**

The electrons required to maintain the discharge are produced from emission events at the cathode as a consequence of bombardment of the cathode by positive ions. The bombarding ion species are thought to become neutralized by a field-emitted electron just before impact with the cathode surface [9]. The neutralization energy is transferred in an Auger-type transition to the lattice electrons which may cause the ejection of secondary electrons from the cathode material. The secondary electron yield for most metals is of the order of 0.1 for incident  $\text{Ar}^+$  ions over the range of bombardment energies typical in the glow discharge (300-500V) [9]. It is believed that the ionization conditions in the cathode region between the electrode and the positive space charge layer must be similar to those in a parallel-plate gap sustaining a potential difference which is practically equal to the minimum sparking potential for that gap [10]. Here electrons leave the cathode and generate avalanches as they proceed to the space charge layer acting as an anode. These electrons pass through this layer and enter the dark spaces and eventually the positive column. They are of the greatest importance because they initiate and maintain the discharge. Electrons in the discharge are finally swept into the anode or become removed from the cathode region by passing through the space charge region. Their number must be replaced, and this replacement takes place at the cathode surface. Thus the values of the electric field and gas



density in the cathode region are such as to set up the appropriate and adequate processes which lead to the continuous emission of the necessary electrons from the cold cathode. This condition is therefore one of self-maintenance in which the electron-gas collision processes in the cathode region set up a mechanism or mechanisms at the cathode for the secondary emission of the requisite number of electrons to maintain the discharge. The emission of the secondary electrons results in a net negative space charge. The current in this region, is carried mainly by the positive ions heading towards the cathode. Due to the recombination of the slow electrons and the incoming positive ions, a thin luminous zone is formed and it is called the Cathode Glow. The non-luminous layer between the cathode and the cathode glow is called the Aston dark space.

Further from the cathode, the electric field becomes weaker, and there the electron is a more efficient excitation and ionization agent, causing ionization of the discharge gas and electron multiplication. On the anode side of the cathode glow, the number of electrons able to cause gas ionization has increased through multiplication, and simultaneously, a large number of positive ions has been created. Since the electron mobility is higher than that of the ion, the collection of charged species leaves a large net positive space charge established throughout the cathode dark space. There is a high, uniform, net positive charge density, in spite of an almost beam-like current of electrons, which suffer some ionizing and a very few exciting collisions. This region emits little visible light though some ultraviolet radiation and is called the Cathode Dark Space. The drift of positive ions towards the cathode ends by setting the steady state glow regime, characterized by a nearly constant positive space charge located near the cathode. This positive space charge produces a large potential

gradient and most of the discharge voltage is taken up here. This makes the field continuously decrease until a very small value is reached. Positive space charge near the cathode determines the cathode fall. The voltage fall across this region is nearly the whole of that across the discharge tube. Approaching the negative glow, further electron multiplication takes place, the electron current density increases, diminishing the positive space charge. By the end of the cathode dark space, the current is nearly all carried by the electrons, present in great numbers [11]. The positive ion current density shows, in turn, a complementary space variation to allow for the current density conservation. Thus the self-sustained discharge condition is fulfilled. Passing through the dark space, the electrons are accelerated to energies high enough to produce a sufficient number of electrons and ions, and another luminous zone develops separated from the cathode by the dark space. This luminous zone is called negative glow.

#### 1.4.2 The Negative Glow

The onset of the negative glow corresponds to the position where the fast cathode electrons have lost a large fraction of their energy through inelastic collisions with other particles. A large population of electrons with energies from a few tens of eV to nearly thermal values is found [12] in this region. This range of electron energies is low enough to allow electron impact excitation and ionization collisions with various atomic species present. This reflects the fact that those energy levels existing at  $\leq 3$  eV above the ground state will be preferentially populated by electron impact. Atomic transitions in long wavelength UV and visible regions of the spectrum may dominate the emission from the negative glow because of

the low excitation energy. Other processes such as ion-electron recombination could also happen in this region. The consequence of these processes will also be observed in the emission spectrum.

The plasma potential in the negative glow region is almost invariable, less than 1 V difference, in comparison with the discharge voltage of around 1000 V or higher. This region has a near zero and almost completely uniform field [13]. The electric field free characteristic in the negative glow has been further confirmed for analytical devices by the electrical probe experiments of Fang and Marcus [14]. However, the negative glow contains high densities of both ions and electrons. There may be two main groups of electrons in the negative glow: fast electrons, produced near the cathode, which have not suffered inelastic collisions in the cathode dark space [15]. This includes a beam-like component, with an energy approaching that of the cathode fall; and slow electrons, those created in the cathode dark space which are less energetic as a result of undergoing inelastic collisions. This is a much larger group having a smooth (but not really thermal) energy distribution from zero to some tens of volts (according to conditions) [10]. Due to their larger number density, the slow electrons are more important than the fast ones in the excitation process and producing the negative glow. The negative glow is a region of intense radiation, the color of which is characteristic of the discharge gas. The maximum brightness of the discharge occurs a short distance away from the leading edge (cathode side) of the negative glow, as there, energy-depleting collisions give rise to electrons having energies at which large inelastic collision cross sections are observed. The high density of both ions and electrons combined with a near-zero field strength, makes ion-electron recombination more efficient.

The fast electrons penetrating further into the negative glow, produce both ionization and excitation, but they gradually lose energy with distance. The collision rate of the high energy electrons slows down drastically during their progression through the neutralized plasma of the negative glow. As the electrons are slowed down, the negative space charge reaches a maximum, and the energy available for excitation and ionization is exhausted. It is at this point another dark region- Faraday dark space begins.

#### 1.4.3 The Faraday Dark Space

Further from the cathode, the decline in the production of excited and ionized species is revealed by a dark space, the Faraday dark space. The zero field situation cannot last beyond this point, since the decrease in electron energy and drift velocity give rise to an accumulation of electrons and form a negative space charge which induces a small field enhancement. In the Faraday dark space, the increased field acts to draw electrons out from the fringe of the negative glow. At the same time, the electron drift velocity increases again avoiding any further extension of the negative space charge. The low energy electrons are unable to pump up the atoms or ions to excited states and the increasing field strength prohibits the recombination of the ions and slow electrons, resulting in an almost complete darkness in this region. When the electrical field reaches a constant value, the formation of the positive column begins.

#### 1.4.4 The Positive Column

Like the negative glow, this region has the property of a plasma-- a partially ionized gas, but having no net space charge. The electric field was

found constant in the positive column. It is usually a region of uniform luminosity and easily molds itself to the shape of the tube containing it. The field takes a value for which the production of charged species by electron impact is balanced by recombination either in volume or at the walls. In spite of the high electron mobility, no positive space charge is formed since the number of electrons entering a positive column section is the same as that leaving the section. This condition could not be fulfilled near the cathode because the secondary effect could not release enough electrons from the cathode to replace each electron leaving the cathode region.

#### 1.4.5 The Anode Regions

In the dc discharge, the anode is usually only a few volts negative with respect to the plasma potential [7]. Since this potential difference is small, the anode does not normally emit any particles and simply collects the electrons. In general, there is a negative space charge region in the neighborhood of the anode which is relatively non-luminous. This produces a small anode fall potential, and slow electrons emerging from the positive column will enter the anode fall region, where they are accelerated toward the anode. An anode dark space and an anode glow are formed as electrons gain enough energy to excite and ionize gas in front of the anode.

### 1.5. Applications

In 1968, a practical glow discharge lamp for spectrochemical analysis with a flat cathode was described by Grimm [1] and attracted much research in this area. Due to the basic properties of the glow discharge, it can be used in many different ways as an analytical source. A glow discharge can be used as an atomization source, ion source and emission

source at the same time. Fig. 1.4 is a schematic diagram showing some of the related techniques with a glow discharge.

a) Atom Reservoir

Sample atoms are generated in this device by sputtering, making it an almost ideal atomization source. Material brought into the plasma in a glow discharge is to a large extent present as a vapor cloud of free atoms, thus glow discharges are suitable as reservoirs for atomic absorption and atomic fluorescence [16-22]. In this respect, some excellent review articles have been published by J.A.C. Broekaert [23] and Caroli [24], and a book entitled *Glow Discharge Spectroscopies* edited by Marcus [7] has recently been published.

b) Ion Source

The sample atoms are also partially ionized in the low-pressure plasma, making it a useful ion source. Glow discharge mass spectrometry (GDMS) has been widely used in the analysis of many kinds of samples. Non-thermal vaporization of the sample occurs making selective volatilization less severe as compared to classic spark sources or vacuum arc ion sources, which is a pre-requisite for reducing matrix interferences. Glow discharges have been successfully coupled to quadrupole mass spectrometers [25,26] and commercially to a sector type mass spectrometer [27] and may be expected to become of considerable interest for trace analysis of solid samples. As shown in many publications, different types of alloys have been analyzed by several groups [28-33] and in this lab [33]. Apart from compact metallic samples, non-conducting powders can also be analyzed with a glow discharge. They can be mixed with a metal powder and the mixture can be briquetted into pellets [34]. Many applications are detailed in the book edited by Marcus [7].

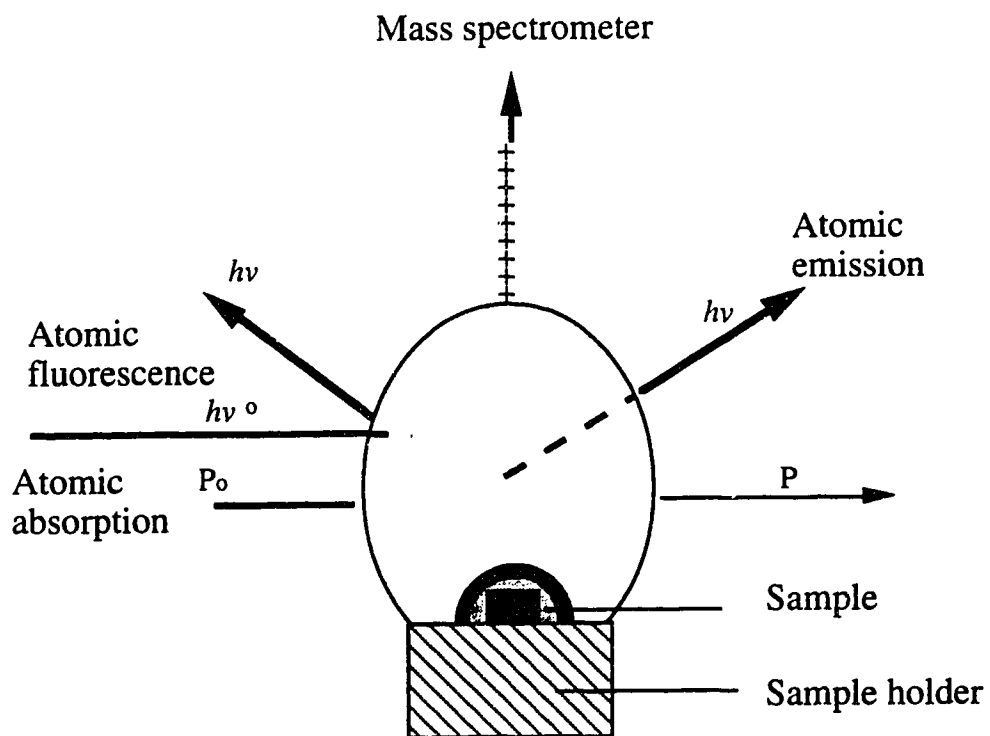


Fig. 1.4 Representation of some glow discharge related techniques.

## **1.6. Problems in This Area**

The use of a glow discharge for spectrometric analysis should benefit from an understanding of the basic phenomena that determine the analytical performance of the glow discharge: atomization, ionization and excitation of the sample material. The fundamental aspects of this technique, however, are not fully understood. The basic parameters obtained by different authors and different techniques are often different from each other. In 1958, Cobin [35] pointed out that no sources are infallible, all proofs should be questioned, and no discharge phenomena are so well understood that data can be applied precisely. According to Chapman [10], the situation was not significantly different in 1979, at least in sputtering and plasma etching discharges. There is a still real need to understand fully and appreciate the operative principles of these discharges [24]. The excitation mechanisms in the glow discharge, for example, have not been thoroughly investigated. Much of the work to date has been of the more empirical approach; much remains to be learned concerning the fundamental phenomena occurring in glow discharges and how their proper optimization may lead to better analytical results [11].

## **1.7 The Objective of the Thesis**

For any type of emission spectroscopy, including glow discharge emission analysis, excitation of the analyte is an essential process. To understand its mechanism is very important, both theoretically and practically. The characteristics of the emission spectrum of the analyte and the discharge gas reveal the population of the atoms in various energy



levels. The population of the atoms at each energy level is directly related to the excitation mechanism(s). The primary focus of this study is to provide a detailed analysis of the spectral character of emission from a glow discharge. Spectral character refers to the specific types of lines emitted by species in the discharge (both ions and atoms of the sample and filler gas) and their relative intensities. In order to get a full picture, complete spectral records (ultraviolet, visible and near-IR) were measured using a UV-Vis-NIR Fourier transform spectrometer. The experimental components are described in the next chapter (Chapter 2) and then some basic parameter studies of the glow discharge are described (Chapter 3). The full spectral studies are presented in Chapter 4 (ions) and Chapter 5 (neutral atoms). A brief summary of this study will be given in Chapter 6.

## References

1. W. Grimm, *Spectrochim. Acta* **23B** 443 (1968).
2. F. Paschen, *Ann. Phys.* **50** 901 (1916).
3. X. Feng, Ph.D Thesis, University of Alberta, 1994.
4. F. Llewellyn-Jones, *The Glow Discharge*, Methuen & Co. Ltd, London, 1966.
5. A.M. Howatson, *An Introduction to Gas Discharges*, Pergamon Press, Elmsford, N.Y., 1976.
6. P.W.J.M. Boumans, *Anal. Chem.* **44** 1219 (1972).
7. D. Fang and R. K. Marcus, *Fundamental Plasma Processes*, Chapter 2, in *Glow discharge Spectroscopies*, Edited by R. K. Marcus, Plenum Press, New York, 1993.
8. E. Nasser, *Fundamentals of gaseous Ionization and Plasma Electronics*, Wiley-Interscience, New York, 1971.
9. G.K. Wehner, in *Methods and phenomena*, Edited by S. P. Wolsky and A. W. Czanderna, Vol. 1, Elsevier Scientific, New York, 1975.
10. B. Chapman, *Glow Discharge Processes*, Wiley-Interscience, New York, 1980.
11. W.W. Harrison and B. L. Bentz, *Prog. Analyt. Spectrosc.* **11** 53 (1988).
12. P.F. Knewstubb and A. W. Tickner, *J. Chem. Phys.* **36** 684 (1962)
13. D. Fang and R. K. Marcus, *Spectrochim. Acta* **45B** 1053 (1990).
14. D. Fang and R. K. Marcus, *Spectrochim. Acta* **46B** 983 (1991).
15. J.M. Anderson, *J. Appl. Phys.* **31** 511 (1960).
16. D.C.McDonald, *Anal. Chem.*, **49** 1337 (1977).

17. H.G. Human, N.P. Ferreira, R. A. Kruger and L. R. P. Butler, *Analyst*, **103** 469 (1978).
18. B.W. Smith, N. Omenetto and J.D. Winefordner, *Spectrochim. Acta*, **39B** 1389 (1984).
19. B.M. Patel and J. D. Winefordner, *Spectrochim. Acta*, **41B** 469 (1986).
20. N.P. Ferreira and H.G. Human, *Spectrochim. Acta*, **36B** 215 (1981).
21. R.M. Lowe, *Spectrochim. Acta*, **31B** 257 (1978).
22. P.E. Walters and H.G. Human, *Spectrochim. Acta*, **36B** 585 (1983).
23. J.A.C. Broekaert, *J. Anal. Atom. Spec.*, **2** 537 (1987).
24. S. Caroli, *J. Anal. Atom. Spec.*, **2** 661(1987).
25. Y. Shao and G. Horlick, *Spectrochim. Acta*, **46B** 165 (1991).
26. N. Jakubowski, D. Stuewer and W. Vieth, *Anal. Chem.*, **59** 1825 (1987).
27. A.P. Mykytiuk, P. Semeniuk and S. Berman, *Spectrochim. Acta Rev.* **13** 1 (1990).
28. M. Dogan, K. Laqua and H. Massmann, *Spectrochim. Acta*, **27B** 65 (1972).
29. R. Klockenkamper, K. Laqua and M. Dogan, *Spectrochim. Acta*, **34B** 527 (1980).
30. R.A. Kruger, L.R. Butler, C.J. Liebenberg and R.G. Bohmer, *Analyst*, **102** 949 (1977).
31. H. Jager *Anal Chim Acta*, **60** 303 (1972).
32. N. P. Ferreira and L. R. Butler, *Analyst*, **103** 607 (1978).
33. X. Feng and G. Horlick, *J. Anal. Atom. Spec.*, **9** 823 (1994).

34. S.El Alfy, K. Laqua and H. Mabmann, *Fresenius Z. Anal Chem.* **1**  
263 (1973).
- 35 J.D. Cobine, *Gaseous Conductors*, New York, N.Y., 1958.

## **Chapter 2. Instrumentation**

In this chapter, the glow discharge devices and the spectrochemical instruments used in our measurement are briefly presented. For the most part, they were developed during previous studies in this laboratory .

### **2.1. Glow Discharge Devices**

Glow discharge devices can be constructed in a variety of configurations. They can be divided into three categories according to the configuration of the cathode-- hollow cathode, planar cathode or pin-type cathode glow discharges. In our experiments, only the later two were used, and they are discussed in the following sections.

#### **2.1.1. Planar Cathode**

A planar cathode glow discharge source introduced by Grimm [1] has been applied extensively as a source for analytical emission spectrometry [2]. A wide variety of solid conducting samples as well as non-conducting powders have been analyzed, and investigations of the fundamental parameters have been published. A planar cathode GD is a device in which the cathode (usually the sample) is a flat disc. An advantage of this configuration is that the cathode (i.e. the sample) is readily machined and interchange of samples is relatively convenient. Because this kind of device is usually constructed in the obstructed way

(anode cylinder is near the cathode surface), the sputtering surface area is fixed and the signal intensity is relatively stable.

A modified version of this type of glow discharge device has been described, in which a ceramic restrictor is placed between the cathode and the anode. As described by Ko [3] and Ferreira et al [4], a GD device in which the anode is further away from the sample and where a ceramic restrictor defines the burning spot is advantageous. The field across the sample is more uniform, which results in a flatter burning spot and, accordingly, in better depth resolution. It was also found that the analytical performance of this lamp in terms of precision and freedom from matrix interferences was even better than that of the original Grimm-type lamp.

An example of a planar cathode glow discharge device built in this laboratory is shown in Fig. 2.1 [5]. The unit was constructed from brass in an obstructed way. The space between the inner surface of the cathode and the insertion of the anode body is so small that a discharge can not happen within this space. The cathode was isolated from the rest of the anode body by a piece of Teflon insulator. A quartz window was mounted at the far end of the anode. Between flat surfaces, there are O-rings to prevent air leaking into the unit. Between the sample disc and the cathode body, an additional piece of conductor was often used to assure that the sample and the cathode body were at the same potential. The unit was designed in the manner that fresh discharge gas entering into the unit sweeps the quartz window first, then flow towards the cathode surface. In this way, the deposition of sputtered materials on the window was minimized. The gas was pumped out through the space between the anode insertion and the cathode, and the redeposition of the sputtered material back to the sample surface is believed significant. Both the anode and the cathode (and the

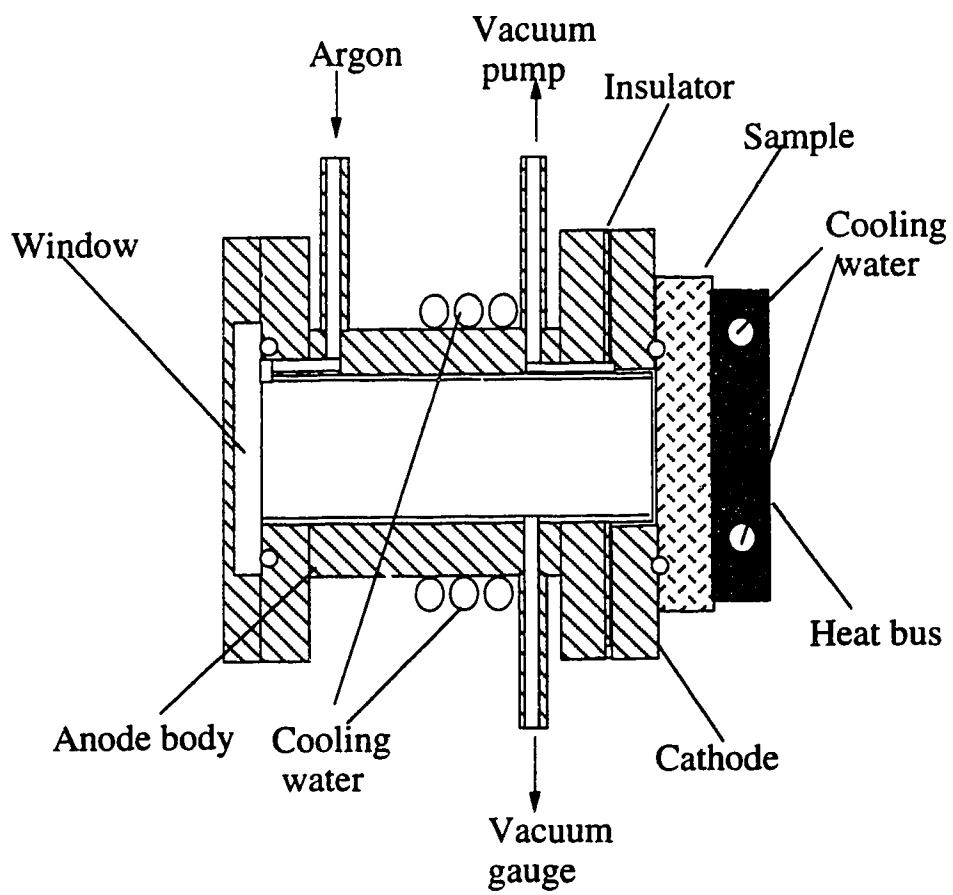


Fig. 2.1 Schematic diagram of a Grimm-type glow discharge source.

sample) were water cooled to minimize the thermal evaporation of the sample and the inner surface of the anode body.

### 2.1.2 Pin-type Glow Discharge

An example of a pin-type glow discharge built in this laboratory [5] is shown in Fig. 2.2.

The samples (Cathode) are metallic pins, 3.1 mm in diameter and about 15 mm long. Materials to be used as samples must be machined into this form. The GD cavity was lined with a thin stainless steel sleeve. This simply provided an inner surface that was easy to clean. The insulator around the pin sample and the cathode is Macor, and the other insulator material is Teflon.

An advantage of a pin-type device is the sample can be small. However, fabrication of the sample takes some time unless a sample rod with the right diameter is available. Also, the sample surface area and the sample shape change during the sputtering process causing the signal intensity to drift. In addition, the plasma around the sample tip is not homogenous in any direction, making certain diagnostic studies of the plasma very difficult.

## 2.2 The Spectrometers

### 2.2.1. The Photodiode Array (PDA) System

Some spectral measurement, particularly most of those presented in Chapter 3, were carried out using a photodiode array spectrometer. The PDA spectrometer was based on a system developed by Lepla and Horlick [6].



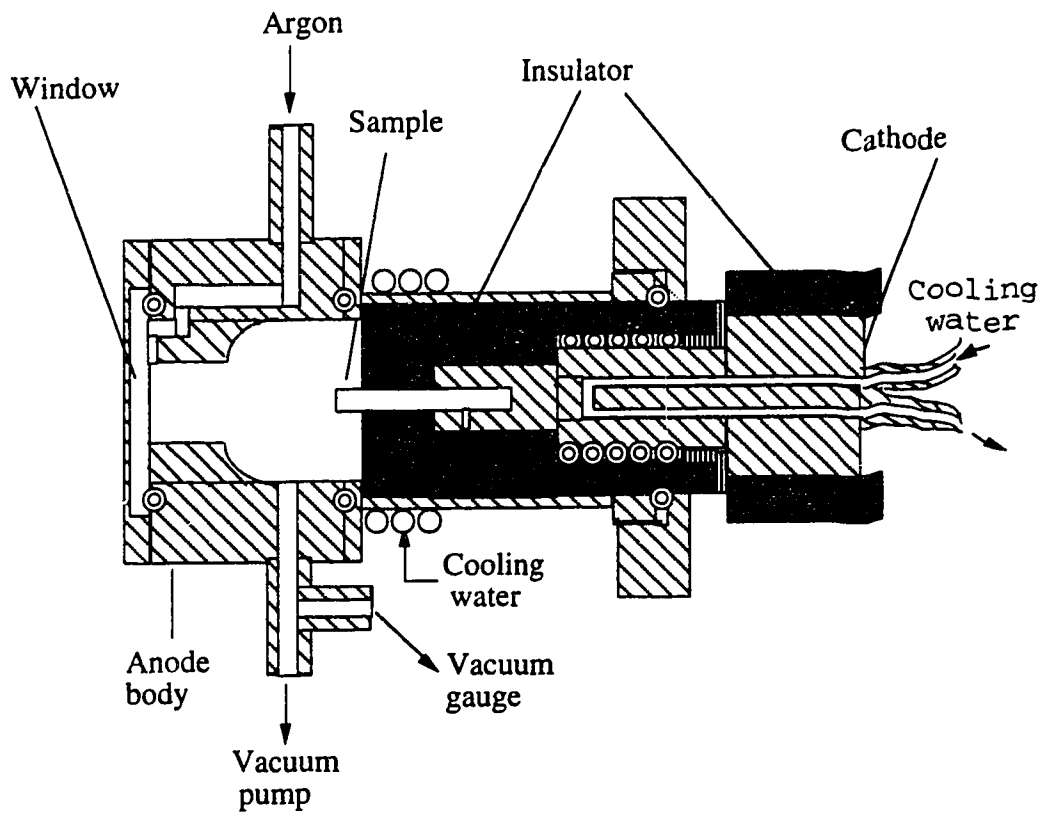


Fig. 2.2 Schematic diagram of a pin-type glow discharge source.

For this work, the PDA (1024 elements, 25.4 mm long) was mounted horizontally in the exit focal plane in a 1 meter spectrometer. The PDA was oriented along the spectral axis, so that multi-wavelength data was obtained. The simultaneous wavelength coverage was limited to a single spectral window of 20 nm.

The PDA system was interfaced to an IBM-PC using a Data Translation DT2801-A A/D I/O board and custom built clock/timer [6]. The DT2801-A is an interface board which plugs into a slot in the IBM-PC and it contains a 16 channel, 12 bit ADC, two 12 bit DAC's and two 8 bit digital I/O ports. The ADC can be external clocked and triggered, and the maximum conversion rate for the ADC is 27.5 kHz.

The maximum integration time is limited by saturation of the array by the signal and/or the dark current. In order to maximize the integration capability of the array for weak signals, it is necessary to cool the array. Without cooling, dark current alone will saturate the array at an integration time of about 10 seconds. The array was cooled by utilizing a Peltier effect cooling module and a copper bus which passes through a slot in the driver board and contacts the back of the PDA chip. The cold side of the Peltier cooler is coupled to the PDA by the copper bus to conduct the heat away from the array. To ensure good thermal contact of the cold copper bus and the back of the array, a thermal conductive paste was used. The warm side of the Peltier device is in contact with a water cooled copper bus. With this design, temperatures of approximately  $-20^{\circ}\text{C}$ , at the array were achieved. The Peltier cooler was operated at approximately 11 volts and 4 amperes making possible integration times of up to 100 seconds. To prevent condensation of water vapor and/or formation of ice

on the PDA, the surface of the array is continually flushed with dry nitrogen.

The data acquisition and analysis were carried out by using software written in Asyst by K. Lepka [7] and modified by the author. The spectra can be either plotted on an HP plotter or transfer to another computer format for further treatment. An example of spectra acquired by the PDA system is shown in Fig. 2.3.

### 2.2.2 Fourier Transform Spectrometer

Most of the spectral measurements presented in this thesis were carried out using a Fourier transform spectrometer (FTS) developed and built in this laboratory [8]. A block diagram of the Fourier transform interferometer is shown in Figure 2.4. In the measurement, each of the frequencies of the light present in the bandwidth is modulated by the interferometer and recorded by the detector. The resulting signal is called an interferogram. An example interferogram is shown in Fig. 2.5. As illustrated, up to 65536 data points are acquired for each interferogram. This recorded time domain signal was converted into a frequency domain signal by the mathematical process of Fourier transform, resulting in a spectrum.

The spectral measurement features of this Fourier transform spectrometer have been detailed by King et al [9]. A key feature is that it allows a direct measurement over a broad spectral range of a complete spectrum. This range is limited only by the detector response and the efficiency limits of the optical components of the instrument and is unmatched by any other measurement system. For the spectral measurements in this study, detectors were used that restricted, to some

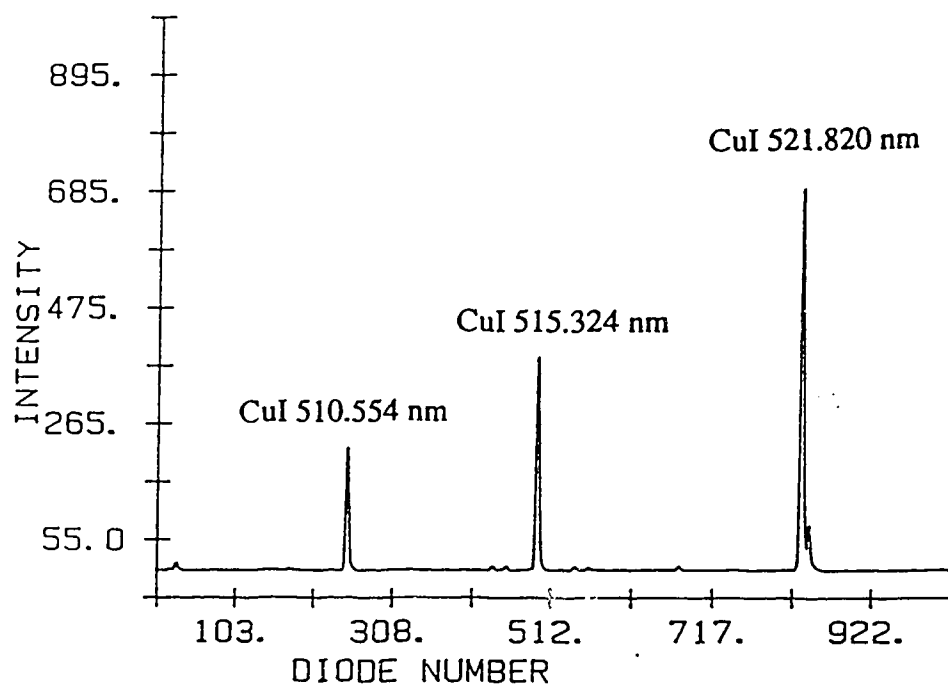


Fig. 2.3 A spectrum obtained from the PDA system and plotted on an HP plotter.

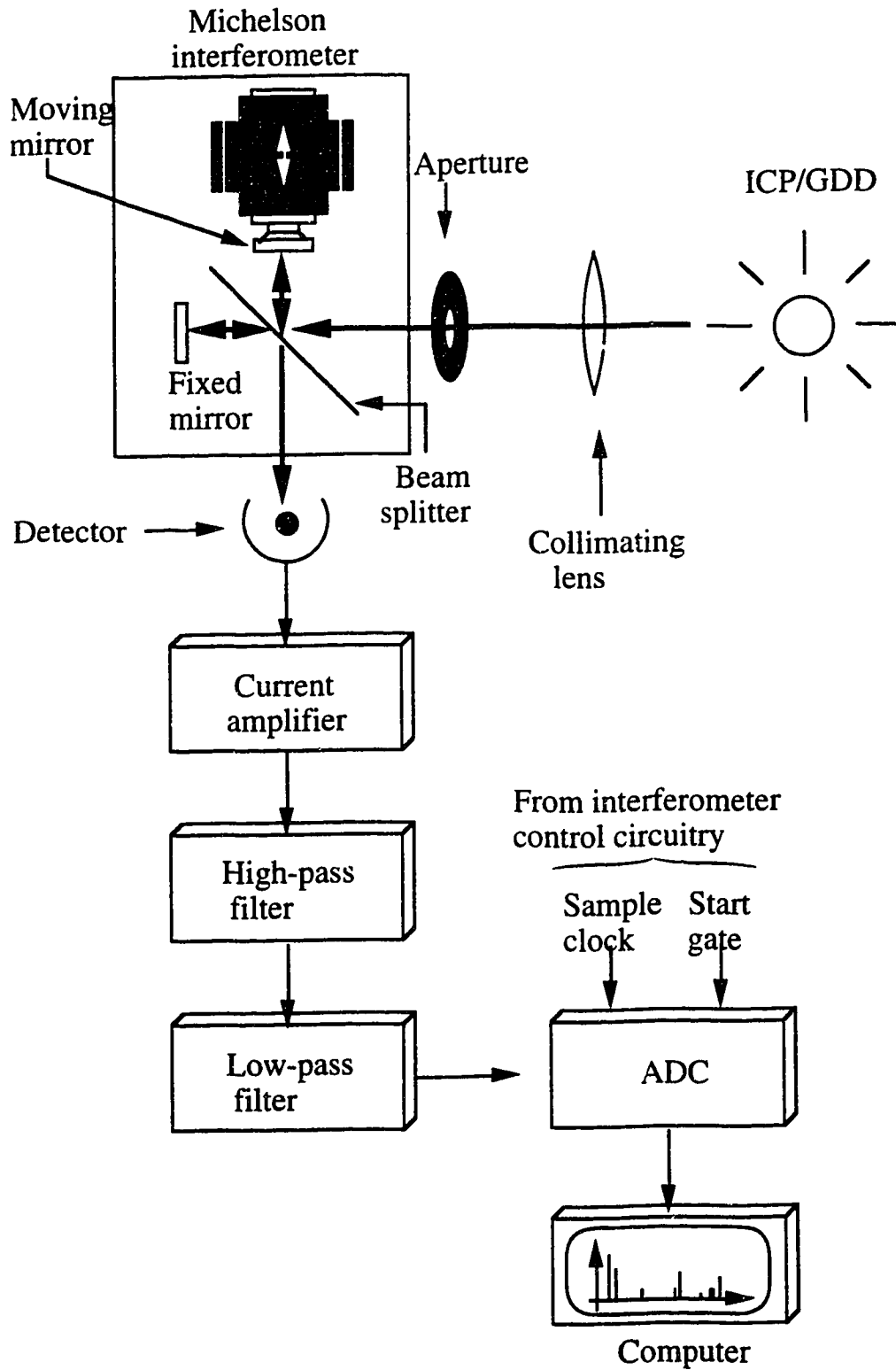


Fig. 2.4 Block diagram of the FTS measurement system.

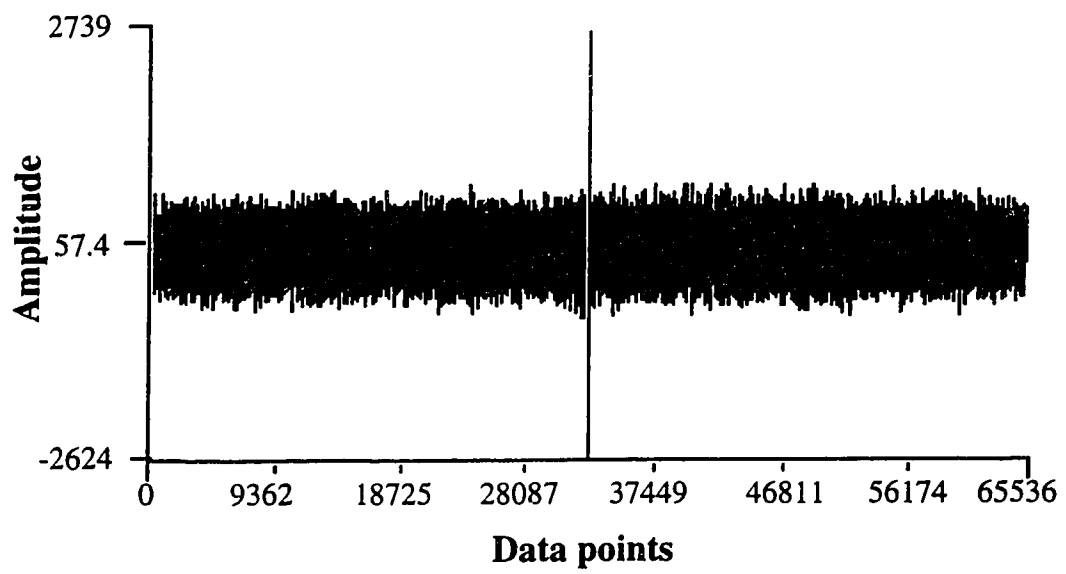


Fig. 2.5 An example of brass interferogram acquired with the FT system.

extent, the spectral bandwidth in order to avoid aliasing complications [See Reference 9]. What we call ultraviolet spectra (UV spectra) were obtained with the FTS system utilizing a solar blind photomultiplier tube (R166). The spectral response of this tube extends from about 300 nm down to below 200 nm. With a data digitization rate of four times the He-Ne laser clock [See Table 1 of Reference 9] an unaliased region from 158 to 316 nm ( $63209 - 31665 \text{ cm}^{-1}$ ) is acquired. An example spectrum is shown in Fig. 2.6a, many of which will be discussed in Chapter 4 and 5.

The visible region spectra were obtained using a 1P21 type photomultiplier tube. This tube has a spectral response extending from about 300 nm to 650 nm. The unaliased region acquired in this case extends from infinities (*i.e.*  $0 \text{ cm}^{-1}$ ) to 316 nm ( $31605 \text{ cm}^{-1}$ ) [9]. A visible region spectrum is shown in Fig. 2.6b. Finally, some near-infrared spectra (NIR) were also acquired. They cover the same range aliased region as acquired for the visible spectra, but are measured using a Si photodiode as the detector [Fig. 2.6c]. The FTS system has very high resolution. In the 200 nm region, the resolution is as high as 2.5 pm. This feature of the system reduces the number of spectral interferences in a given spectrum. For this research, this is a very valuable feature. It is vital to have pure isolated lines for fundamental spectrophysical studies of an excitation source like the ICP or GD. Overlap between the spectral lines could lead to misinterpretation of the spectrum or unresolved lines may result in wrong conclusions in the study of excitation mechanisms. Also, FTS has high degree of accuracy in the measurement of wavelength, which is a big problem with both direct readers and monochrometers. Only a single internal He-Ne laser is required to calibrate the entire scale of the spectrum. The accuracy of the wavelength is limited only by the accuracy

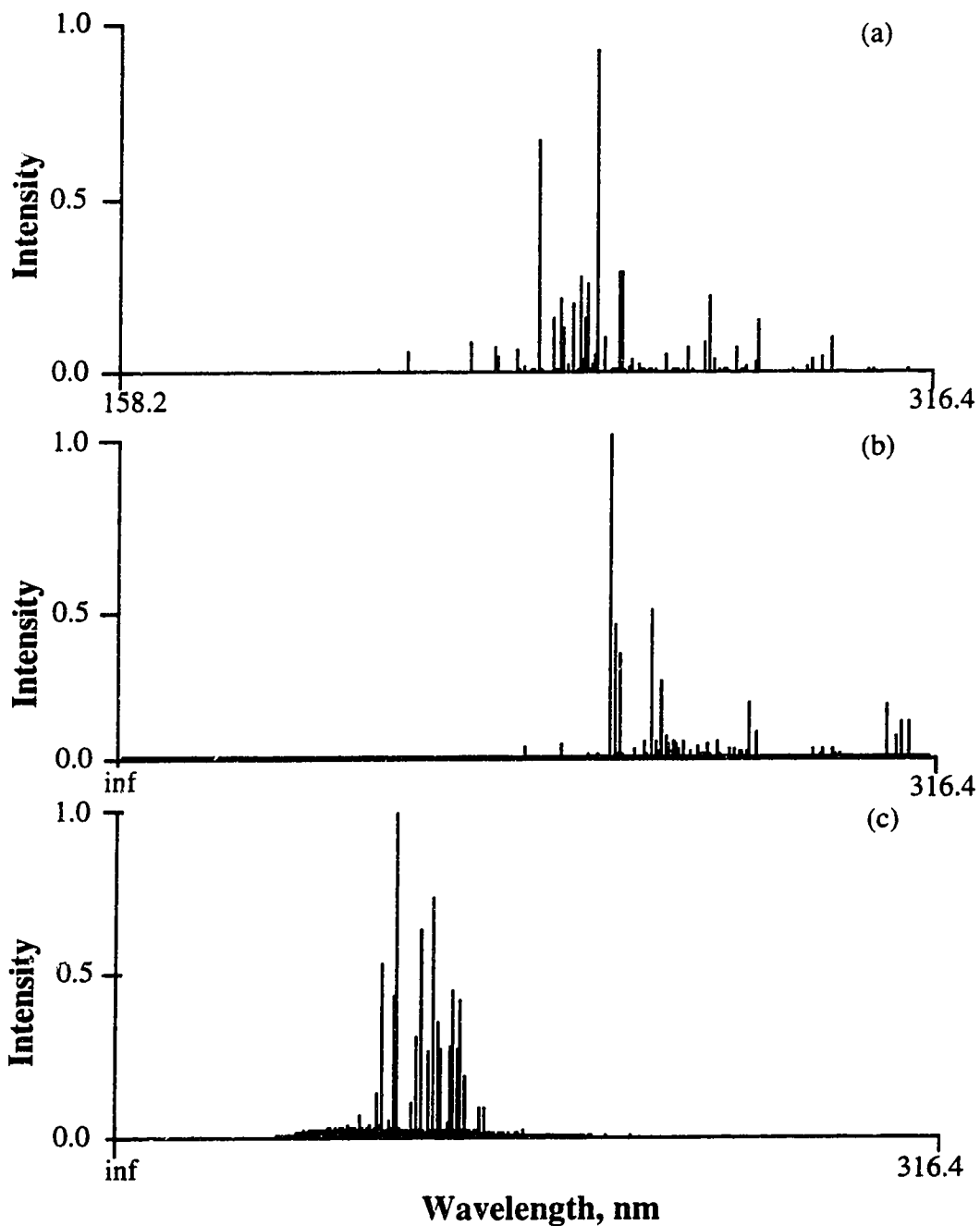


Fig. 2.6 Example spectra acquired with the FT system in different wavelength regions. a: UV region with an R166 solar-blind PMT; b: Visible region with a 1P21 PMT; c: Near infrared region with a silicon photodiode detector. Sample: brass.



with which the wavelength of the laser is known, and by the alignment of the optics in the interferometer system. The spectrometer has been shown to have an absolute wavelength accuracy of 1 pm and a wavelength precision approaching 0.1 pm. These three important characteristics - wide spectral range, high resolution and high wavelength accuracy make the FTS an almost perfect tool for this study.

The work-up and detailed spectral analysis of the results presented in Chapter 4 and 5 would not have been possible without the support program SpectroPlot [10]. This program was developed by G. B. King and has extensive display and analysis options to deal with the large data sets that are acquired using the FTS system.

## References

1. W. Grimm, *Spectrochim. Acta* **23B** 443 (1968).
2. R.K. Marcus, Ed "*Glow Discharge Spectroscopies*" Plenum Press, NY. 1993.
3. J.B. Ko, *Spectrochim. Acta* **39B** 1405 (1984).
4. N.P. Ferreira, J.A. Strauss and H.G.C. Human, *Spectrochim. Acta* **38B** 899 (1983).
5. Y. Shao and G. Horlick, *Spectrochim. Acta* **46B** 165 (1991).
6. K.C. Lepla and G. Horlick, *Appl. Spectrosc.* **43**, 1187 (1989).
7. K.C. Lepla , Ph.D Thesis, University of Alberta, 1989.
8. B.R. Todd and G. Horlick, *Spectrochim. Acta* **47B** 275 (1992).
9. G.B. King, B.R. Todd and G. Horlick, *Spectrochim. Acta* **47B** E333 (1992).
10. G.B. King and G. Horlick, *Spectrochim. Acta* **47B** E353 (1992).

## **Chapter 3. Glow Discharge Parameter studies**

### **- Comments and Measurements**

In a glow discharge, the discharging parameters have a fundamental influence on the source performance. Studies of these parameters could generate valuable information for both diagnosis and the application of the source. In this chapter, the parameters which affect the nature of a glow discharge will be briefly discussed and some measurement of the parameters relative to the diagnosis of the source will be made.

#### **3.1 Current - Voltage - Pressure**

The operation of a glow discharge in the abnormal mode is defined by three globe parameters, pressure (P), current (I) and voltage (V), of which only two can be changed independently. This means that for a given pressure, a choice of current or voltage automatically fixes the other variable. The voltage-current relationship determines the conditions under which the source operates and from the viewpoint of analytical applicability, a selection of these parameters must be made to ensure sufficient sputtering and spectral radiance. The analytically suitable current and voltage range is within which sufficient sputtering occurs and, on the other hand, micro-melting does not take place. The sputter rate of a cathode sample in a GD is dependent on the energy of the noble gas ions and atoms striking the cathode surface. This ion energy is determined by the operation voltage of the discharge and, owing to the multiple collisions in the gas phase, the operation voltage then gives the maximum energy (in

electron volts) of an ion hitting the sample. The pressure defines the mean free path and thus the number of collisions an ion undergoes while it is accelerated in the cathode dark space. If the voltage determines the mean energy of the bombarding ions for a given pressure, the effect of the current manifests itself in the number of ions hitting the surface. Both account for the sputter rate of a sample in a glow discharge.

The relationship between the discharge current and the discharge potential, and between the discharge current and the gas pressure were measured separately. The measurements were made using argon as the discharge gas. The potential was directly read from the power supply and the current was measured using a digital milliamper meter. In the measurement of the relationship between the potential and the current, the gas pressure was fixed at 1650 millitorr, which is a moderate pressure often used in our low current glow discharge study. The potential was varied by adjusting the setting on the power supply. A plot of the resulted current against the discharge potential is shown in Fig. 3.1a.

The same equipment was used in the measurement of the relationship between the discharge current and the gas pressure. The discharge potential was set at 800 V and the pressure was varied by adjusting a needle valve which was inserted into the gas delivery line. The actual gas pressure was measured by a baratron [ model 122AA - 01000AB, MKS Instruments Inc.]. The upper limit of the gas pressure is the point at which sparking in the glow discharge was observed. The plot of the current against the pressure is shown in Fig. 3.1b.

From Figs. 3.1a and 3.1b, one can see that the discharge potential and the gas pressure have a similar effect on the discharging current. The current density at the cathode surface must be increased for any current

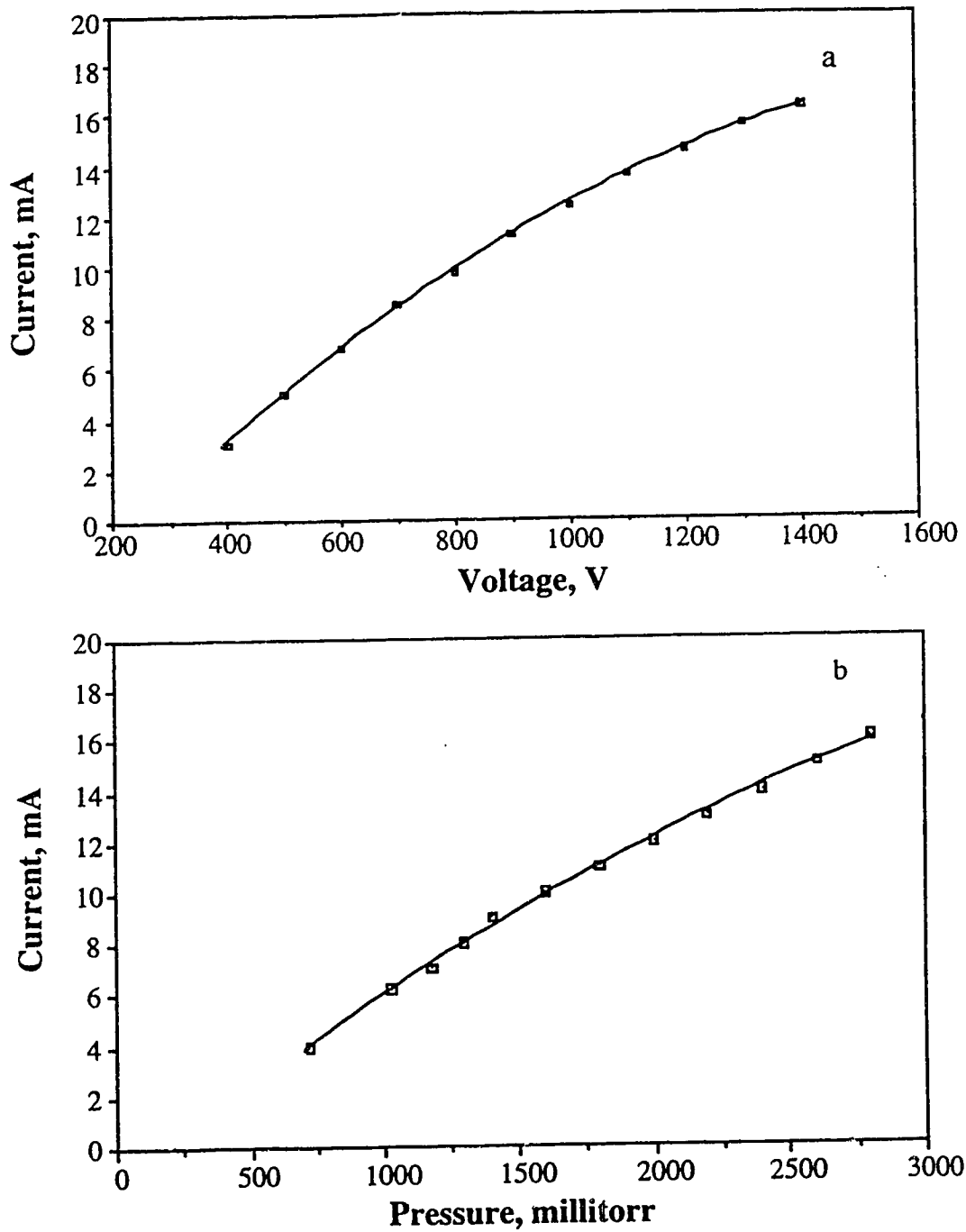


Fig. 3.1 Variation of discharge current with applied voltage (a) and gas pressure (b).

increase, because the device is operating at abnormal conditions. However, the mechanism of increasing the current may not be the same in each case. At a constant gas pressure, the current increase results from the more efficient bombardment from each individual incident particle on the cathode surface. At higher voltage and lower pressure, the cathode dark space thickness is increased [1]. The cathode fall is larger than at a lower potential. On one hand, the longer acceleration distance for the incoming ions gives them a higher kinetic energy. The higher average electron energy prohibits recombination between the ions and the electrons thus making more ions available for the bombardment of the cathode. On the other hand, the higher negative potential makes the cathode surface more vulnerable to attack from the incoming particles. The ejection of secondary electrons, and the atoms which form the cathode material as well, happens more readily. The other factor is that at a high potential the electrons released from the cathode acquire more energy in their passage of the cathode dark space and penetrate further towards the anode. The average electron energy is higher than in the lower potential case. Ionization collisions between the electrons and neutral atoms may be more effective, and increase the number of the ions and electrons.

At a lower potential and an increased gas pressure, the increased current density comes from the larger number of incident bombarding ions. When the pressure is high, even though the average electron energy is lower, the free path length of the electrons is short. The electrons have more chances to hit and ionize the gas atoms. More ions and electrons will be concentrated in the front of the cathode surface. A large number of positive and negative particles travel in opposite directions, resulting in a high discharge current. With high pressure, the cathode dark space is

significantly thinner than in the lower pressure case [1]. In the far end of the negative glow (the electrons get there mainly by diffusion), the field strength will be weak. The fraction of the total electrons that pass this curtain without losing momentum will be significantly smaller. Ion-electron recombination will be more efficient, and the nature of the plasma will be dominated by recombination process.

### 3.2 Pre-burning

For a new sample, after the voltage has been turned on, the discharge needs a period of time before it becomes stable. This process is called pre-burning. In this process, at a given potential and pressure, the discharge current may vary significantly. The composition of the surface changes according to the ease of sputtering of each component which constitutes the sample. The atomic population of various species in the plasma and at the surface do not represent the bulk composition of the sample. The easy to sputter components have a higher population in the plasma, the hard to sputter components have a higher concentration at the surface of the sample. During this period, analyte signal may not be very constant. The length of the pre-burning period is determined by quite a few factors which include: the effectiveness of the vacuum system, the cleanliness of the sample surface, the sample composition, the discharge gas and its purity, the gas pressure, the discharge current density and the discharge potential. For samples, such as copper and silver, which have a high resistance to oxidation, the pre-burning period can be very short or non-existent. For samples, such as magnesium, aluminum and some alloys, which are very easily oxidized, the pre-burning time can be as long as half an hour. The prolonged pre-burning time is due to the trace amount of air

in the discharging gas which oxidizes the surface of the cathode. In this period, at a given discharge potential and gas pressure, the discharge current is abnormally high and unstable. The discharge may form a microarc at some spot on the cathode surface. The high current and low sputtering efficiency are believed to be the result of thermal electron emission at these hot spots. Monitoring the emission spectrum of an aluminum sample between 300 and 316 nm using the PDA system clearly demonstrated the influence of this factor. The aluminum signal does not show much intensity until the band spectrum of O-H disappears. A glow discharge mass spectrometry study carried out by Feng [2] demonstrated the same phenomenon.

### **3.3 Cathodic Sputtering**

It is easily seen that the walls of a discharge tube become darkened after prolonged use, and in the case of glass, the effect eventually can make the tubes opaque. At the same time, the cathode becomes eroded and the material condensed from the vapor deposits on nearby objects, whether other electrodes, insulating supports or the walls. This phenomenon (removal of material from the cathode) is known as sputtering. This process brings the cathode sample into the plasma and forms the back-bone of glow discharge analysis. The phenomenon was first described by Grove [3] and later accounts have been given by Thomson and Thomson [4]. Massey and Burhop [5] and Wehner [6] also reported the phenomenon. Cathode sputtering was exploited by Grimm in 1968 for rapid analyses of conductive samples in the glow discharge device [7]. In 1972, Boumans [8] reported a detailed quantitative analysis of cathodic sputtering. By now, the



phenomenon has been studied for more than a century. However, there still are difficulties in quantitatively describing this process.

### 3.3.1 Description of Cathodic Sputtering

The phenomenon of cathodic sputtering is closely related to the effects of bombardment of the cathode by massive high-speed particles such as fast ions or neutral atoms. Such particles then eject atoms off the target, whether singly or in aggregates, by some direct collisional process. It is thus easy to see why cathode sputtering is readily brought about in a glow discharge because the electrode is subjected to intensive bombardment of fast positive ions generated in the cathode dark space. The extent to which the phenomenon occurs depends on the current density and increases with the value of the cathode fall. The rate of sputtering is therefore dependent on the gas pressure. It is reported that the sputtering rate increases as the gas pressure decreases [9].

There are many views about the precise mechanisms of cathodic sputtering. However, there is still lack of general agreement between the experimental data related to the loss rate of sputtered material to the discharge parameters. Nevertheless, the facts are that for cathodic sputtering: the target is bombarded by ions or neutral atoms of different masses (originating from the discharge gas and the sample material); the ions have a wide energy range because they originate from various parts of the cathode fall and experience frequent symmetric charge transfer processes, and there is a wide angular distribution of the impact due to collisions; the sample is inhomogeneous, both physically (multi-crystalline) and chemically (alloy, inclusions).

The sputtering process is very often compared to the break in a game of atomic billiards in which the cue ball strikes the neatly arranged pack (the atomic array of the target), scattering balls (target atoms) in all directions, including some back towards the player, *i.e.* out of the target surface. As illustrated in Fig. 3.2 [10], when an ion approaches the surface of the cathode, as described by Chapman [11], a number of phenomena may occur:

- a) The ion may be reflected, probably being neutralized in the process.
- b) The impact of the ion may cause the target to eject an electron, usually referred to as a secondary electron.
- c) The ion may become buried in the target. This is the phenomenon when the oncoming particle has very high kinetic energy. In glow discharges used in analytical chemistry, this phenomenon rarely happens.
- d) The ion impact may also be responsible for some structural rearrangements in the target material. "Rearrangements" may vary from simple vacancies (missing atoms) and interstitial (atoms out of position) to more gross lattice defects such as changes of stoichiometry (*i.e.* relative proportions) in alloy or compound targets, or to changes in electrical charge levels and distributions, and are usually collectively referred to as radiation damage.
- e) The ion impact may set up a series of collisions between atoms of the target, possibly leading to the ejection of one of these atoms. This ejection process is known as sputtering. This is the most important aspect from the point of view of analysis.

It is implied in this description of the basic interactions that the incident particle could be either an ion or a neutral atom. The ions are

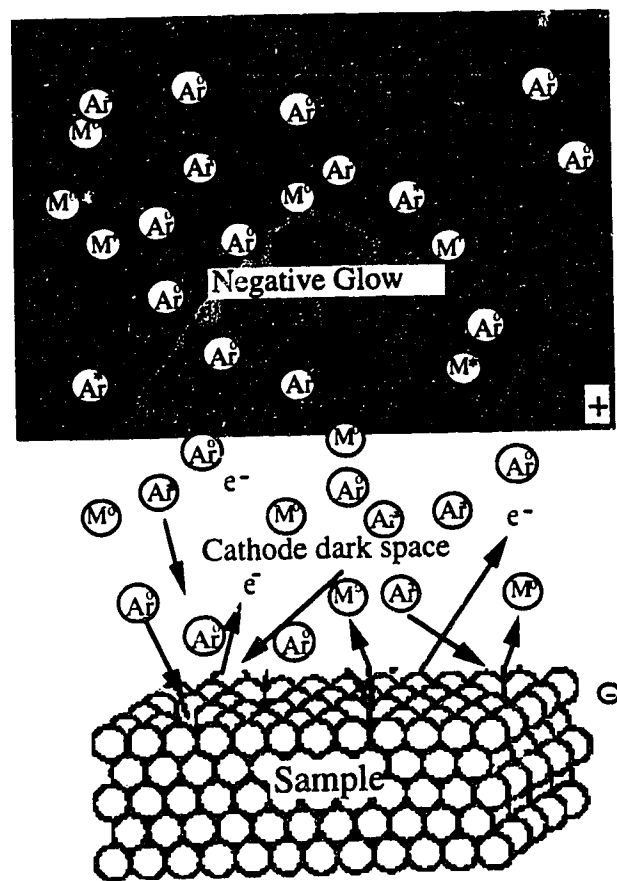


Fig. 3.2 Illustration of cathodic sputtering in a glow discharge.

likely to be neutralized by the Auger emission of an electron from the target as the ion approaches [11], so that the impacting species are actually mostly neutral.

The series of collisions in the target, generated by the primary collision at the surface, is known as a collision cascade. This cascade leads to the sputter ejection of an atom from the surface (which will require at least two collisions) or the cascade heads off into the interior of the target, gradually dissipating the energy of the primary impact, ultimately to lattice vibrations, *i.e.* heat. Therefore the sputter ejection is rather inefficient, with typically only 1% [12] of the incident energy reappearing as the energy of the sputtered atoms.

The large number of ions existing in the near-zero field within the negative glow are almost equally likely to travel in any direction. Most ions once they enter the strong field of the dark space will reach the cathode. Bodarenko [13] made a measurement of ion energy distribution in an abnormal plane cathode discharge (one in which the discharge column completely covers the cathode) and found that the majority of the  $\text{Ar}^+$  ions had energies of less than half the fall voltage, and noted a small peak of high energy  $\text{Ar}^{2+}$ .

At the potentials used in most discharges, ions will not lose energy by exciting or ionizing neutrals unless charge transfer process is available. There will be some elastic scattering, but this is not held to account for much change in ion energies. The principle factor in preventing ions from reaching the cathode with energy equal to the full accelerating voltage is considered by Little and Von [14] and other writers to be "symmetrical charge exchange". In this process a fast moving ion, and an atom of the same gas, can transfer an electron; this results in a new ion of only thermal

speed, and a fast atom which has no electrical effect. If this occurs with any frequency many ions reaching the cathode will have much less than the maximum available energy. The total effect on ion energy distribution will depend on the number of collisions, and hence the pressure and the dark space length.

The interactions in a sputtering target are sufficiently short range that only the interactions between immediate neighbors (including the incident ion) need to be considered. A binary collision is characterized by the energy transfer function [11]:  $4m_i \cdot m_t / (m_i + m_t)^2$  where  $m_i$  and  $m_t$  are the masses of particles (i - incident; t - target) involved in the collisions. A useful parameter in the discussion of cathode sputtering is the sputtering yield  $S$ , defined as the number of target atoms (or molecules) ejected per incident ion. From the binary collision model, one would expect the sputtering yield to depend on the masses of the incident ion and the target atom, and on the energy  $E$  of the incident ion. However, the sputtering process is not just a question of transferring energy to the target atoms, but also that this energy should be transferred mostly to the surface layers. We would therefore expect the sputtering yield  $S$  to be proportional to the energy deposited in a thin layer near the surface. Therefore the surface binding energy should play an important role in the ejection of the sputtered atoms. For low bombardment energies ( $E$ ) up to about 1 kV, an expression due to Sigmund [15] can be used to predict the sputtering yield  $S$ :

$$S = (3a/4p) \times (4m_i \cdot m_t / (m_i + m_t)^2) \times (E/U_0) \quad (3.1)$$

Here  $U_0$  is the surface binding energy of the material being sputtered, and  $a$  is a monotonic increasing function of  $m_t/m_i$  which has values of 0.17 for  $m_t/m_i = 0.1$ , increasing up to 1.4 for  $m_t/m_i = 10$ .

This expression for  $S$  predicts that the yield will increase linearly with  $E$ . Carter described a similar relationship between the sputtering yield and the energy in 1968 [16]. At a constant pressure, this means that the sputtering yield will increase linearly with the discharge potential. As discussed in the previous section, the incident particle energy is determined by both the discharge potential and the pressure. At high potential and low pressure, one may expect a higher sputtering yield. It is observed that when the potential increases the sputtering efficiency increases; by increasing the gas pressure, the sputtering efficiency increases as well. However, the potential has a stronger influence on sputtering than does the pressure because there is less redeposition at lower pressure.

In practice, the sputtering yield is difficult to measure. Variation of flux of the incident particles is not easily controlled or accurately calculated. Redeposition of the sputtered material back to the cathode is difficult to quantify. A portion of sputtered atoms are back-scattered by initial collisions onto the cathode surface. For most glow discharge devices, filler gas is introduced toward the cathode which impedes transport of sputtered species to the negative glow. Due to the high concentration and low kinetic energy of the sputtered atoms adjacent to the cathode surface, the majority of these atoms will diffuse back to the cathode. Furthermore, a portion of sputtered species is ejected from the cathode as positive ions, which would be returned to the cathode surface driven by the electric field and contribute to the redeposition. It has been shown that these processes combined can re-deposit up to 90% of the sputtered atoms onto the surface of the cathode for a 0.1 torr discharge sustained between parallel electrodes [17]. Therefore, the relationship between discharge current and voltage at a given source pressure in a glow discharge device, along with the effects of

redeposition, determine the rate of cathodic sputtering. The rate of loss of material depends on electrical discharge parameters such as the value of the abnormal cathode fall, current density, and on other factors such as the material of the cathode and the mass of the impinging positive ions, and the temperature of the gas and the cathode. It is also influenced by chemical reactions. The cathode material nature should be one of the most important factors due to the surface bonding energy and the relative atom mass ratio to the bombarding particles. The rate of sputtering also appears to increase with the mass of the incident positive ion. Experience shows that with pure helium as the sputtering gas and a brass cathode, a long sputtering time is required to have a detectable loss. One would expect the over all sputter rate of a material to increase proportionally to the sputtering current for a given cathode material.

### 3.3.2 Some Sputtering Measurements

#### 3.3.2.1 Differential Sputtering

To demonstrate the different sputtering efficiencies for different materials under identical discharge conditions, the following experiment was carried out. A piece of pure cadmium metal was tightly inlaid into a larger piece of aluminum. The surface of the piece was ground to a smooth finish without any space between the two metals. This piece of binary metal was machined to a suitable size for a cathode and put onto a Grimm type glow discharge unit in a way that part of the sputtering spot was on the cadmium and the rest on the aluminum. The sputtering was carried out under a discharge potential of 900 V and 15 mA current for 30 minutes including the pre-burning period. The surface was unevenly eroded as

shown in the photograph [Fig. 3.3], the cadmium side is twice as deep as the aluminum side. The difference may be explained by the surface binding energy of the material. Wehner and Anderson [18] related the threshold energy of sputtering to the heat of sublimation of the target material. The atomic mass and radii may also play a role as well.

### 3.2.2.2 Sputtering Rate Measurement

Considering that the sputtering rate may be different in the pre-burning period from the rest of the burn, two methods could be used to correct this problem. One approach is to subtract the preburning time from each sputtering operation (the end of preburn could be monitored from the emission spectrum), and the weight loss of the sample is subtracted from the total loss as well. Each time the difference is used to calculate the loss rate. The second approach is to use a slope method. Assume the preburning time is  $t_0$  and the sample weight loss is  $m_0$  in this period. In a sputtering period of  $t$ , the sample weight loss is  $m$ . Then the loss rate of sputtering will be

$$S = (m - m_0) / (t - t_0) \quad (3.2)$$

Rearranging this equation, one can get:

$$m = S t - S t_0 + m_0 \quad (3.3)$$

Further assuming  $S$  is constant at a given set of operation conditions, the equation can be simplified as

$$m = S t + C \quad (3.4)$$

where  $C$  is a constant. A plot of the mass loss ( $m$ ) against sputtering time ( $t$ ) will generate a linear curve, with the slope as the mass loss rate. In this study, the second approach was used.

The sputtering efficiency for our working conditions was measured





Fig. 3.3 A photograph showing a differential sputtering.  
top: cadmium; bottom: aluminum.

by weighing a sample before and after a given period of sputtering time with argon as sputtering gas and brass as the sample. At 15 mA discharging current, the sample loss rate was 0.807 mg/min [Fig. 3.4]. At a 55 mA discharge current, the sample loss rate was 2.08 mg/min [Fig. 3.5]. The loss rate increased with an increase of the discharge current at a given discharge potential. However, it fell short of being directly proportional to the discharge current. The loss rate at higher current is lower than that predicted by the linear relationship between the current density and the sputtering yield [8]. The reason for this may be the fact that at a given discharge potential, the increased current was realized by increasing the gas pressure. The short cathode dark space and the high density of the sputtered material atoms adjacent to the cathode surface likely enhanced the redeposition back to the sample. As shown in Figs. 3.4 and 3.5, the relationship of the mass loss and the sputtering time is fairly linear and the intercept of the curve with the time axis is close to zero. This may be an indication that the loss rate in the pre-burning period is not significantly different from that during the rest of the sputtering time, or the pre-burning period really needed may actually be very short.

### **3.4 Species Number Densities**

#### **3.4.1 Sputtered Atoms**

The redeposition of the sputtered atoms in a glow discharge source makes it impossible to compare the atomic sputtering rate from the solid surface with the density of atoms in the plasma. The density of sputtered atoms in the plasma source is usually obtained by measuring the absorption of radiation from a hollow cathode source and computing the

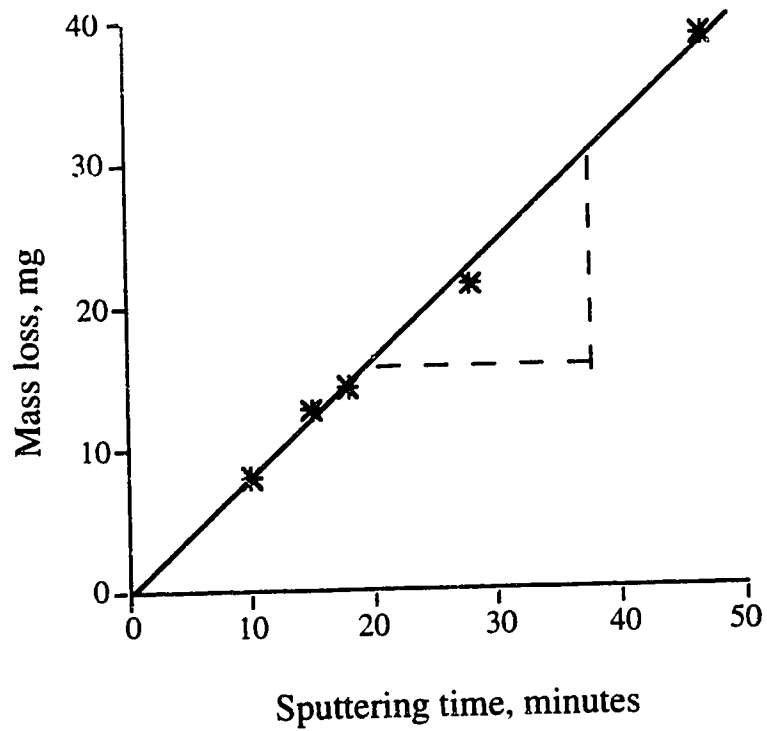


Fig. 3.4 Plot showing the mass loss of a brass sample in different sputtering time. 15 mA, 1200 V; Sputtering diameter: 7.0 mm

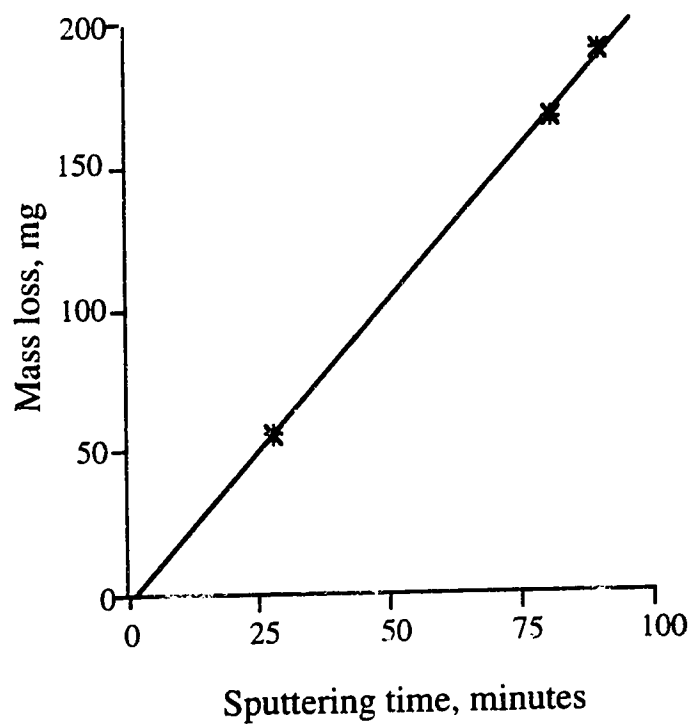


Fig. 3.5 Plot showing the mass loss of a brass sample in different sputtering time. 55 mA, 1000 V; Sputtering diameter: 7.0 mm

optical density, taking the measured line profiles of the emission source and the absorbing medium into account [19]. A linear increase in the density with the current was found for single element sample and alloy samples [8]. The voltage also influences the atom density, as a result of the fact that the sputtering rate of a metal depends on the energy of the bombarding species which increases with voltage. It was found that the atom density is at a maximum between 1 and 1.5 mm from the cathode surface [19]. This is attributed to sputtering of material from the cathode as atomic clusters which, on leaving the cathode, are then dissociated by electron, atom and ion collisions. The actual atomic number density also depends on operating conditions such as the gas flow rate into the discharge unit.

#### 3.4.2 Metastables

It is generally recognized by spectroscopists that metastable rare gas atoms may play an important role in excitation in weakly ionized plasmas such as the glow discharge and inductively coupled plasma. To assess such effects in the glow discharge attempts have been made to measure the concentration of metastable argon atoms. The concentration of metastables was determined by Ferreria *et al* utilizing absorbance measurements [20]. In their studies, the Ar(I) 696.5 nm transition was chosen. A non-uniform distribution of metastables was obtained, decreasing from a maximum at the cathode surface to a minimum at ~1.5 mm from the cathode, and rising again to a broad maximum at 4-6 mm. Carefully studying their data, one can find the following trends: The maximum metastable population exists at the cathode surface, with a steep decline throughout the cathode dark space. In all cases, there is a second maximum at a distance just beyond the interface of the cathode dark space and the negative glow. The magnitude

and the distance from the cathode surface of the second maximum is dependent on the pressure, current and, in turn, the discharge potential. The maximum is higher with a higher discharge current regardless of the way the higher current is achieved. At a given current, however, the second maximum appears closer to the cathode surface when the pressure is higher. This corresponds to the interface of the cathode dark space and the negative glow. At a given current, there is a larger population of metastables with a higher pressure and low potential. Doughty and Lawler [21] presented similar profiles when they measured the metastable densities in a helium glow discharge. Winchester and Marcus [22] presented an almost identical plot by using a diode geometry device. Such a distribution was explained by the authors in the following way: The high density of metastable atoms at the cathode surface is the result of neutralizing collisions of the sputtering argon ions and the secondary electrons at the surface. The metastable atoms formed there may transfer into the bulk of the plasma by diffusion, or redeposit onto the cathode surface, thus results a minimum within the cathode dark space. The correlation between the second maximum and the interface of the cathode dark space and the negative glow corresponds to the region of the discharge where secondary electrons have lost sufficient energy to depopulate the metastable levels. The decrease in metastable atom densities at farther distances reflects the lower-energy electron distributions in the negative glow. (However, I personally think that there is another possible explanation to this profile: The metastable formation is mainly an ion-electron recombination process. This process requires that the electron energy be low to be efficient. At the cathode surface, the electrons have not been accelerated by the cathode fall yet. The cross section of the recombination should be fairly large. One

could expect a maximum in the metastable population at the surface. This is the origin of the cathode glow. In the cathode dark space, the electrons have been gradually accelerated by the cathode fall, the cross section of the recombination becomes smaller, the metastable population has a minimum at this point. However, as the electrons acquire more kinetic energy, the gas ionization by electron impact become more and more intense. That is why there is not much light emission in this region. Further from the cathode surface, some of the electrons lose most their energy by inelastic collisions with the gas atoms, at the same time, the number of electrons and ion number increases because of the multiplication process. With a large number of low energy electrons, together with a large population of gas ions, the ion-electron recombination becomes efficient again, and thus the second maximum appears. Corresponding to this maximum, there should be intense emission from this region, and that is observed in practice.)

### 3.4.3 Electrons

In the voltage range in which most glow discharges operate, the secondary electron emission coefficient, is on the order of 0.1 electron per ion for argon ion bombardment [11].

Ferreira *et al.* [23] determined the electron density as a function of distance from the cathode using a side view device, by measuring the Stark broadening of the He 447.1 nm line, when helium was added to the argon carrier gas. From the knowledge of the gas temperature, the Lorentzian-Stark width of the line was deconvoluted from the measured line width, which was a convolution of the Doppler and Stark widths. Three electron groups are believed to exist in the negative glow (NG) region of a glow discharge according to literature [24]: Group I is the secondary electrons

emitted from the cathode surface, which gain kinetic energy through the cathode dark space (CDS) and attain an electron temperature ( $T_e$ ) of 20 - 25 eV (so-called fast or primary electrons) and a number of density on the order of  $10^6 \text{ cm}^{-3}$ ; group II is the secondary electrons generated by gas-phase ionization collisions with electron temperatures of  $\sim 2-10 \text{ eV}$  and number densities in the range of  $10^7-10^8 \text{ cm}^{-3}$ ; and group III (ultimate or slow electrons) are the electrons from either group I or group II that have experienced several elastic and inelastic collisions with particles in the plasma and thus have an electron temperature of only 0.05-0.6 eV, having densities in the range of  $10^9-10^{11} \text{ cm}^{-3}$  [25].

Electron energy and density in a glow discharge measured by optical methods are often inconsistent. The reasons are that the glow discharge plasma is not at thermal equilibrium or even local thermal equilibrium, and the number density of electrons in a glow discharge are usually low. The  $H\beta$  broadening method generate abnormally large numbers when electron densities are low. Langmuir probe techniques [26-28] are considered the best way to measure localized electron temperature, electron number density, average electron energy and the electron energy distribution. These authors [26-28] have found that the electron number density is proportional to the discharge current, while the axial density distribution in the NG region is fairly constant up to 13 mm from the cathode surface. The authors also claimed that the densities of gas phase ions (discharge gas and sputtered species) are two to five fold larger than the electron populations. Some of the results obtained by different authors are summarized in Table 3.1.

### 3.5 Spectrophysical Parameters



Table 3.1 Some fundamental parameters in glow discharge

Value	Device	Method	Ref.
<b>Electron number density (<math>10^{12} \text{ cm}^{-3}</math>)</b>			
0.25 - 0.35	Flat-Cathode	L - probe	[26, 28]
2.2 - 8.2	(He + Hg) Al, 8 mA	L - probe	[1]
130 - 320	Grimm type	Stark broadening	[23]
16 - 102	Grimm, 20 - 30 mA	H $\beta$ broadening	[29]
<b>Ion number density (<math>10^{11} \text{ cm}^{-3}</math>)</b>			
3.7 - 6.2			[26]
<b>Gas temperature, K</b>			
1000 - 1500		Doppler	[23]
420 - 1170			
<b>Electron temperature, eV</b>			
0.25 - 0.30	Flat Cathode	L - probe	[26, 28]
0.05 - 0.07	(He + Hg) Al, 8 mA	L - probe	[1]
0.07 - 0.11	Grimm 40 - 80 mA	Doppler	[23]
0.83 - 2.24	Hollow cathode	L - probe	[30]

### 3.5.1 Gas temperature

The gas temperature in a glow discharge is defined as the kinetic energy of the gas molecules. The first measurements [31] of gas kinetic temperature in a glow discharge were made on a commercial glow discharge source using the Doppler broadening method. A maximum value of metal temperature was found some distance from the cathode. It was qualitatively explained on the grounds that the atoms near to the cathode had directional velocity normal to the cathode, as a result of the mechanical sputtering process. This leads to a Doppler narrowing when viewed perpendicularly to the direction of motion.

Ferreira *et al.* [23] found that at 2 mm from the surface the temperature values measured with argon and metal are approximately equal. Under 800V, 60 mA discharge conditions, the temperature value was close to 1500 K, a similar value to that obtained in the study by West *et al.* [31]. The increase of temperature with discharge current is clearly shown in these studies.

In our study, the discharge current was significantly lower than they used. It is reasonable to assume that the gas temperature is not higher than 1500 K.

### 3.5.2 Electron Temperature

Quite a few authors have measured the electron temperature in low pressure discharges. Some of the results are also shown in Table 3.1. Differences in temperatures are dependent on the measurement method. Most of them are based on the assumption that the electrons' behavior obeys the Maxwellian distribution. The calculations used in the data interpretation are based on an accurate knowledge of the electron number

density which is usually estimated or measured based on a local thermal equilibrium model. Nevertheless, the common conclusion of these measurements is that the electron temperature in the Grimm type glow discharge under normal analytical conditions is significantly lower than 0.3 eV. This is considered a low temperature compared to the electron temperature found in, say, an inductively-coupled plasma which is about 0.7 eV. Fang and Marcus showed that the electron temperature is not affected very much by the discharging current, while the electron average energy increases with the increase of the discharge current [28]. It seems to me that the electron energy is a more accurate term to describe the behavior of the electrons in the glow discharge, as its measurement can be accomplished without the assumption of thermal equilibrium.

Fang and Marcus [28] compared the measured electron energy distribution with the Maxwell-Boltzmann distribution with an average energy of 0.832 eV, and found that in the negative glow of the glow discharge plasma, there is an obvious depletion of high energy electrons. The electron temperature obtained by the authors based on Maxwell-Boltzmann distribution is 0.287 eV (or 2200 K), at 3 torr and 21 mA current, 700 V. The number density of the electrons and the electron energy distribution is not sensitive to the distance from the cathode surface up to 13 mm. Average electron energy is higher in a low pressure plasma than in a higher pressure one at a given current (fixed current, low pressure needs high voltage). They concluded that in the negative glow there are very few electrons with energies greater than 4 eV. The slow electrons do not play significant roles in maintaining the discharge, either through electron impact or Penning ionization, but are utilized primarily for electronic excitation. The average electron energy is reported to be

about 0.9 eV with a very small portion beyond 2 eV. From the diagram shown in the work of Marcus and Fang [26], at a given gas pressure, the average electron energy increases with the potential in the region which is far from the cathode surface. While at a given current, the average electron energy decreases with the pressure. Borodin and co-workers [32] studied a hollow cathode discharge and found that a high energy group, with the energy larger than 25 eV, indeed exist with a large number centered around the cathode fall potential. These would be electrons formed at the cathode surface that had not experienced inelastic collision as they traversed the NG from side to side.

### 3.5.3 Excitation temperature

One of the most commonly measured plasma parameters in diagnostic studies is the excitation temperature ( $T_{exc}$ ).  $T_{exc}$  describes the distribution of an analyte species among its electronic energy levels and is useful in describing the condition of the plasma as an emission source which is in thermal equilibrium or local thermal equilibrium.  $T_{exc}$  is described by the Boltzmann distribution:

$$N_p = N_a [g_p / Z_a(T)] \exp(-E_p / k T_{exc}) \quad (3.7)$$

Where  $N_p$  is the concentration of atoms (or ions) in energy level  $p$ ,  $N_a$  is the total concentration of atom (or ion)  $a$ ,  $g_p$  is the statistical weight of level  $p$ ,  $Z_a(T)$  is the partition function of the atom (or ion)  $a$ ,  $E_p$  is the excitation energy of level  $p$ , and  $k$  is the Boltzmann constant. The absolute intensity of a spectral line emitted in the transition from state  $p$  to state  $q$  is

proportional to the number population of that emitting species in the p state, which can be expressed as  $I_{pq}$ :

$$I_{pq} = (4\pi) A_{pq} N_p h\nu_{pq} \quad (3.8)$$

where  $l$  is the thickness of the radiation source,  $A_{pq}$  is the Einstein's transition probability from state p to state q,  $h$  is the Planck's constant and  $\nu_{pq}$  is the frequency emitted by the transition from the state p to q.

Combining Equation 3.8 and 3.9 and making the necessary rearrangements, results in a linear function between the  $\log(I_{pq}\lambda_{pq}/g_p A_{pq})$  and the excitation energy  $E_p$ .

$$\log(I_{pq}\lambda_{pq}/g_p A_{pq}) = \log(N_a hc/4\pi Z_a(T)) + (-E_p/2.303kT(\text{exc})) \quad (3.9)$$

According to Equation 3.9, the excitation temperature ( $T(\text{exc})$ ) can be calculated from the slope of the plot of  $\log(I_{pq}\lambda_{pq}/g_p A_{pq})$  against  $E_p$ . In a Grimm-type glow discharge, excitation temperatures lower than 3000 and higher than 10000 K are reported [33], depending on the lines used in the measurement.

### 3.5.4 Ionization temperature

The measurement of the ionization temperature in a plasma is often done using the Saha equation method, which needs again a knowledge of the electron number density and the relative emission intensity of atom lines and ion lines from the same element. However, the validation of this method is based on the assumption that both the ion lines and atom lines are excited by the same mechanism. The other requirement for the use of this

equation is that the ionization and the excitation of these species be thermal in nature, which is doubtful in the low pressure glow discharge. This critical parameter in other thermal emission sources is less important (if not meaningless) in a glow discharge.

### 3.6 Not All Lines Are Created Equally

The inconsistency in the excitation temperatures reported for the glow discharge in the literature reflect a fact that not all lines are created (*i.e.* excited thermally) equally. Studies on the effect of discharge operation parameters on spectral intensities may reveal some of the mechanisms which governing the excitation and the ionization of the analyte atoms in the glow discharge.

#### 3.6.1 The effect of filler gas - a mixed gas study

It is well known that the sample spectral intensity is affected by the nature of the support gas under similar operating conditions. This is true in ICP and glow discharges. In ICP emission spectrometry, people attribute the effects to the different temperature of the source, which in turn influences the extent of vaporization, atomization, excitation and ionization. In glow discharges, the situation is more complicated. In addition to temperature effects, the sputtering rate is also altered. Another aspect is the nature of this technique. As mentioned in section 3.1, among the three parameters- pressure, voltage and current, only two can be independently varied. The third parameter varies according to the setting of the other two. Because different filler gases have different ionization potentials, at the same pressure and voltage, one can not get the same current. In other

words, it is not possible to make all the operation conditions identical in order to compare spectral intensities. In analytical practice, people usually chose the optimum operating conditions for the discharge gas they are using. Among all the gases available to us, argon is the first choice because of its high sputtering efficiency. Helium is another often used gas because of its high ionization potential.

In one study conducted earlier in this work, a mixture of argon and helium at different ratios was used to see the effect on the emission intensity of the analyte from a brass cathode. Ar and He at different ratios were introduced into a pin-type glow discharge unit with a brass sample. The detection system was the computer controlled PDA spectrometer. The description of this device was given in Chapter 2. The sample was machined as a pin, 3 mm in diameter and about 15 mm long. Gas mixing was controlled by two separate needle valves connected to an argon gas tank and a helium gas tank respectively. The discharge potential was adjusted to keep the current constant at 10 mA when helium was introduced. The integration time was 10 seconds for each of the spectra obtained.

Variation of signal intensity for some lines is shown in Fig. 3.6. In pure Ar, the CuI (neutral atom) lines are more intense than the CuII (ion lines) and ZnII lines. With an increasing amount of He in the filler gas the ion lines grew in intensity relative to the neutral atom lines. Take the 239.263 nm copper atom line and the 254.480 nm copper ion line as an example. At 0% helium, the intensity of the copper ion line is barely measurable. It is lower than one percent of the atom line. With an increase in the percentage of the helium in the filler gas, this ion line gets stronger and stronger, while the atom line gets weaker and weaker. Eventually at

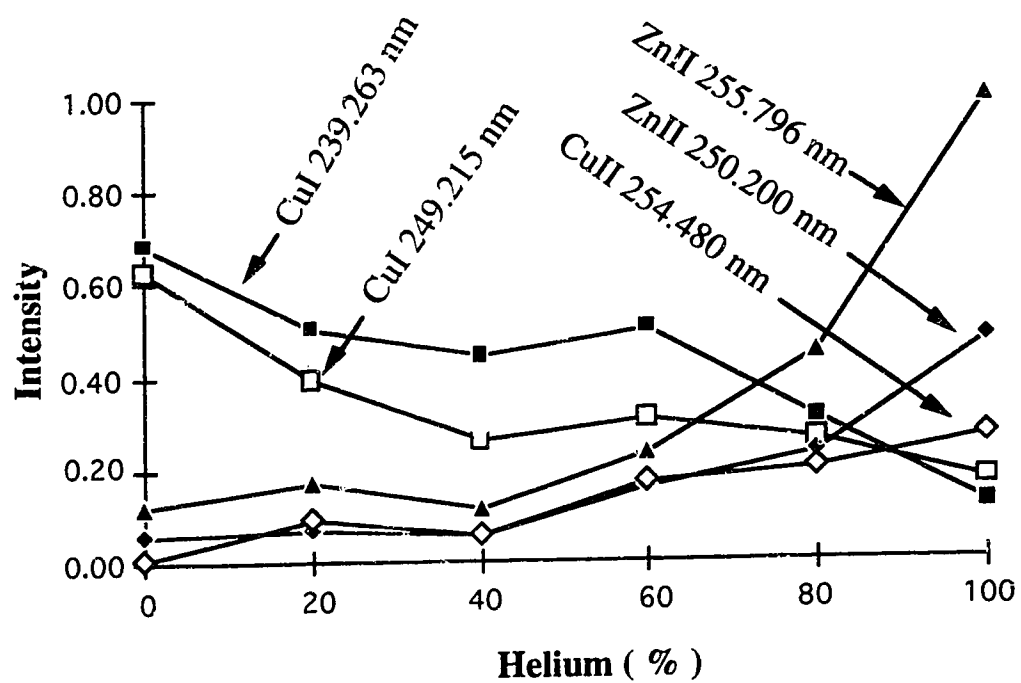


Fig. 3.6 Signal variation with helium content in the filler gas.

Filler gas: Ar-He mixture, Sample: Brass. 10 mA.



100% helium, the ion line became stronger than the atom line. The increase in the intensity of the two zinc ion lines 250.200 and 255.796 nm with the percentage of the helium is even more dramatic. Because all the ion line transitions have higher excitation energies [34], it is easy to make the simple conclusion that the helium discharge has a higher excitation temperature. However, further studies do not support this argument as will be detailed in the following chapters.

### 3.6.2 The effect of pressure and potential

The effect of pressure and potential on the discharge current was discussed in the first section of this chapter and it was demonstrated that variations of potential and pressure have a similar effect on the discharge current [Fig. 3.1]. If the intensities of the analyte signals were solely determined by the discharge current, then they would show similar intensities as long as the discharge current was kept constant, or the signals would behavior similarly when the current was varied. Experiments have shown that this is not the case. On one hand the intensities of different lines show different variation when the current changes. On the other hand, at constant current, the signals vary according to the pressure and the voltage. The data for Fig. 3.7 were obtained at a constant discharge current of 6.0 mA and the plots show the line intensities vs. voltage. Note that the pressure had to be lowered to keep the current constant when the voltage was increased. In Fig. 3.8 the plots are for line intensities versus pressure at 6.0 mA current. Similarly, the voltage has to be decreased to keep the current constant when the pressure was increased. All six copper lines showed a maximum in intensity at 600 V and 1650 millitorr. A possible explanation is that as the voltage is increased, the pressure becomes too low

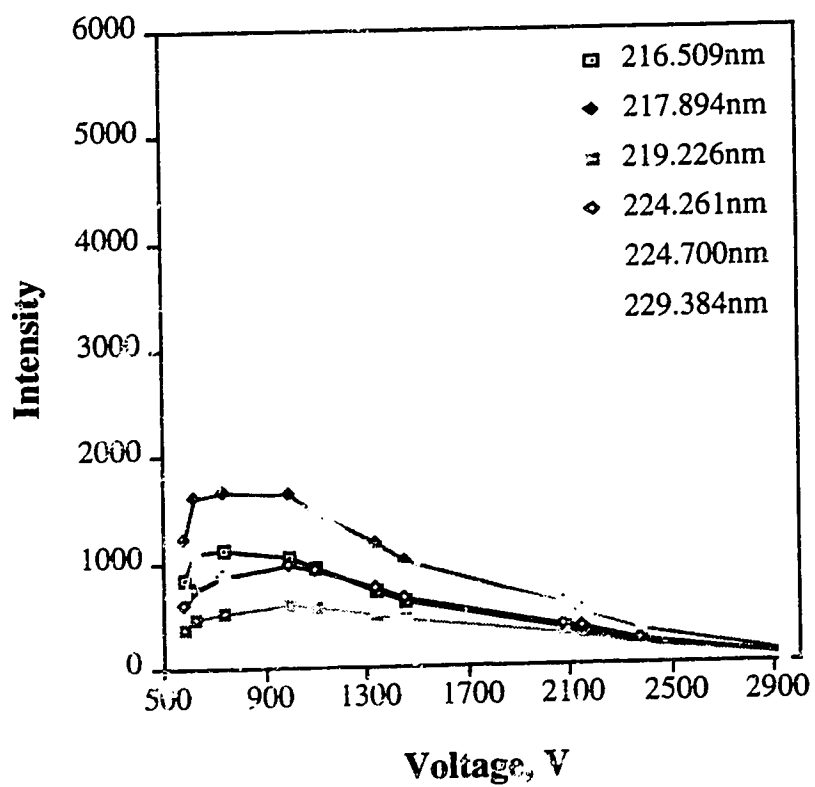


Fig. 3.7 Signal variation when the voltage is increased at constant current, 6.0 mA.

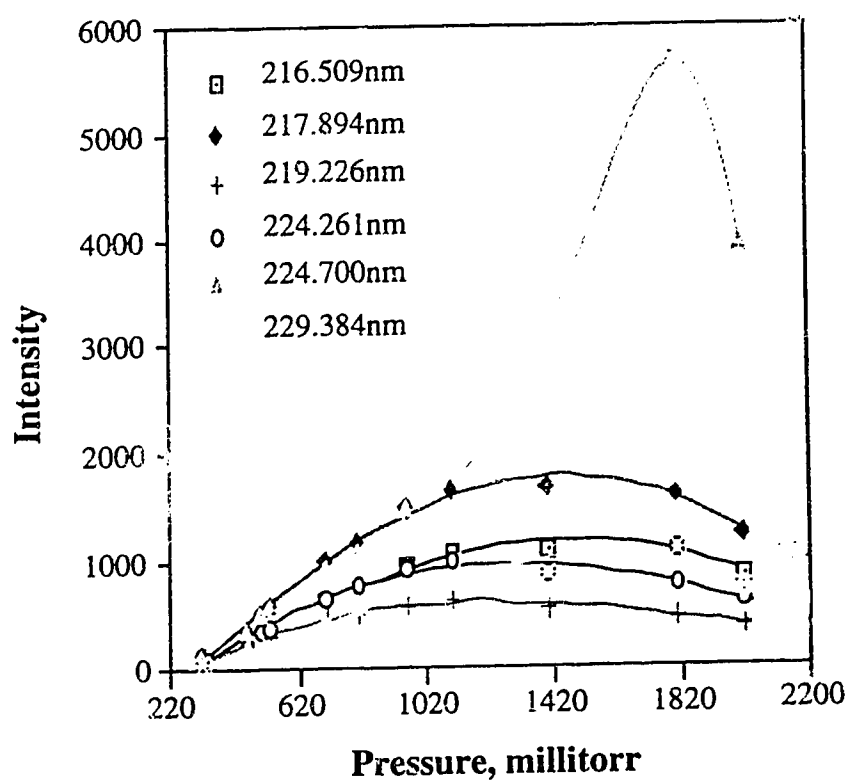


Fig. 3.8 Signal variation when the pressure is increased at constant current, 6.0 mA.

to be efficient on cathodic sputtering and/or excitation; increasing pressure makes the voltage too low to be efficient for cathodic sputtering and/or ionization. Other authors [35] have also found similar maxima. Among the six lines there are five copper atom lines. All of their intensities showed a similar variation. The other line is the 224.700 nm copper ion line. It obviously varies differently from the other five. This may suggest a different excitation process. Whether other ion lines show a similar variation or not would have to be further investigated.

Fig. 3.9 contains the plots showing the variation of the signal when the current is changed by different means. Signals in (a) were obtained when the current was increased by changing the voltage and keeping the pressure constant at 1600 millitorr, while in (b) the current was increased by changing the pressure and keeping the voltage at 800 V. It is obvious that the behavior of the signals depends on how the current is increased. When the voltage was increased (a), all the lines showed a maximum in intensities at around 15 mA, while when the pressure was increased, all the lines became more and more intense. Changes in voltage or pressure, will certainly alter the character of the discharge plasma. The relative contribution of each excitation - ionization processes will also altered as a consequence. Further studies on the excitation processes may give an explanation to the observed signal behavior, and this will be commented again at the end of Chapter 5.

### 3.6.3 Configuration

The configuration of the glow discharge device and even the cathode alone has some influence on the signal intensity and the relative intensities

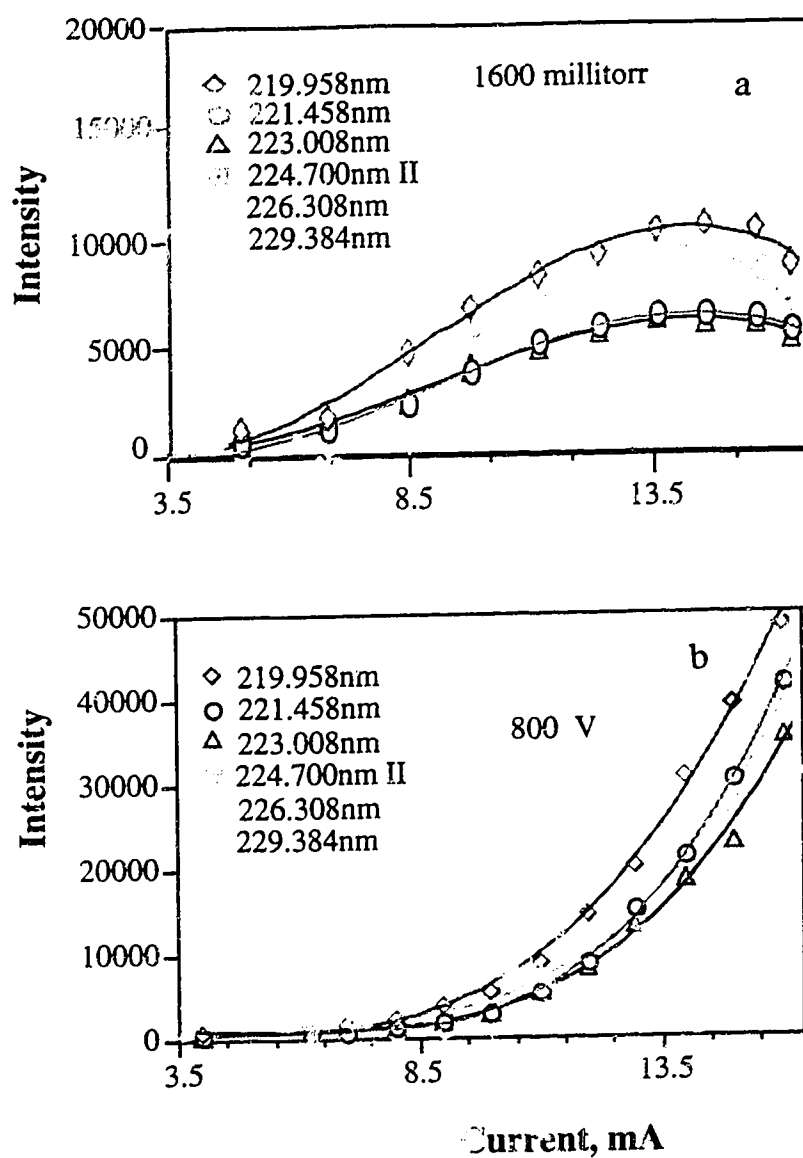


Fig. 3.9 Signal variation following the discharge current by changing voltage (a) and pressure (b).

among different lines. Experiment shows that for overall intensity at the same operation conditions, the hollow cathode glow discharge generates the highest radiation, following by the Grimm-type and then the pin-type. The spectra of brass in He discharge shown in Fig. 3.10 demonstrate the signal differences from our pin-type and Grimm-type discharge sources. While some variation in the relative intensities is observed, the overall picture is similar. Thus, similar conclusion should be reached about excitations using either source.

### 3.7 The Excitation Temperature Paradox

A common measure of the excitation power of a radiation source is the excitation temperature,  $T_{exc}$ , typically determined by the Boltzmann method mentioned above. If a source is not in thermal equilibrium, such a temperature, while it can be measured, may have little real meaning and may be seriously misleading. However, in the knowledge of the existence of this limitation, it is useful to measure the  $T_{exc}$  of a source, particularly for both a set of neutral atom (I) and ion (II) lines. The values obtained for  $(T_{exc})_I$  and  $(T_{exc})_{II}$  and the manner in which they deviate from each other can provide clues as to the true excitation character of the source.

The temperature measurements were carried out using pure iron as the sample and three different gases - argon, neon and helium as filler gases. The Fourier transform system was used for the spectral measurements. The operating conditions were listed in Table 3.2. The UV spectra obtained are shown in Fig. 3.11a for argon, b for neon and c for helium. These spectra were used to obtain the intensities of FeII lines for the measurement of  $(T_{exc})_{II}$ . Visible region spectra were also acquired for

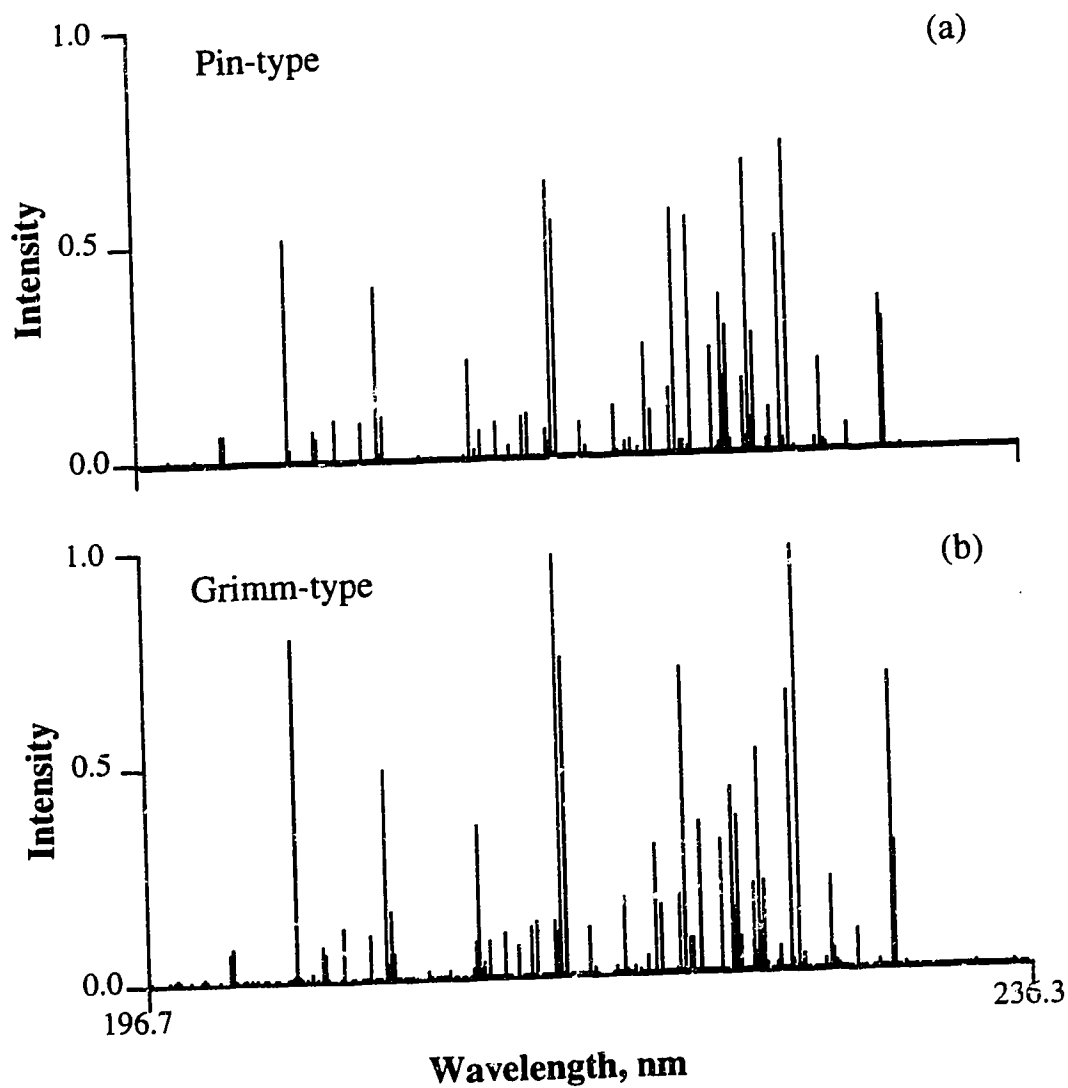


Fig. 3.10 Comparison of partial brass spectra in helium obtained from a pin-type and a Grimm-type glow discharge unit.

Table 3.2 Operating parameters for the temperature measurement

Filler gas	Pressure, torr	Current, mA	Voltage, V
argon	3.7 - 3.9	14	750
neon	5.0	12	1100
helium	11.0	10	1800



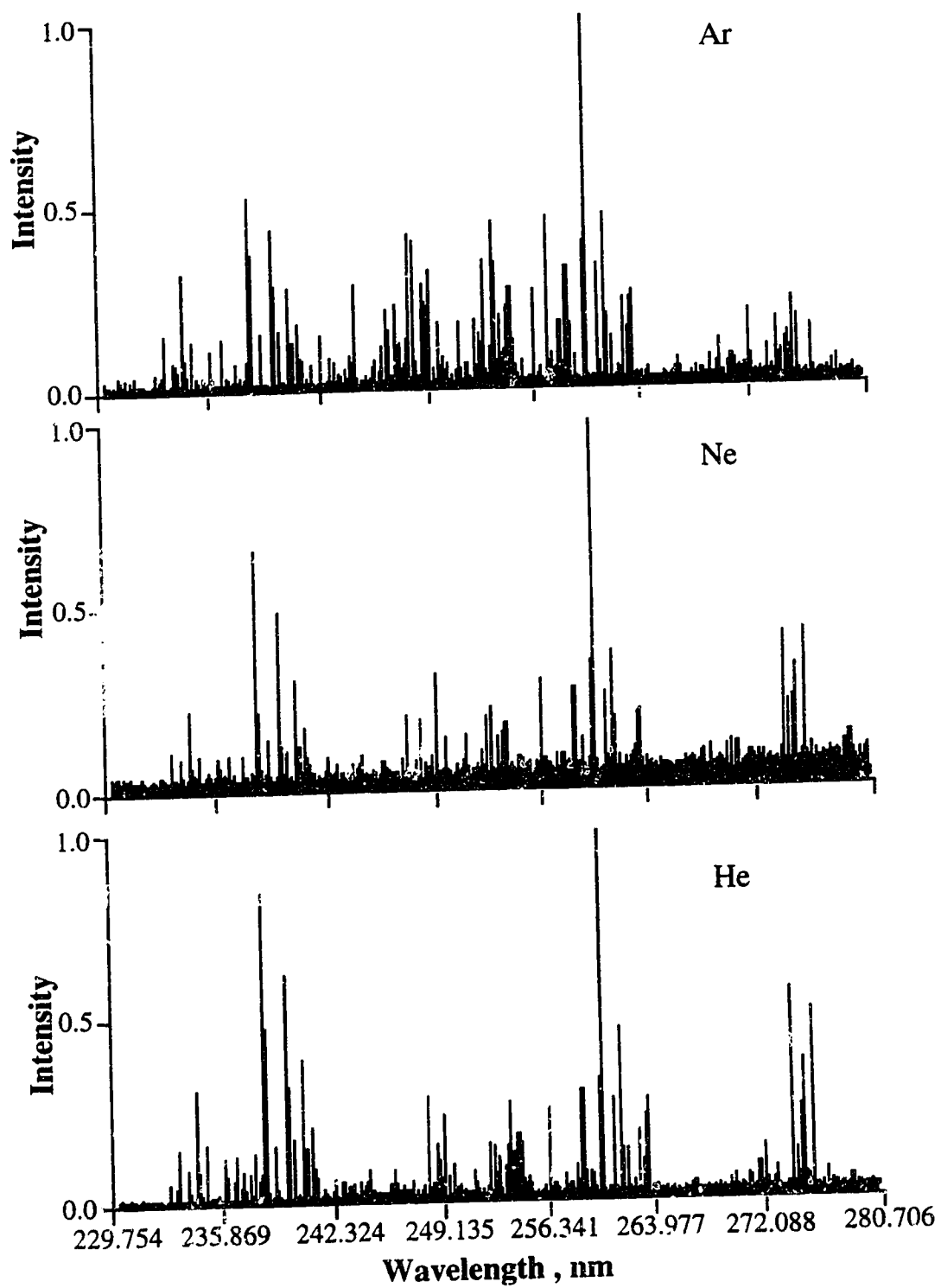


Fig. 3.11 Partial Fe UV spectra from glow discharge emission.

the measurement of the FeI lines. The lines used in the Boltzmann plot and their excitation energies along with their transition probabilities are listed in Table 3.3. An example plot is shown in Fig. 3.12 for neutral atoms, and Fig. 3.13 for ions of iron. From the plots, the excitation temperatures based on iron neutral atoms were 3560 K for argon, 3550 K for neon and 3910 K for helium. The excitation temperatures based on iron ions were 13200 K, 12800 K and 11400 K for argon, neon and helium respectively.

The temperature obtained from the ion lines is about three times that obtained from the neutral atom lines. This is a clear indication of non-thermal excitation behavior and that a single "temperature" can not be assigned to the glow discharge. The fact that the ion line temperature is so high, also is indicative of the presence of excitation mechanisms favoring the population of energetic ionic levels.

Using the same sets of Fe lines, excitation temperatures were obtained for the ICP. The spectral data and Boltzmann plots are shown in Figs. 3.14 and 3.15. The neutral atom temperature obtained was 6100 K and that using the ion lines was 7700 K. These results are typical for an ICP, with the two values in rough agreement and  $(T_{exc})_{II}$  a little greater than  $(T_{exc})_{I}$ .

It is interesting to note that the atom line temperature for the glow discharge is about half that of the ICP, while the ion line temperature is about twice that of ICP. Boltzmann temperatures, in non-thermal situations can be very dependent on the nature of the lines used to construct the plot. For example, the neutral atom lines (Table 3.3) are all of relatively low excitation energy. The above temperature results imply that relative to the ICP, the neutral atom levels are underpopulated and the ionic levels are overpopulated. The ICP is generally close to local thermodynamic

Table 3.3 Iron lines used in the excitation temperature measurement

Wavelength, nm	Type	Exc. energy, $\text{cm}^{-1}$	$gA$ , ( $10^8 \text{ s}^{-1}$ ) [35]
258.588	II	38626	6.44
261.187	II	38626	8.71
260.709	II	39030	6.63
275.574	II	44190	21.1
273.955	II	44432	15.4
271.441	II	44755	3.86
266.466	II	64834	26.5
266.663	II	65076	24.1
385.991	I	25885	0.796
371.994	I	26853	1.79
382.043	I	33062	6.16
361.876	I	35642	5.09
360.886	I	35884	4.16
381.584	I	38142	8.15

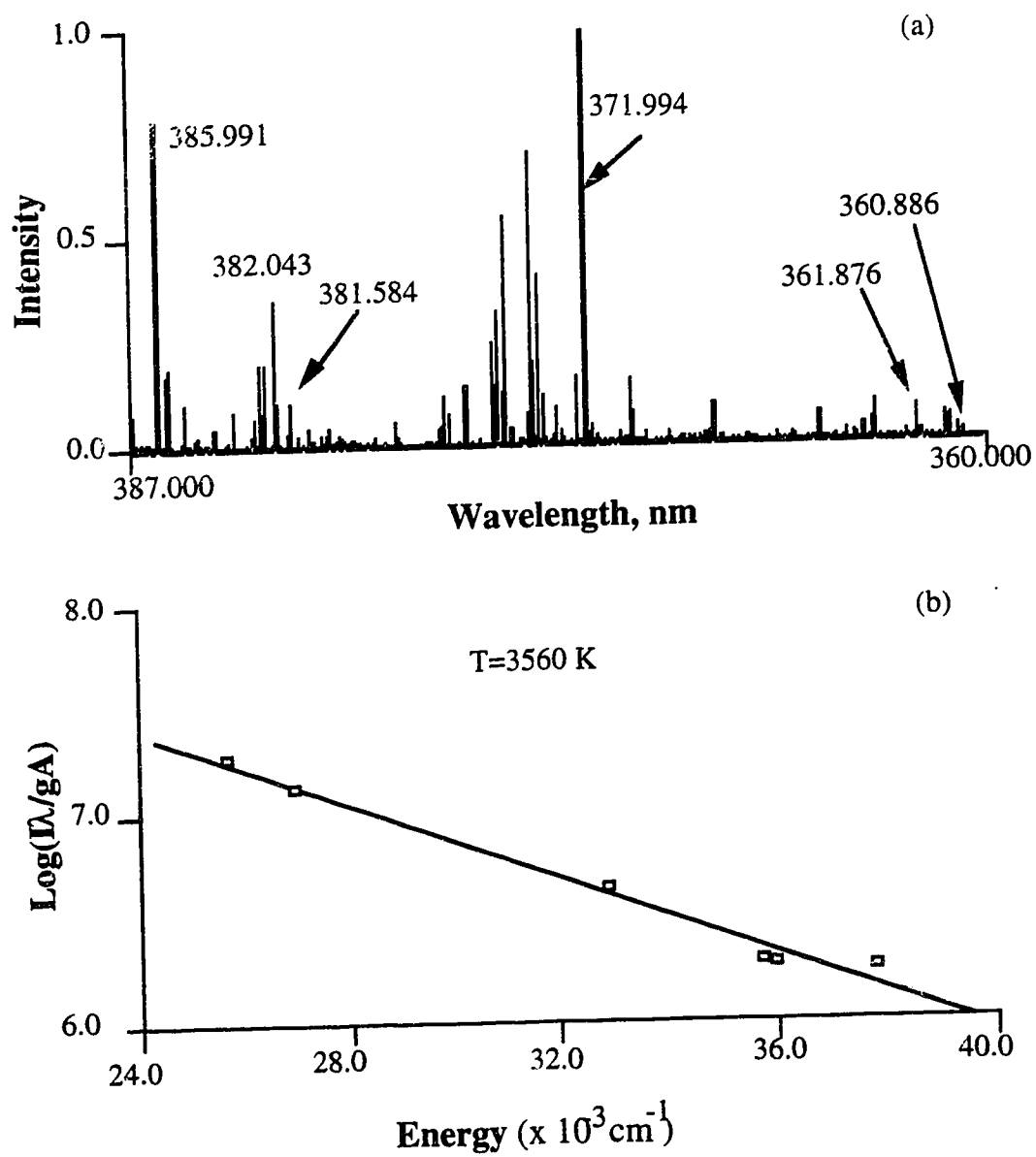


Fig. 3.12 Partial visible spectrum from Fe-Ar glow discharge and the Boltzmann plot.

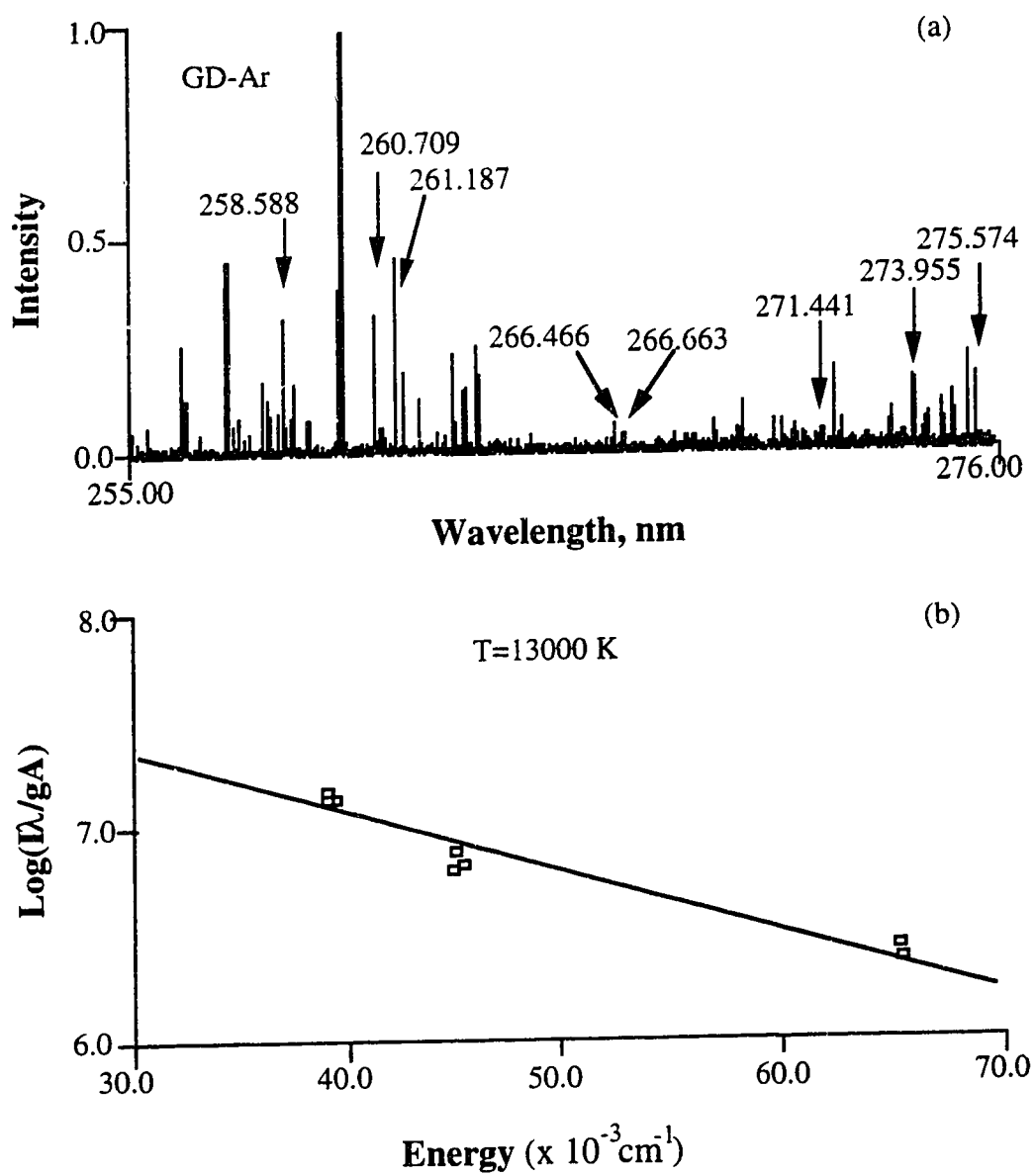


Fig. 3.13 Partial UV spectrum from Fe-Ar glow discharge and the Boltzmann plot.

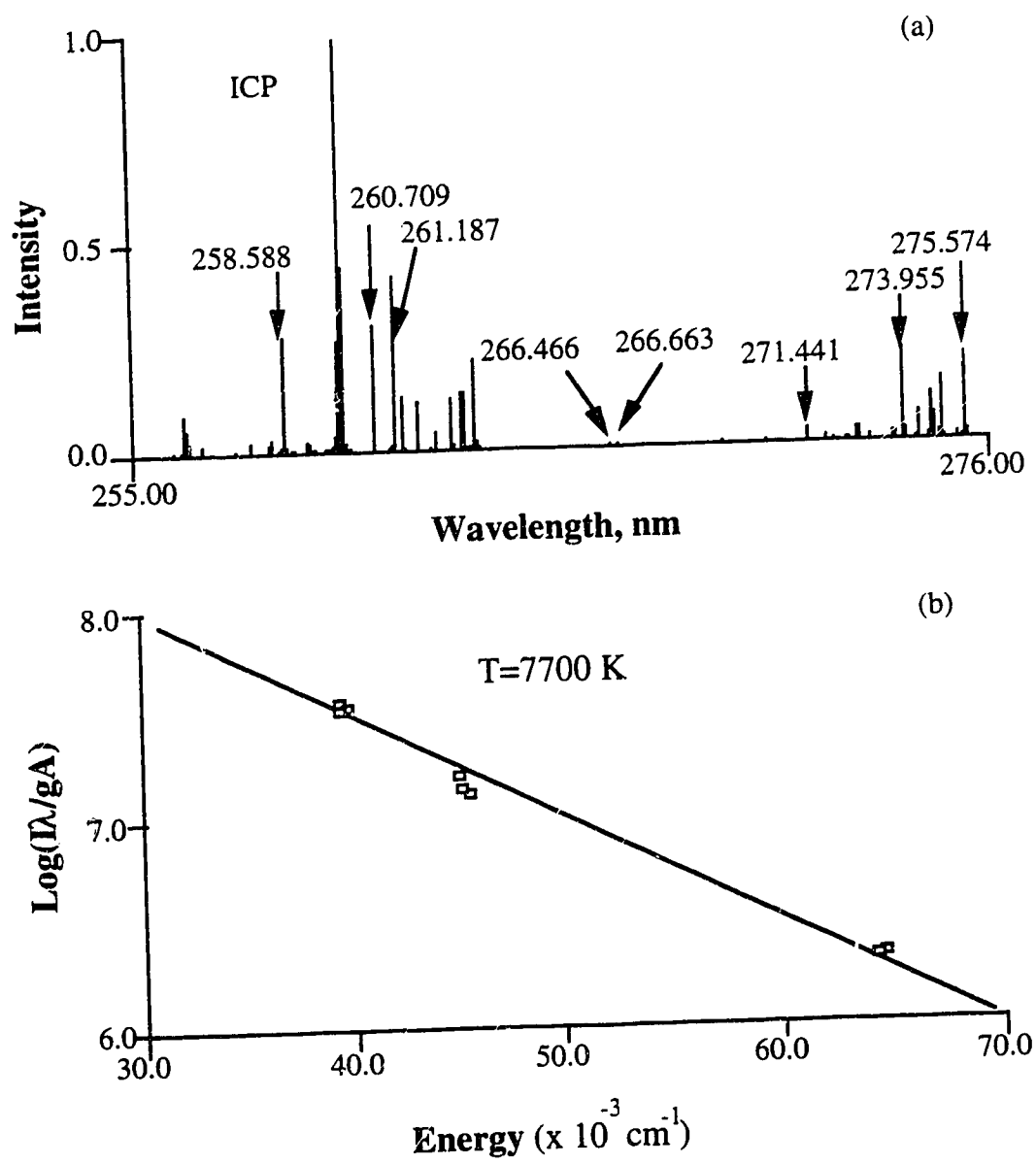


Fig. 3.14 Partial Fe UV spectrum from the ICP emission and the Boltzmann plot.

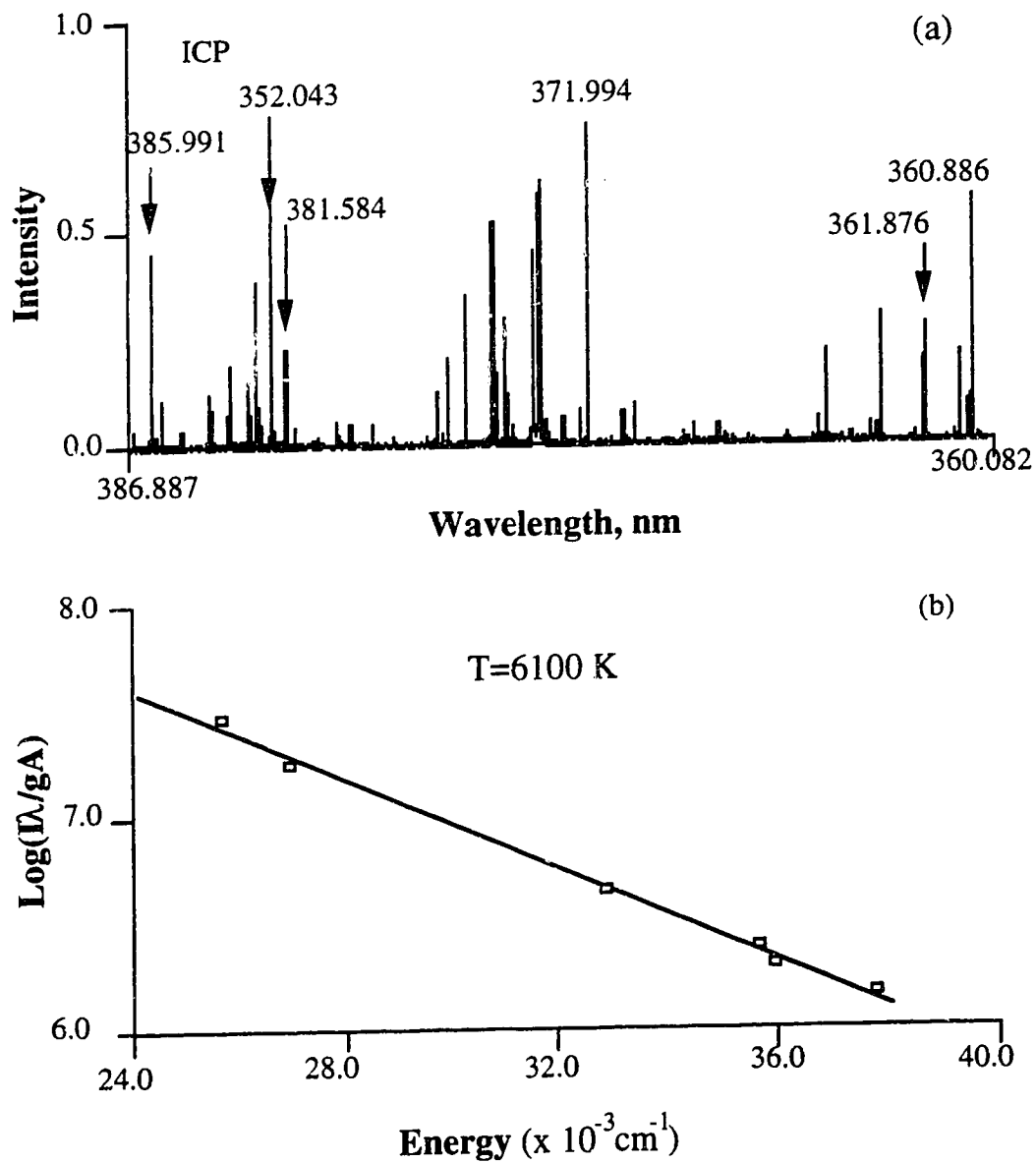


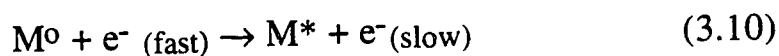
Fig. 3.15 A section of Fe visible spectrum from ICP and the Boltzmann plot.

equilibrium (LTE), so additional excitation mechanisms must be operative in the GD to create the above indicated populations.

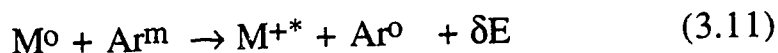
McWhirter's [37] work demonstrated that the low pressure (1.5 - 15 torr) electrical discharge with electron density below  $10^{15} \text{ cm}^{-3}$  does not satisfy the condition of complete TE or local TE. A single temperature can not describe the nature of the system which is not in total or local thermal equilibrium. The gas temperature, the electron temperature, the ionization temperature and the excitation temperature may all have different values. It may be more meaningful just talking about the distribution of the species among various energy states instead of the excitation temperature.

In a low pressure glow discharge, the excitation and ionization must be determined by various collisional processes. According to the literature, the most important collision processes which are related to excitation and ionization include the following:

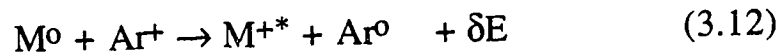
- Electron impact



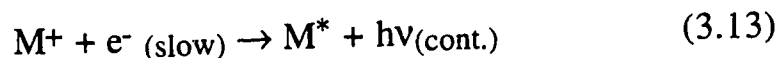
- Penning collision



- Charge transfer



- Electron-ion recombination



In all these equations, the symbols have the following meaning:  $M^0$  - an analyte atom in the ground state,  $M^*$  - an analyte atom in the excited state,  $M^+$  - an analyte ion in the ground state,  $M^{+*}$  - an analyte ion in the excited state,  $Ar^+$  - an argon ion in its ground state,  $Ar^0$  - an argon atom in its ground state,  $Ar^m$  - an argon atom in metastable state,  $\delta E$  - a small



amount of energy. In the situation for other filler gases, the Ar symbol could be replaced by that gas symbol (*i.e.* Ne or He) and the equations are still valid.

The actual discharge conditions, the gas identity, the sample nature and the source geometry may determine the relative roles of these processes and eventually determine the emission characteristics of the analyte. Using different filler gases to study the excitation and ionization mechanisms may be a good approach. It may give a reasonable explanation of the phenomena observed in the glow discharge emission. This will be discussed in more detail in Chapter 4 and 5.

## References

1. J.M. Anderson, *J. Appl. Phys.*, **31** 511 (1960) .
2. X. Feng, *Ph.D thesis*, University of Alberta, 1994.
3. W.R. Grove, *Philos. Trans. R. Soc. London* **142** 87 (1852).
4. J.J. Thomson and G.P. Thomson, *Conduction of Electricity Through Gases*, Vol. II, Cambridge, University Press, 1933.
5. H.S. W. Massey and E.H.S. Burhop, *Electronic and Ionic Impact Phenomena*, Oxford: Clarendon Press, 1952.
6. G.K. Wehner, *Advances in Electronic and Electron Physics*, Chapter 7, Academic Press, New York, 1955.
7. W. Grimm, *Spectrochim. Acta*, **23B** 443 (1968).
8. P.W.J.M. Boumans, *Anal. Chem.*, **44** 1219 (1972).
9. F. Llewellyn-Jones, *The Glow Discharge and an Introduction to Plasma Physics*, Methuen, London, 1966.
10. D. Fang and R.K. Marcus, *Fundamental Plasma Processes*, Chapter 2, in *Glow discharge Spectroscopies*, Edited by R. K. Marcus, Plenum Press, New York, 1993.
11. B. Chapman, "*Glow Discharge Processes, Sputtering and Plasma Etching*," Wiley, New York (1980).
12. R.V. Stuart and G.K. Wehner, *J. Appl. Phys.* **35** 1819 (1964).
13. A.V. Bodarenko, *Sov. Phys. Tech. Phys. (Engl. Transl.)* **18** 515 (1973).
14. P.F. Little and A. von Engel, *Proc. Roy. Soc., London*, **224A** 209 (1954).
15. P. Sigmund, *Phys. Rev.* **184** 383 (1969).
16. G. Carter and J. S. Colligan, *Ion Bombardment of Solids*, Chapter 7, Heinemann, London, 1968.

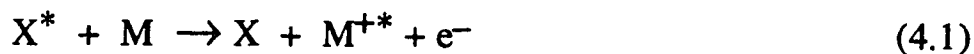
17. C.G. Bruhn and W. Harrison, *Anal. Chem.* **50** 16 (1978).
18. Wehner and Anderson, 1970 Chapter 3.
19. N.P. Ferreira and H.G.C. Human, *Spectrochim. Acta* **36B** 215 (1981).
20. N.P. Ferreira, J.A. Strauss and H.G.C. Human, *Spectrochim. Acta*, **37B** 947 (1982).
21. D.A. Doughty and J.E. Lawler, *Plasma Processing, Mater. Res. Soc. Symp. Proc.* **68** 141 (1986).
22. M.R. Winchester and R.K. Marcus, *16th Annu. Meet. Fed. Anal. Chem. Spectrosc. Soc.* 1989, Paper No. 327.
23. N.P. Ferreira, H.G.C. Human and L.R.P. Butler, *Spectrochim. Acta*, **35B** 287 (1980).
24. W. Stern, *Beitr. Plasmaphys.* **9** 59 (1969).
25. J.W. Coburn and E. Kay, *Appl. Phys. Lett.* **18** 435 (1971).
26. D. Fang and R.K. Marcus, *Spectrochim. Acta* **45B** 1053 (1990).
27. D. Fang and R.K. Marcus, *J. Anal. at. Spectrom.* **5** 569 (1990).
28. D. Fang and R.K. Marcus, *Spectrochim. Acta* **46B** 983 (1990).
29. M. Kuraica, N. Konjevic and M. Platisa, *Spectrochim. Acta* **47B** 1173 (1992).
30. D.M. Mehs and T.M. Niemczyk, *Appl. Spectrosc.* **32** 269 (1978).
31. C.D. West and H.G.C. Human, *Spectrochim. Acta* **31B** 81 (1976).
32. V.S. Borodin, Y.M. Kogan and R.I. Lyaguschenko, *Sov. Phys. Tech. Phys. (Engl. Transl.)* **11** 887 (1967).
33. J.A.C. Broekaert, *J. Anal. At. Spectrom.* **2** 537 (1987).
34. A.G. Shenstone, *Proc. Roy. Soc.* **A253** 297 (1936).
35. M.K. Levy, D. Serxner, A.D. Angstadt, R.L. Smith and K.R. Hess, *Spectrochim. Acta* **46B** 253 (1991).

- 36 W.L. Wiese and G.A. Martin in *Wavelength and Transition Probabilities for Atoms and Atomic ions*, National Bureau of Standards, Washington, D C, 1980.
37. R.W.P. McWhirter, in *Plasma Diagnostic Techniques*, edited by R. H. Huddlestone and S. L. Leonard, Academic Press, New York, 1965, p201.

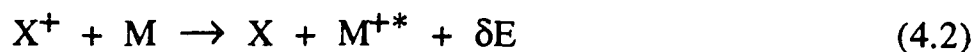
## Chapter 4. A Spectral Study of Charge Transfer and Penning Processes in Glow Discharges

### 4.1 Introduction

Studies of the fundamental processes which are relevant in determining the intensity of emission in a glow discharge have been ongoing now for many years. Within about the last decade a reasonably consistent picture of ionization and excitation processes has emerged. A particular focus of many studies has been on the role of charge transfer in the generation and excitation of singly charged analyte ions. In 1985 Wagatsuma and Hirokawa [1] pointed the way in a paper dealing with the effects of different filler gases (Ar, Ne and N<sub>2</sub>) on the emission characteristics of Cu, Ag, Sn and Al. They clearly showed that the nature of the filler gas could have a drastic effect on the character of the spectrum emitted by these elements. Their interpretive focus, however, centered on the role of filler gas metastables in ionization and excitation (*i.e.* Penning ionization). Penning ionization is a reaction between a metastable rare gas atom (X\*) and an analyte atom (M) resulting in an ionized and often excited ion:



In contrast to Penning ionization/excitation, charge transfer involves a reaction between an ionized rare gas atom (X<sup>+</sup>) and an analyte atom (M) resulting in an excited analyte ion:



In this case there is no third party (*i.e.* the electron in Equation 4.1) to carry off any excess energy and thus  $\delta E$  must be small. It has been generally established [2] that  $\delta E$  should be in the range of +0.1 to +0.5 eV for the reaction to proceed with the positive sign indicating that the energy of  $X^+$  exceeds that of  $M^{+*}$ .

Steers and his colleagues have made many contributions to our understanding of charge transfer processes in glow discharges. In 1987 Steers and Fielding [3] pointed out that charge transfer from argon ion could explain the unusually high intensity of emission from CuII 224.700 nm relative to other lines originating from the same level (4p) with about the same energy. This was a key paper that clearly showed that when charge transfer was operative, it could have a major influence on relative spectral line intensities in a glow discharge.

Wagatsuma and Hirokawa [4,5,6] continued their studies on the effects of different filler gases and filler gas mixtures on emission in glow discharges. In particular, their studies with Ne and Ar-He discharges began to reveal that charge transfer with  $Ar^+$ ,  $Ne^+$  and  $He^+$  was generally active as an ionization/excitation mechanism in glow discharges. A detailed paper in 1991 by Wagatsuma and Hirokawa [7] presented numerous charge transfer processes involved in the excitation of  $Cu^+$  in glow discharges with Ar, Ne, He-Ne, and Ar-He filler gases.

Steers and his colleagues also continued to carry out work that helped to elucidate the role of charge transfer in excitation processes in glow discharges. In particular they studied microwave-boosted glow

discharges [8,9,10,11]. Anomalies in enhancements or lack thereof revealed and clarified the existence of transitions populated by charge transfer from filler gas species. Finally, Levy *et al.* [12] also studied charge transfer processes in glow discharges with specific focus on  $\text{Ar}^+$  and the  $\text{CuII}$  224.700 nm line.

Charge transfer is by no means a new concept and many studies predate the above. Farnsworth and Walters [13] discussed the potential role of charge transfer between  $\text{Ne}^+$  and Cu in the excitation of  $\text{CuII}$  270.096 nm in an r.f.-boosted pulsed hollow cathode lamp. As well there is a large amount of literature concerning hollow cathode metal ion lasers [14,15,16,17] in which it is shown that charge transfer with  $\text{He}^+$  and  $\text{Ne}^+$  is a key process populating the lasing transitions of species such as Cu, Zn and Cd.

Predating all of this, of course, is the work of Duffendack in the 1920s and 30s. Some literature still refers to charge transfer as the "Duffendack reaction". It is interesting to note that Duffendack and Thomson [18] did observe enhanced emission as a result of charge transfer for several  $\text{CuII}$  lines in a Ne arc and  $\text{AgII}$  lines in a He arc, very similar to that observed in current glow discharge studies.

The study of charge transfer in analytical spectroscopy is not limited to glow discharges. Charge transfer processes in helium microwave induced plasmas (He-MIPs) have been studied by Carnahan and colleagues [19,20]. Goldwasser and Mermet [21] and Burton and Blades [22] among others have studied charge transfer processes in argon inductively coupled plasmas (ICPs).

From this brief review of the literature, it is clear that the type of filler gas in a glow discharge device plays a key role in determining the

exact nature of charge transfer processes. It was felt that a broad and comprehensive picture of charge transfer processes in glow discharges could be obtained by measuring, in a single study, the emission from a glow discharge device operated with either Ar, Ne or He as the filler gas (*i.e.* no mixed gases). This should provide the most unambiguous picture of specific charge transfer processes. In addition a broad picture can only be provided by complete spectral information. Charge transfer processes manifest themselves all over the UV-vis spectral range. To this end complete UV and Vis spectra were measured in this study using a Fourier transform spectrometer.

## **4.2 The experiment**

The elements studied in this experiment include Cu, Zn (as NIST Naval brass SRM 1107), Ag, Cd, and Fe. The samples were run as either pins or discs using the glow discharge devices described in Chapter 2. Argon, helium and, for some cases, neon were used as the filler gases. The parameter settings used in this study depended on the sample, the nature of the discharge gases and are indicated in each of the specific measurement [Table 4.1]. The measurement of the emission signals was made by using the Fourier Transform Spectrometer described in Chapter 2. The data were collected and processed by using a Macintosh II computer with the software SpectroPlot as mentioned in Chapter 2. The optical coupling between the glow discharge and the interferometer was achieved by placing a 30 cm focal-length quartz lens at its focal length distance from the discharge. Collimating light was directed into the interferometer through an aperture set at a diameter of 8 mm. The detectors used were R166 solar-



Table 4.1. Parameter settings in the emission measurement

Sample	Gas	Pressure, torr	Voltage, V	Current, mA
Brass	Ar	3.37	740	15
	Ne	6.50	1200	12
	He	11.85	1700	10
Fe	Ar	3.67	750	14
	Ne	4.95	1100	12
	He	11.0	1800	10
Ag	Ar	3.55	800	16
	He	11.5	1600	12
Cd	Ar	3.10	800	15
	He	12.2	1400	14

blind photomultiplier tube (Hamamatsu Photonics K. K.) for the ultraviolet spectral region (200 - 316 nm) and 1P21 photomultiplier tube (Hamamatsu Photonics K. K.) for the visible spectral region (316 - 600 nm). Both were operated at a potential of 660V. For each spectrum, 32 interferograms were co-added to increase the signal-to-noise ratio. All the spectra obtained in this chapter were calculated from 64k interferograms sampled with a frequency 4 times of that of the clock derived from the He-Ne laser. The acquired interferograms were multiplied by a Gauss function and, for some interferograms, 4 times zero filled, followed by a mathematical Fourier transform to yield the resultant spectra.

### 4.3 Results and Discussion

Complete UV spectra (200 to 316 nm) acquired for the brass sample normalized to their most intense lines are shown in Fig. 4.1. Three spectra are shown, one for each filler gas, Ar (a), Ne (b) and He (c). Viewing the complete spectra presented in Fig. 4.1 clearly indicates that they are each very different. As has been commented on in the literature [1,4,5,6,7] almost the entire spectral character of the discharge is altered by a change in filler gas. A prominent difference in the spectra is that the most intense line is different in each spectrum. For the Ar case the most intense line is CuII 224.700 nm, for Ne it is CuII 248.579 nm and for He it is ZnII 255.796 nm, all ion lines. However, many other spectral differences exist and will be highlighted later. An interesting aspect of most of the spectral differences is that they tend to be dramatic, a strong spectral feature in one spectrum is often almost completely absent in another spectrum.

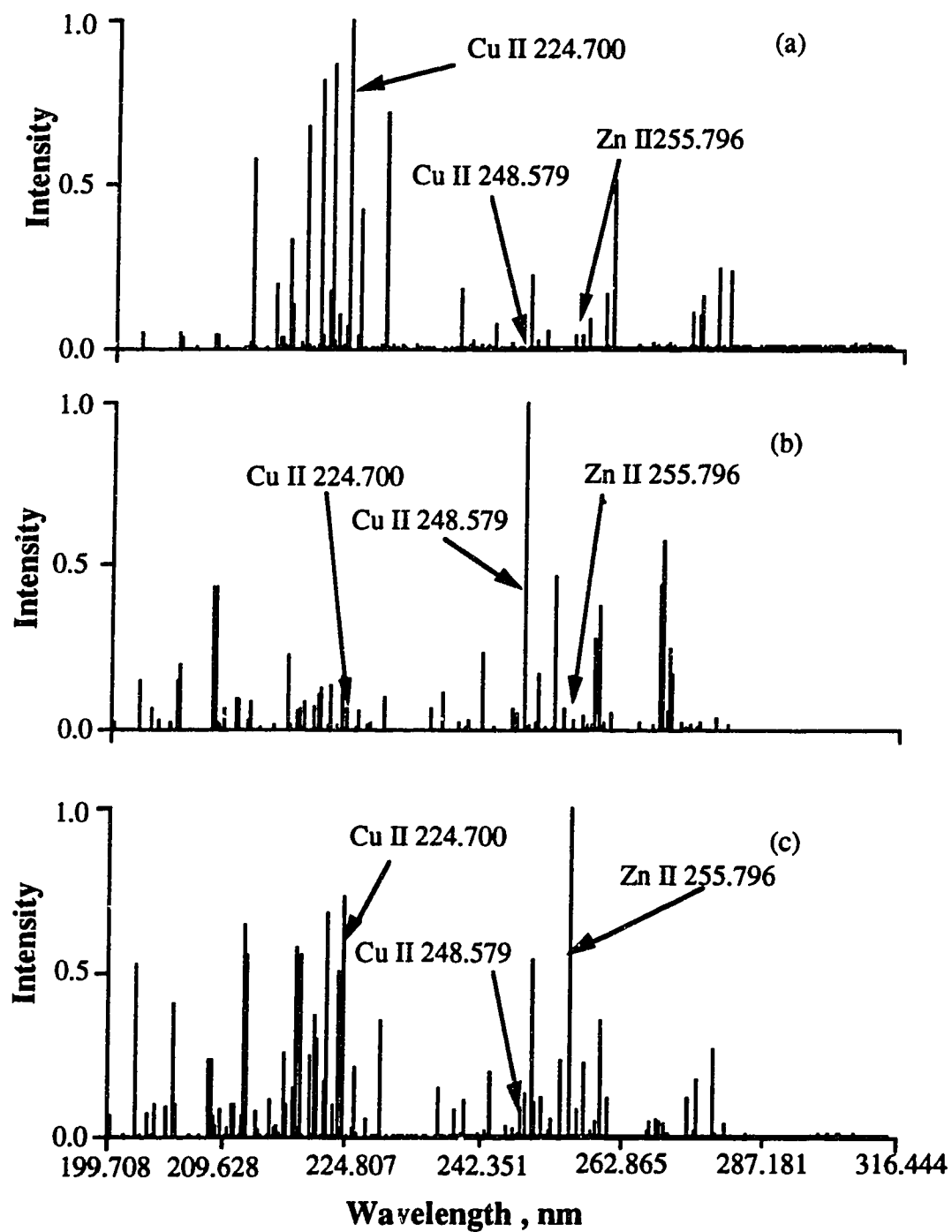


Fig. 4.1 UV spectra of brass in three discharge gases: (a) argon, (b) neon and (c) helium.

Dramatic spectral differences such as these are suggestive of highly specific excitation mechanisms most likely driven by certain filler gas species. The three gases (Ar, Ne and He) provide a range of energetic species (metastables and ions) that are available to participate in Penning and charge transfer processes. The species and their energies are listed in Table 4.2.

#### 4.3.1 Copper Ion Lines

A simplified energy level diagram (Grotrian diagram) for copper ion is shown in Fig. 4.2. Superimposed on the same diagram are the metastable and ground state ion energy levels of Ar, Ne and He. This figure is an adaptation of a similar diagram presented by Wagatsuma and Hirokawa [7]. Two energy scales are given, one from the  $\text{Cu}^0$  ground state and one from the  $\text{Cu}^+$  ground state. Transitions observed in most emission sources from copper ions are illustrated in the diagram. Detailed terms are omitted in this and the following diagrams for reasons of simplicity.

The most intense line in the spectrum with Ne as the filler gas (Fig. 4.1) is the  $\text{CuII}$  line at 248.579 nm. Expanded scale spectra in the general vicinity of this line are shown in Fig. 4.3. This line has an excitation energy (from the ion ground state) of 13.64 eV and results from a transition from the 5s level of  $\text{Cu}^+$  to the 4p level. It is but one of many lines of roughly comparable energy that are the result of transitions from the 5s to the 4p level (see Table 4 of ref. 7). Other examples include the 252.930, 259.053 and 260.027 nm lines also noted in Fig. 4.3 and the 270.096, 270.318, 271.351, 271.878, and 272.168 nm lines noted in the expanded spectral region shown in Fig. 4.4. In all cases noted above the

**Table 4.2 Metastable energy levels and ionization potential of helium, neon and argon.**

<b>Gas</b>	<b>Metastable (<math>X^*</math>) Energy, eV</b>	<b>Ionization (<math>X^+</math>) Potential, (eV)</b>
<b>He</b>	19.82, 20.62	24.58
<b>Ne</b>	16.6, 16.7	21.56, 21.66
<b>Ar</b>	11.55, 11.72	15.76, 15.94

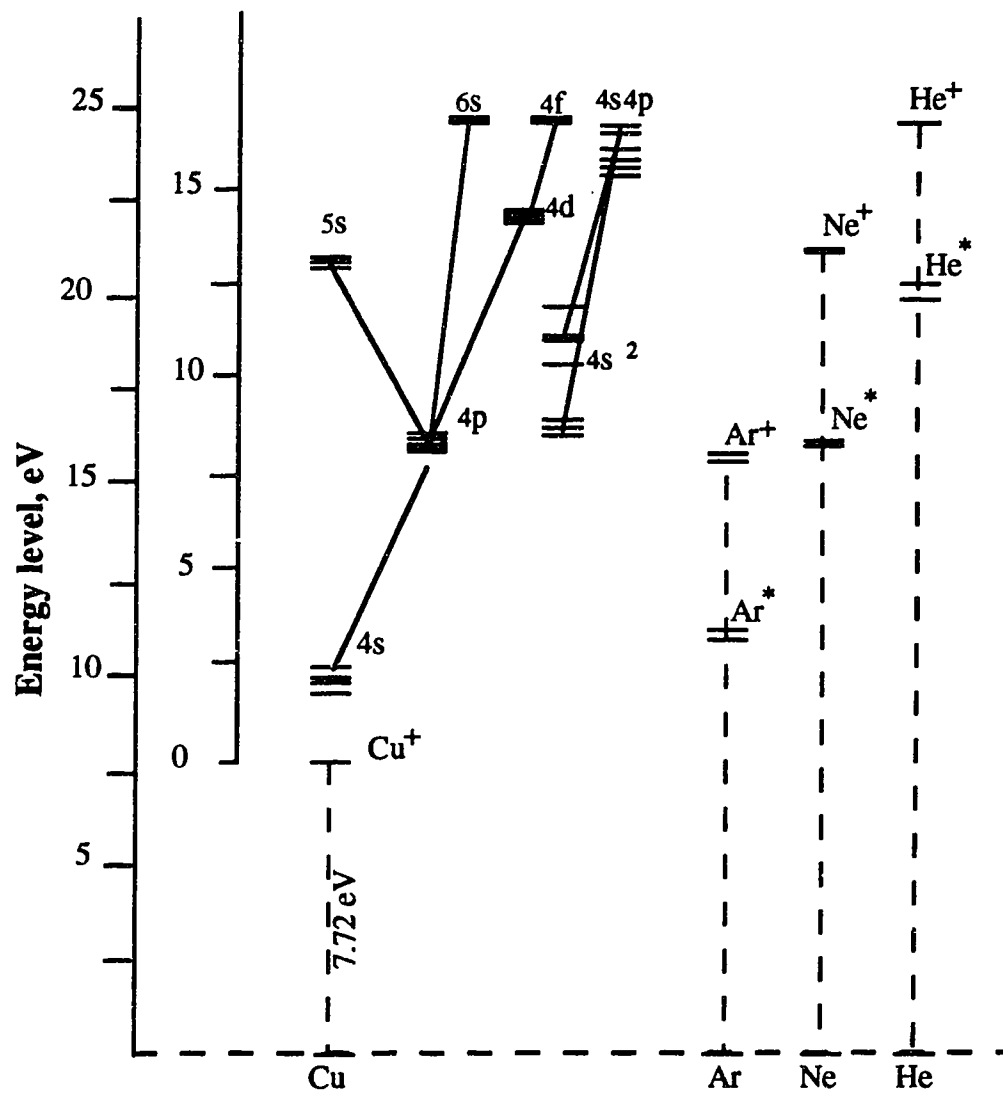


Fig. 4.2 A simplified energy diagram of Cu ion and the metastable and ionization potentials of the discharge gases.

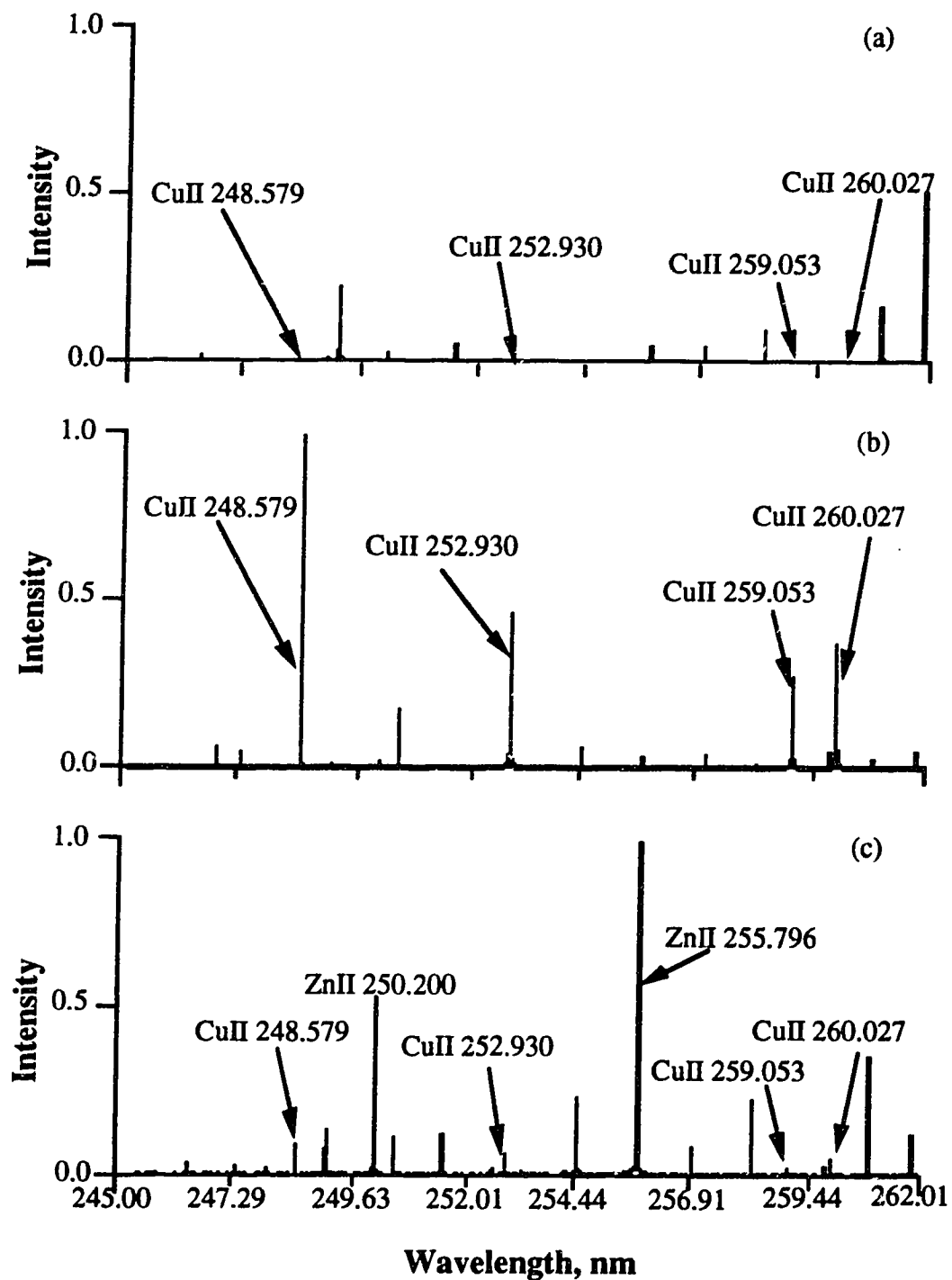


Fig. 4.3 A portion of brass spectra showing the relative intensities of the CuII lines in the vicinity of 248.579 nm. (a) Ar, (b) Ne, (c) He.

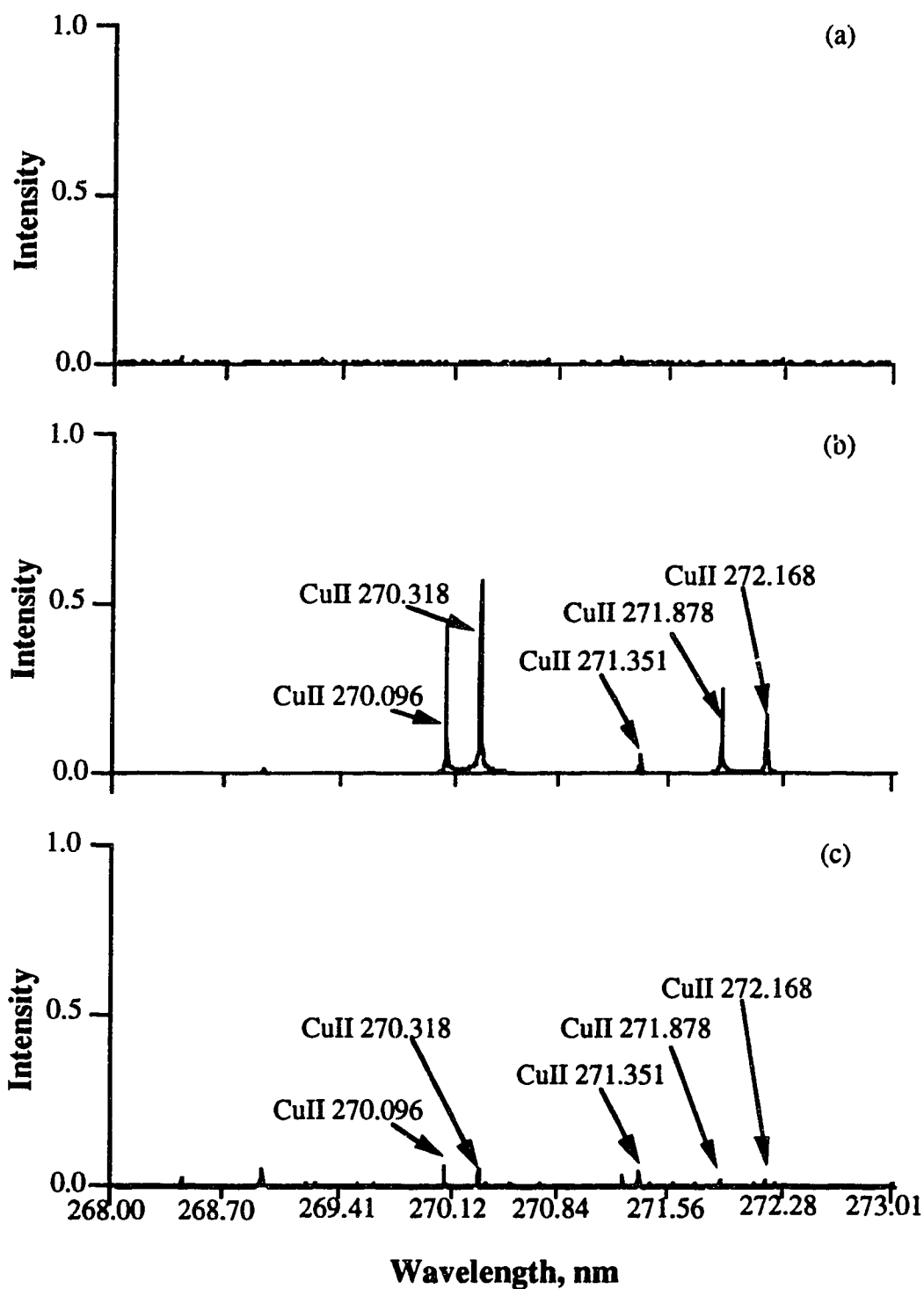


Fig. 4.4 Expanded spectra region showing some of the CuII lines from the 5s to 4p transitions enhanced by Ne. (a) Ar, (b) Ne and (c) He.



intensity of the particular line is dramatically enhanced when Ne is the filler gas in contrast to the spectra for which Ar or He is the filler gas. It is almost as if these lines in Ne were turned on by a switch.

In fact, a switch is a good analogy for what is happening. The switch mechanism is charge transfer and it is activated by  $\text{Ne}^+$ . The copper ion 5s excited state has four levels;  $^3\text{D}_1$  (13.65 eV),  $^3\text{D}_2$  (13.43 eV),  $^3\text{D}_3$  (13.39 eV), and  $^1\text{D}_2$  (13.68 eV) [7]. The  $\text{Ne}^+$  ground levels are 21.56 eV and 21.66 eV. Adding the ionization potential of copper (7.72 eV) to the above 5s energies results in total excitation potentials of 21.37, 21.15, 21.11, and 21.40 eV. All these values are just below the  $\text{Ne}^+$  levels (0.16 to 0.55 eV) and thus we have an almost perfect situation to drive charge transfer (*i.e.* a small positive energy defect). Therefore the major factor determining these copper ion line intensities when Ne is the filler gas is charge transfer to the 5s level. This process is illustrated on the energy level diagram shown in Fig. 4.5. Charge transfer processes in the Ne-Cu system are the basis of certain hollow cathode metal ion lasers [16,17]. The CuII 248.579 nm line is a prominent lasing transition in such lasers, and lasing action has been observed for most of these 5s to 4p transitions. As well, back in 1933 Duffendack and Thomson [18] observed enhancements of these lines in a neon arc which they attributed to charge transfer.

Referring back to Fig. 4.1, the most intense line in the spectrum with Ar as the filler gas is the CuII 224.700 nm line. The spectral region around this line is shown in Fig. 4.6 for each of the filler gases. This line is the lowest energy transition (8.235 eV) between the 4p and 4s states of copper ion (see Fig. 4.2). A more detailed diagram of these levels is shown in Fig. 4.7 which was adapted from reference 12. Three transitions are shown; CuII 224.700 nm (15.96 eV), CuII 221.810 nm (16.15 eV) and

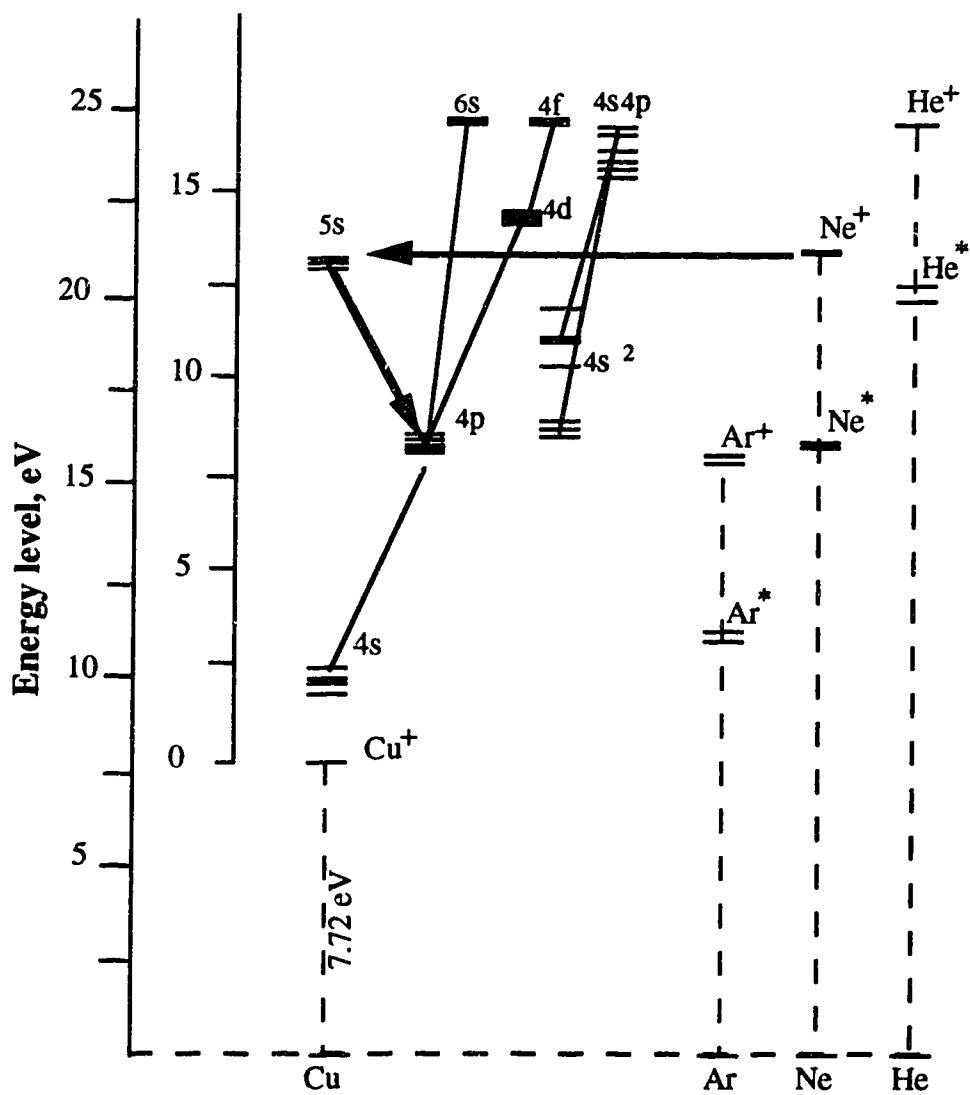


Fig. 4.5 A schematic diagram illustrating the charge transfer from neon ions to copper atoms populating the 5s levels.

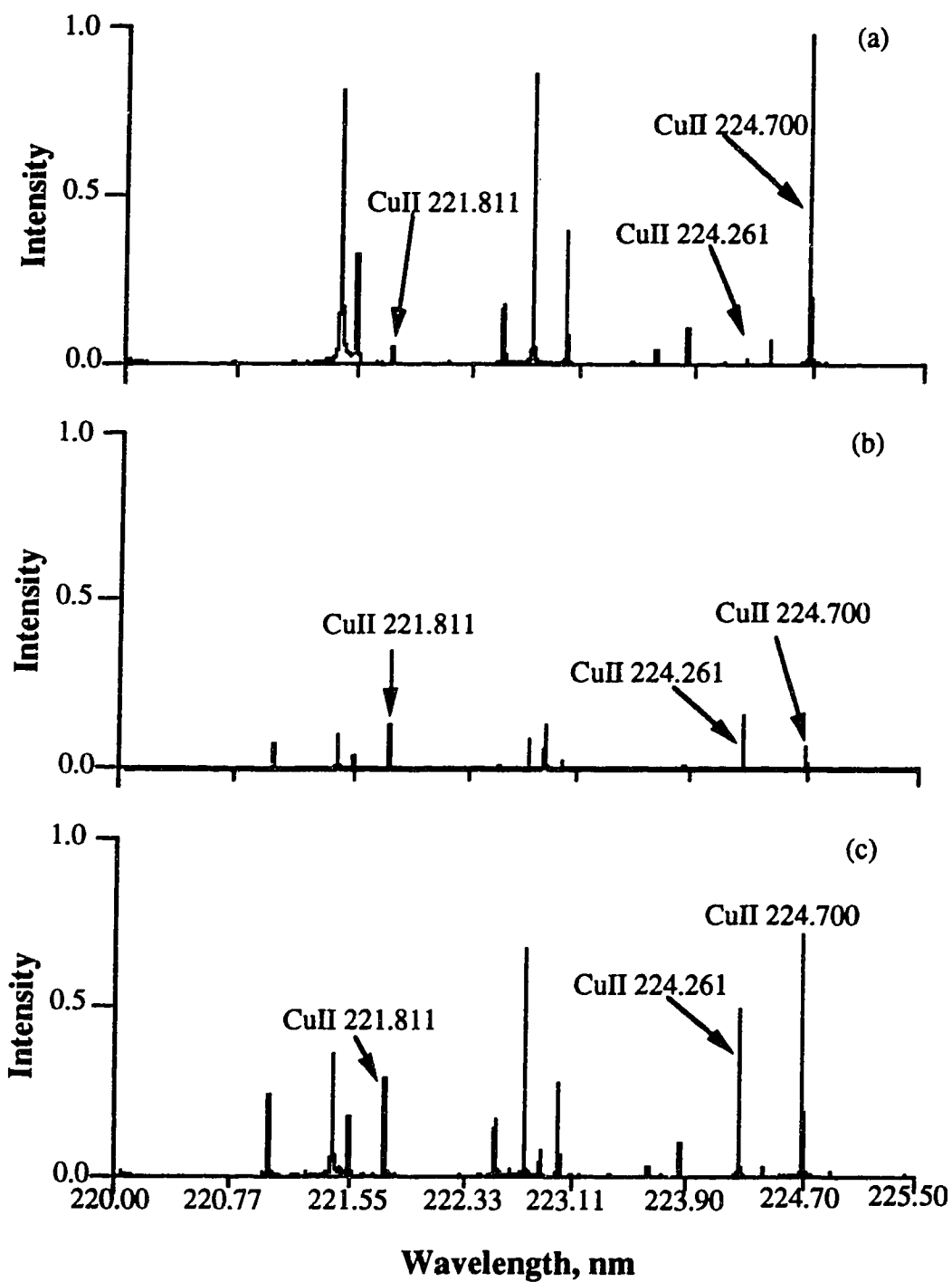


Fig. 4.6 A portion of spectra showing the extraordinary intensity of CuII 224.700 nm line in Ar. (a) Ar, (b) Ne, (c) He.

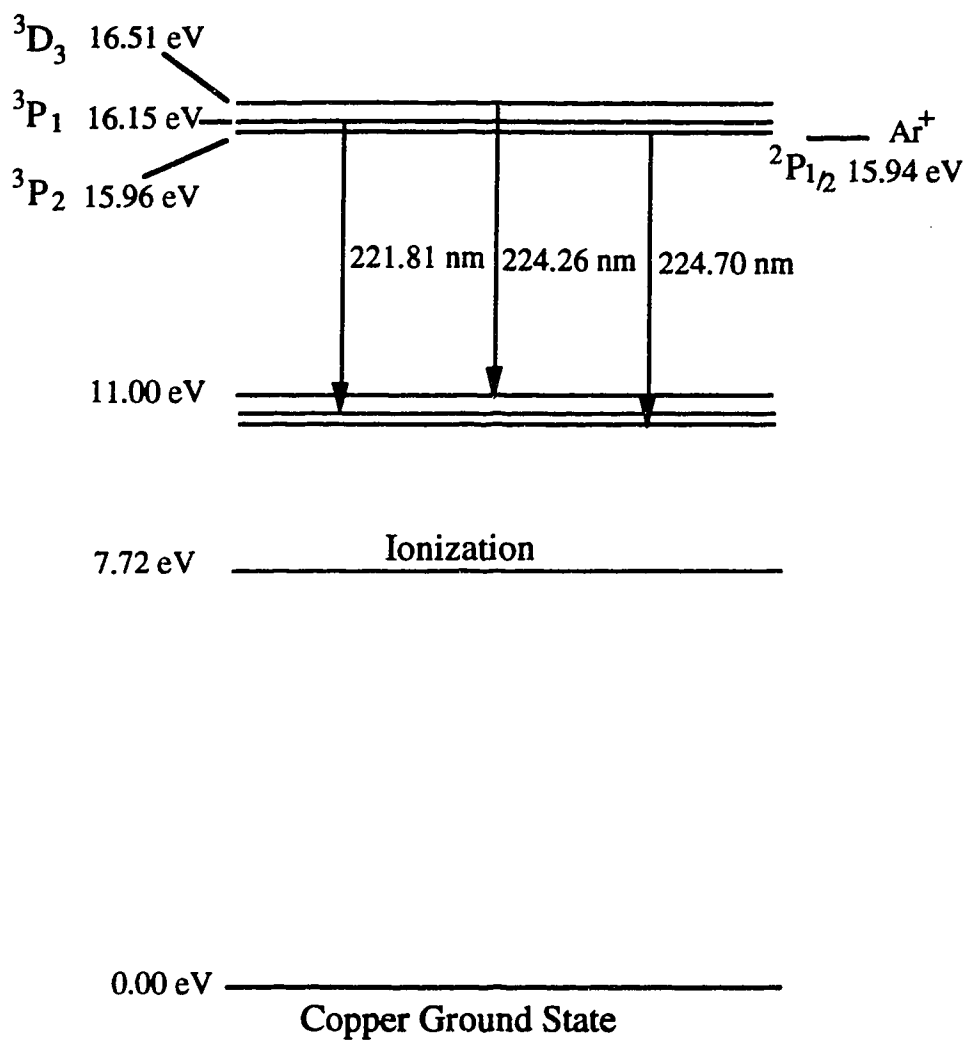


Fig. 4.7 A detailed diagram showing the availability of charge transfer in Ar-Cu discharge.

CuII 224.261 nm (16.51 eV). The energies noted are from the copper atom ground state.

Each of these lines is specifically noted in the spectra shown in Fig. 4.6. Clearly, of this group the CuII 224.700 nm line is selectively and significantly enhanced in the presence of Ar. Steers and Fielding [3] presented a nice analysis of this case explaining the selective excitation of the CuII 224.700 nm line on the basis of charge transfer with Ar<sup>+</sup>. At first glance the ground state energy of Ar<sup>+</sup> (15.76 eV) would not supply enough energy (defect is -0.2 eV) to effect charge transfer. Charge transfer can proceed with small positive energy defects (< about +0.5 eV) but the process is not very tolerant of even small negative energy defects. Steers and Fielding [3] noted however that Ar<sup>+</sup> has a metastable level 0.18 eV above the ion ground state. This level then has a total energy of 15.94 eV, bringing the energy defect to only -0.02 eV. The collision partners in the charge transfer process can bring this much energy in via translational energy and, as illustrated by the data, charge transfer proceeds selectively into this level. Both Wagatsuma and Hirokawa [7] and Levy *et al.* [12] have further discussed and illustrated this case. This selective charge transfer process is illustrated in Fig. 4.8.

Referring back to Figs. 4.6 and 4.7, it is interesting to note the relative intensities of all three of these lines in each of the filler gas spectra. While 224.700 nm is significantly enhanced relative to 224.261, and 221.810 nm in the Ar spectrum, such is not the case for the Ne and He filler gas spectra. For the Ne case, all three lines are readily observable and have, within about a factor of two, comparable intensities. For the He case the lines are quite strong and again of comparable intensity. For Ne it might be possible for a Penning process to populate these levels (Ne

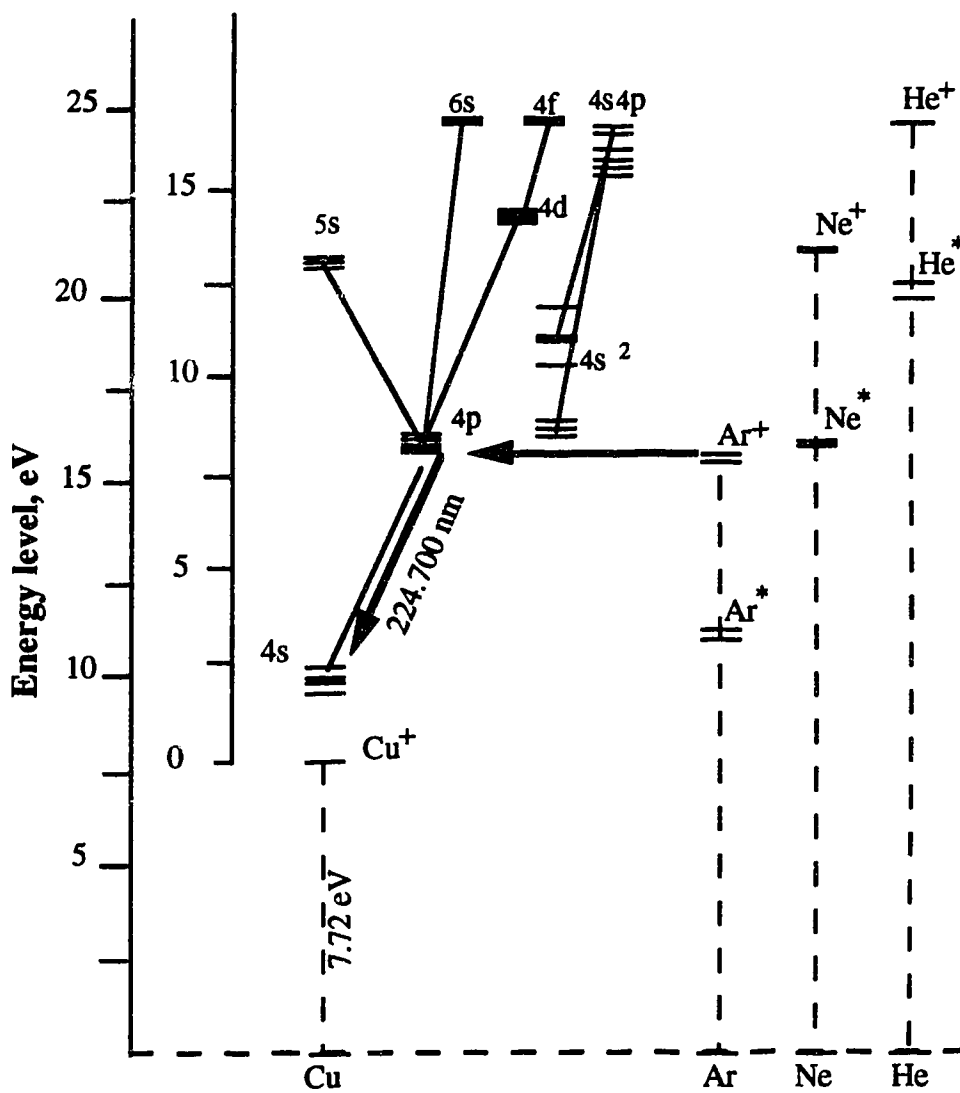


Fig. 4.8 A schematic diagram illustrating the charge transfer from argon ions to copper atoms populating one of the 4p levels.

metastables level are 16.6 and 16.7 eV, Table 4.2). But also possible, is population of the 4p levels by stepwise de-excitation from the 5s level, a level we already know is selectively and effectively populated by charge transfer from  $\text{Ne}^+$ . Wagatsuma and Hirokawa [7] also suggested this mechanism for the population of these levels in a Ne discharge. This process is illustrated in Fig. 4.9.

Wagatsuma and Hirokawa also reported the excitation of the copper ion 6s levels via charge transfer with  $\text{He}^+$  [7]. These levels relax via transitions to the 4p levels. The spectral lines resulting from 6s to 4p transitions in copper ion occur in the vacuum ultraviolet and could not be directly observed in this study. However, the 4p to 4s spectral lines observed in Fig. 4.6 for the He case can, in part, be explained by stepwise de-excitation from 6s to 4p to 4s after charge transfer population of the 6s levels by  $\text{He}^+$ .

Wagatsuma and Hirokawa also recently reported evidence for charge transfer by  $\text{He}^+$  into the 4f levels of copper ion [23]. This sets up transitions from the 4f to the 4d levels of copper ions. These transitions result in the emission of several lines in the visible region of the spectrum [23]. In the course of this study we have also measured complete visible spectra for the brass sample with all three filler gases. These spectra are presented in full and discussed in more detail in Chapter 5 which deals with ion-electron recombination processes in glow discharges. However, certain expanded scale sections of these spectra will be presented here to further illustrate the existence of charge transfer processes.

The two most intense 4f to 4d lines noted by Wagatsuma and Hirokawa [23] were 493.165 and 490.973 nm. Both these lines were observed in our He discharge spectrum and they are shown in Fig. 4.10. A

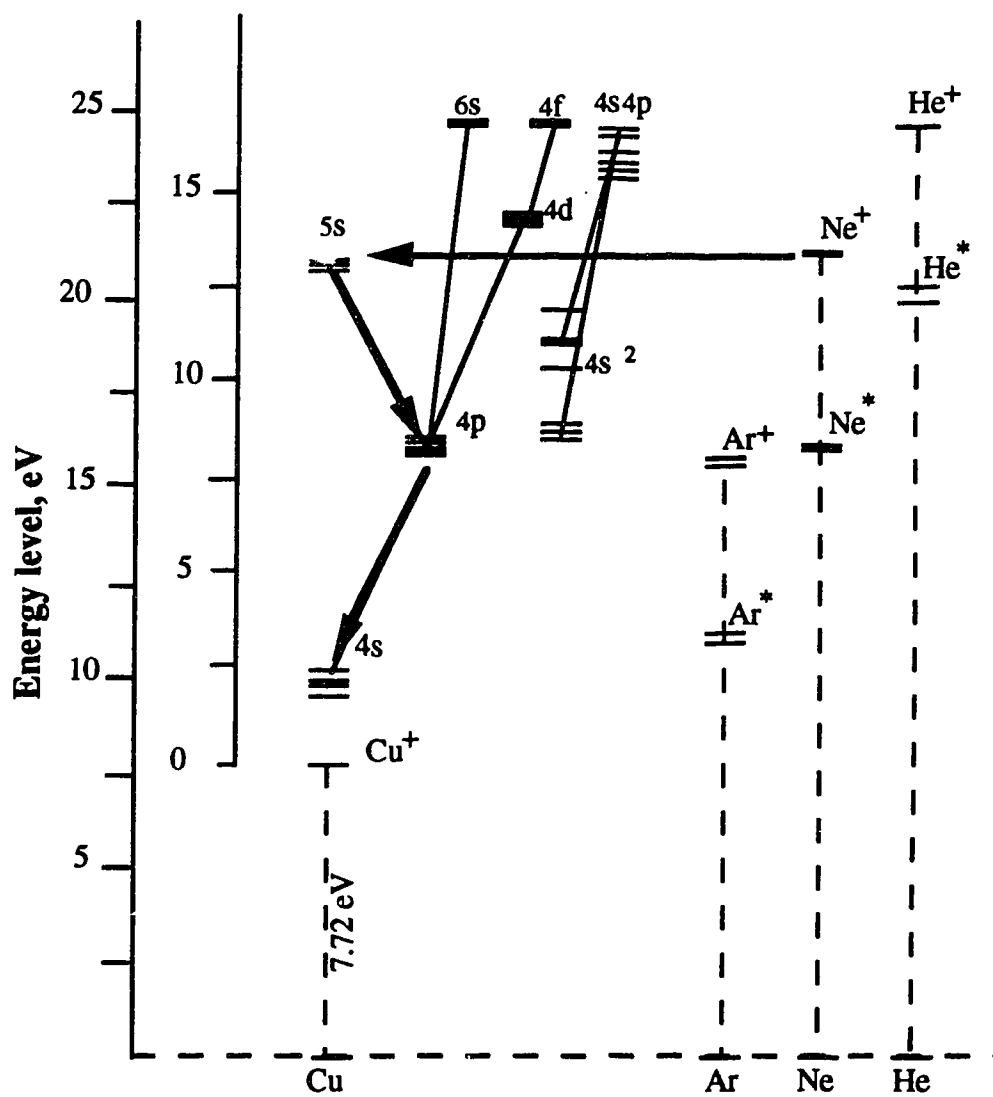


Fig. 4.9 A diagram showing the 4p to 4s transitions enhanced by charge transfer in Ne-Cu discharge.



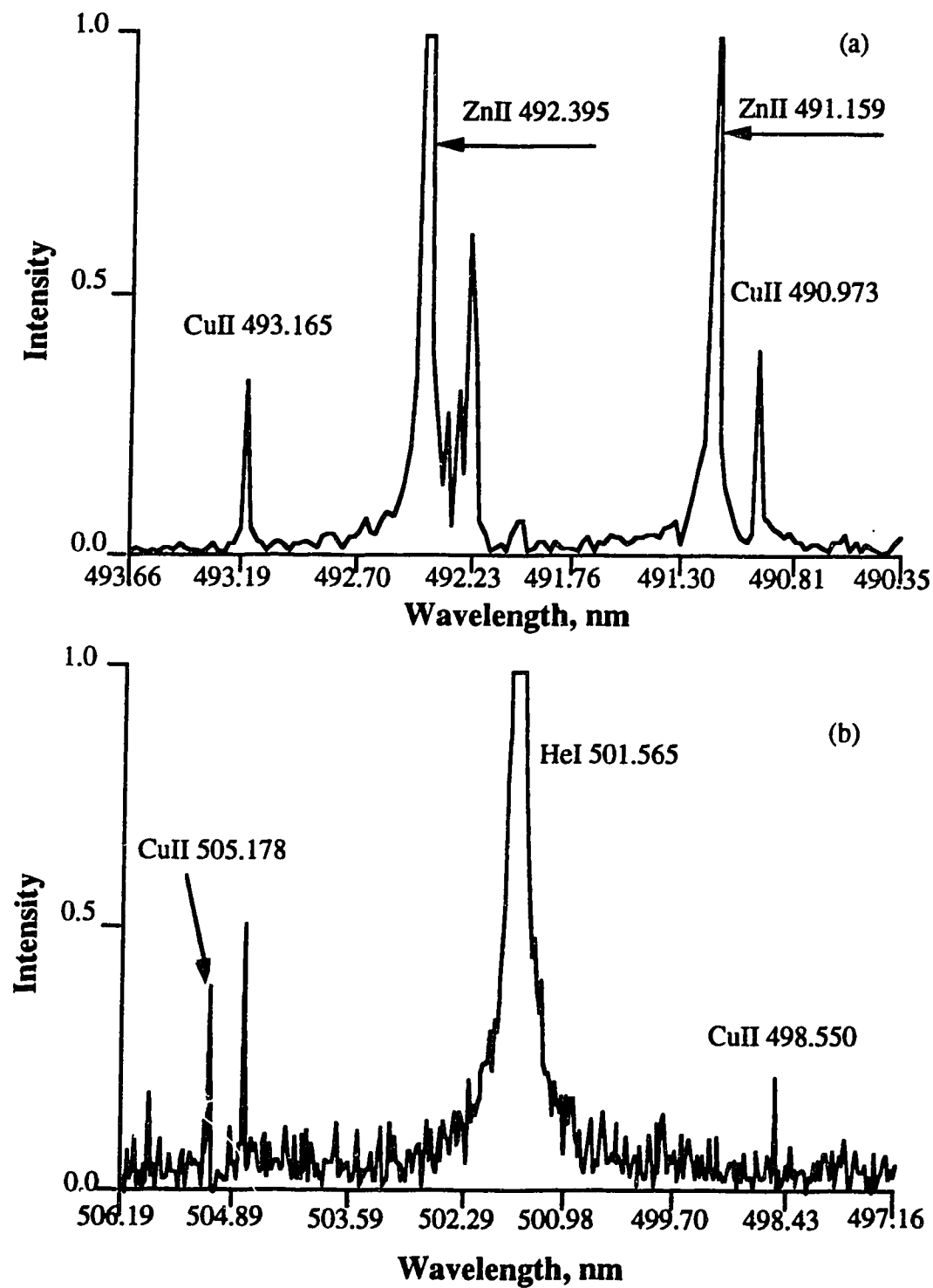


Fig. 4.10 A portion of visible spectrum of brass in helium showing some 4f to 4d transition lines.

couple of weaker but identifiable 4f to 4d lines are also shown in Fig. 4.10b (505.178 and 498.550 nm). With the FTS acquired spectra and SpectroPlot the wavelengths of these lines can be pin pointed to within about 1 pm and thus unambiguously identified. None of the above lines were observed in the spectra for the Ar and Ne filler gas cases.

The 490.973 and 493.165 nm lines have a listed excitation energy of 16.853 eV. Adding in the IP for Cu (7.72 eV) results in a total excitation energy for these lines of 24.577 eV. The energy of  $\text{He}^+$  is 24.58 eV, thus there is an almost zero energy defect and charge transfer excitation is certainly possible. For the 505.178 nm (16.88 eV) and the 498.550 nm (16.878 eV) lines the energy defect is about -0.02 eV and again, although the defect is negative, charge transfer is a possible excitation mechanism.

Referring then back to Fig. 4.6, the 4p to 4s transitions observed for the He discharge are most likely driven by stepwise de-excitation of the 6s and 4f levels of copper ion which are populated by charge transfer from  $\text{He}^+$ . These processes are summarized in Fig. 4.11.

### 4.3.2 Zinc Ion Lines

Referring back to the spectrum with He as the filler gas shown in Fig. 4.1, it is seen that the ZnII 255.796 nm line is the strongest line in the spectrum, stronger even than the ZnI neutral atom resonance line at 213.856 nm. In the expanded views of these spectra shown in Fig. 4.3 this line along with ZnII 250.200 nm are highlighted. As can be seen in the spectra presented in Fig. 4.3, both of these lines are relatively weak in both the Ar and Ne filler gas cases. Thus it appears that some type of selective excitation of these lines is occurring in the He based discharge.

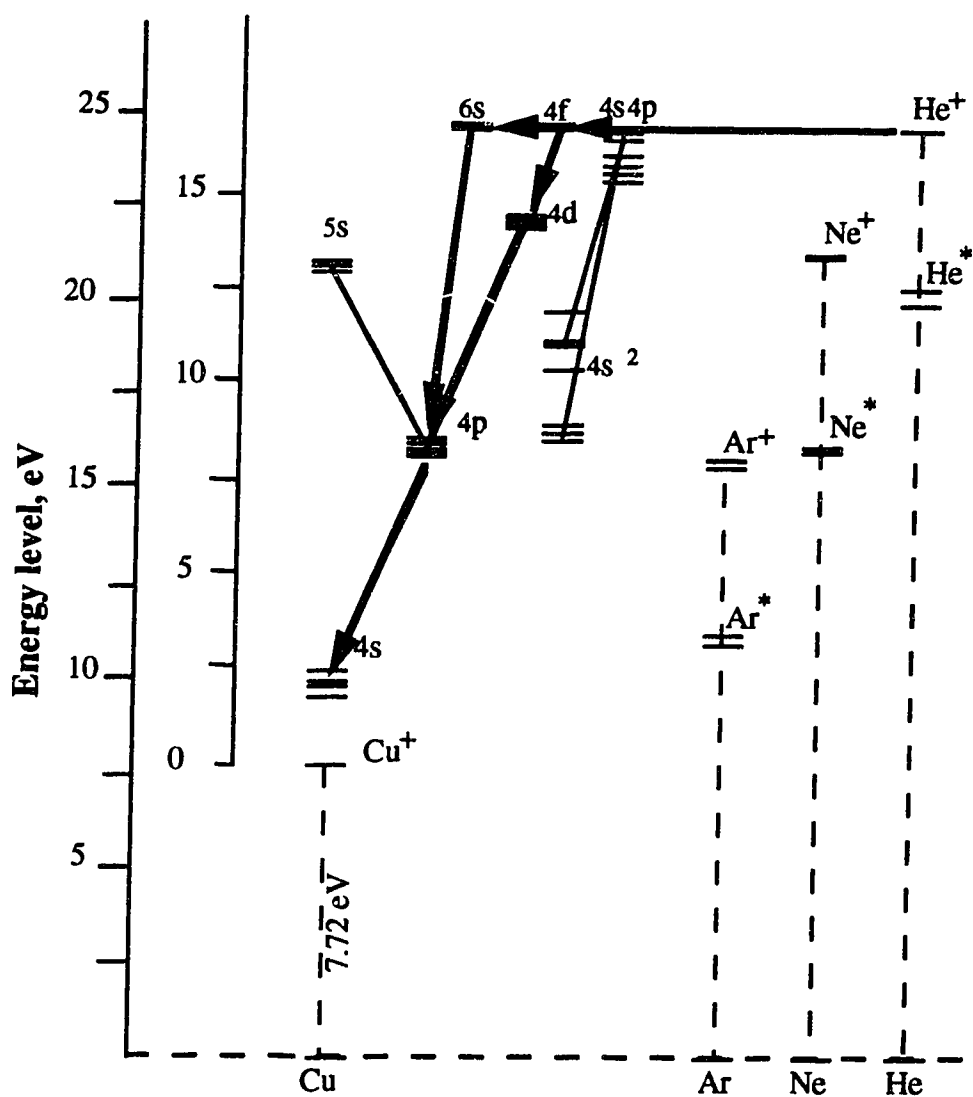


Fig. 4.11 Illustration of the population of CuII 6s, 4f levels by charge transfer and followed by stepwise de-excitation.

A simplified energy level diagram for zinc ion is presented in Fig. 4.12. Also superimposed on the energy level diagram are the metastable and ion energy levels of Ar, Ne and He. The Zn ion lines noted above originate in transitions from the 5s to the 4p levels. The excitation energies of these two lines are 10.97 eV (ZnII 255.796 nm) and 10.98 eV (ZnII 250.200 nm). Adding in the ionization potential of Zn (9.39 eV) the total excitation energies for these lines are 20.36 eV and 20.37 eV. The metastable levels of He are 19.82 eV and 20.62 eV [5]. Thus it is possible, via a Penning process with He\* to populate the 5s levels responsible for these zinc ion lines. This process is shown schematically in Fig. 4.13. As will be seen in a moment, it is also possible to populate certain upper levels of zinc ion via a charge transfer process with He<sup>+</sup>. The 5s level could thus also be populated via stepwise de-excitation from the upper levels. Green *et al.* [24] have indicated that such a process could be possible for the population of this level.

In addition to the UV spectra of the glow discharges shown in Fig. 4.1, complete visible range spectra for the three discharges (Ar, Ne and He) have also been measured for the brass sample. The nature of these spectra are discussed in the next chapter which deals primarily with the excitation of neutral atom lines in glow discharges. However, parts of these spectra are pertinent to this discussion of the excitation of ZnII lines.

Expanded sections of the visible spectra of the Ar, Ne and He based glow discharges are shown in Fig. 4.14. The spectra are centered on the ZnII 491.166 nm and ZnII 492.404 nm lines. The lines are clearly only present in the He glow discharge spectra. These lines are the result of transitions from the 4f to the 4d states of Zn<sup>+</sup> [14,15] and both lines have excitation potentials of 14.54 eV. Adding in the ionization potential for Zn

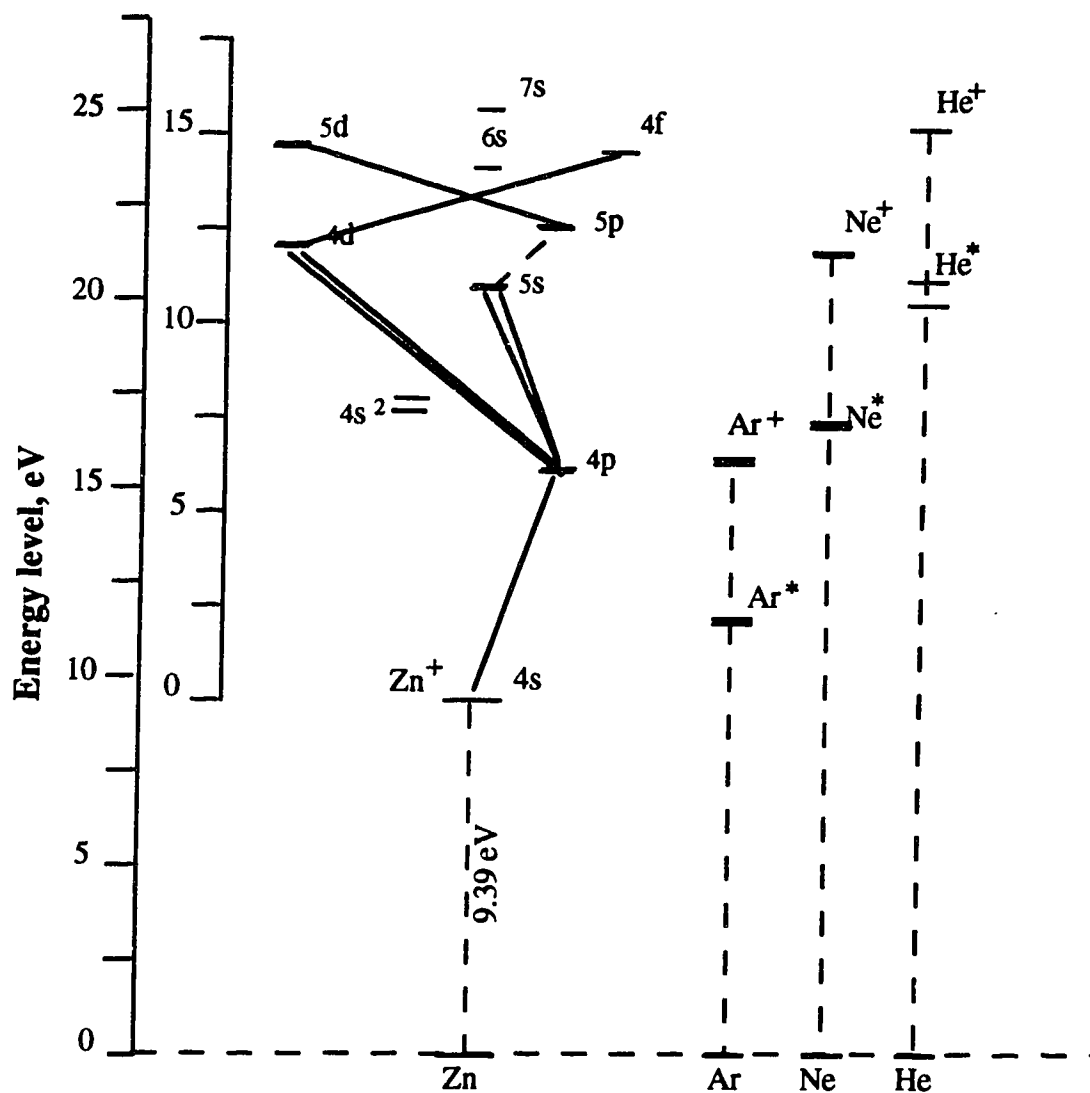


Fig. 4.12 A simplified energy diagram of Zn<sup>+</sup> with the metastable and ionization potentials of the discharge gases.

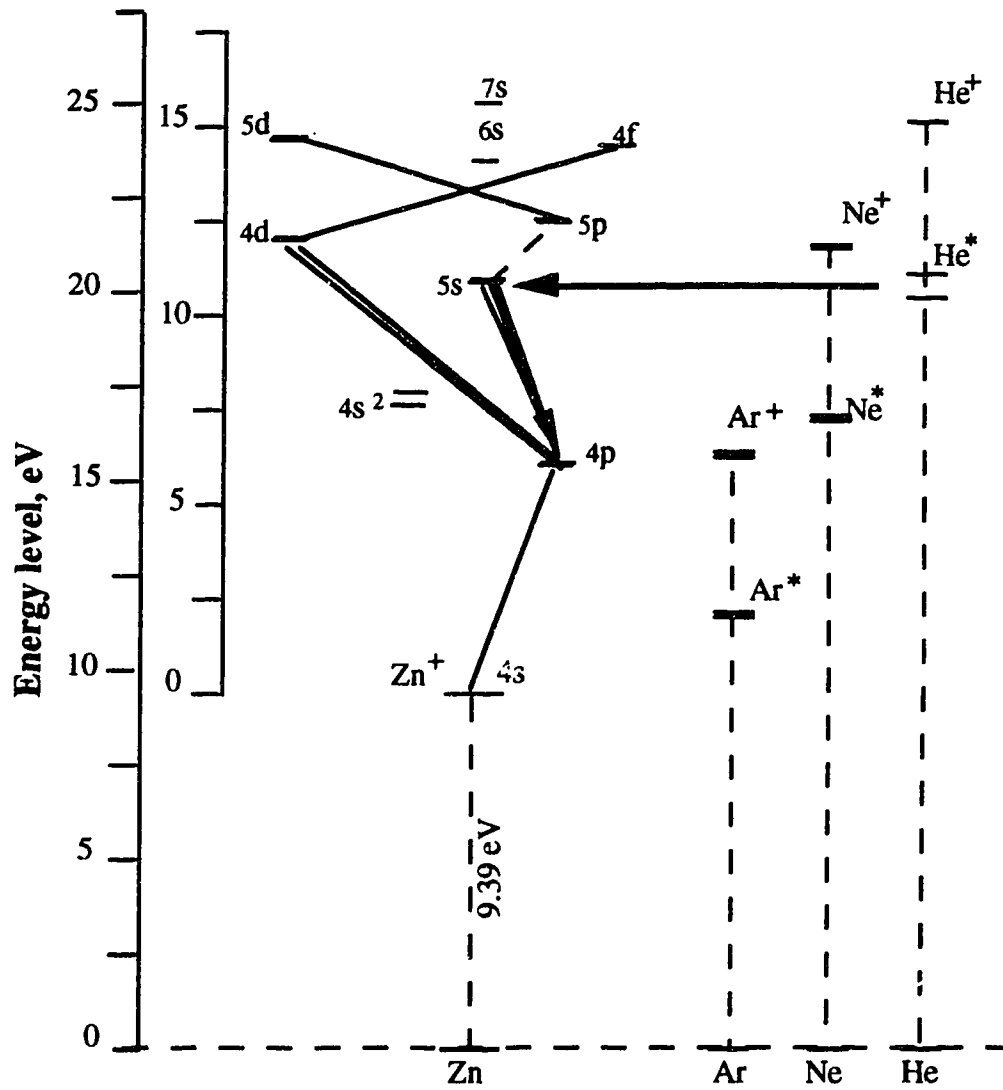


Fig. 4.13 A schematic diagram illustrating a possible Penning process in He-Zn discharges.

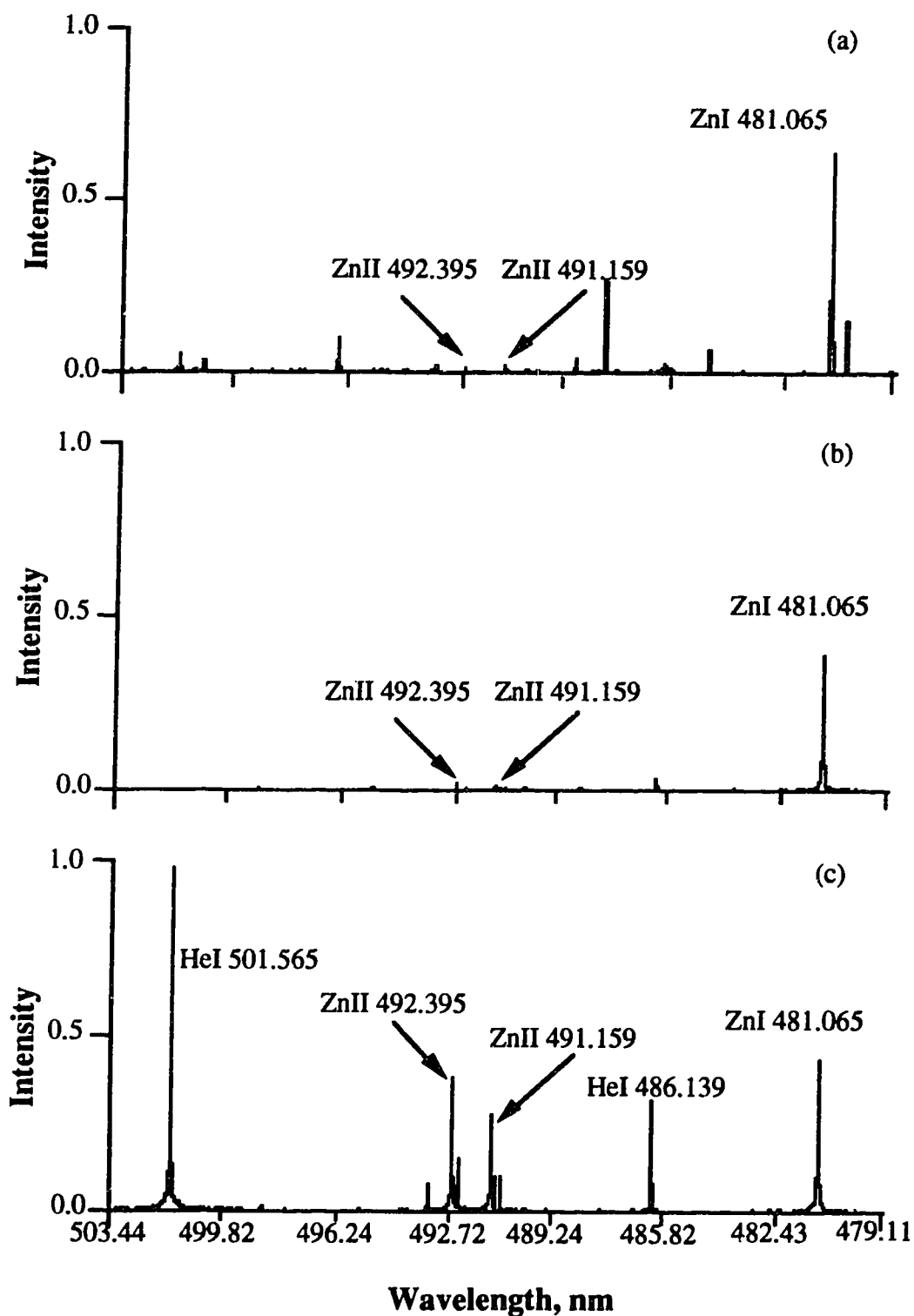


Fig. 4.14 Relative intensity of ZnII 491.166 and 492.404 nm lines in different gases. (a) Ar, (b) Ne, (c) He.

(9.39 eV) the total excitation energy for these lines is 23.93 eV. This energy is below and reasonably close to the  $\text{He}^+$  energy (24.58 eV), but the energy defect (+0.63 eV) is a bit on the large side for efficient charge transfer.

These transitions are well established lasing lines in He-Zn ion lasers. It has been suggested, however, by Green *et al.* [24] that it is the 5d level that is first populated by charge transfer from  $\text{He}^+$  and that the 4f level is populated by collisional de-excitation. In He-Zn ion lasers the 5d level is also a source of lasing transitions with the transitions occurring from the 5d to the 5p levels of Zn ion at wavelengths of 610.254 nm and 602.126 nm. These lines are observable in our He glow discharge and are shown in Fig. 4.15. The excitation energy of these lines is 14.63 eV. The total excitation energy (14.63 + 9.39) is now 24.02 eV resulting in an energy defect of +0.54 eV, smaller than for the 4f levels but still somewhat on the large side. However, all these lines do exist specifically in the He discharge spectra (Figs. 4.14 and 4.15) and in He-Zn lasers [14,15]. Charge transfer driven by  $\text{He}^+$  seems the most logical explanation for the excitation of these levels. This process is summarized in Fig. 4.16.

An interesting group of ZnII lines is found just above 200 nm and spectra of this region for the three discharge filler gases are shown in Fig. 4.17. For the Ar discharge the most intense line in this region is the ZnI 213.856 nm neutral atom resonance line but somewhat weak emission (in a relative sense) is also seen from the ZnII lines at 202.551 nm and 206.191 nm and the ZnII lines at 206.425 nm and 209.986 nm. The first two of these Zn ion lines are low energy ion lines with excitation potentials of 6.12 eV and 6.01 eV respectively. They are the result of transitions from the 4p to the 4s levels of  $\text{Zn}^+$  (see Fig. 4.12) and are the ground state



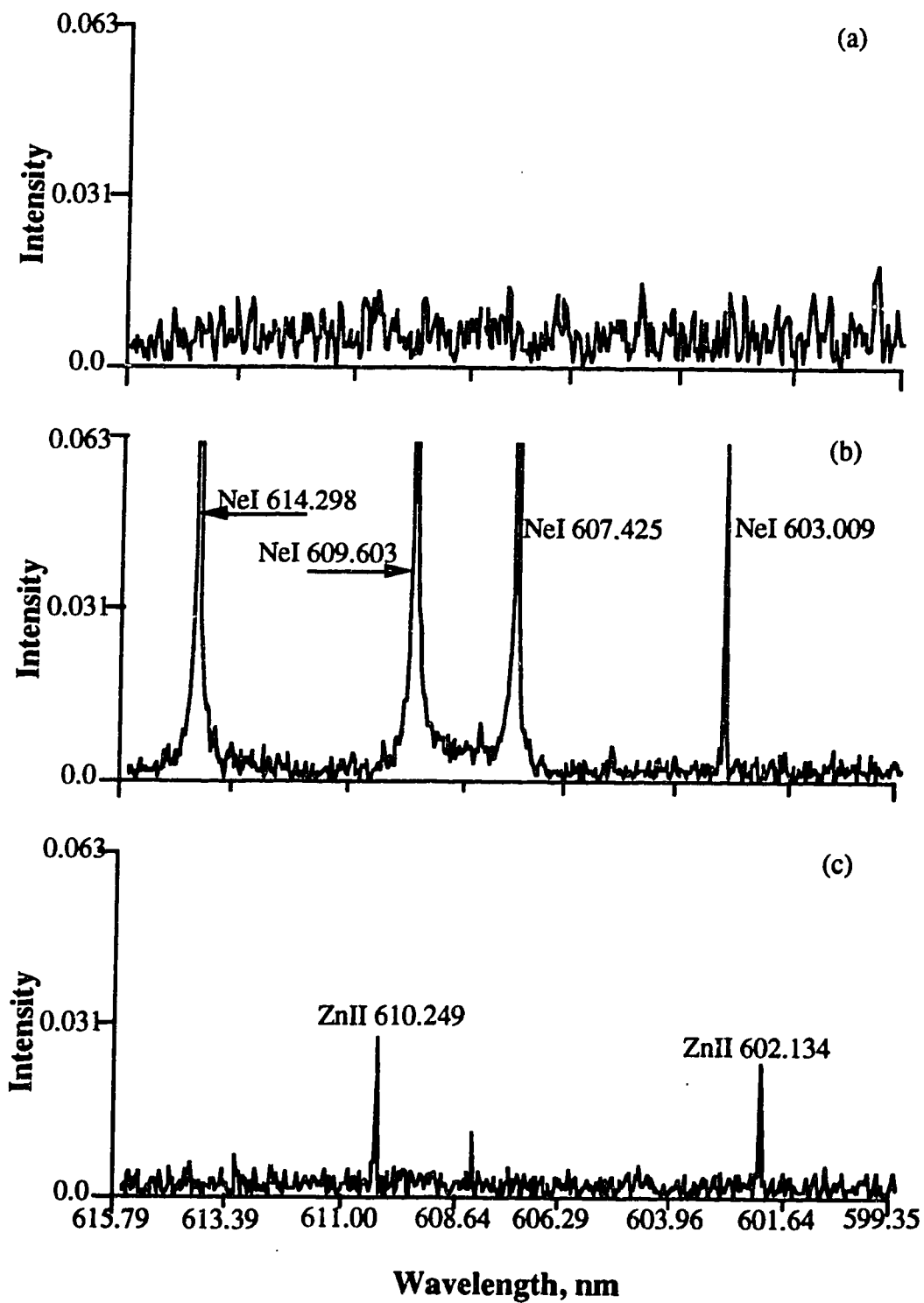


Fig. 4.15 ZnII lines from 5d to 5p transitions populated by He<sup>+</sup> - Zn Charge transfer.

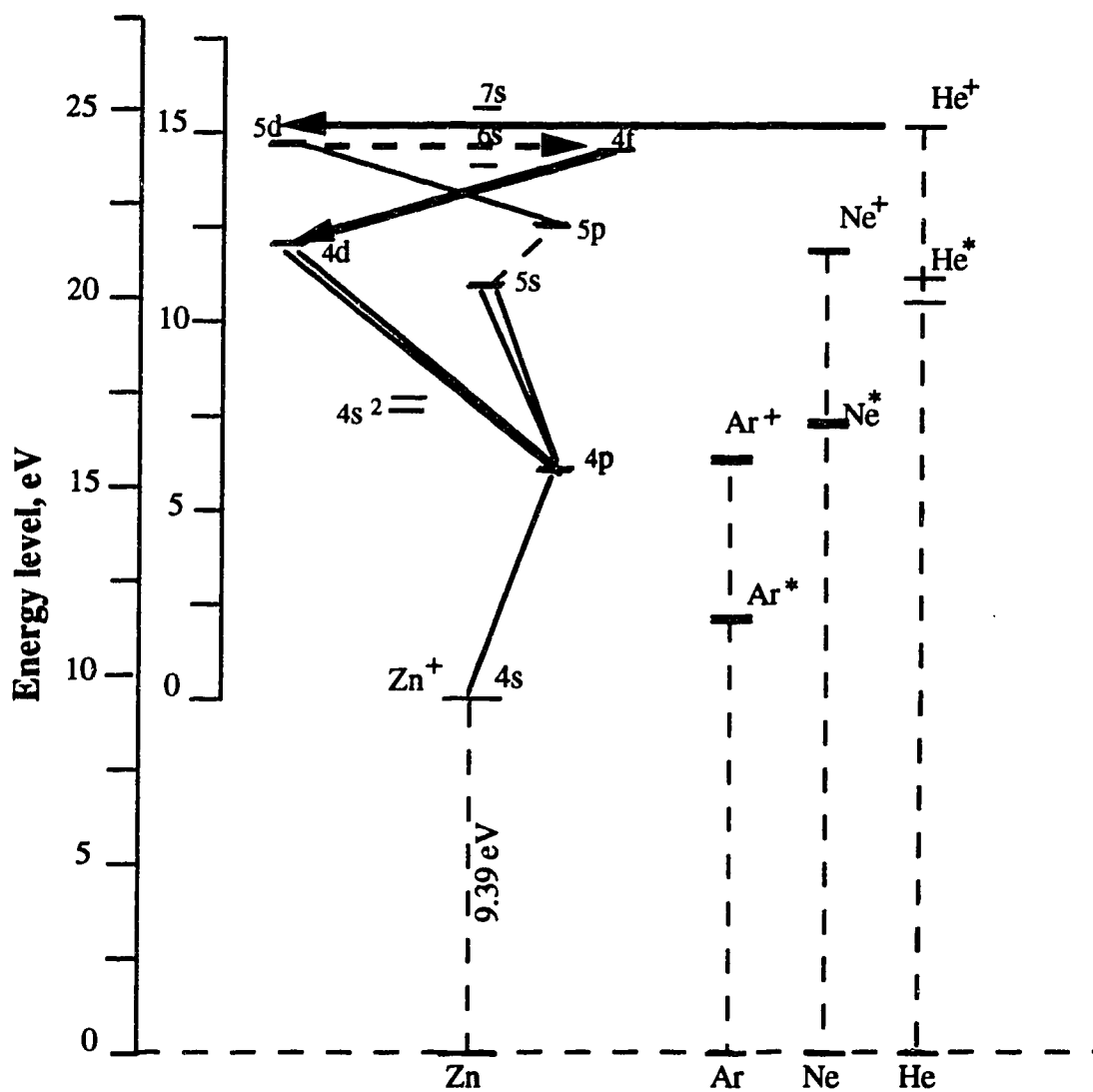


Fig. 4.16 Illustration of the 4f - 4d transitions enhanced by He<sup>+</sup> - Zn Charge transfer.

resonance lines of the ion. The second two Zn ion lines mentioned above are higher energy lines with excitation potentials of 12.03 eV and 12.02 eV respectively. They are the result of transitions from the 4d to the 4p levels of  $\text{Zn}^+$  (see Fig. 4.12).

It would appear that charge transfer with  $\text{Ar}^+$  has the potential to populate the 4p levels of  $\text{Zn}^+$ . Adding in the IP of Zn (9.39 eV) the total excitation potentials for these lines are 15.51 eV (202.551 nm) and 15.40 eV (206.191 nm). The energy defects for these lines with the ground state of  $\text{Ar}^+$  (15.76 eV) are +0.25 eV and +0.36 eV. Certainly we have seen cases in this chapter before where charge transfer has occurred with energy defects of this magnitude but, in this case, a dramatic enhancement of the intensity of these lines is not observed.

On the other hand, there is a dramatic alteration in the relative intensities of these lines in the spectrum for the Ne discharge (see Fig. 4.17). All four Zn ion lines are now quite prominent and all are more intense than the ZnI 213.856 nm neutral atom line. The most intense line in this region is now ZnII 209.986 nm, one of the higher energy Zn ion lines originating in a transition from the 4d to the 4p level.

In this case, charge transfer driven by  $\text{Ne}^+$  seems to be operative. For the ZnII 209.986 nm line the total excitation energy is 21.41 eV. The energy defect with respect to  $\text{Ne}^+$  (21.56 eV) is now only +0.15 eV. For ZnII 206.425 nm the defect is +0.14 eV. With this smaller energy defect, charge transfer with  $\text{Ne}^+$  to populate the 4d levels of  $\text{Zn}^+$  seems to be an effective process.

Not only are the 4d to 4p lines quite strong in the Ne discharge spectrum (Fig. 4.17), but the lower energy 4p to 4s lines (ZnII 202.551 nm and ZnII 206.191 nm) are also quite strong. This seems to be a case again

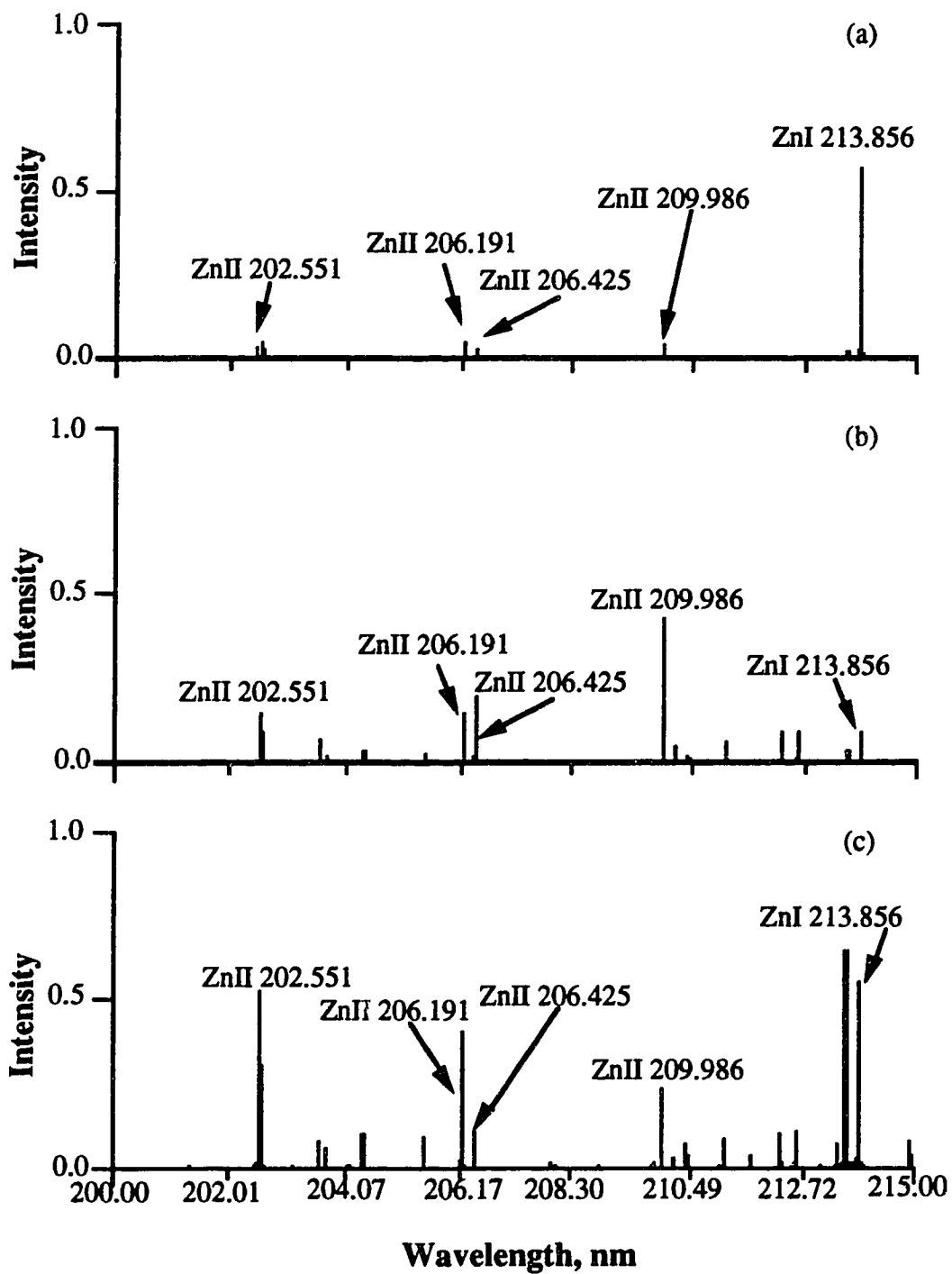


Fig. 4.17 ZnII lines in the vicinity of 206 nm region. (a) Ar, (b) Ne, (c) He.

of stepwise de-excitation driving the excitation of the 4p level with subsequent emission of these lower energy lines analogous to the stepwise de-excitation processes discussed earlier in conjunction with the Cu ion spectra. These steps are schematically illustrated in Fig. 4.18.

Finally, both of these pairs of high and low energy ZnII lines are observed in the He discharge spectrum shown in Fig. 4.17. The lines are all quite strong and on a relative scale, comparable in intensity to that of the ZnI 213.856 nm line. As shown earlier the 4f level of Zn<sup>+</sup> can be populated by charge transfer processes involving He<sup>+</sup>. Stepwise de-excitation would lead to emission from these 4d to 4p and 4p to 4s transitions. These excitation and stepwise de-excitation processes involving He<sup>+</sup> charge transfer are summarized in Fig. 4.19.

### 4.3.3 Ag Ion Lines

The UV spectra for a glow discharge with a silver cathode are shown in Fig. 4.20 for Ar and He filler gas situations. In this case spectra were not obtained with Ne as the filler gas. The two spectra shown in Fig. 4.20 are dramatically different and clearly the excitation conditions in He are quite different than in Ar, a point noted by Duffendack and Thomson back in 1933 [18]. The six most intense lines for the Ar case are listed in Table 4.3 along with the four most intense lines for the He case. All the lines listed for the Ar filler gas spectrum are ion lines with excitation energies above the ground state ion of about 10 to 11 eV and all due to transitions from the 5p level of the ion to the 5s level [25] (see Fig. 4.21). Three of the lines listed for the He case are also 5p to 5s lines but are considerably enhanced, in a relative sense, compared to some of the other 5p to 5s lines. The fourth line listed for the He case is 271.206 nm and it does not appear

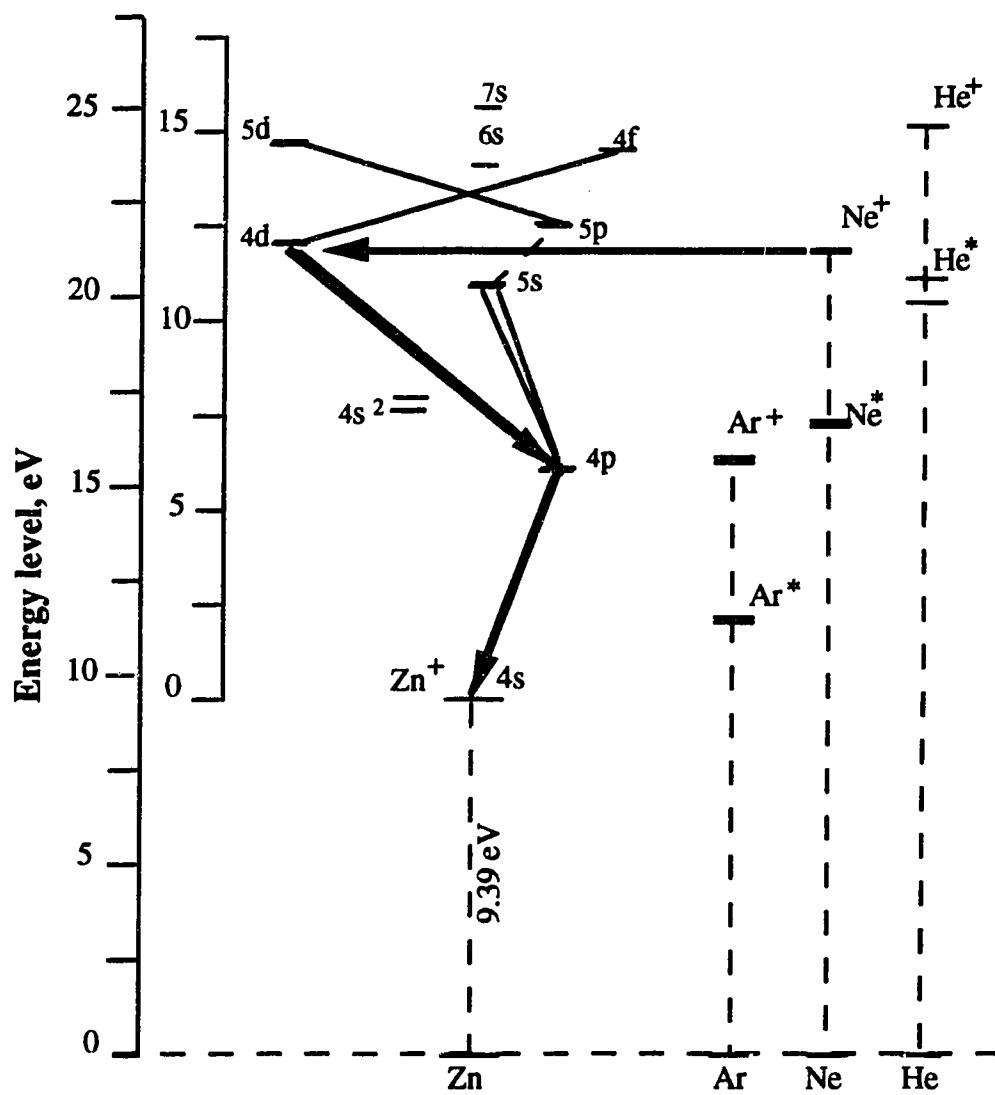


Fig. 4.18 A schematic diagram illustrating the charge transfer from  $Ne^+$  to Zn populating the  $Zn^+$  4d states followed by cascading.

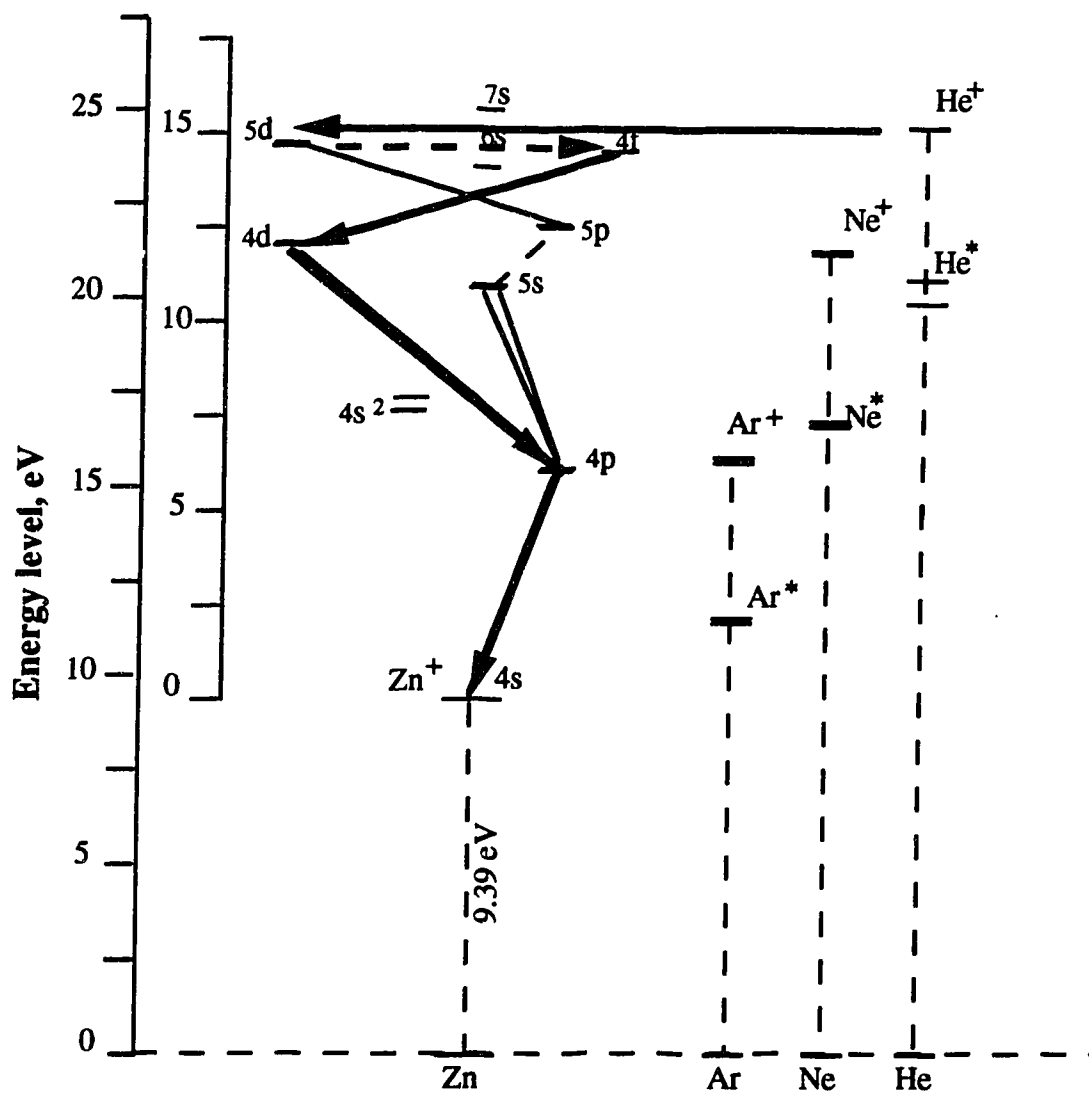


Fig. 4.19 He<sup>+</sup> populating Zn<sup>+</sup> 5d level by charge transfer and enhancing the 4d-4p and 4p-4s transitions.

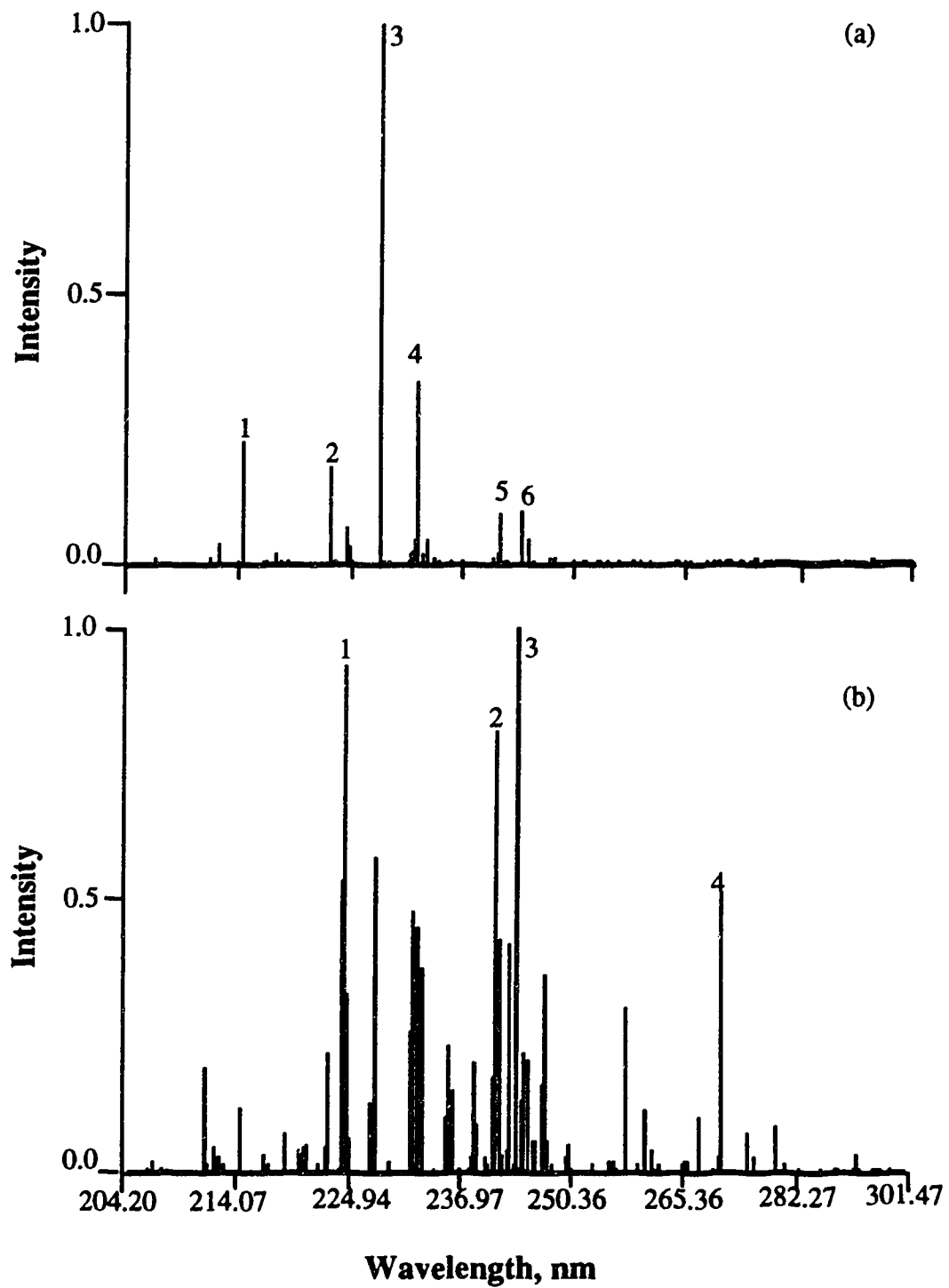


Fig. 4.20 Comparison of Ag UV spectra in argon and helium discharges.

(a) argon, (b) helium.



**Table 4.3. Major AgII Lines Observed in the UV Spectra**

**(a) AgII lines for Ar filler gas case**

No.	Wavelength, nm	Energy, eV
1	214.561	11.20
2	222.952	11.27
3	227.998	11.13
4	232.029	11.05
5	241.318	10.18
6	243.779	9.98

**(b) Ag II lines for He filler gas case**

No.	Wavelength, nm	Energy, eV
1	224.642	10.36
2	241.318	10.18
3	243.779	9.98
4	271.206	14.94

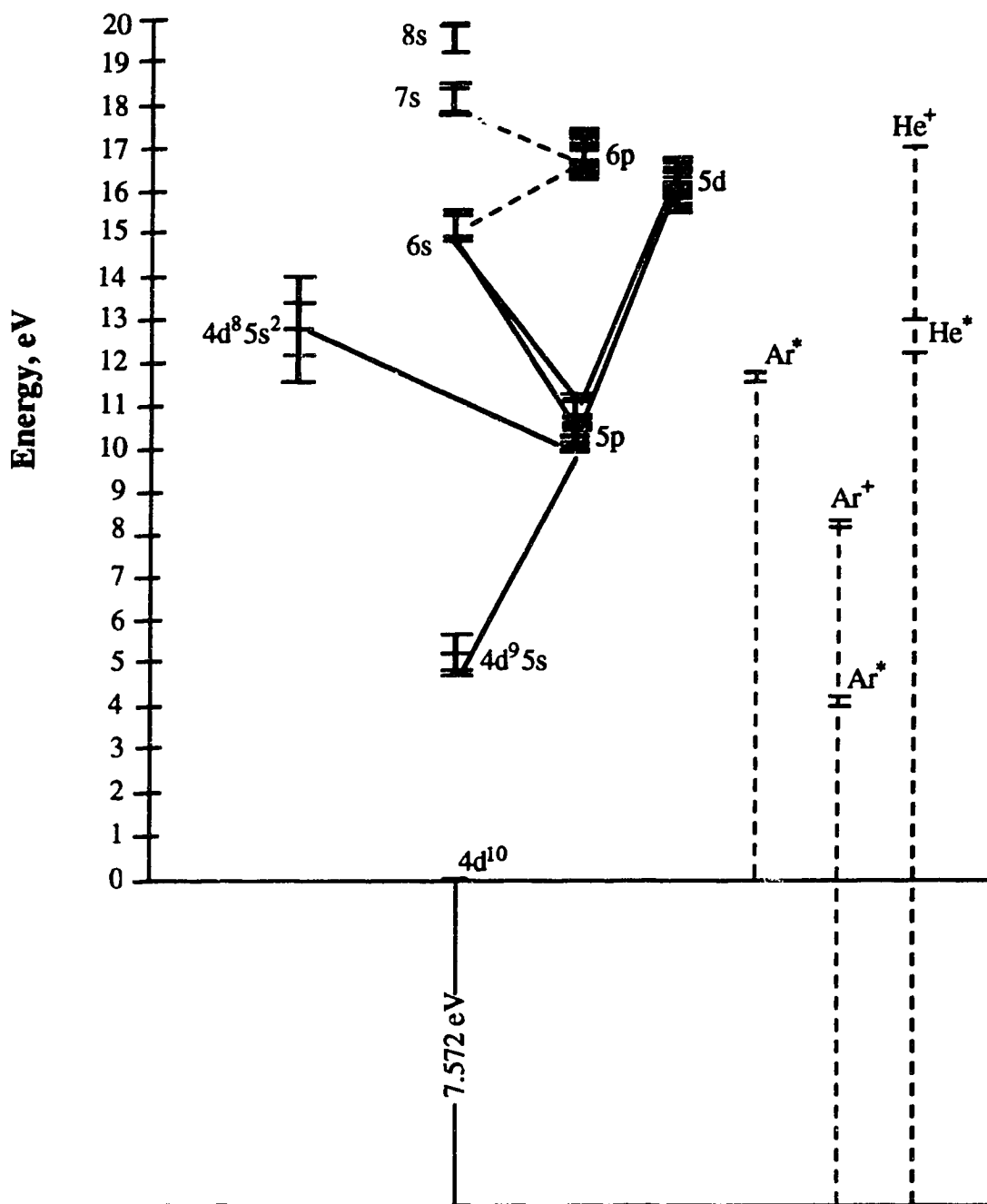
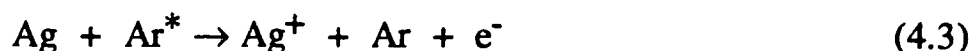


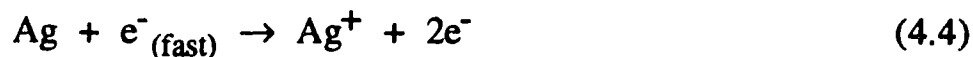
Fig. 4.21 A simplified energy diagram of Ag ion and the metastable and ionization potentials of the discharge gases.

when Ar is the filler gas. This line has an excitation potential of 14.94 eV and is the result of a transition from the 6s level to the 5p level of silver ion [25].

As mentioned above, all the silver lines observed in this region with Ar as the filler gas are ion lines. They are also all the result of transitions from the 5p to the 5s level. The excitation energies of the 5p levels of silver above the ground state ion fall just below the energy level of the Ar metastable level ( $\text{Ar}^*$ ) which has an energy of 11.56 eV. It seems that the excitation mechanism in this case involves a two step process. In the first step silver is ionized, perhaps by Penning ionization:



or direct electron impact:



and then the ion is excited to the 5p level by collision with an argon metastable:



This second reaction would require energy matching on a par with charge transfer reaction ( $\leq 0.5$  eV). Such is the case for the  $\text{Ar}^*$  (11.56 eV) and most of these 5p levels. This process is depicted schematically in Fig. 4.22.

In order to clarify excitation processes when He is the filler gas, it is necessary to look at expanded sections of the spectra shown in Fig. 4.20.

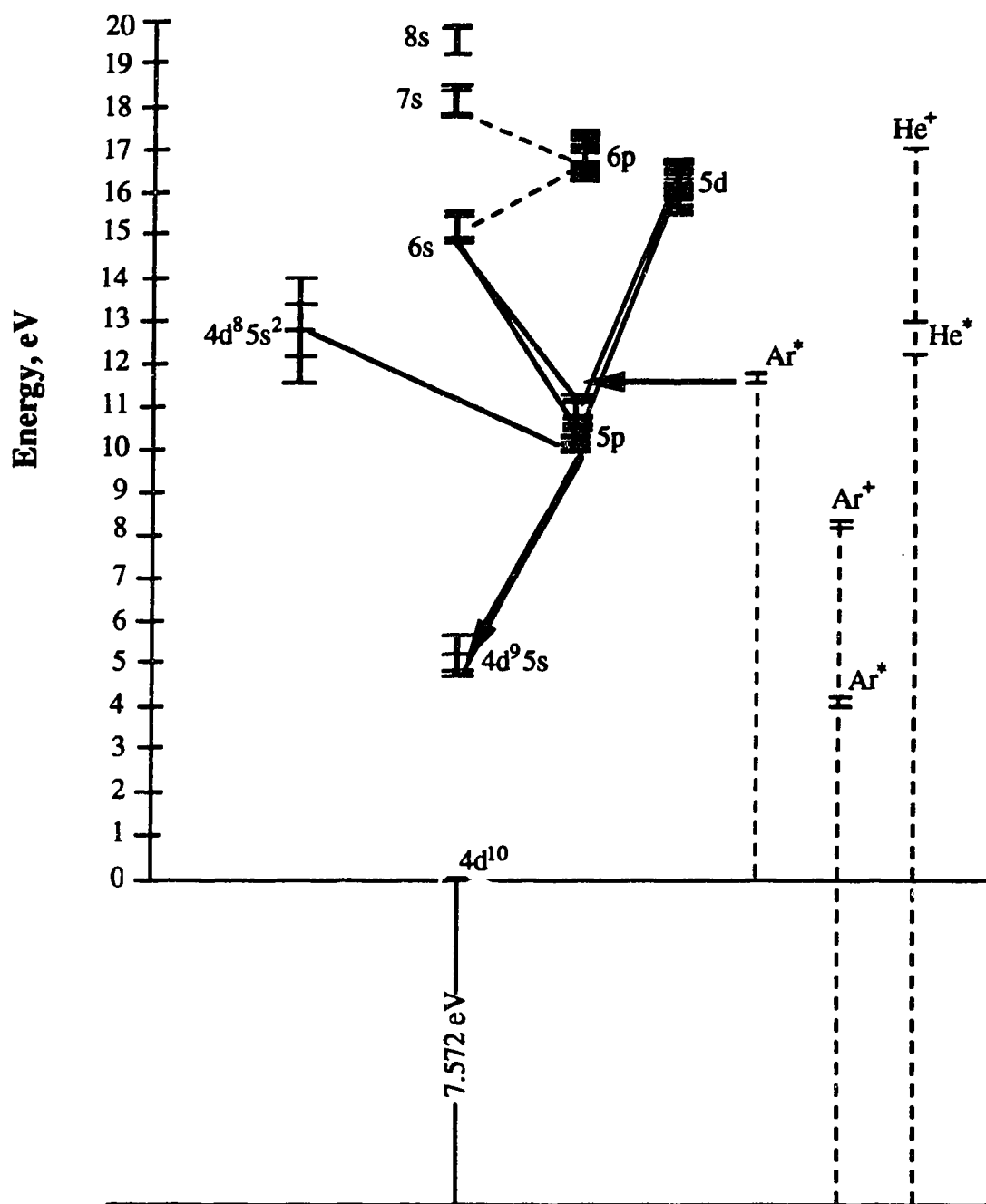


Fig. 4.22 A possible path of excitation of  $\text{Ag}^+$  by Ar metastable atoms.

Expanded scale spectra centered at about 242 nm are shown in Fig. 4.23. The eight most intense lines are listed in Table 4.4. The three lines observed in both spectra (lines 2, 5 and 7) are all 5p to 5s transitions. The other five lines (1, 3, 4, 6, 8) were only observed when He was the filler gas. These lines are all of higher excitation energy, as high as 16.38 eV, and are all 5d to 5p transitions. Adding in the ionization potential for Ag (IP = 7.57 eV) the total excitation energy is 24.13 eV. This leaves a +0.63 eV energy defect for charge transfer with  $\text{He}^+$  (24.58). Thus, for the He discharge, the 5d levels of  $\text{Ag}^+$  can be excited by charge transfer with  $\text{He}^+$  and the observed emission of 5d to 5p and then 5p to 5s lines is a result of stepwise de-excitation. This process is depicted schematically in Fig. 4.24.

This same scenario can be verified throughout this spectral region. Expanded spectra in the 213 nm region are shown in Fig. 4.25 and the lines are listed in Table 4.5. Again the lower energy 5p to 5s transitions are observed in both spectra while the higher energy 5d to 5p transitions are seen only when He is the filler gas.

He-Ag hollow cathode discharges have been the basis of  $\text{Ag}^+$  lasers [17,26-28]. In the UV region the two lines cited for lasing action are the 224.344 and 227.743 nm lines, both a result of 5d to 5p [17] transitions. In this literature, charge transfer from  $\text{He}^+$  is the suggested excitation mechanism for these lines. Expanded scale spectra in the vicinity of these two lines are shown in Figs. 4.26 and 4.27 and the observed lines and energies are listed in Table 4.6. The two lasing transitions are distinctly and exclusively observed in the He filler gas spectra. Thus the  $\text{He}^+$  charge transfer into the 5d level of  $\text{Ag}^+$  with subsequent stepwise de-excitation to the 5p and 5s levels sets much of the spectral character of  $\text{AgII}$  in the UV spectral region in the He filled glow discharge.

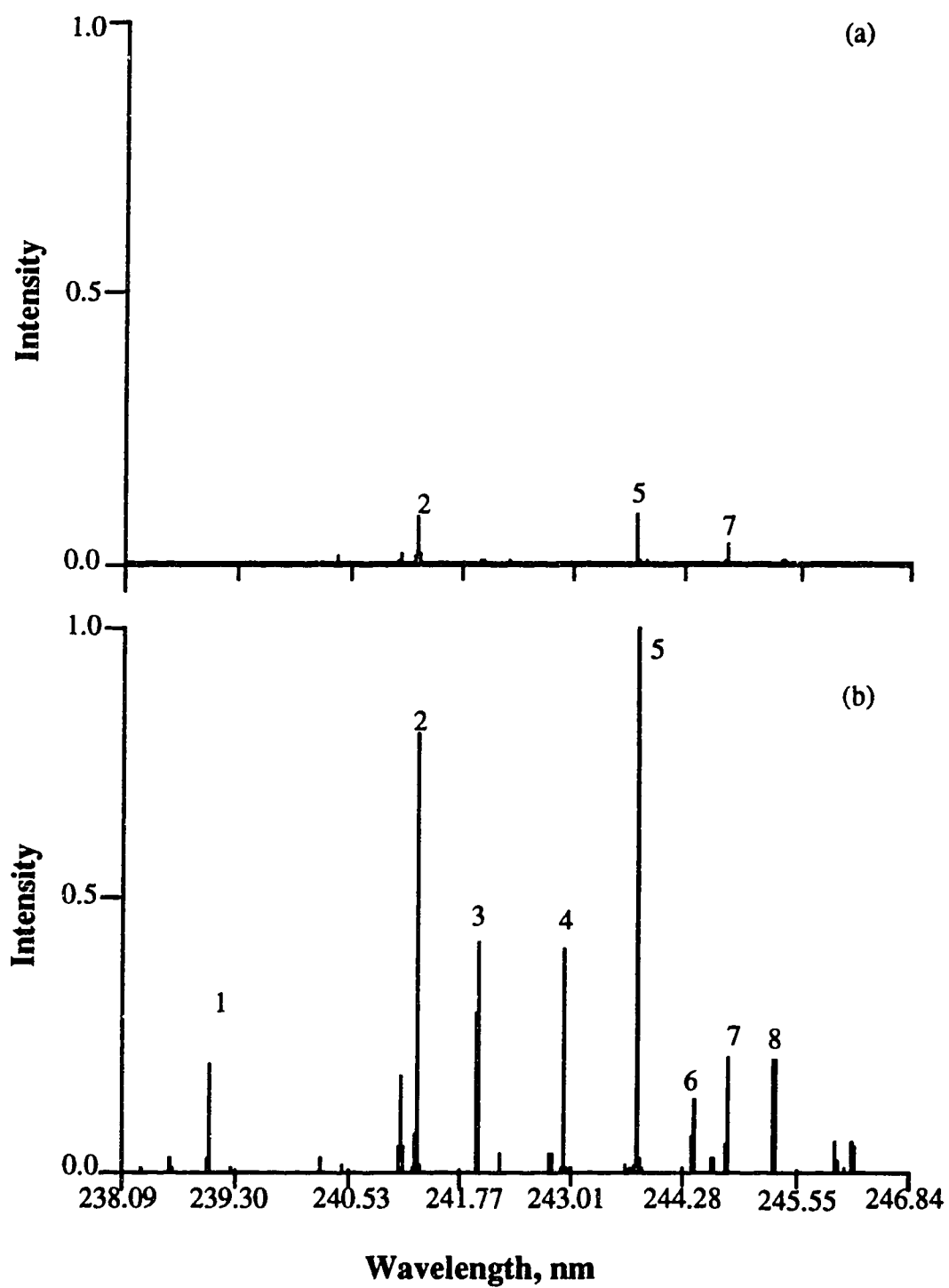


Fig. 4.23 A section of Ag<sup>+</sup> spectra in the 242 nm region showing the difference of line intensities in the two gases. (a) Ar, (b) He.

Table 4.4. AgII Lines in the 242 nm Region

No.	Wavelength, nm	Energy, eV	Spectrum
1	239.054	16.38	He
2	241.318	10.18	Ar, He
3	242.007	16.38	He
4	242.964	15.81	He
5	243.779	9.93	Ar, He
6	244.421	16.33	He
7	244.789	10.77	Ar, He
8	245.333	15.76	He

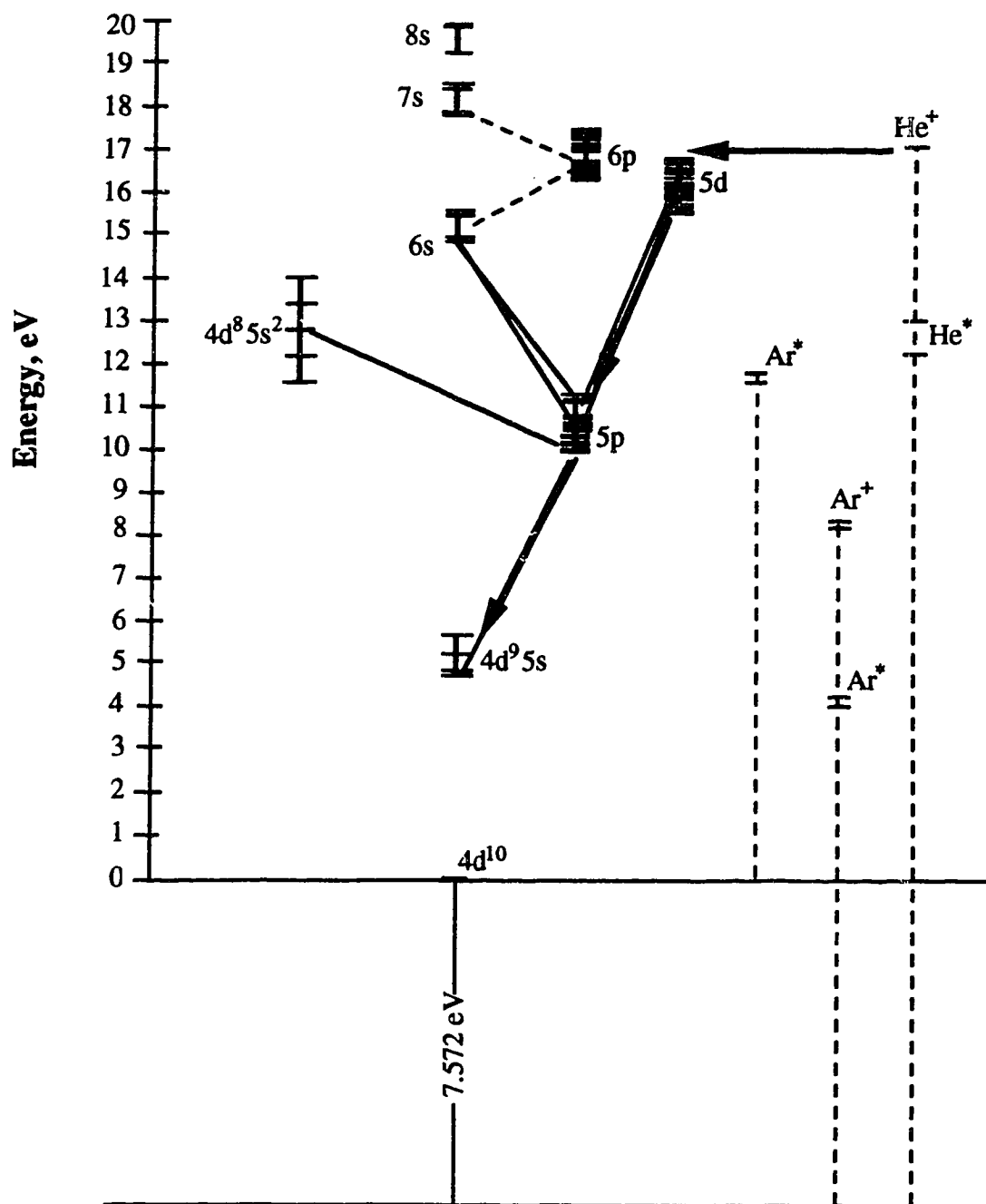


Fig. 4.24 Illustration of charge transfer between He<sup>+</sup> and Ag populating the 5d level and a cascading process.



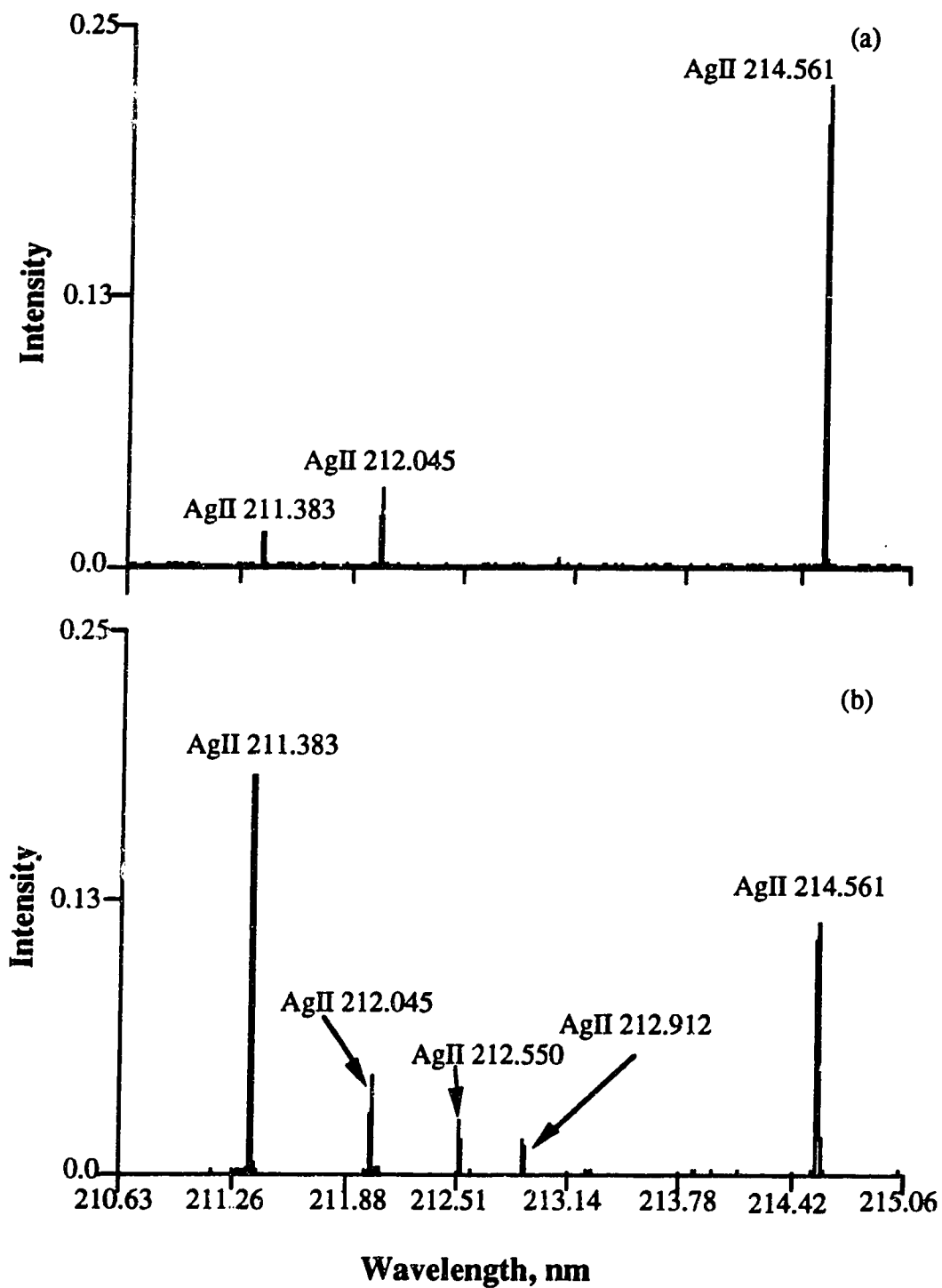


Fig. 4.25 A portion of AgII spectra showing the lines from 5d - 5p transitions only appear in the He discharge. (a) Ar, (b) He.

**Table 4.5. Ag II lines in the 213 nm Region**

<b>No.</b>	<b>Wavelength, nm</b>	<b>Energy, eV</b>	<b>Spectrum</b>
1	211.383	10.71	Ar, He
2	212.045	11.27	Ar, He
3	212.550	15.77	He
4	212.912	16.37	He
5	214.561	11.20	Ar, He

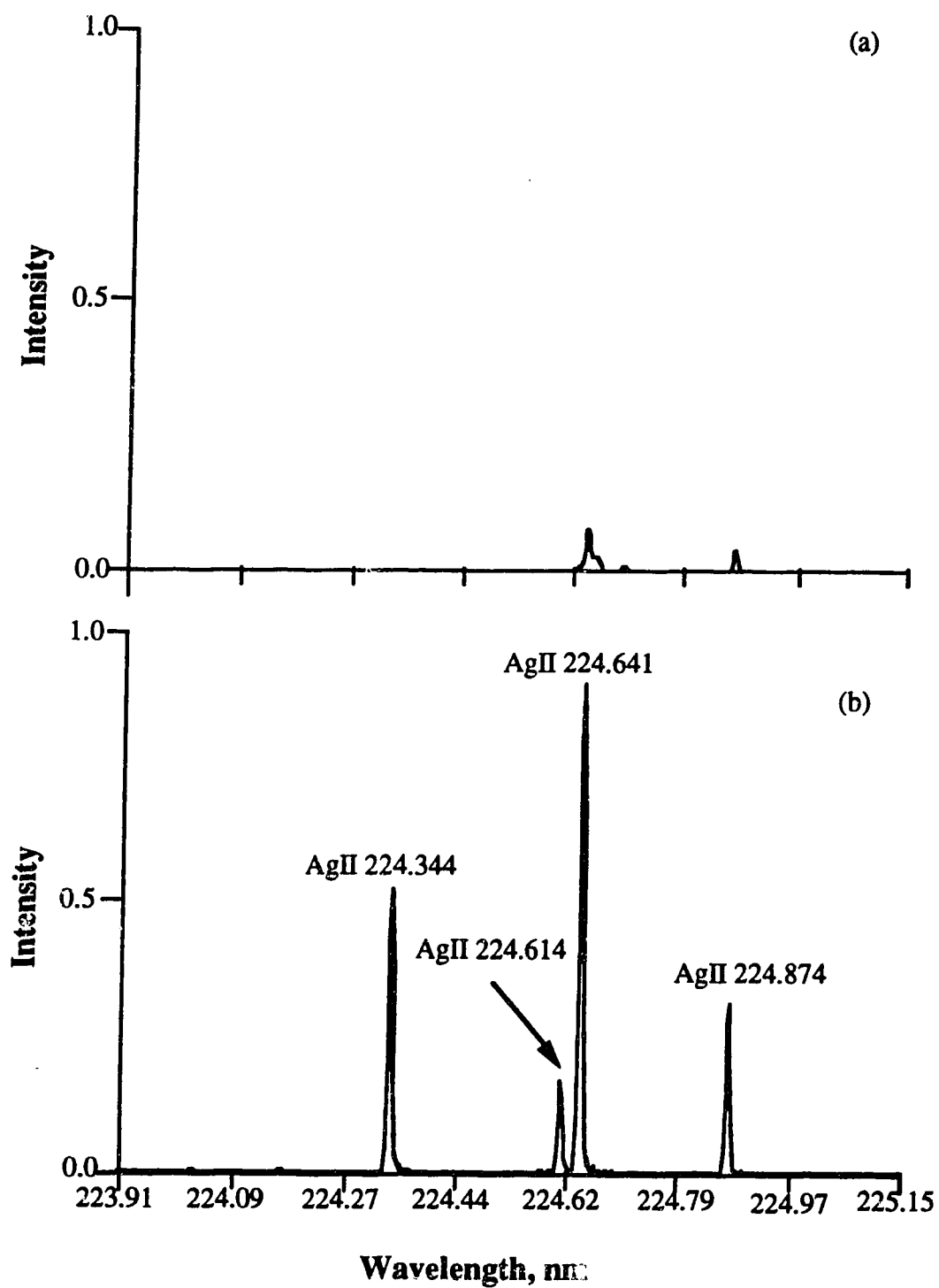


Fig. 4.26 Some of the AgII lines in the vicinity of 224 nm generated from the 5d - 5p transitions. (a) Ar, (b) He.

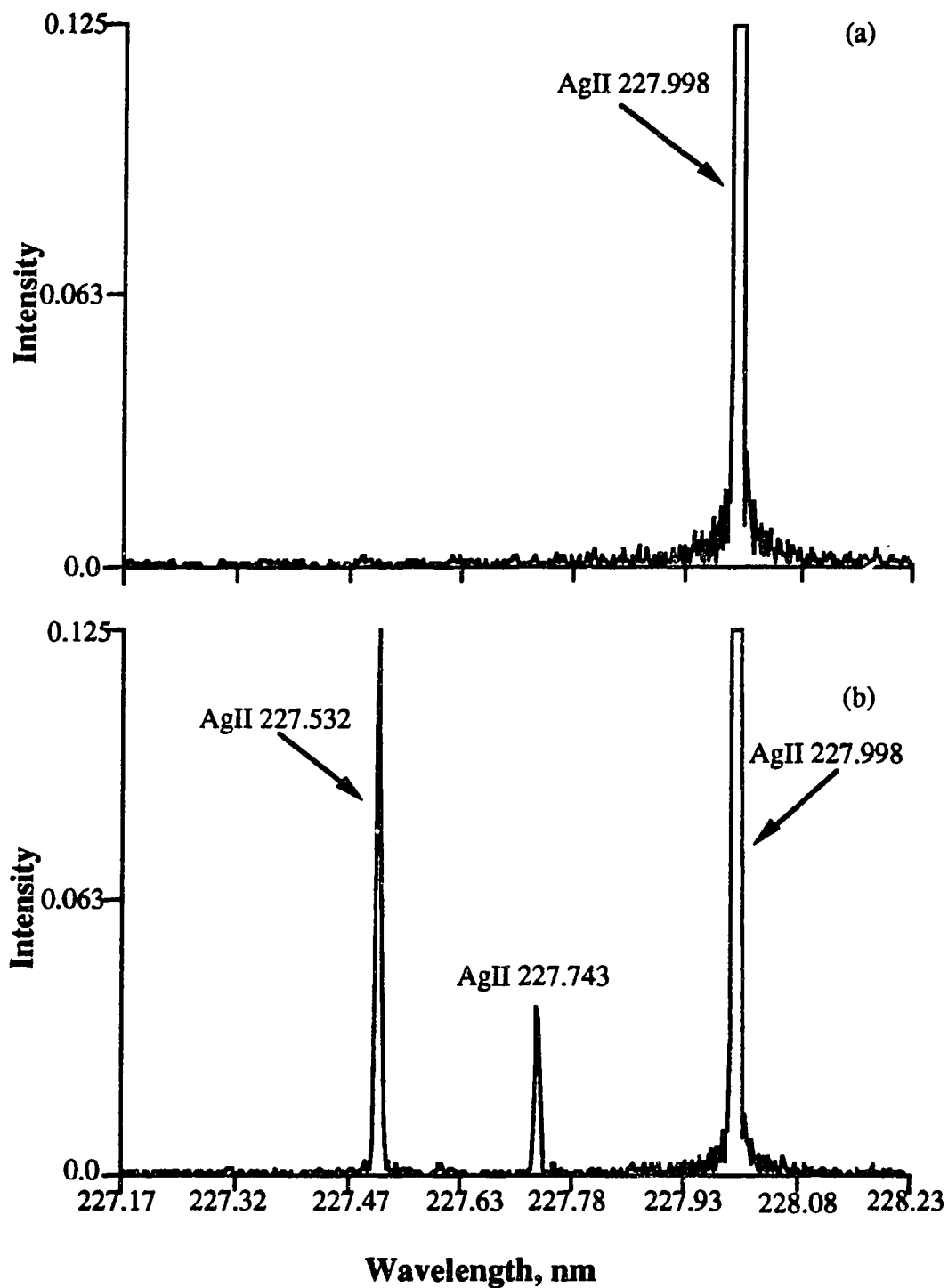


Fig. 4.27 Expanded spectra showing AgII 227.532 and 227.743 nm lines only appear in the He discharge.(a) Ar, (b) He.

**Table 4.6. AgII Lines in the 224 and 228 nm Spectral Regions**

**(a) 224 nm Region**

No.	Wavelength, nm	Energy, eV	Spectrum
1	224.344	16.50	He
2	224.614	15.70	He
3	224.641	10.36	Ar, He
4	224.874	10.55	Ar, He

**(b) 228 nm Region**

No.	Wavelength, nm	Energy, eV	Spectrum
1	227.532	15.82	He
2	227.743	15.81	He
3	227.998	11.13	Ar, He

An interesting and somewhat different charge transfer and stepwise de-excitation process is indicated by the spectral lines present in the 268 nm spectral region. Expanded scale spectra for this region are shown in Fig. 4.28 and the major lines observed are listed in Table 4.7. As can be clearly seen from the spectra, these lines were only observed when He was the filler gas. All these lines are the result of transitions from the 6s level of silver ion to the 5p level [25]. Several of these lines have an excitation energy of about 15 eV. The total excitation energy is then  $(15 + 7.57)$  22.57 eV which leaves a large energy defect of about 2 eV with respect to charge transfer excitation by  $\text{He}^+$ . It is not expected that charge transfer would occur for such a large energy defect. Nevertheless, the lines are there.

However lasing action has been observed in the near-infrared for the silver ion lines at 840.38, 825.47 and 800.54 nm [28]. These lines have excitation potentials of 16.41, 16.49 and 16.49 eV and are the result of transitions from the 6p level of silver ion to the 6s level. For the 16.49 eV lines the energy defect for charge transfer with  $\text{He}^+$  is now only +0.52 eV, a value at which charge transfer with  $\text{He}^+$  clearly occurs. We did not make measurements to directly observe these lines, but stepwise de-excitation of the 6p to the 6s to the 5p level can explain the observation of the 6s to 5p transitions shown in Fig. 4.28. These processes are shown schematically in Fig. 4.29.

#### 4.3.4 Cd Ion Lines

The UV spectra for a glow discharge operating with a cadmium cathode are shown in Fig. 4.30 for Ar and He filler gas situations. In this case the same major lines are observed in both spectra and they are listed in

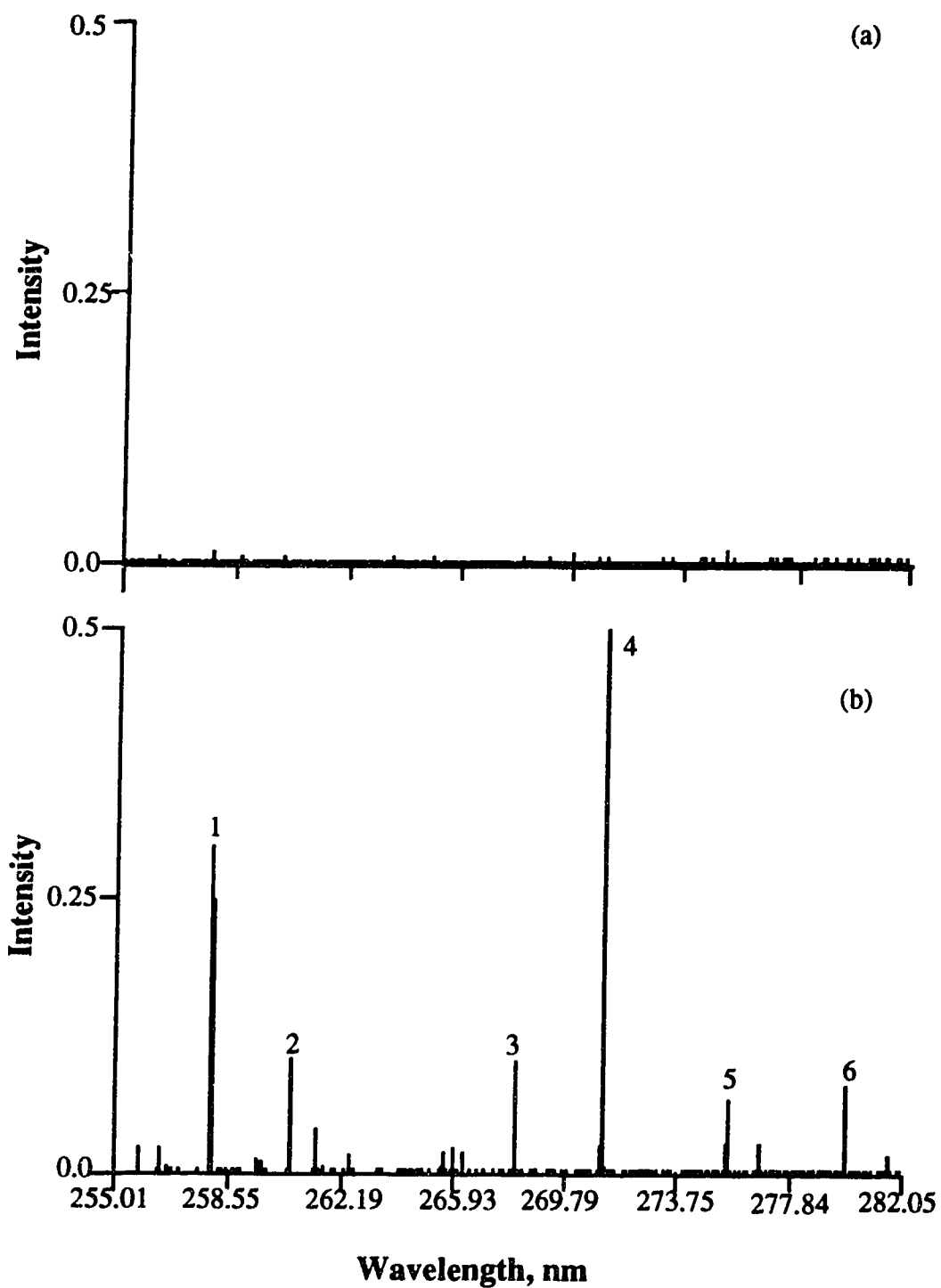


Fig. 4.28 Expanded spectra section in the vicinity of 268 nm showing the 6s -5p transition lines in He discharge. (a) Ar, (b) He.

**Table 4.7. AgII Lines in the 268 nm Region**

No.	Wavelength, nm	Energy, eV
1	258.074	14.98
2	260.616	14.94
3	268.138	14.98
4	271.651	15.54
5	275.651	15.54
6	279.966	14.98



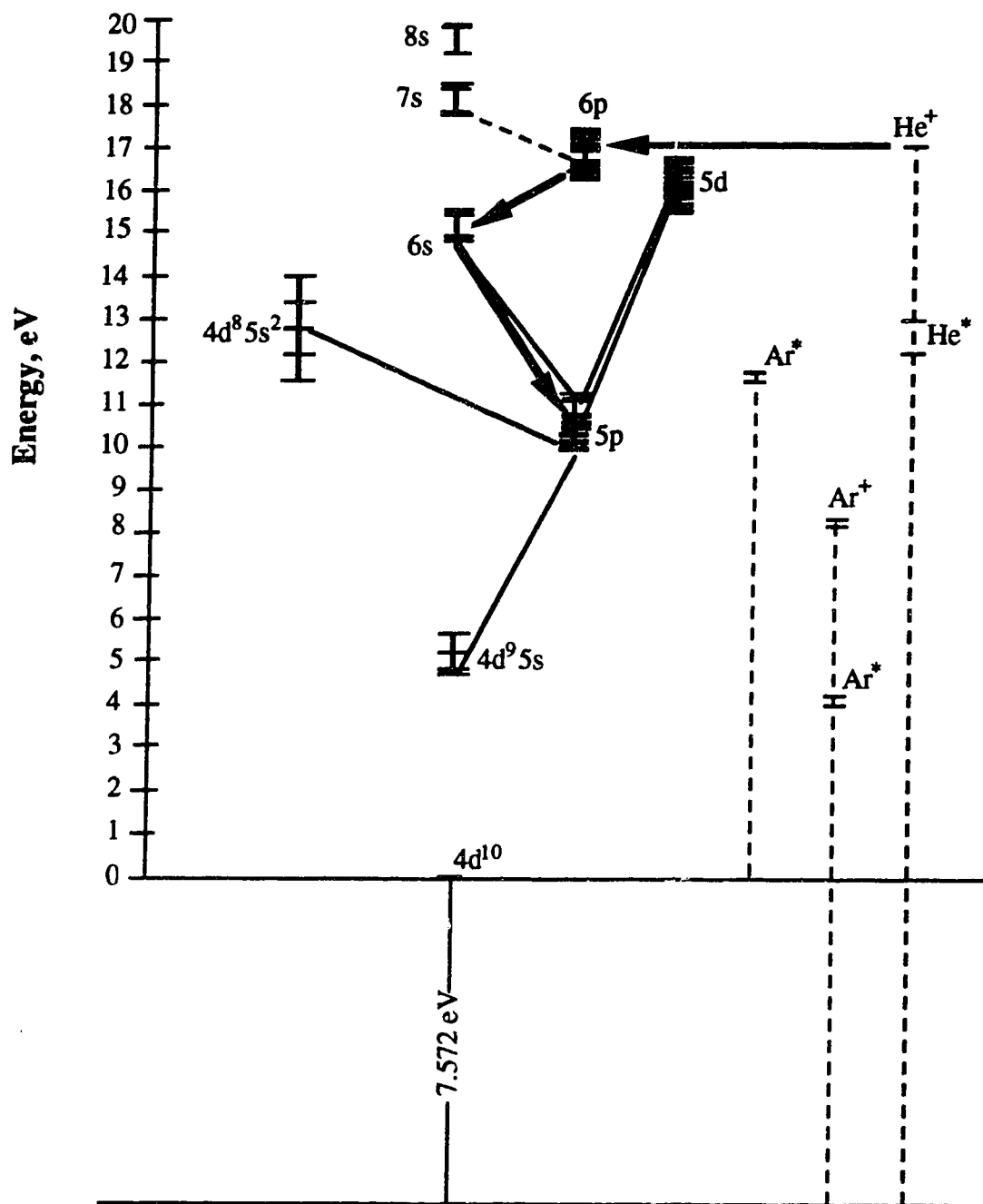


Fig. 4.29 A path of  $He^+$  - Ag charge transfer enhancing the 6s - 5p transitions.

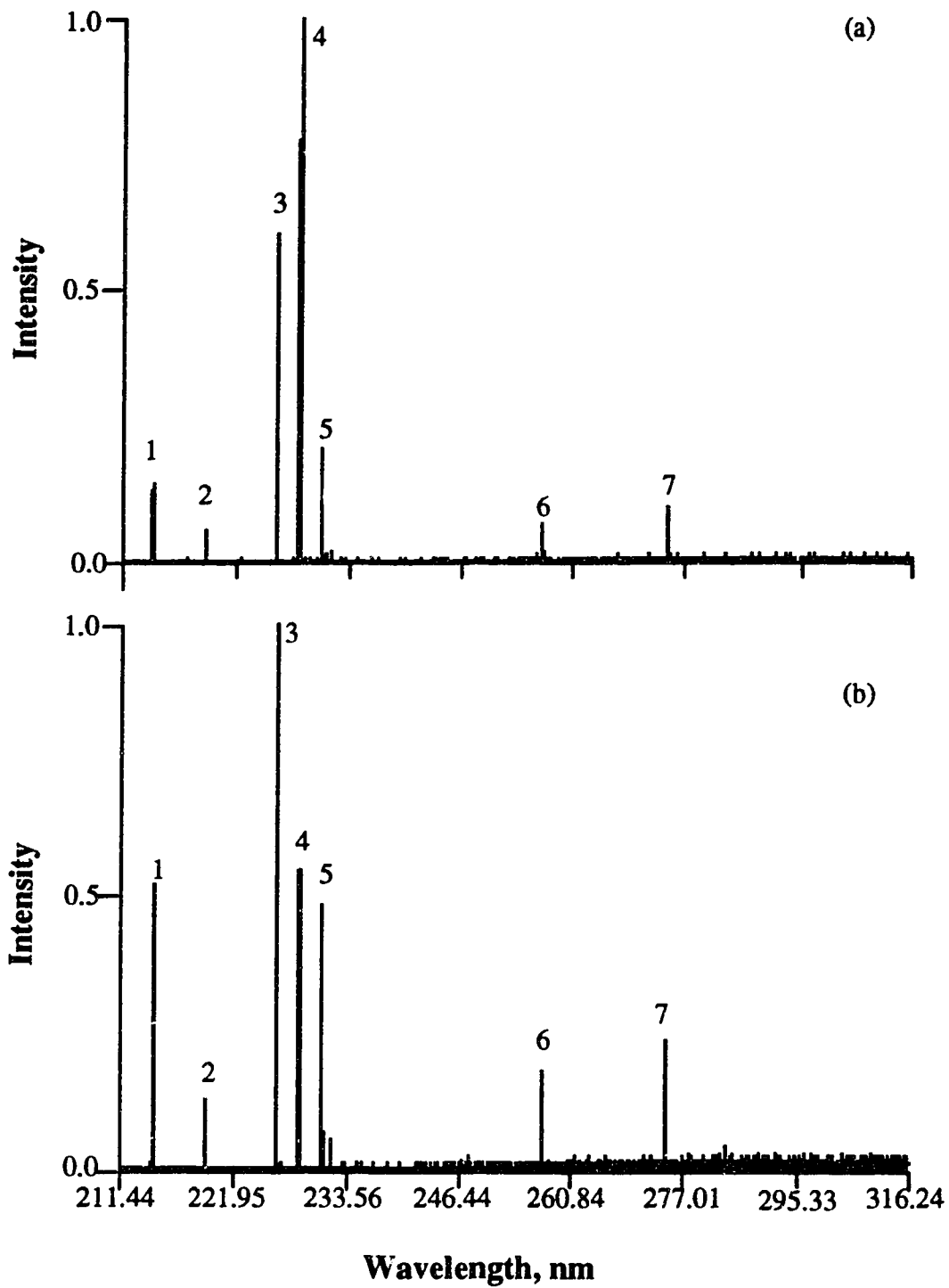


Fig. 4.30 Comparison of Cd<sup>+</sup> spectra in Ar (a) and He (b) discharges.

Table 4.8. All the lines except the 228.802 nm line are ion lines. The main difference between the two spectra are that the ion line intensities are all enhanced relative to the neutral atom line in the He filler gas spectrum compared to the Ar filler gas spectrum.

The higher energy cadmium lines (219.456 / 231.277, and 257.293 / 274.858 nm) come from different transitions. The 219 / 213 pair are a result of 5d to 5p transitions and the 257 / 274 pair are a result of 6s to 5p transitions [29]. The low energy lines (226 / 214) are a result of 5p to 5s transitions (See Fig. 4.3).

The presence of ion lines for the Ar filler gas case can be explained by a two step excitation process, followed by stepwise de-excitation. As suggested earlier for silver, Cd is first ionized and then the ions are excited by collision with an argon metastable. The energy of the argon metastable (11.72 eV) is an almost exact match for the 6p level of CdII (11.74 eV). Referring to Fig. 4.31, what seems to happen is that the 6p level of Cd<sup>+</sup> is populated by energy exchange from the argon metastable. The 6p level then relaxes radiatively through 6s→5p→5s or 5d→5p→5s levels. Lines for the 6p to 6s transitions (806.6 and 853.2 nm) occur in the near-IR and have been seen in CdII based metal ion lasers [14]. These processes are illustrated in Fig. 4.32.

For the He filler gas situation the intensities of the lines from both of these levels are enhanced relative to that of the 228.802 neutral atom lines. Based on previous observation presented in this chapter, one could speculate that this is driven by a charge transfer process to higher cadmium ion levels driven by He<sup>+</sup>. This higher cadmium ion level then cascades down stepwise to populate the 6p, 6s, 5d and 5p levels. This can be confirmed by observations in the visible region of the cadmium spectrum.

Table 4.8. Major Cd Lines Observed in the UV Spectra

No.	Type	Wavelength, nm	Energy, eV	Levels
1	CdII	214.441	5.78	5p to 5s
2	CdII	219.456	11.12	5d to 5p
3	CdII	226.502	5.47	5p to 5s
4	CdI	228.802	5.41	?
5	CdII	231.277	11.14	5d to 5p
6	CdII	257.293	10.28	6s to 5p
7	CdII	274.858	10.28	6s to 5p

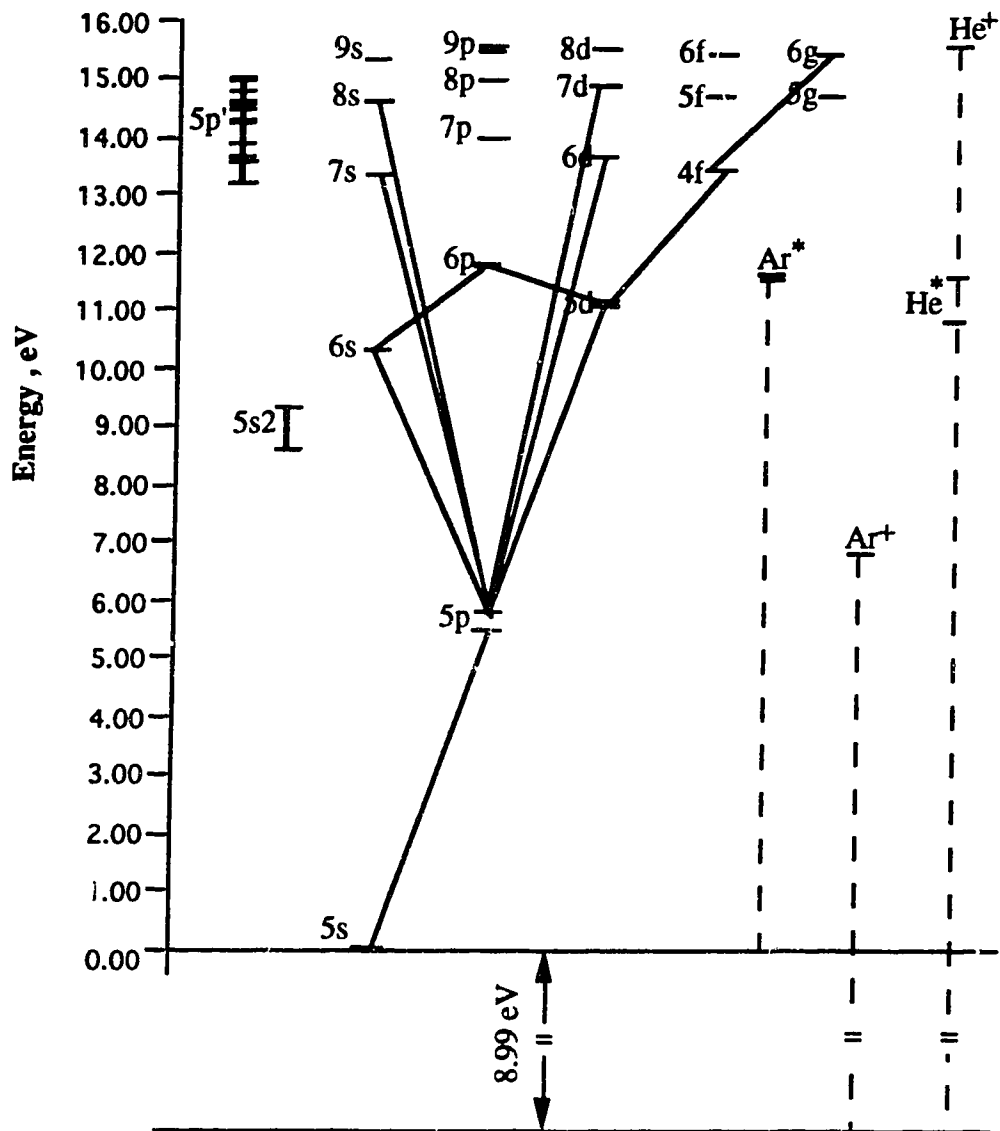


Fig. 4.31 A simplified energy diagram of Cd ion and the metastable and ionization potentials of the discharge gases.

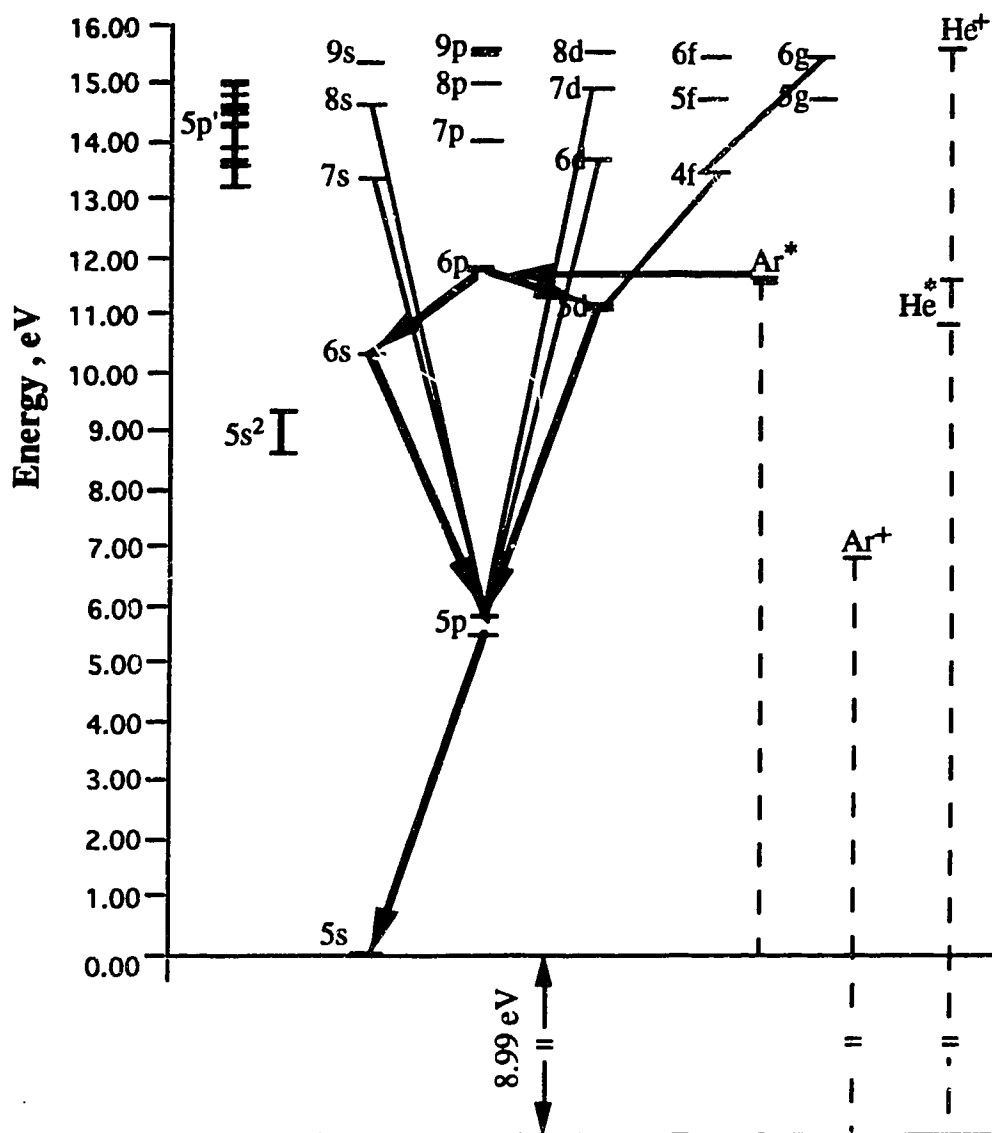


Fig. 4.32 A possible mechanism populating the 6p excited states of Cd<sup>+</sup> and followed by stepwise de-excitations.

Expanded scale spectra in the 520 nm region are shown for both the Ar and He filler gas cases in Fig. 4.33. The CdII 537.809 and 533.753 nm lines are considerably enhanced in a relative sense with respect to the CdI 508.582 nm line in the He situation compared to Ar. These lines are the result of transitions from the 4f to the 5d level of Cd<sup>+</sup> and have an excitation potential of 13.44 eV. The ionization potential of Cd is 8.99 eV, thus the total excitation potential for these lines is 22.43 eV. With respect to He<sup>+</sup> (24.58 eV) the energy defect is +2.15 eV and thus, direct charge transfer excitation of this level is unlikely. However, these transitions are observed in He-Cd metal ion lasers [14] along with CdII 635.993 and Cd 635.472 nm. These lines are a result of transitions from the 6g to the 4f level of Cd<sup>+</sup> and have an excitation energy of 15.39 eV. Now the case for charge transfer is excellent (energy defect +0.2 eV) and the 4f level can be populated by stepwise de-excitation providing a mechanism for excitation of the 537 and 533 nm lines. In fact the stepwise de-excitation can continue all the way down to the 5s level. So in the He filler gas case for Cd<sup>+</sup>, the spectral data indicate that the 6g levels of cadmium ion can be populated by charge transfer with He<sup>+</sup> and the stepwise de-excitation occurs from:



The process is shown schematically in Fig. 4.34.

Collins [14] also observed, as noted above, lasing action for the near IR 6p to 6s transitions at 806.6 and 853.1 nm. He indicated that the 6p level was populated by stepwise de-excitation of the 9s (15.34 eV) and 8d (15.45 eV) levels that were subject to population by charge transfer with He<sup>+</sup>. These processes are also shown in Fig. 4.34. Thus, the observed spectral

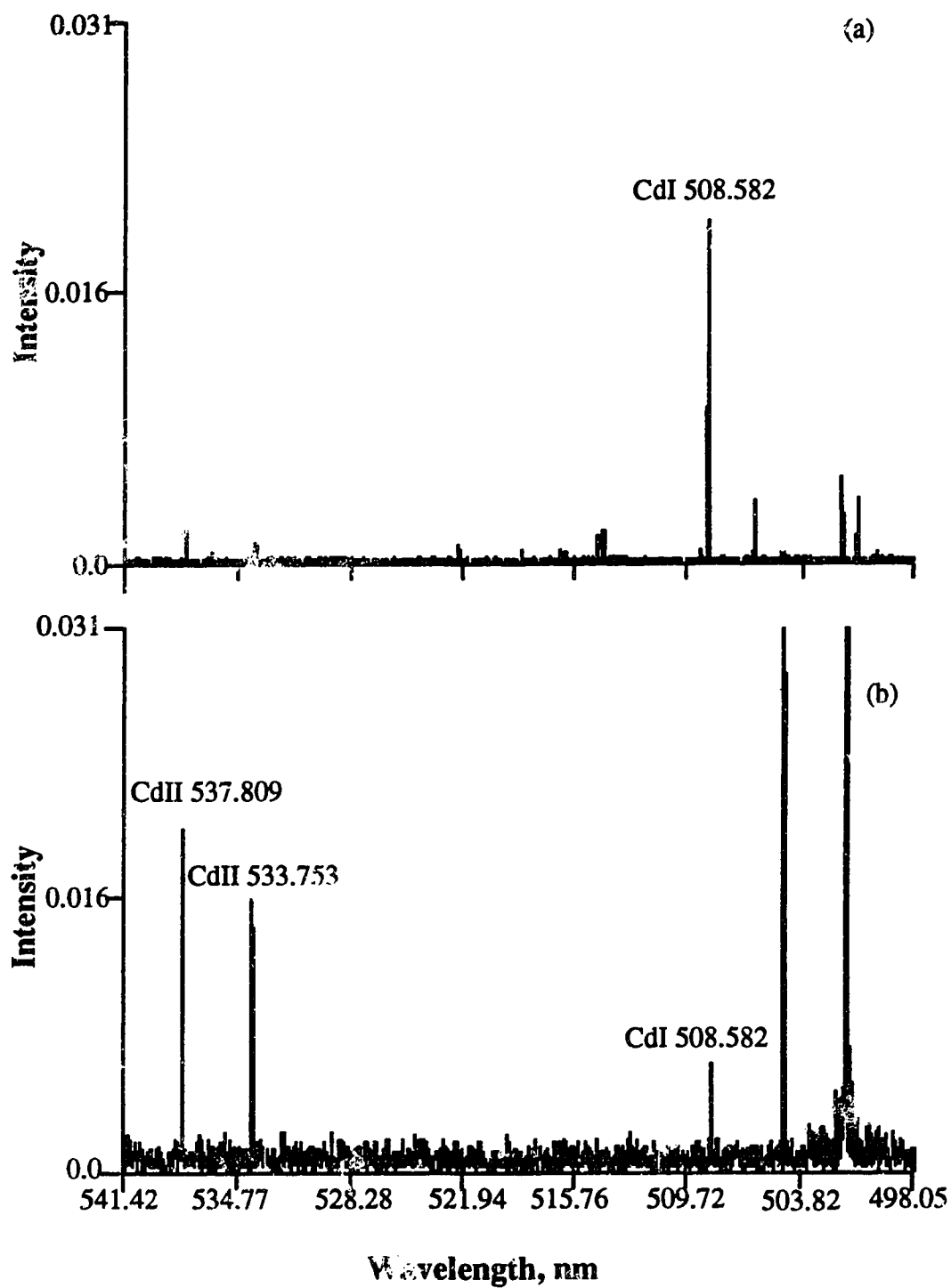


Fig. 4.33 The relative intensities of CdII 537.809 and 533.753 nm lines to the CdI 508.582 nm in Ar (a) and He (b) discharges.



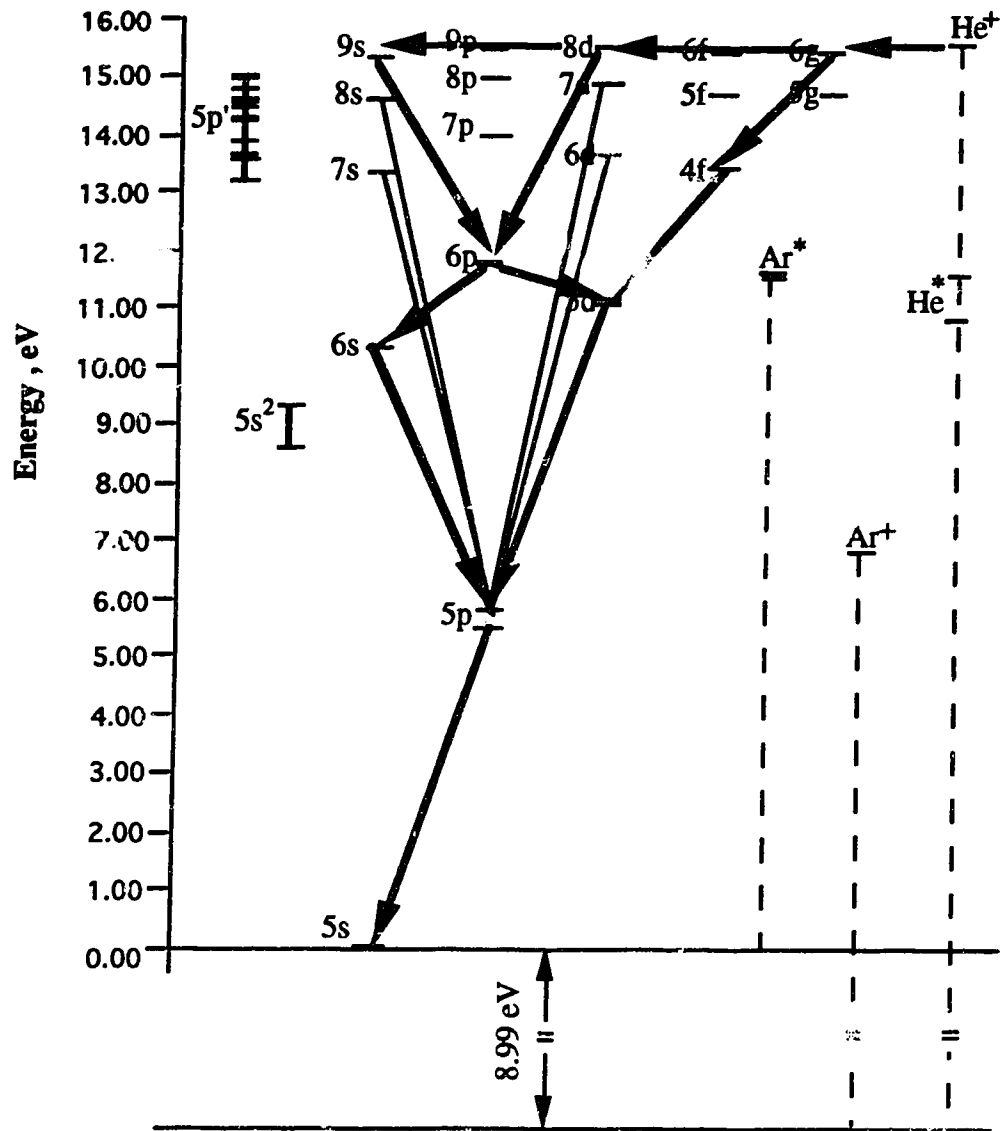


Fig. 4.34 Charge transfer between He<sup>+</sup> and Cd and stepwise de-excitation.

lines in the He discharge reveal an extensive pattern of charge transfer driven excitation followed by many stepwise de-excitation processes.

Collins [14] also observed lasing action from the CdII 441.563 nm line. This line is a result of a transition from a  $5s^2$  level to the 5p level and the line has an excitation potential of 8.59 eV. Its total excitation energy is 17.58 eV and Collins indicated that it was excited by a Penning process by  $\text{He}^*$  [14]. This line was observed in our visible spectra and was certainly enhanced in the case of the He filler gas case (see Fig. 4.35.)

### 4.3.5 The Iron Spectra

The iron spectrum obtained from either the argon discharge, neon discharge, or helium discharge [Chapter 3] is very complicated. However, a general comparison among the spectra obtained from each of these discharges gives us some indication of the dominating processes in the excitation of the ionic transitions. Fig. 4.36 is a portion of the spectra just illustrating the relative intensities of the Fe transitions. Table 4.9 is a list of some of the Fe II lines with their excitation energies and the relative intensities emitted from the three discharge gases. The charge transfer effect is not as outstanding as in the copper and zinc spectra, but we still can see the enhancement of some lines by one of the discharge gases. Fig. 4.37 is a plot of the relative intensity of ionic iron emissions from each of the three discharge plasmas versus the excitation energy. From this figure, it is clear that at the low excitation energy end, all three gases have a similar power of excitation. The selectivity is shown at the high excitation energy end. The most obvious effect is for argon on the Fe II transitions which have excitation energies around 7.6 to 8.0 eV. Because the ionization potential of iron is 7.87 eV, any charge transfer enhancement by argon has

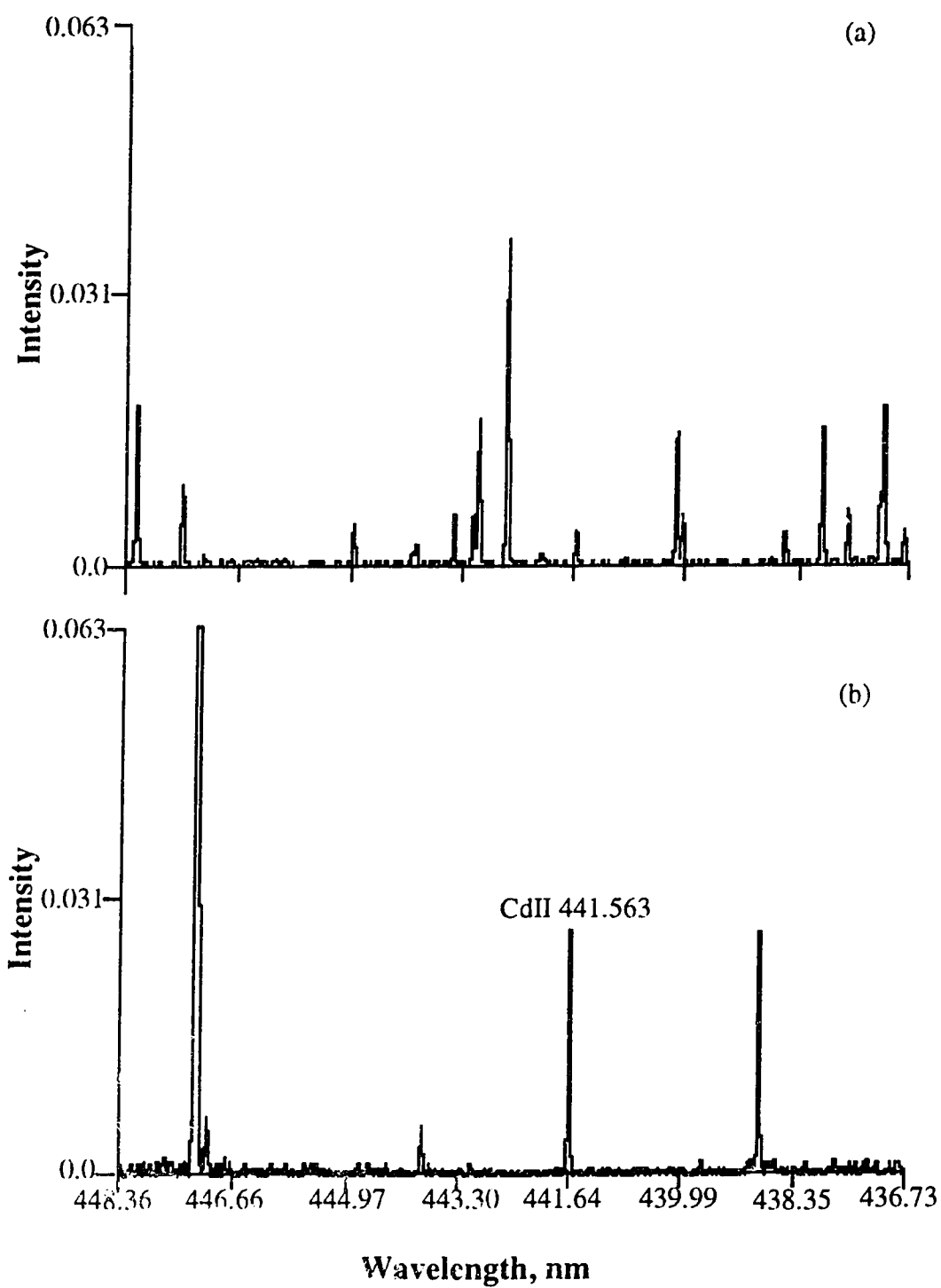


Fig. 4.35 Expanded portion of Cd spectra showing the CdII 441.563 nm line in He discharge. (a) Ar, (b) He.

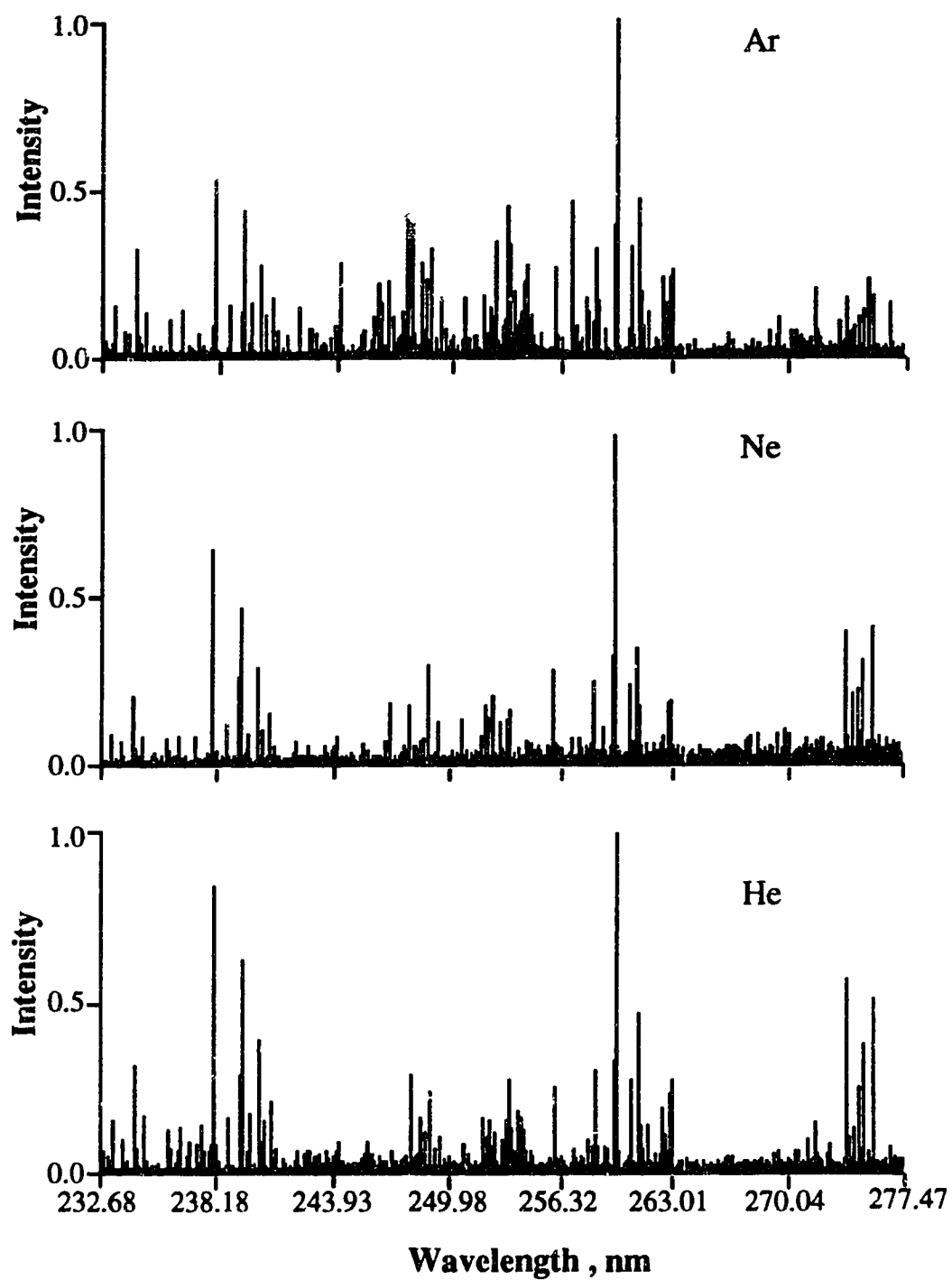


Fig. 4.36 A section of iron UV spectra in three discharge gases.

Table 4.9 Relative intensity of iron ion lines in glow discharge emission (UV)

Wavelength (nm)	Excitation Energy(eV)	Relative intensity		
		Ar	He	Ne
232.739	5.41	4.5		5.3
233.135	5.55	4.3		
233.280	5.36	15.0	13.1	13.4
233.800	5.41	7.6	8.3	
234.349	5.29	31.4	28.2	25.1
234.396	5.59	2.7		
234.428	5.41	5.7	6.3	
234.810	5.51	11.2		
234.830	5.36	14.2	13.3	11.3
235.447	7.94	3.8		
235.910	10.50	10.8	11.2	
235.999	5.48	6.1		
236.029	5.55	6.4		
236.483	5.29	14.0	11.3	11.3
236.859	5.58	4.1		
236.996	10.45	8.0		
237.643	10.42	3.5	12.3	
237.927	5.51	5.5		
238.076	5.29	9.1	6.6	
238.207	5.20	51.0	75.8	71.0
238.863	5.24	14.6	13.4	16.2
239.562	5.22	43.1	53.8	52.0
239.924	5.25	15.2	14.8	12.4
240.488	5.24	29.9	32.2	33.7
240.666	5.26	12.5	12.3	14.7
241.052	5.25	17.8	17.0	21.1
241.107	5.26	8.2	8.3	
241.331	5.26	7.5	6.4	
241.506	7.98	2.7		
242.414	7.92	14.0		
243.007	7.93	8.6		
243.227	7.94	7.4		
244.451	7.65	20.6	7.3	
244.511	10.27	6.3		
244.556	7.77	28.6		
246.045	10.52	8.5		
246.667	7.86	14.8		

Table 4.9 Relative intensity of iron lines in glow discharge emission (UV)(contd.)

Wavelength (nm)	Excitation Energy(eV)	Relative intensity		
		Ar	He	Ne
246.681	7.86	15.5		
247.066	7.84	24.4		
247.243	7.86	6.8		
247.331	7.79	12.5		
247.857	7.84	13.4		
248.016	7.80	40.8		
249.086	7.80	23.7		
249.326	7.60	33.0	19.5	34.0
251.176	7.62	17.0	6.9	16.2
251.712	7.70	6.1		
252.539	7.54	7.2	9.0	21.3
252.629	7.49	15.8	12.3	18.9
252.629	7.49	15.8	12.3	
252.955	7.61	35.3	9.9	24.7
	7.71			
253.442	7.58	6.7		
253.548	7.69	43.7	13.1	
253.682	7.56		8.0	
253.900	7.52	6.8	10.9	20.4
254.067	7.70	9.6		
254.343	7.71	6.7		
254.667	7.69	26.2		
254.940	7.71	12.7		
255.507	7.69	7.2		
255.545	7.70	2.8		
256.253	5.82	25.5	22.1	33.8
256.347	5.87	12.9	11.3	
256.691	5.90	5.2		
257.437	7.40	6.8		
257.792	5.90	5.6		
258.258	5.87	9.3	8.0	
258.588	4.79	32.7	24.4	29.5
259.154	5.82	8.4	7.0	
259.837	4.82	38.9	27.6	39.0
259.940	4.77	98.1	90.2	109.4
260.709	4.84	33.7	22.5	28.2

**Table 4.9**      **Relative intensity of iron lines in glow discharge emission (UV)(contd.)**

Wavelength (nm)	Excitation Energy(eV)	Relative intensity		
		Ar	He	Ne
261.187	4.79	48.5	37.9	40.0
261.382	4.85	18.9	11.5	21.9
261.762	4.82	13.6	11.3	
262.567	4.77	23.3	17.3	
262.829	4.84	16.3	8.8	
263.105	4.82	23.6	21.7	
	7.54			
263.132	4.79	25.0	22.4	23.5
266.466	8.04	6.7		
266.663	8.07	5.0		
270.399	7.94	8.0		
270.906	7.77	19.8		
271.441	5.55	3.8	8.4	
271.622	7.99	5.2		
272.754	5.58	7.6		
273.955	5.51	19.9	46.3	44.8
274.320	5.61	9.2	12.0	24.9
274.648	5.59	12.0	19.8	29.5
274.932	5.55	13.5	32.1	38.7
275.329	7.77	24.1		
275.574	5.48	17.7	46.9	46.8
277.930	7.72	4.4		
278.370	7.70	6.2		

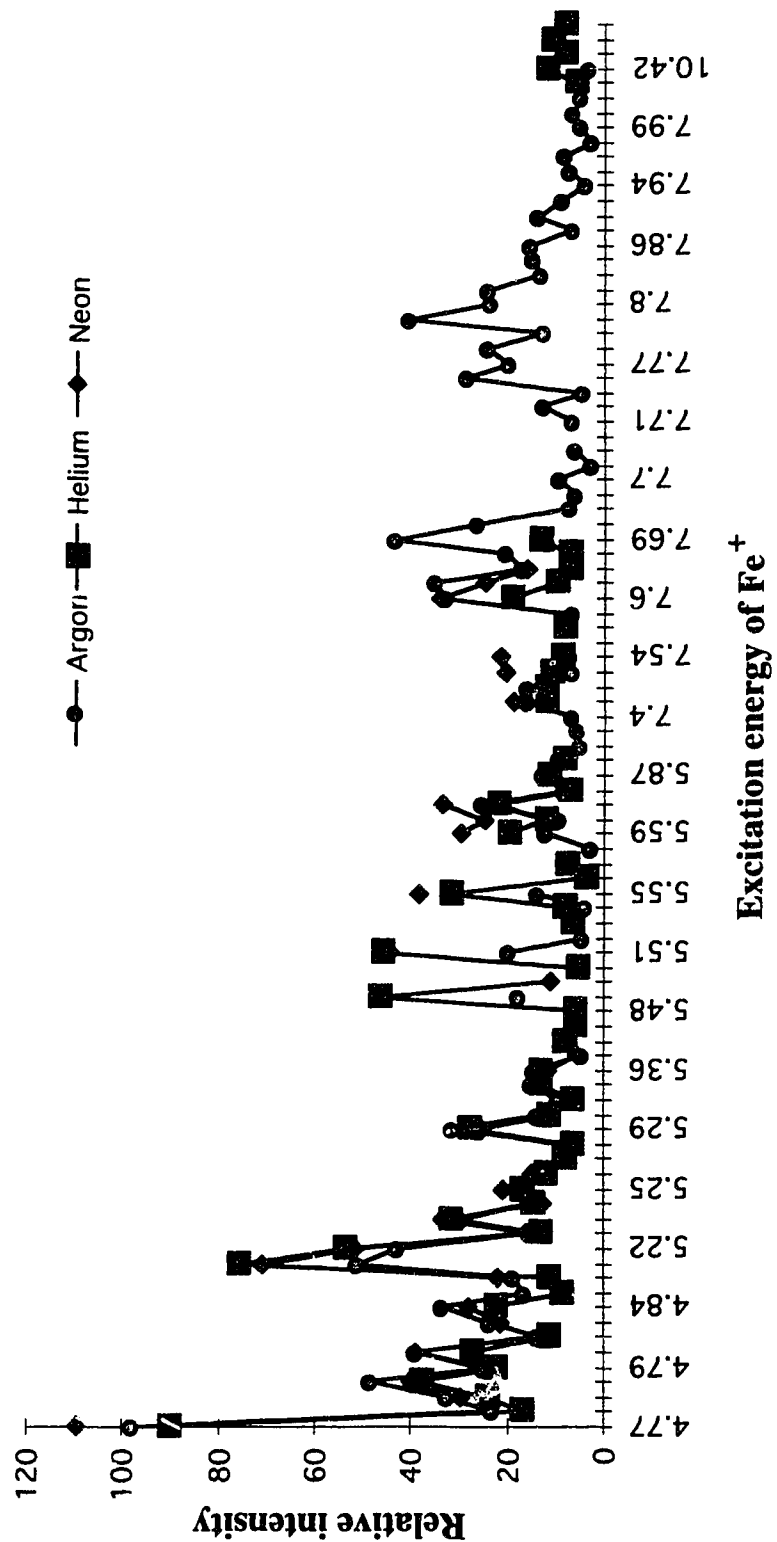


Fig. 4.37 A plot showing the relative intensity of some Fe ion lines altered by different gases in glow discharge



the requirement for the excitation energy of  $15.76 - 7.87 = 7.89$  eV or at a close level. This is consistent to the observations from the spectra.

#### **4.4 The Factors That Influence Charge Transfer Reaction**

Any process which changes the population of one or both the collision partners will change the extent of charge transfer. Different filler gases have different sputtering rates, and this results in a different population of the analyte atoms in the ground state level. For the same gas, a discharge operating at different conditions will generate significantly different results. In the study of Farnsworth and Walter [13] on the Cu II emission with a radio frequency (r.f.) burst and current pulse method in a neon gas discharge, it was found that the 270.1 nm emission drops in intensity with the r.f. burst. The intensity drop was attributed to the removal of one of the charge exchange reactants, the ground state copper atoms, by the r.f. With added microwave excitation in an argon plasma, Steers and Leis [8] found that the intensity of Cu II 224.700 nm line falls, but Cu II lines emitted from higher states become more intense. They reasoned that it was possibly due to the number density of ground state copper atoms being decreased by the microwave boost. Absorption measurements have confirmed that, with the added microwave excitation, the number density of metastable copper atoms increases greatly, whereas the number density of ground state atoms falls [9].

A current change in the glow discharge often means a change in the population of gas ions. Variation in the discharge current also alters the charge transfer extent. Take the  $\text{Ar}^+ - \text{Cu}$  transfer as an example. At low

discharge current (say < 3 mA), the 224.700 nm line may just be a few times more intense than other CuII lines which are not populated by charge transfer. At high discharge current (> 20 mA for instance), however, the difference can be more than a hundred fold.

As discussed by Turner-Smith et al.[2], the reaction probability is highest when the energy levels of the partners overlap. The selective enhancement on the transition of the Cu II 224.700 nm line by argon, and the transitions of Cu II  $3d^95s$  to  $3d^94p$  by neon is the result of this effect. The probability of energy transfer increases with decreasing energy difference between the two states. In this case, matching of the excitation energy between the particles involved in the collisions can be assumed to be a critical factor. It is stated by F. Llewellyn-Jones [30] that at the situation of  $\delta E/h U \sim 1$  (where  $U$  is the relative velocity between the collision partners and  $h$  is Plank's constant), charge transfer will be efficient. At the same gas temperature, the average relative velocities of the gas ions to the analyte atoms will be Ar, Ne and He in increasing order, because of the mass of the filler gas atoms. Therefore the range of  $\delta E$  that the charge transfer process can tolerate will be the largest in He, and the smallest in Ar. Furthermore, gas temperature is often higher in He than in the other gases because of the higher potential used for the same discharge current. The higher temperature will enhance this effect. This may partially explain the phenomenon that He often shows charge transfer consequences even if the energy gap is relatively large and Ar charge transfer processes are more energy specific.

The efficiency of the charge transfer process is also dependent on the sample and the plasma matrix. This process is not as efficient in the iron and silver case as in the copper and zinc cases. One reason is the lack of

direct match between the energy levels, the other is the availability of other processes. No matter what kind of system it is, there is always a competition between all the possible excitation mechanisms. It is the matter which one or ones are dominating. When one process is suppressed, the other processes will show a strong influence.

It has been found that charge transfer is also dependent on the quantum term of the upper state of the transition. At the same energy discrepancy, charge transfer favors the triplet levels [Fig. 4.38]. Duffendack and Thomson [18] discussed this phenomenon half a century ago, and they thought this might be related to the spin direction of the unpaired electron in the excited ions.

#### 4.5 Conclusion

From the discussion above, the following conclusions can be made: first, the characteristics of the emission spectrum in a low-pressure glow discharge are very much dependent on the filler gas, and the ionic lines of the analyte show the most difference; second, ion lines in some spectra are mainly excited by the charge transfer process, and this mechanism contributes most to the population of the high level state of the analyte ions; third, Penning ionization might play an important role for the generation of analyte ions and its contribution to the excitation of these ions is possible. There is always a competition among all the possible excitation processes. The charge transfer and Penning process are excitation energy specific, electronic impact is more universal. For most of the low excitation energy transitions, like in the case of iron, electron impact may contribute the most. For the high energy excitation transitions, the emission would be

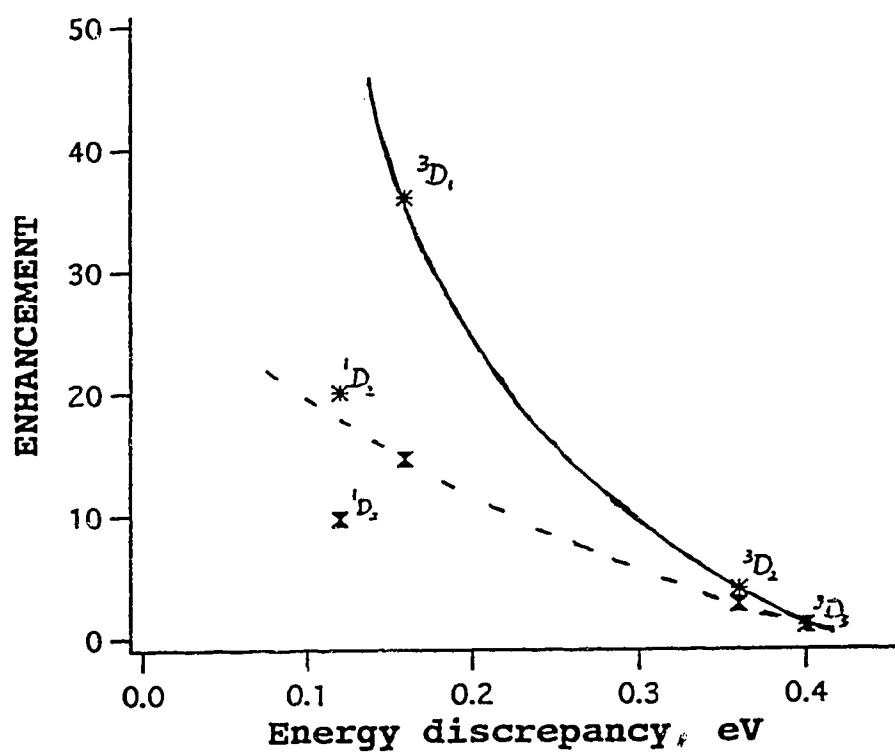


Fig. 4.38 A diagram showing that charge transfer in Ne - Cu system favors the  $^3D$  terms.

very weak if electron impact operates alone, for the high energy electrons have a low number density in a low current glow discharge.

Stepwise de-excitation is another main processes governing excitation of some ion lines. For example, the Cu II lines are greatly enhanced by using helium or neon as filler gas. Only a few of the higher levels match the charge transfer or Penning processes, and most of the lines are from the stepwise de-excitation of these levels.

## References

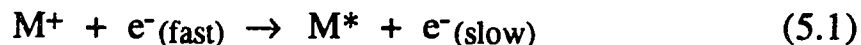
1. K. Wagatsuma and K. Hirokawa, *Anal. Chem.* **57** 2901 (1985).
2. A.R. Turner-Smith, J.M. Green and C.E. Webb, *J. Phys. B: Atom Molec. Phys.* **6** (1973).
3. E.B.M. Steers and K.J. Fielding, *J. Anal. At. Spectrom.* **2** 239 (1987).
4. K. Wagatsuma and K. Hirokawa, *J. Anal. At. Spectrom.* **4** 525 (1989).
5. K. Wagatsuma and K. Hirokawa, *Anal. Chem.* **60** 702 (1988).
6. K. Wagatsuma and K. Hirokawa, *Spectrochim. Acta* **42B** 523 (1987).
7. K. Wagatsuma and K. Hirokawa, *Spectrochim. Acta* **46B** 269 (1991).
8. E.B.M. Steers and F. Leis, *J. Anal. At. Spectrom.* **4** 199 (1989).
9. E.B.M. Steers and F. Leis, *Spectrochim. Acta* **46B** 527 (1991).
10. F. Leis, J.A.C. Broeckaert, and E.B.M. Steers, *Spectrochim. Acta* **46B** 243 (1991).
11. E.B.M. Steers and A.P. Thonre, *J. Anal. At. Spectrom.* **8** 309 (1993).
12. M.K. Levy, D. Derxner, A.D. Angstadt, R.L. Smith, and K.R. Hess, *Spectrochim. Acta* **46B** 253 (1991).
13. P.B. Farnsworth and J.P. Walters, *Spectrochim. Acta* **37B** 773 (1982).
14. G.J. Collins, *J. Appl. Phys.* **44** 4633 (1973).
15. J.A. Piper and P. Gill, *J. Phys. D: Appl. Phys.* **8** 127 (1975).

16. F.J. de Hoog, J.R. McNeil, G.J. Collins, and .B. Persson, *J. Appl. Phys.* **48** 3701 (1977).
17. D.C. Gerstenberger, R. Solanki, and G.J. Collins, *IEEE Journal of Quantum Electronics* **QE-16** 820 (1980).
18. O.S. Duffendack and K. Thomson, *Phys. Rev.* **4** 106 (1933).
19. K.J. Jones and J.W. Carnahan, *Spectrochim. Acta* **47B** 1229 (1992).
20. J.W. Carnahan and G.M. Hieftje, *Spectrochim. Acta* **47B** 731 (1992).
21. A. Goldwasser and J.M. Mermet, *Spectrochim. Acta* **41B** 725 (1986).
22. L.L. Burton and M.W. Blades, *Spectrochim. Acta* **46B** 819 (1991).
23. K. Wagatsuma and K. Hirokawa, *Spectrochim. Acta* **48B** 1039 (1993).
24. J.M. Green, G.J. Collins and C.E. Webb, *J. Phys. B: Atom. Molec. Phys.* **6** 1545 (1973).
25. A.G. Shenstone, *Phys. Rev.* **31** 317 (1928).
26. J.R. McNeill, W.L. Johnson and G.J. Collins, *Appl. Phys. Letters* **29** 172 (1976).
27. R.D. Reid, D. Gerstenberger, J.R. McNeil and G.J. Collins, *J. Appl. Phys.* **48** 3994 (1977).
28. R.D. Reid, W.L. Johnson, J.R. McNeil, and G.J. Collins, *IEEE Journal of Quantum Electronics*, **7** 78 (1976).
29. A.G. Shenstone and J.T. Pittenger, *J. Opt. Soc. Am.* **39** 219 (1949).
30. F. Llewellyn-Jones, *The Glow Discharge and an Introduction to Plasma Physics*, Methuen, London, 1966, p23.

## Chapter 5 Excitation and Emission Characteristics of Neutral Atoms in Glow Discharges - with Comparison to Inductively Coupled Plasmas

### 5.1 Introduction

The glow discharge is now widely used in a variety of analytical spectroscopies [1]. In its use as an atomic emission source the most sensitive lines for determination typically are the neutral atom resonance lines of the sought for elements. The excitation mechanism for these lines is often stated to be electron impact, *i.e.*



However, it is also well established that the distribution of excited states in neutral atoms is non-Boltzmann. This is manifested in the difficulties in obtaining meaningful temperature measurements of the glow discharge by the Boltzmann method [2]. This point was illustrated at the end of Chapter 3. This implies that the energy distribution of electrons in the glow discharge is non thermal, a fact that is generally accepted [3,4]. In addition, mechanisms other than electron impact (Equation 5.1) could be responsible for the generation of excited state neutral atoms. In particular, ion-electron recombination is a possible major mechanism for generating excited state neutral atoms, *i.e.*





For example, Steers and Leis [5] indicated that recombination was a major source of excited copper atoms.

The key to delineating ion-electron recombination processes in a glow discharge is to study the complete character of neutral atom emission. Ion-electron recombination processes will be reflected in the spectral character of neutral emission in that high energy neutral atom lines and stepwise de-excitation paths should reveal themselves.

In this chapter the spectral character of the neutral atom emission of copper, zinc, silver and cadmium in a glow discharge will be presented. In order to obtain complete and accurate spectral coverage, spectra were measured using the Fourier transform spectrometer described in Chapter 2. In contrast to the study of the spectral character of ion emission presented in Chapter 4, the emphasis in this chapter is on an interpretation of the visible spectra of these elements although portions of the UV spectra will also be presented. While spectra are presented for glow discharges utilizing different filler gases (i.e. Ar, Ne and He) it will be seen that the nature of the filler gas has considerably less effect on the character of the neutral atom spectra compared to the effects seen for the ion spectra. However, an interesting and dramatic contrast is provided by comparing the glow discharge (GD) spectra (Ar filler gas) to that for the same element in an Ar Inductively Coupled Plasma (ICP). In addition, a comparison of the argon neutral atom and ion emission spectra between the GD and the ICP provides some insight on excitation processes in the two discharges.

## 5.2 Experimental

The operation of the glow discharge emission source was carried out in the same way as described in Chapter 4. The spectral measurement and data treatment for both the ICP emission and glow discharge used the same FTS system and operated with the same parameter settings as in Chapter 4. The operation conditions for the ICP are listed below:

Forward power	1.2 kW
Reflected power	0.05 kW
Frequency	27 MHz
Nebulizer gas	1.1 l/min
Auxiliary gas	1.1 l/min
Coolant gas	15 l/min
Viewing zone	18 mm from load coil.

## 5.3 Results and Discussion

### 5.3.1 Overview of the Brass Visible Spectra

Visible region spectra are presented in Fig. 5.1 for the brass sample (NIST Brass 1107) with Ar, Ne and He as the filler gas. Some major copper and zinc lines observed in these spectra are noted on Fig. 5.1a. All the noted lines are neutral atom lines and most, as will be detailed later in this chapter, originate from high energy states of the respective atoms.

Except for the filler gas lines (see Figs. 5.1b and 5.1c), the copper and zinc lines observed throughout the three spectra shown in Fig. 5.1 are all the same and generally of the same relative intensity. This is in contrast to the spectral character of the UV spectra (i.e. ion lines) presented for this

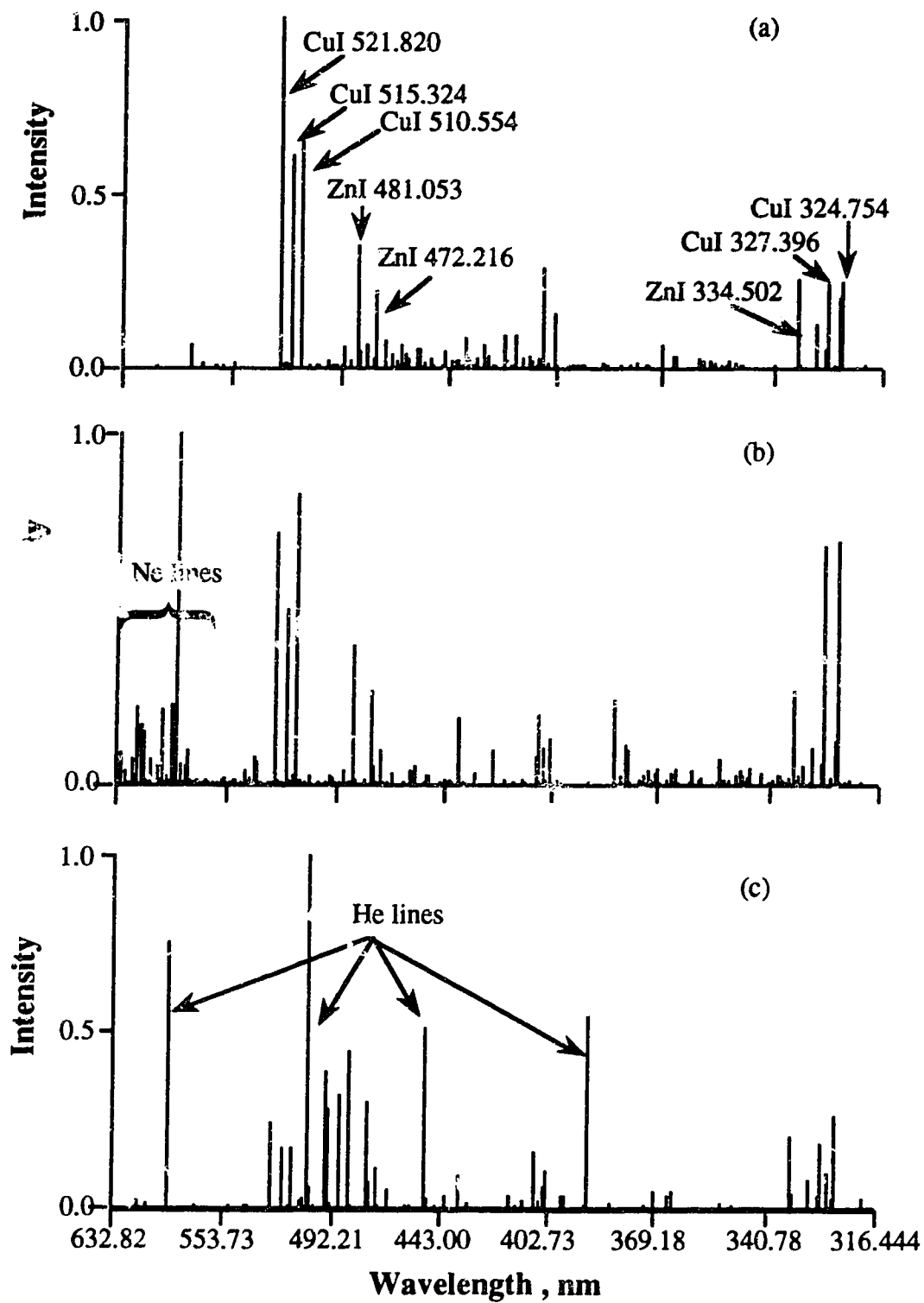


Fig. 5.1 Visible region spectra of brass in different discharge gases  
(a) Ar, (b) Ne and (c) He.

brass sample and discussed in Chapter 4 (Fig. 4.1). Thus, the drastic alteration in spectral character that was observed for ion lines caused by the nature of the filler gas is not observed for neutral atom line emission. This implies that some common mechanism, operative in all the discharges, might be responsible for the generation of excited neutral atoms.

In marked contrast, however, are the glow discharge (GD) and inductively coupled plasma (ICP) emission spectra for the brass sample. These are shown in Fig. 5.2, both for argon based discharges. In the ICP spectrum the high energy neutral atom lines of both copper and zinc are absent and the only strong lines seen from the sample in this spectral region are the two copper resonance lines at 324.754 and 327.396 nm. It is also clear from these two spectra that the resonance lines of copper are self absorbed to some degree in the glow discharge spectra. These lines should have about a 2:1 ratio as seen in the ICP spectrum. This means that the relative intensity of the higher energy copper lines to that of the resonance lines is not accurately portrayed in Fig. 5.1. These spectra (the GD spectra) can, however, be used to illustrate the presence of these high energy neutral atom lines and relative intensities among themselves. In addition, there is a major difference in the nature of the argon emission between the spectra shown in Fig. 5.2. For the ICP, all argon emission lines are neutral atom lines, i.e. ArI lines. For the glow discharge, however, in addition to ArI lines, several strong argon ion lines (i.e. ArII lines) are clearly present, lines that are conspicuous in their absence from the ICP spectrum. This aspect of these spectra will be discussed and explained later in this chapter, but first the character of the Cu and Zn neutral atom emission will be documented and discussed in more detail.

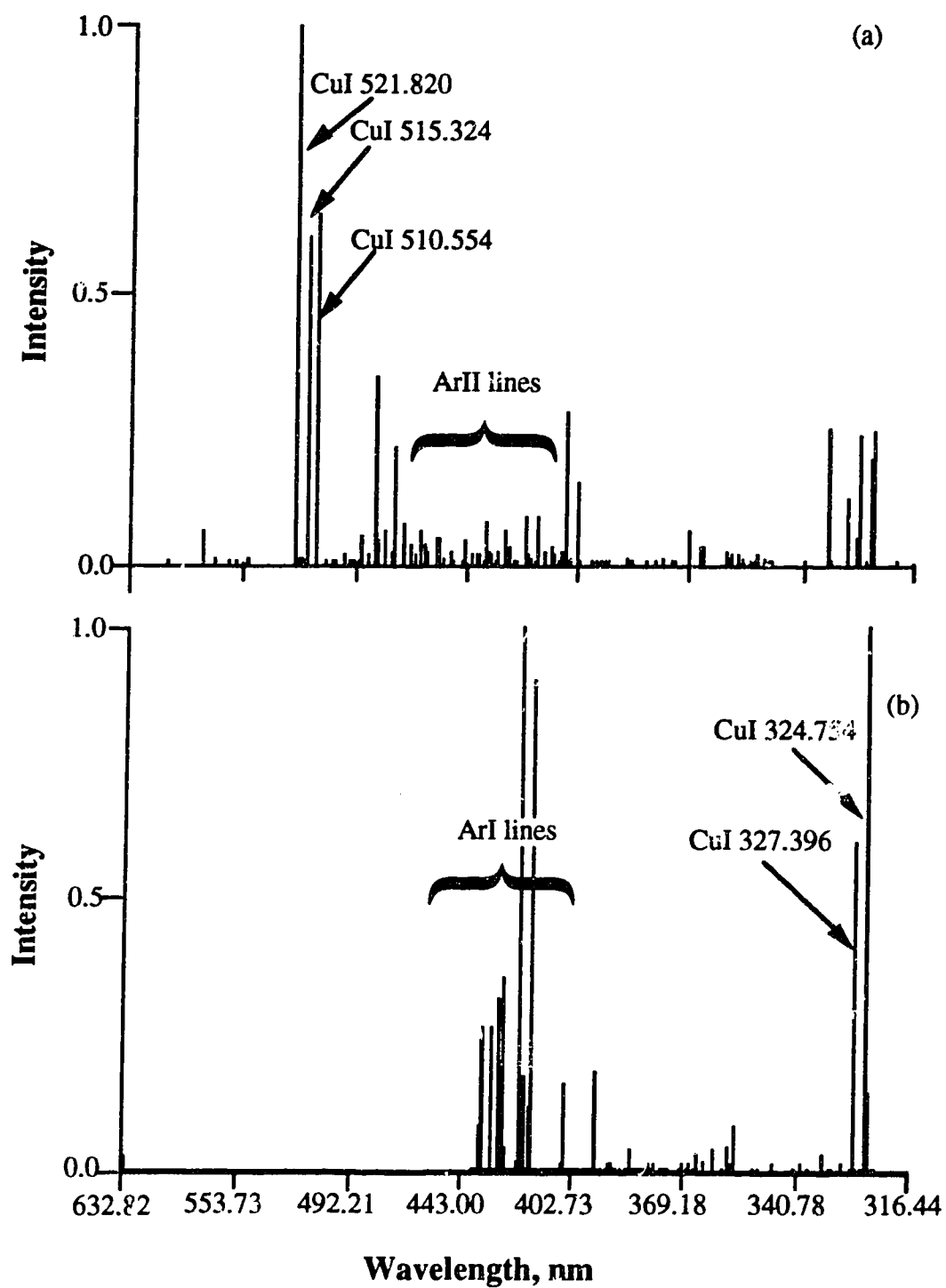


Fig. 5.2. Comparison of brass visible spectra in argon based GD (a) and ICP (b).

### 5.3.2 Copper Neutral Atom Lines - Visible Region

An expanded scale spectrum of the so-called copper green lines in the GD is shown in Fig. 5.3a and for reference an energy level diagram for CuI is shown in Fig. 5.4. The transitions emphasized on the energy level diagram indicate those observed in the glow discharge spectra presented in this study. The energy level diagram is an adaptation and extension of that presented by Candler [6].

The 522.007, 521.820 and 515.324 nm lines are the result of transitions from the  $3d^{10}4d$  level to the  $3d^{10}4p$  level (see Fig. 5.4 and Table 5.1). The 510.554 nm line is the result of a transition from the  $3d^{10}4p$  level to the  $3d^94s^2$  level, a level that is about 1.39 eV above the  $3d^{10}4s$  ground state of copper. Lines that result from two weaker  $3d^{10}4p$  to  $3d^94s^2$  transitions occurring at 578.213 and 578.024 nm are shown in Fig 5.3b. These transitions and their terms are summarized in Fig. 5.5 and Table 5.1. The energy level diagram presented in Fig. 5.5 highlight transitions originating on the  $3d^{10}$  side of the copper energy level diagram.

Note that throughout this chapter, the wavelengths and excitation energies of the lines were obtained from Zaidel *et. al* [7] and cross checked with the MIT wavelength tables [8]. The levels and terms for CuI were obtained from Shenstone [9].

As indicated in Fig. 5.5, a number of other upper level transitions can occur from the  $3d^{10}6d$ ,  $3d^{10}5d$  and  $3d^{10}6s$  levels to the  $3d^{10}4p$  level. Lines from all these transitions are observed in the glow discharge spectra. Expanded scale spectra for the Ar based glow discharge illustrating lines for all these transitions are shown in Fig. 5.6 and listed in Table 5.1. Except for the copper resonance lines at 324.754 and 327.396 nm, none of

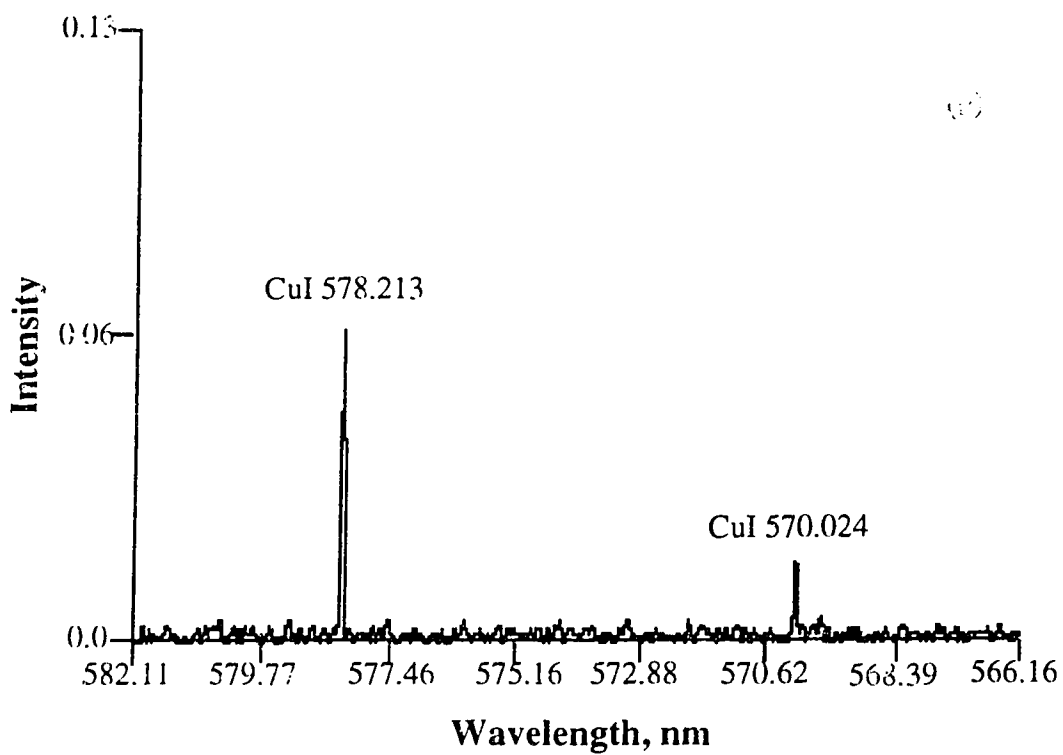
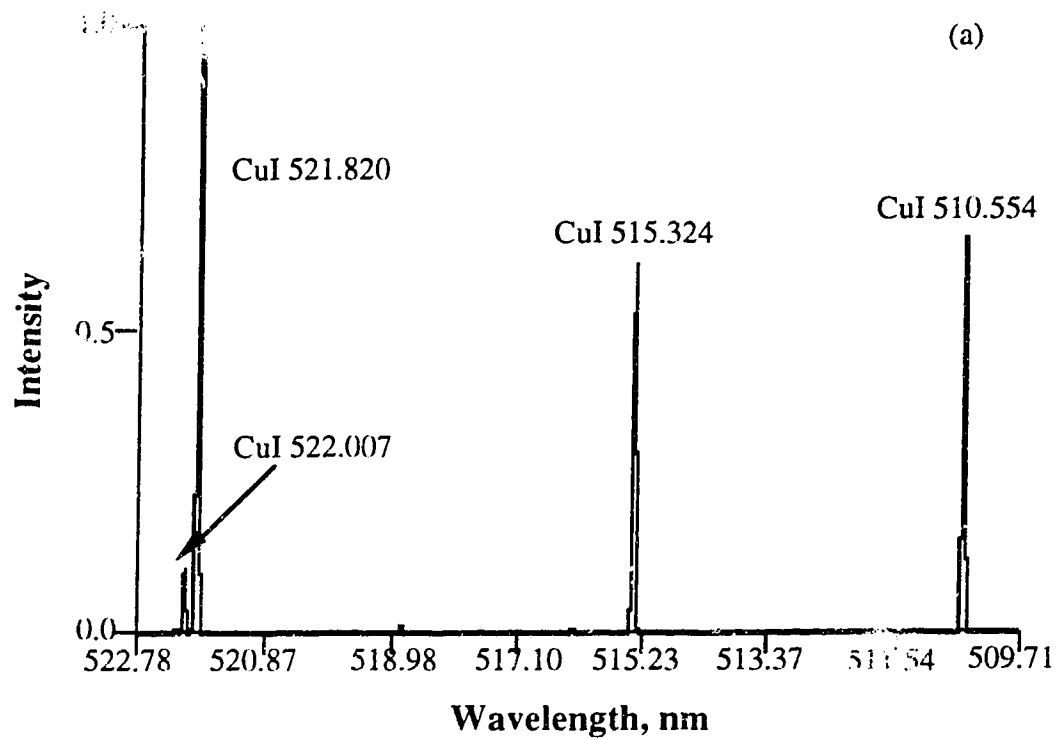


Fig. 5.3 Some CuI lines in argon glow discharge (a) 509.7- 528.8 nm and (b) 566.2 - 582.1 nm.

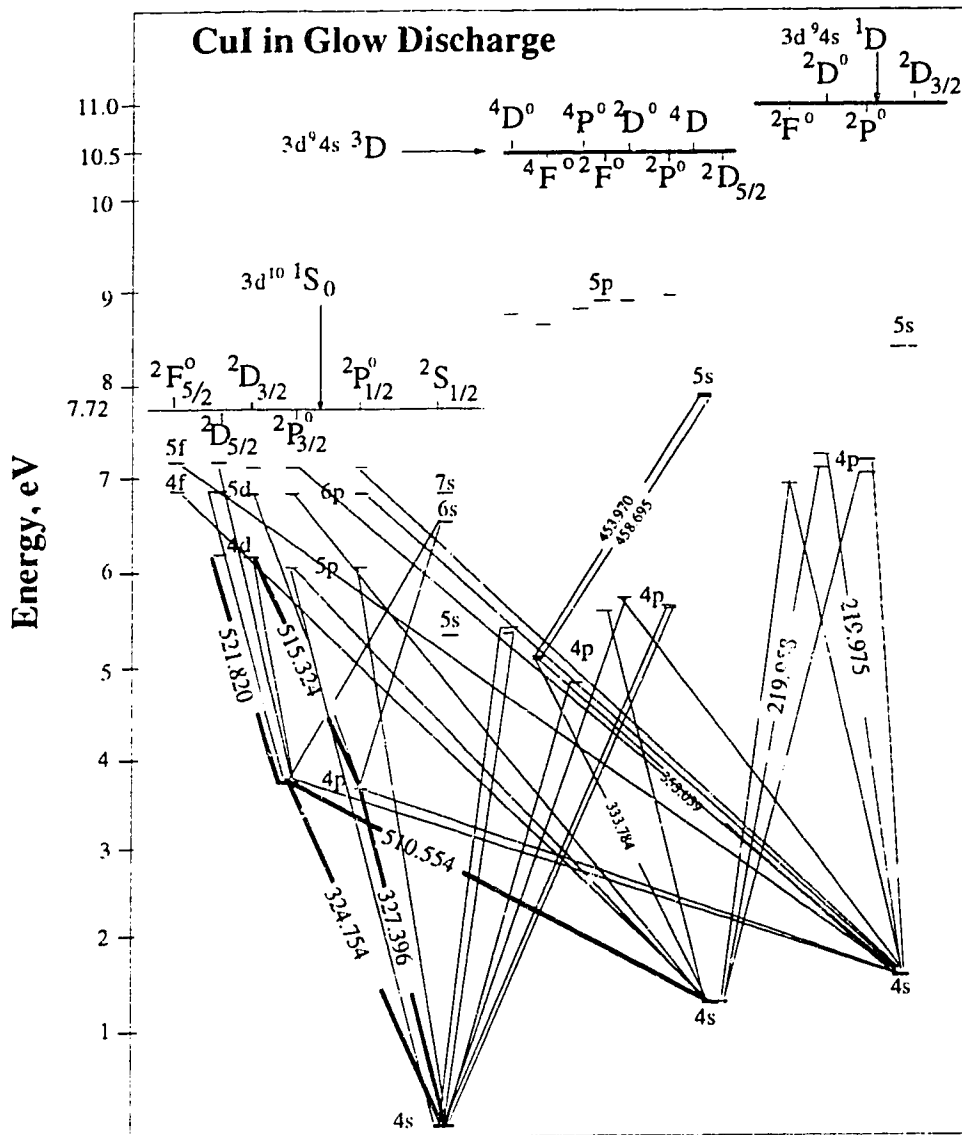


Fig. 5.4 Energy level diagram (or Grotrian diagram) of CuI. Lines showing the major transitions observed in GD. Thickness of the lines is a rough representation of the intensity of the lines.



**Table 5.1 Summary of copper atom lines in the visible spectral region  
( $3d^{10}$  upper states)**

Type	Wavelength, nm	Energy, eV	Transition [9]
CuI	327.396	3.78	$3d^{10}4p - 3d^{10}4s$
CuI	324.754	3.82	$3d^{10}4p - 3d^{10}4s$
CuI	522.007	6.19	$3d^{10}4d - 3d^{10}4p$
CuI	521.820	6.19	$3d^{10}4d - 3d^{10}4p$
CuI	515.324	6.19	$3d^{10}4d - 3d^{10}4p$
CuI	578.213	3.79	$3d^{10}4p - 3d^9 4s^2$
CuI	570.024	3.82	$3d^{10}4p - 3d^9 4s^2$
CuI	510.554	3.82	$3d^{10}4p - 3d^9 4s^2$
CuI	368.744	7.17	$3d^{10}6d - 3d^{10}4p$
CuI	365.430	7.18	$3d^{10}6d - 3d^{10}4p$
CuI	406.329	6.87	$3d^{10}5d - 3d^{10}4p$
CuI	406.270	6.87	$3d^{10}5d - 3d^{10}4p$
CuI	402.266	6.87	$3d^{10}5d - 3d^{10}4p$
CuI	453.082	6.55	$3d^{10}6s - 3d^{10}4p$
CuI	448.035	6.55	$3d^{10}6s - 3d^{10}4p$

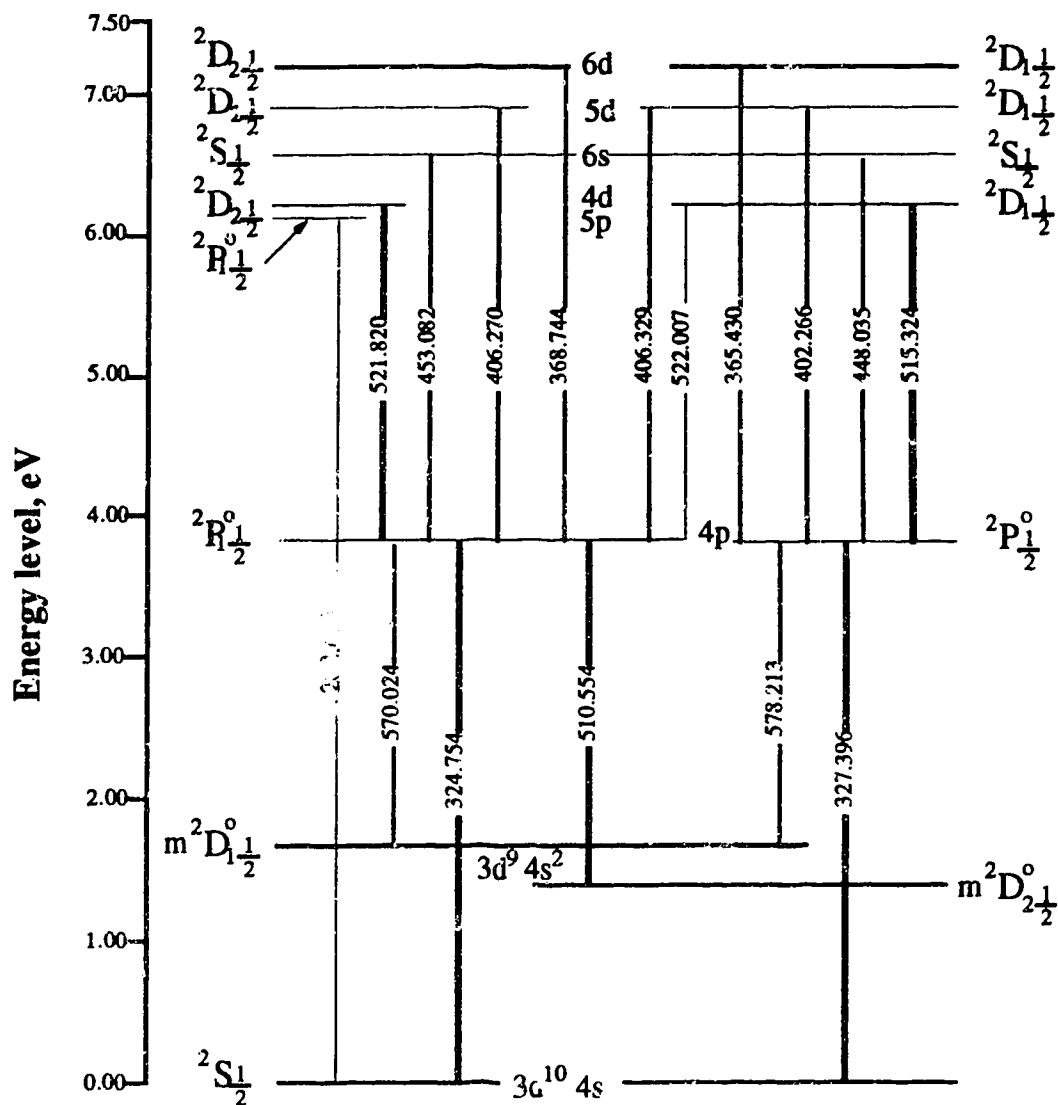


Fig. 5.5 Detailed energy diagram illustrates transitions originated from  $3d^{10}n_x$  configurations.

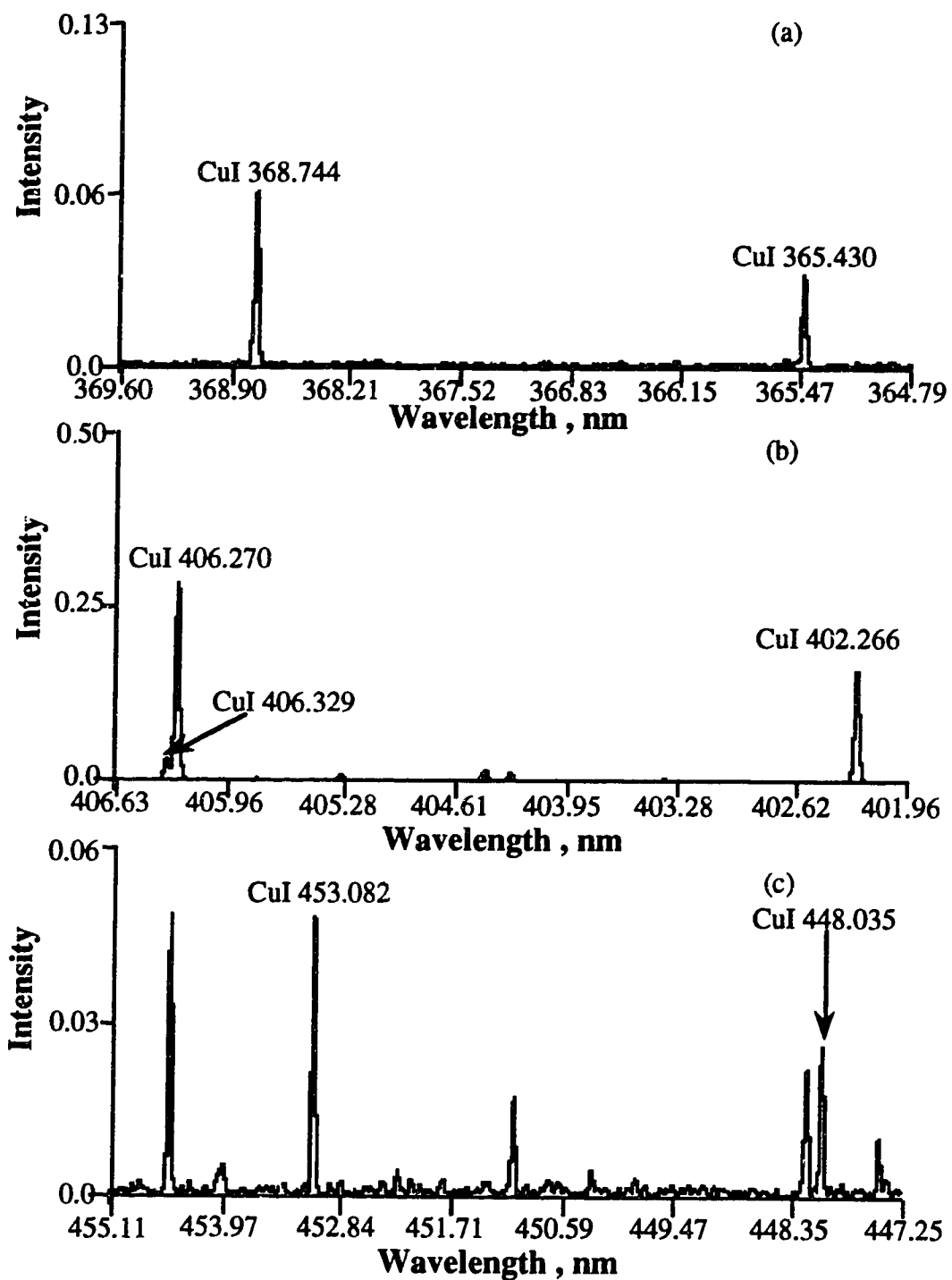


Fig. 5.6 Some CuI lines generated from the transitions illustrated in Fig. 5.5.

the lines shown in Figs. 5.3 and 5.6 were observed in the ICP spectrum of the brass sample.

The presence of these lines in the GD spectra originating in the upper energy levels of the  $3d^{10}$  system clearly indicates that some mechanism is operative populating these levels and followed by stepwise de-excitation. The whole process is a "top-down" excitation. Such a process would also generate similar spectral characteristics for neutral atom emission independent of the nature of the filler gas and this was observed as shown in Fig. 5.1. This is not to state that excitation does not also occur via electron impact. Some of the lines, and in particular the resonance lines at 324.754 and 327.396 nm, are most likely excited by electron impact (Equation 5.1) in addition to the contribution of stepwise de-excitation from the upper levels.

Further spectral evidence that supports the occurrence of the "top-down" excitation assumption in the GD is shown in Fig. 5.7. The 458.695 nm line shown in Fig. 5.7a is the result of a  $3d^9 4s 5s$  to  $3d^9 4s 4p$  transition (see Fig. 5.4) and the line has an excitation potential of 7.80 eV, a value that is larger than the first ionization potential (IP) of Cu (7.724 eV). The  $3d^9$  lines are summarized in Table 5.2.

The lines shown in Fig. 5.7b and 5.7c (427.513 and 465.113 nm) are again both the result of transitions from  $3d^9 4s 5s$  to  $3d^9 4s 4p$  levels. The excitation energy for these lines is 7.733 eV, just above the ionization limit of Cu. The lines shown in Fig. 5.7 are all from transitions that occur on the  $3d^9$  side of the copper energy level diagram (see Fig. 5.4) and the upper levels of these transitions (i.e. above the IP of copper) are subject to auto-ionization. Transitions from these levels may be broad and the 458.695 line (Fig. 5.7a) is clearly a broadened line.

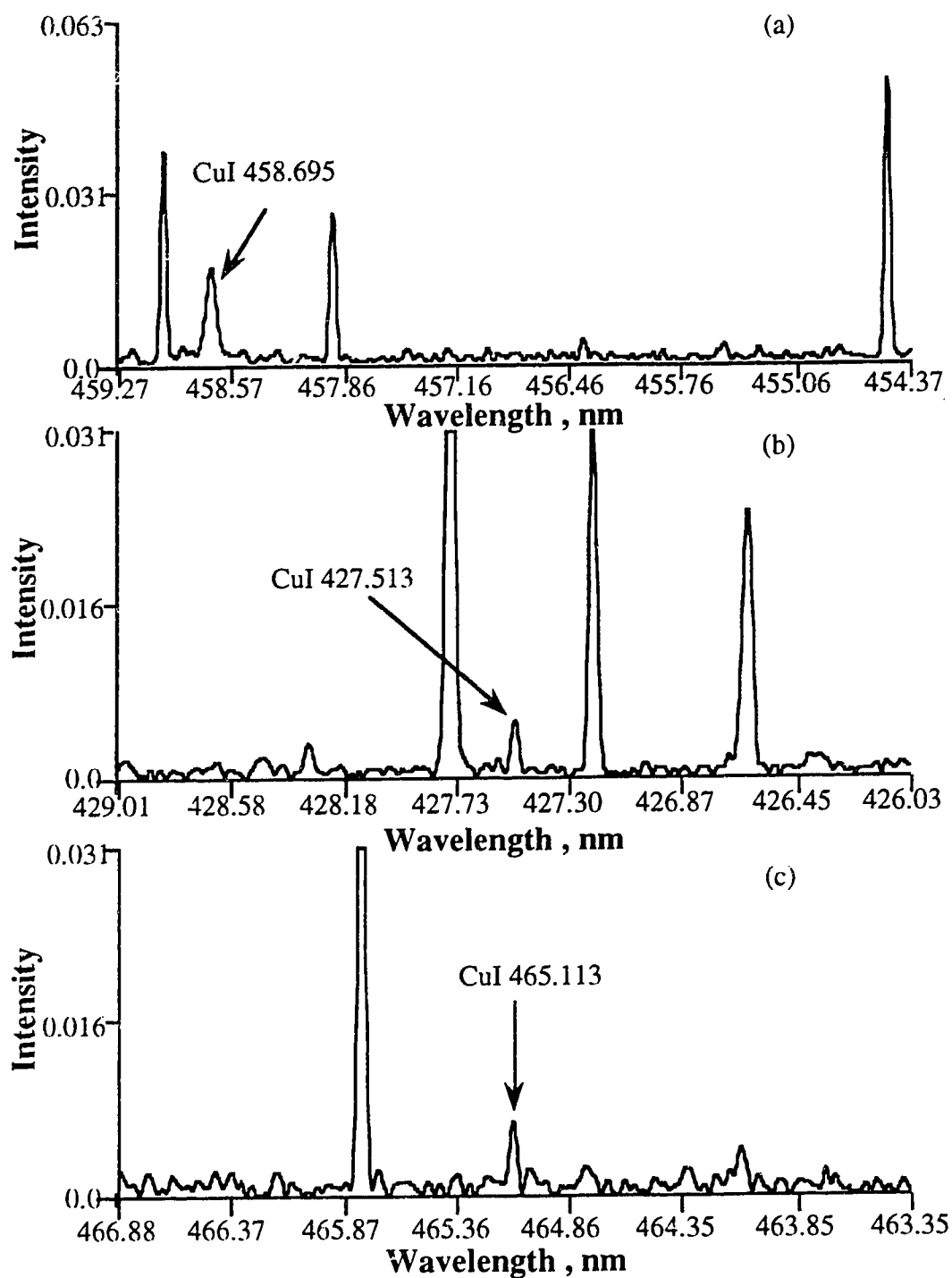


Fig. 5.7 A portion of CuI spectra showing the diffusion lines from the auto-ionizing excited states.

Table 5.2 Summary of copper neutral atoms in the visible spectral region  
( $3d^9$  upper states).

Type	Wavelength, nm	Energy, eV	Transition [9]
CuI	427.513	7.73	$3d^9 4s 5s - 3d^9 4s 4p$
CuI	465.113	7.73	$3d^9 4s 5s - 3d^9 4s 4p$
CuI	458.695	7.80	$3d^9 4s 5s - 3d^9 4s 4p$
CuI	453.970	7.88	$3d^9 4s 5s - 3d^9 4s 4p$
CuI	333.784	5.10	$3d^9 4s 4p - 3d^9 4s^2$
CuI	353.039	5.15	$3d^9 4s 4p - 3d^9 4s^2$

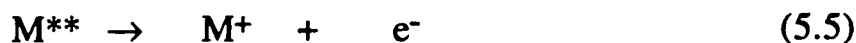
A mechanism by which these excited states can be generated is a process called dielectric recombination [10]:



where  $M^{**}$  designates a doubly excited atom. This species can relax radiatively:



or by reformation of the ion (autoionization):



The presence of the lines shown in Fig. 5.7 in the glow discharge system indicates that these states are formed and that, in part, they are relaxing radiatively.

Finally, spectral evidence for stepwise de-excitation on the  $3d^9$  side of the energy level diagram is found in the observation of the 333.784 nm copper line [Fig. 5.8]. It is the result of a  $3d^9 4s 4p$  to  $3d^9 4s^2$  transition and has an excitation potential of 5.10 eV. The upper level [8] of this line ( $z^4F^{\circ}_{7/2}$ ) is the same as the lower level of the 458.695 nm line just discussed (Fig. 5.7a). Another pair of transitions indicative of stepwise de-excitation is shown in Fig. 5.9. The 453.970 nm line shown in Fig. 5.9a is the result of a  $3d^9 4s 5s$  to  $3d^9 4s 4p$  transition. It has an excitation potential of 7.88 eV and its broadened width is indicative of an autoionizing transition. The lower level of this line is  $z^4F^{\circ}_{5/2}$  [9]. The line shown in Fig. 5.9b (353.039 nm) is the result of a transition from the  $3d^9 4s 4p$  level to the  $3d^9 4s^2$  level

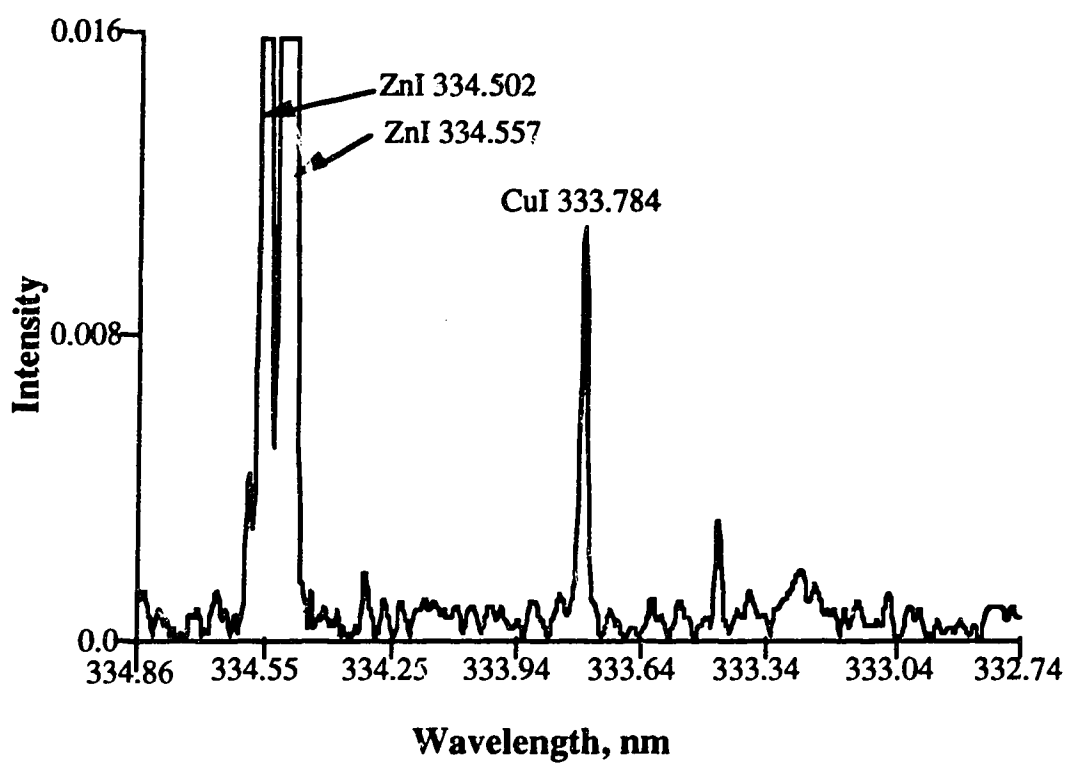


Fig. 5.8 A CuI line generated from stepwise de-excitation.



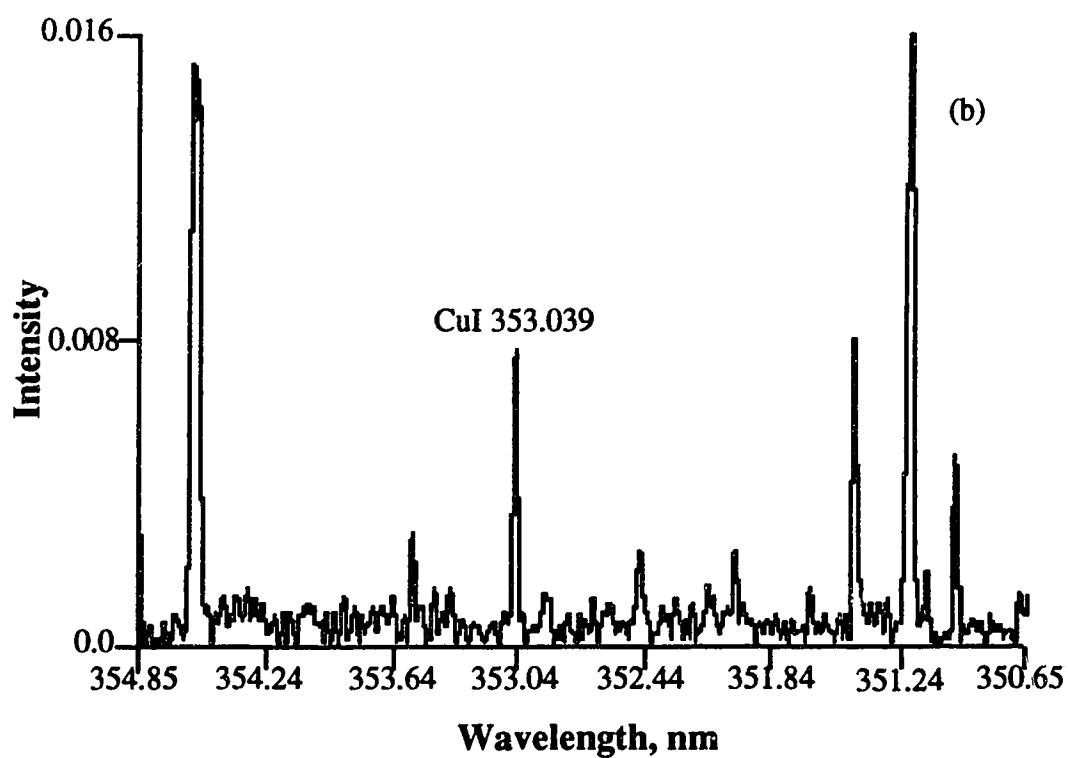
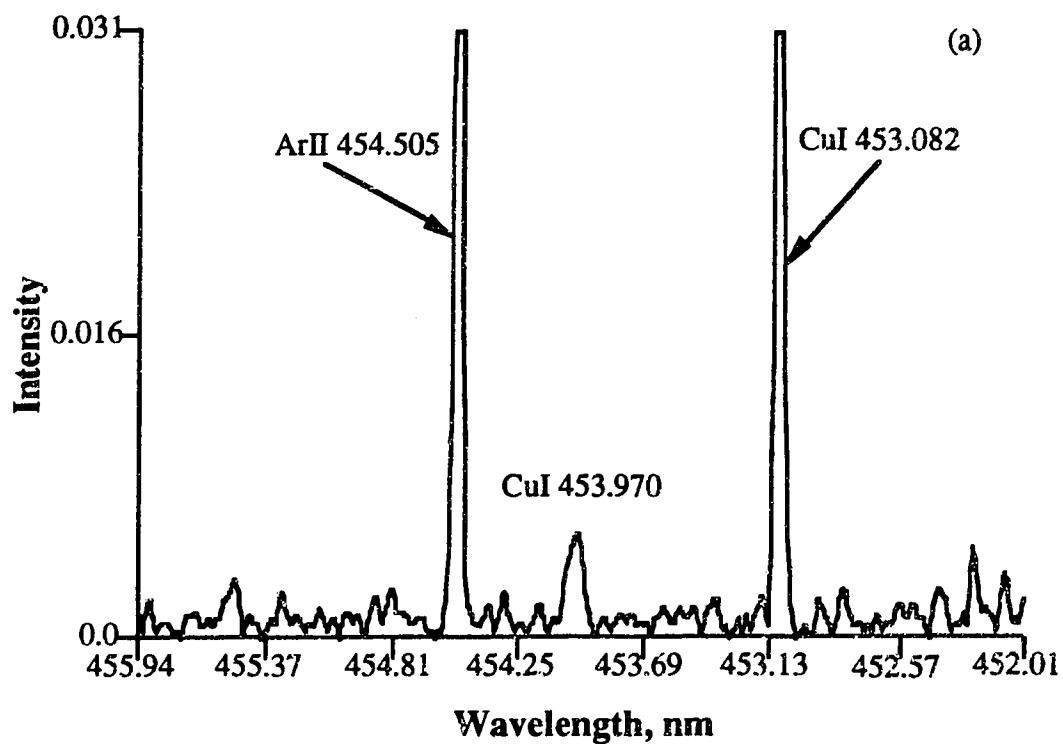


Fig. 5.9 A pair of CuI lines generated from the transitions  $4d^9 4s 5s \rightarrow 4d^9 4s 4p \rightarrow 4d^9 4s^2$ .

and its upper state is  $z\ 4F^{\circ}_{5/2}$  [9], exactly the same as the lower level for the 453.970 nm line. Thus these data and that presented earlier for the  $3d^{10}$  side of the copper energy level diagram provide clear spectral evidence for the occurrence of the excitation of the high energy levels, followed by stepwise de-excitation as a major process establishing the spectral character of the neutral atom emission of Cu in the glow discharge.

### 5.3.3 Copper Neutral Atom Lines - Ultraviolet Region

The ultraviolet spectra of the brass sample for the Ar based glow discharge and the inductively coupled plasma are shown in Fig. 5.10. Although there are clear differences in some regions of the spectra, there are also many similarities, certainly more so than was the case for the visible region spectra (Fig. 5.2). The differences and similarities are, at times, subtle. Several spectral regions will be analyzed in this section and in the section later dealing with zinc. The Ar based glow discharge spectrum has already been discussed in Chapter 4 with respect to copper ion emission. The focus here will be on neutral atom lines.

Several interesting line can be found centered around the CuII 224.700 nm line and expanded scale spectra (GD and ICP) are shown in Fig. 5.11 for this region. Eleven lines, not all in each spectrum, are noted and the type (CuI or CuII), wavelength, excitation energy, and transition are all listed for each line in Table 5.3.

The most prominent line in each spectrum (No. 9) is the CuII 224.700 nm ion line. The excitation of this line in the Ar based glow discharge was dealt with in some detail in Chapter 4. It was noted that charge transfer from  $Ar^+$  could selectively excite this transition and such a process also seems to be operative in the ICP. In the Ar glow discharge the

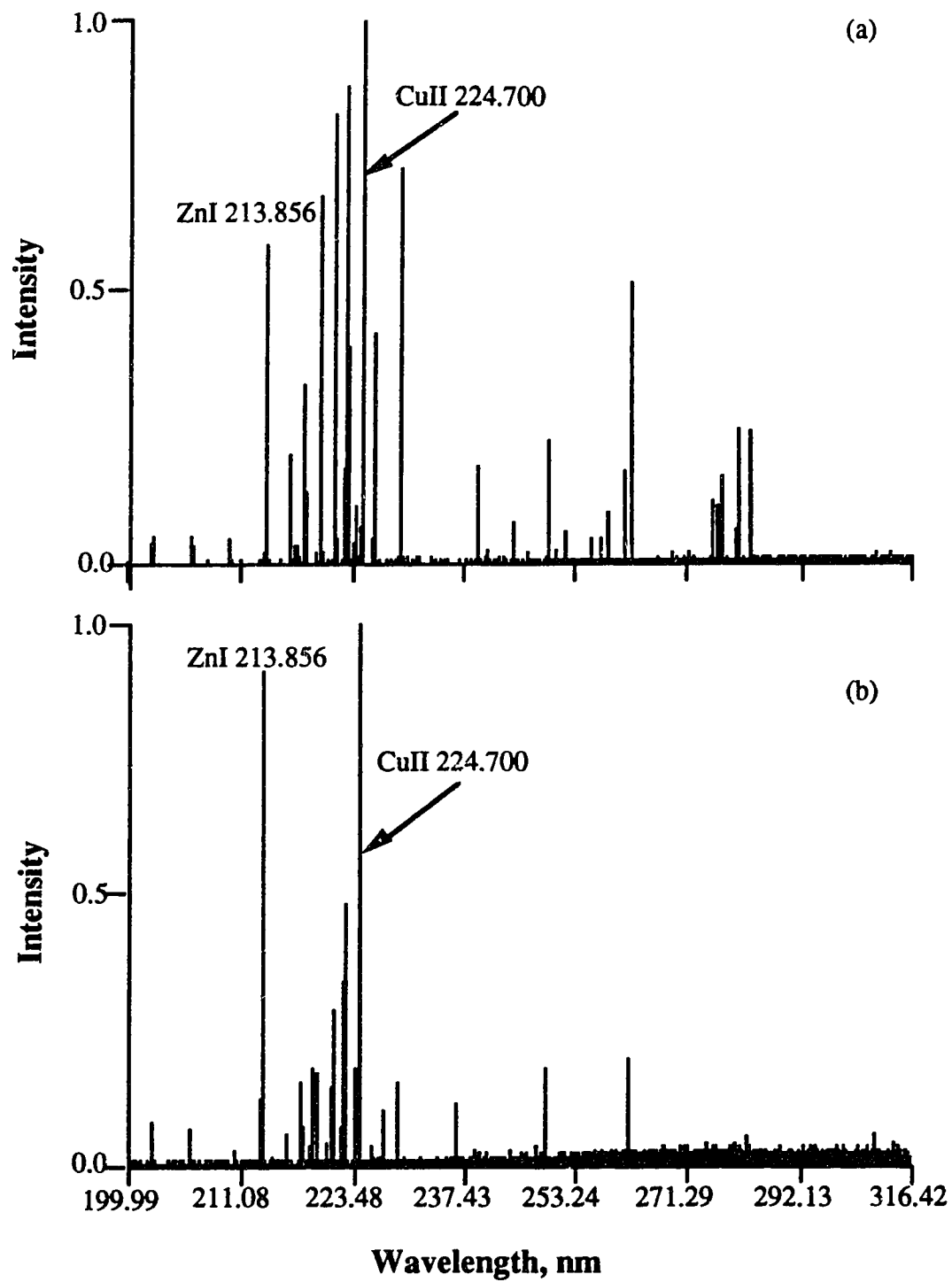


Fig. 5.10 Comparison of brass ultraviolet spectra in argon based GD (a) and ICP (b).

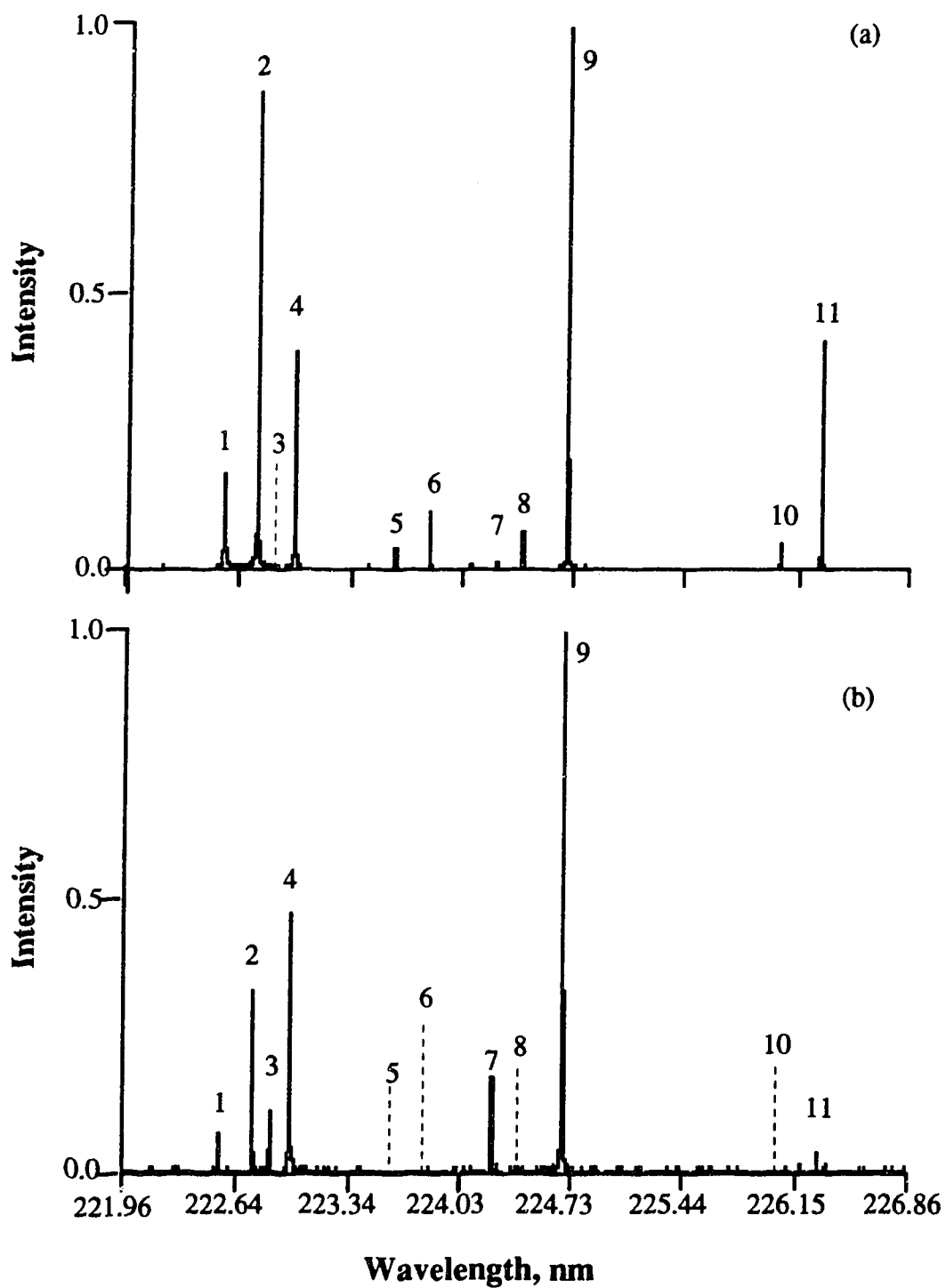


Fig. 5.11 A portion of brass spectra in the vicinity of 224.700 nm (a) GD and (b) ICP.

Table 5.3 Some characteristics of the GD and ICP lines noted in Figure 5.11.

No.	Type	Wavelength, nm	Energy, eV	Transition
1	CuI	222.570	5.57	$3d^9 4s 4p - 3d^{10} 4s$
2	CuI	222.778	7.20	$3d^9 4s 4p - 3d^9 4s^2 (D_{3/2})$
3	CuII	222.886	8.54	$3d^9 4p - 3d^9 4s$
4	CuI	223.008	6.94	$3d^9 4s 4p - 3d^9 4s^2 (D_{5/2})$
5	CuI	223.628	7.18	$3d^{10} 7p - 3d^9 4s^2 (D_{3/2})$
6	CuI	223.845	7.18	$3d^{10} 5f - 3d^9 4s^2 (D_{3/2})$
7	CuII	224.261	8.78	$3d^9 4p - 3d^9 4s$
8	CuI	224.427	5.52	$3d^9 4s 4p - 3d^{10} 4s$
9	CuII	224.700	8.23	$3d^9 4p - 3d^9 4s$
10	CuI	226.053	6.87	$3d^{10} 4f - 3d^9 4s^2 (D_{5/2})$
11	CuI	226.308	7.12	$3d^{10} 7p - 3d^9 4s^2 (D_{3/2})$

excitation was quite selective and only this lowest energy level of the 4p state of the copper ion was excited.

In the ICP spectrum two other CuII lines are observed (line 3 and 7). Both of these lines are also a result of 4p to 4s transitions. Line 3 does not appear in the GD spectrum and line 7 is very weak. It appears then, that other 4p to 4s CuII lines can be excited more readily in the Ar based ICP than the Ar based glow discharge. To explain the ion lines in the ICP, the following factors might be considered. Due to the high power in the ICP, the ion population relative to the neutral atoms is much higher (> 95% ionization was reported in the literature). The high electron number density and the high electron energy make electron impact excitation more effective. Electron impact may play a significant role in the excitation processes in the ICP. This may be one of the reasons why the ICP is a radiation source close to local thermal equilibrium. Charge transfer certainly can contribute to the excitation of some ion lines. Perhaps the higher gas kinetic energy of the ICP allows for more latitude in negative energy barrier charge transfer processes. All these possible processes could make the ion emission in ICP stronger than those in the glow discharge.

The rest of the lines noted in Fig. 5.11 are CuI lines. If like transitions are assessed as group some interesting trends and correlations emerge. Lines 2 and 4 are relatively strong in both discharges. They are both the result of  $3d^9 4s 4p$  to  $3d^9 4s^2$  transitions. However, line 2 is a slightly higher energy transition in that its upper level is just above that for line 4 [9] and its lower level is the higher energy level ( $D_{3/2}$ ) of the  $3d^9 4s^2$  ground state. Line 4's upper level is just below that of line 2 and it terminates in the lower level ( $D_{5/2}$ ) of the  $3d^9 4s^2$  ground state. A CuII state

( $3d^94d$ , 14.62 eV) also emits at this wavelength, its contribution to the intensity of this line may be bigger in ICP than in GD.

It is clear that these lines are readily excited in both discharges. However, the excitation of the higher energy lines is favored over the lower energy line in the GD, with the opposite being the case in the ICP. While, at first perhaps, seeming to be a trivial observation, this trend was observed for several other similar transitions in this region. Another example is shown in Fig 5.12 for the two closely spaced CuI lines at 219.958 and 219.975 nm. Again, the intensity of the slightly higher energy line is favored in the GD, while the lower energy line is favored in the ICP. The energy level diagram for these two lines is shown in Fig. 5.13. A possible explanation for this trend is that in the GD the upper levels are being populated primarily from above followed by stepwise de-excitation. While in the ICP, excitation proceeds primarily from lower levels upwards by electron impact.

Now lets return to Fig. 5.11. Lines 1 and 8 are similar based on their transitions. Both are the result of transition from  $3d^94s4p$  levels to the  $3d^{10}4s$  ground state. Both are stronger in the GD than in the ICP, with line 8 hardly even visible in the ICP spectrum. Their higher intensity in the GD could be favored by an excitation process which first populates the upper levels then followed by stepwise de-excitation.

Finally lines 5, 6, 10 and 11 form a group in that they all originate in upper levels (7p, 5f, 4f, 7p) of the  $3d^{10}$  states and all terminate in the  $3d^94s^2$  ground states. As can be seen from the spectra presented in Fig. 5.11, these lines are essentially present only in the GD spectrum and are absent , except for a weak line 11, from the ICP spectrum. This again, as did the visible spectral data discussed earlier, indicates that a mechanism,

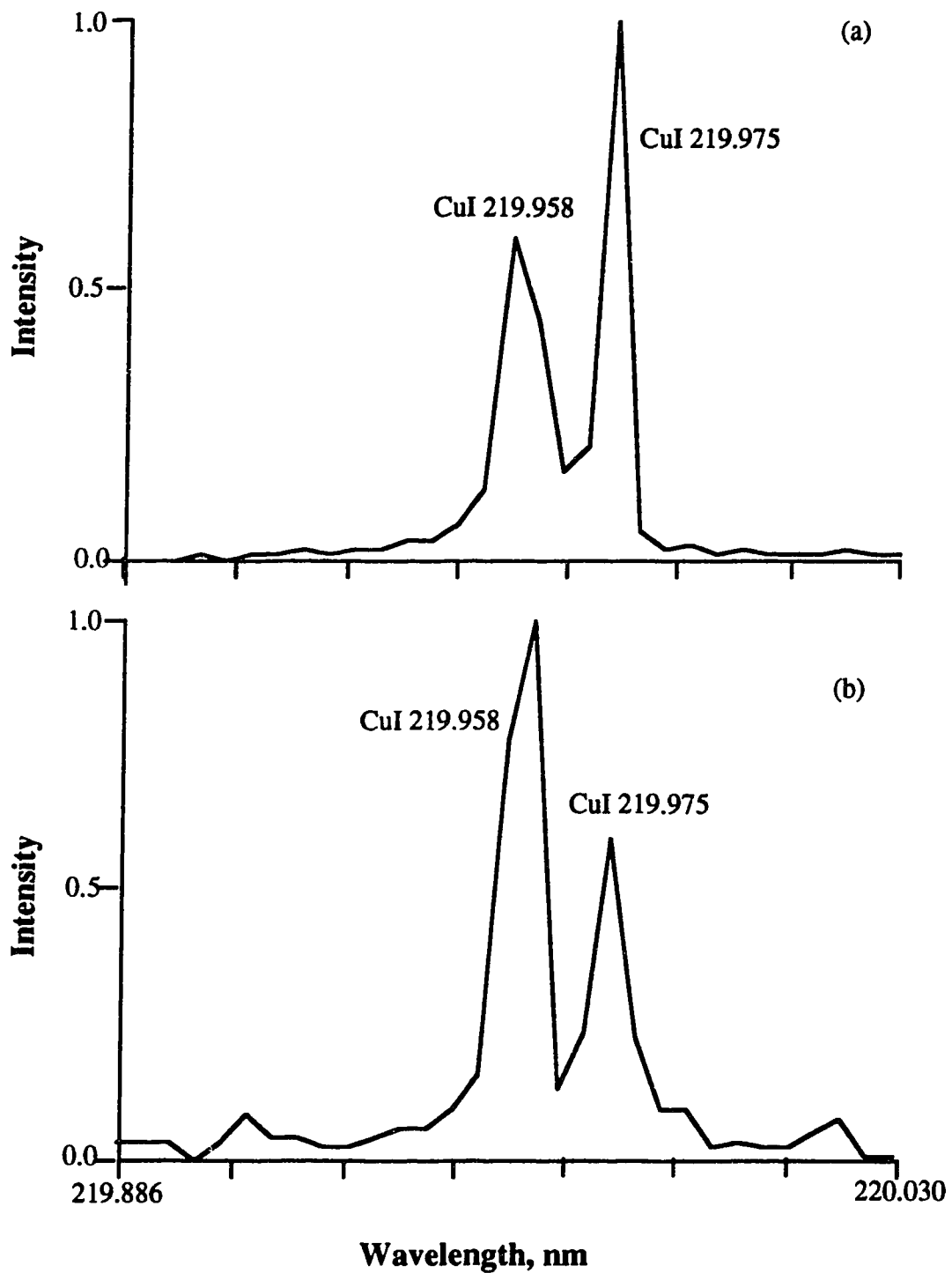


Fig. 5.12. Relative intensities of two closely spaced CuI lines in GD (a) and ICP (b).



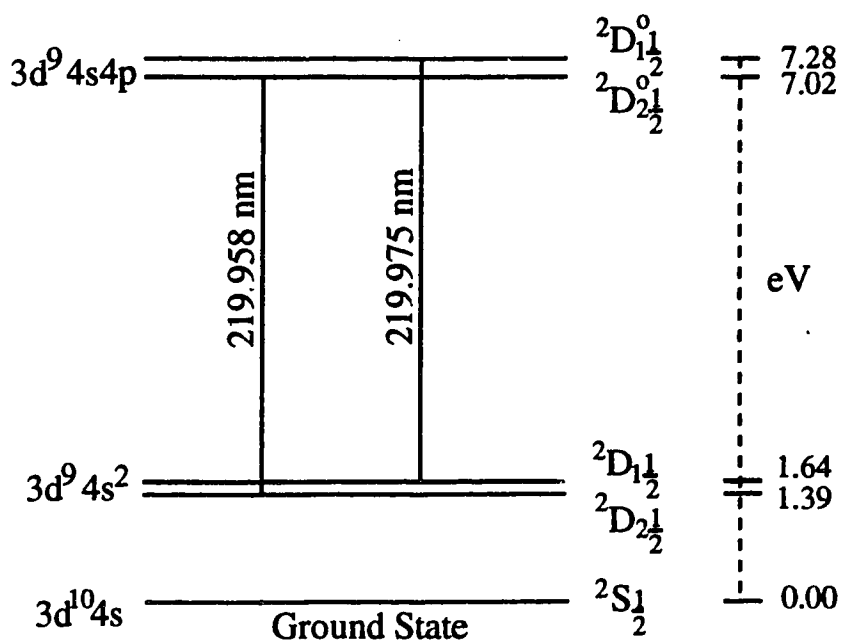


Fig. 5.13 Energy levels involved in the transitions generating 219.958 and 219.975 nm CuI lines.

the "top-down" process, is operative in the GD source populating these upper levels of the  $3d^{10}$  system of states.

An interesting comparison to the spectra shown in Fig. 5.11 is provided by the Ne and He spectra in the same wavelength region shown in Fig. 5.14. As discussed in Chapter 4, for these discharges the 4p to 4s CuII lines (lines 3, 7 and 9) are, more or less, excited, by stepwise de-excitation, to about the same degree. All the neutral atom lines (lines 1, 2, 4, 5, 6, 8, 10 and 11) have generally the same relative emission character as in the Ar GD (Fig. 5.11a). This is in keeping with the statement made earlier with respect to the filler gas not having much effect on the character of the neutral atom line spectrum.

These basic trends in the neutral copper spectrum can be confirmed throughout this spectral region. For the spectra shown in Fig. 5.15, the CuII lines (4p to 4s copper ion transitions) are much stronger in the ICP spectrum than in the GD spectrum. The CuI lines noted are both a result of  $3d^9 4s 4p$  to  $3d^9 4s^2$  transitions. In this case, both lines are more intense in the GD but the higher energy line (CuI 221.565 (7.23 eV) vs. CuI 221.458 (6.98 eV)) is much stronger, in a relative sense, in the GD compared to the ICP discharge.

Seven lines are noted on the spectra shown in Fig. 5.16 and their wavelength, energies, and transitions are summarized in Table 5.4. Line 4 is emitted from lead (PbI), a minor component of the brass sample. Line 6, present in the ICP spectrum and absent in the GD spectrum is a CuII (4p to 4s) line. Lines 2 and 3, presented only in the GD spectrum are CuI lines resulting from transitions from the 8p level of the  $3d^{10}$  states to the ground states of the  $3d^9 4s^2$  level. Lines 1, 5 and 7, present in both discharges, result from transitions from the  $3d^9 4s 4p$  levels to the ground state of the

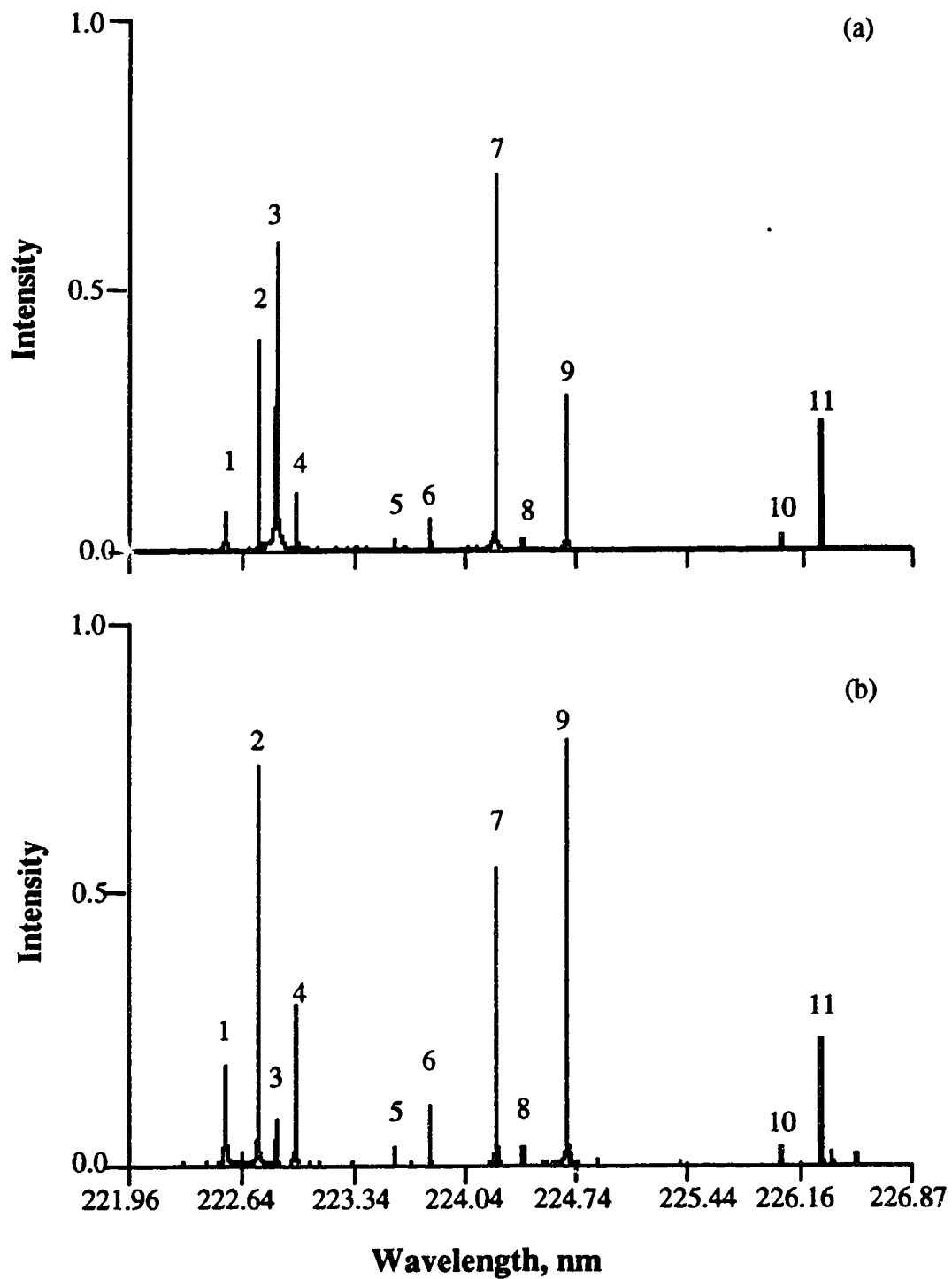


Fig. 5.14 A portion of brass ultraviolet spectra from Ne (a) and He (b) discharges.

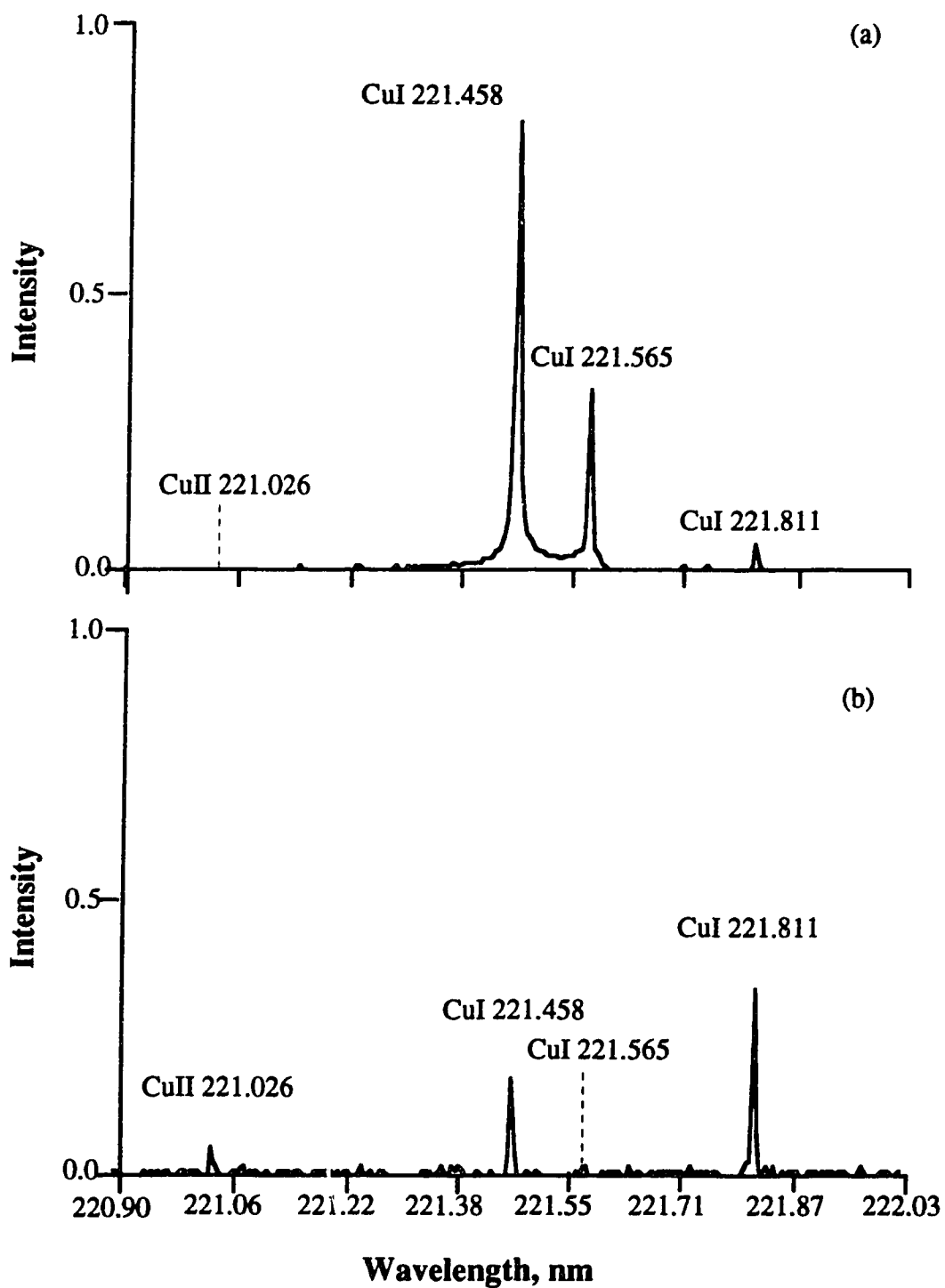


Fig. 5.15 Comparison of CuII and CuI line relative intensities between GD (a) and ICP (b) in the vicinity of 221 nm.

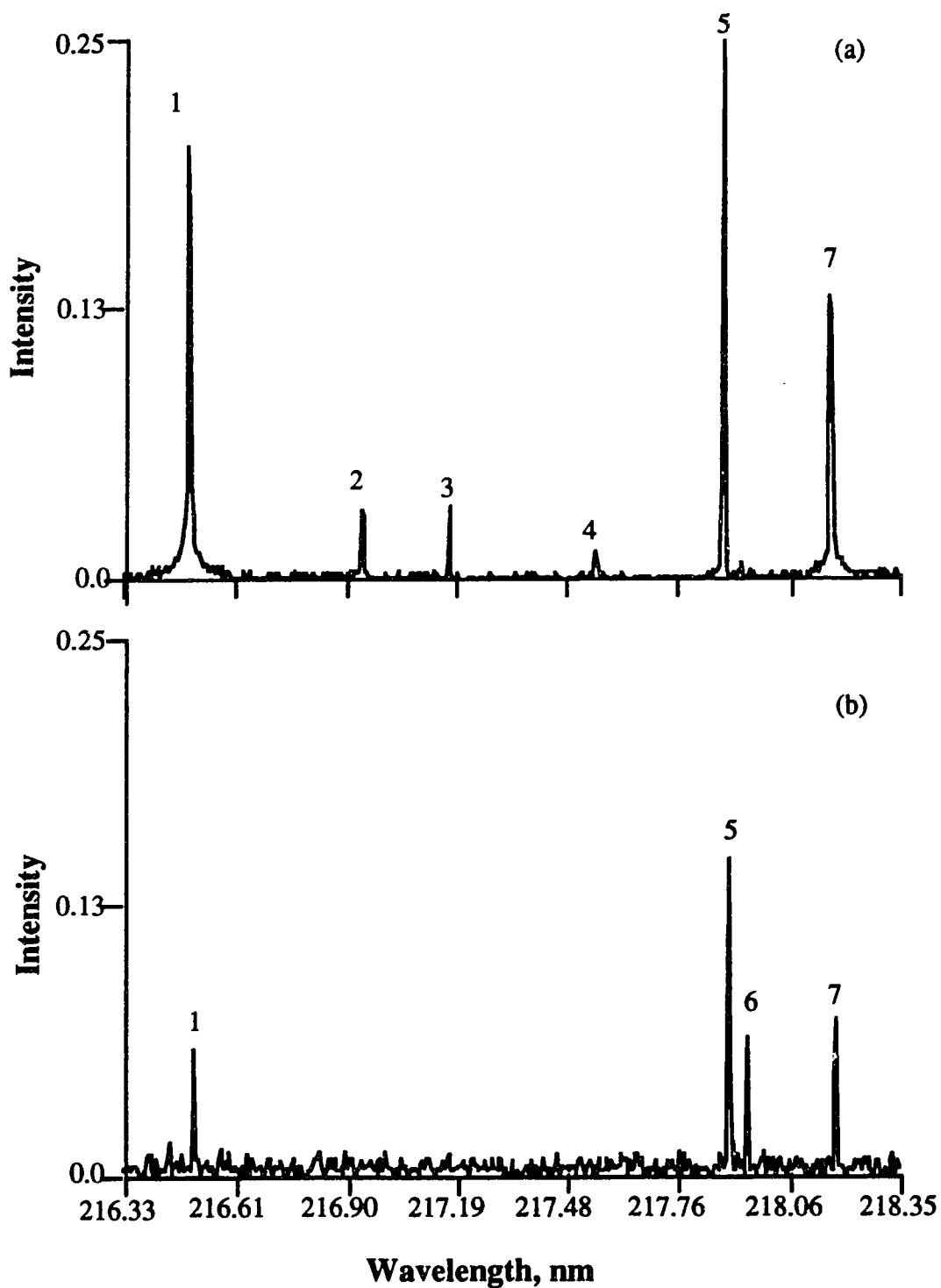


Fig. 5.16 Comparison of CuII and CuI line relative intensities between GD (a) and ICP (b) in the vicinity of 217 nm.

Table 5.4 Line data for Fig. 5.16

No.	Type	Wavelength, nm	Energy, eV	Transition
1	CuI	216.509	5.72	$3d^9 4s 4p - 3d^{10} 4s$
2	CuI	216.953	7.35	$3d^{10} 8p - 3d^9 4s^2 (D_{3/2})$
3	CuI	217.176	7.35	$3d^{10} 8p - 3d^9 4s^2 (D_{5/2})$
4	PbI	217.558	7.02	?
5	CuI	217.894	5.69	$3d^9 4s 4p - 3d^{10} 4s$
6	CuII	217.940	8.66	$3d^9 4p - 3d^9 4s$
7	CuI	218.172	5.68	$3d^9 4s 4p - 3d^{10} 4s$

$3d^{10}4s$  level. All these trends are analogous to those discussed with respect to the lines shown in Fig. 5.11.

Three pairs of GD and ICP spectra are shown in Fig. 5.17. In the first pair, the CuI 202.433 nm line is seen only in the GD spectrum. This line has an excitation energy of 6.12 eV and is the result of a transition from the  $3d^{10}5p$  level directly to the ground state  $3d^{10}4s$  level. In the next two pairs of spectra (Fig. 5.17 c and d, and Figs. 5.17 e and f) the two main lines illustrated (CuI 229.384 nm) and CuI 239.263 nm) are both the result of transitions from the  $3d^{10}6s$  levels to the  $3d^9 4s^2$  ground states. While not absent from the ICP spectra, they are considerably more intense in the GD spectra. In previous examples, lines of this nature were either absent from the ICP spectrum or quite weak (see line 11 in Fig. 5.11). Also the CuII line at 229.436 nm (Figs. 5.17 c and d) is present in both spectra and with about the same intensity. At first, this seems to disagree with the trends seen earlier for the CuII lines. However, this CuII line is a  $4p$  to  $4s$  line which has exactly the same upper state ( $4s^3 P^0_2$ ) [9] as the CuII 224.700 nm. Thus it should be subject to charge transfer by  $Ar^+$  and thus have a comparable sensitivity in the GD and ICP spectra, which is what is observed in Figs 5.17 c and d.

An energy level diagram is shown for copper in Fig. 5.18 b highlighting the major transitions observed in the ICP spectra. The copper GD energy level diagram (Fig 5.4) is duplicated as Fig 5.18a in order that they can be directly compared. The difference are quite striking. The glow discharge scenario is such that lines seem to be raining down from above. The ICP in contrast seems to be driven from the bottom (*i.e.* electron impact) with the low lying  $3d^9 4s^2$  levels acting also as a pseudo ground state along with the  $3d^{10}4s$  level. These mechanisms are not mutually

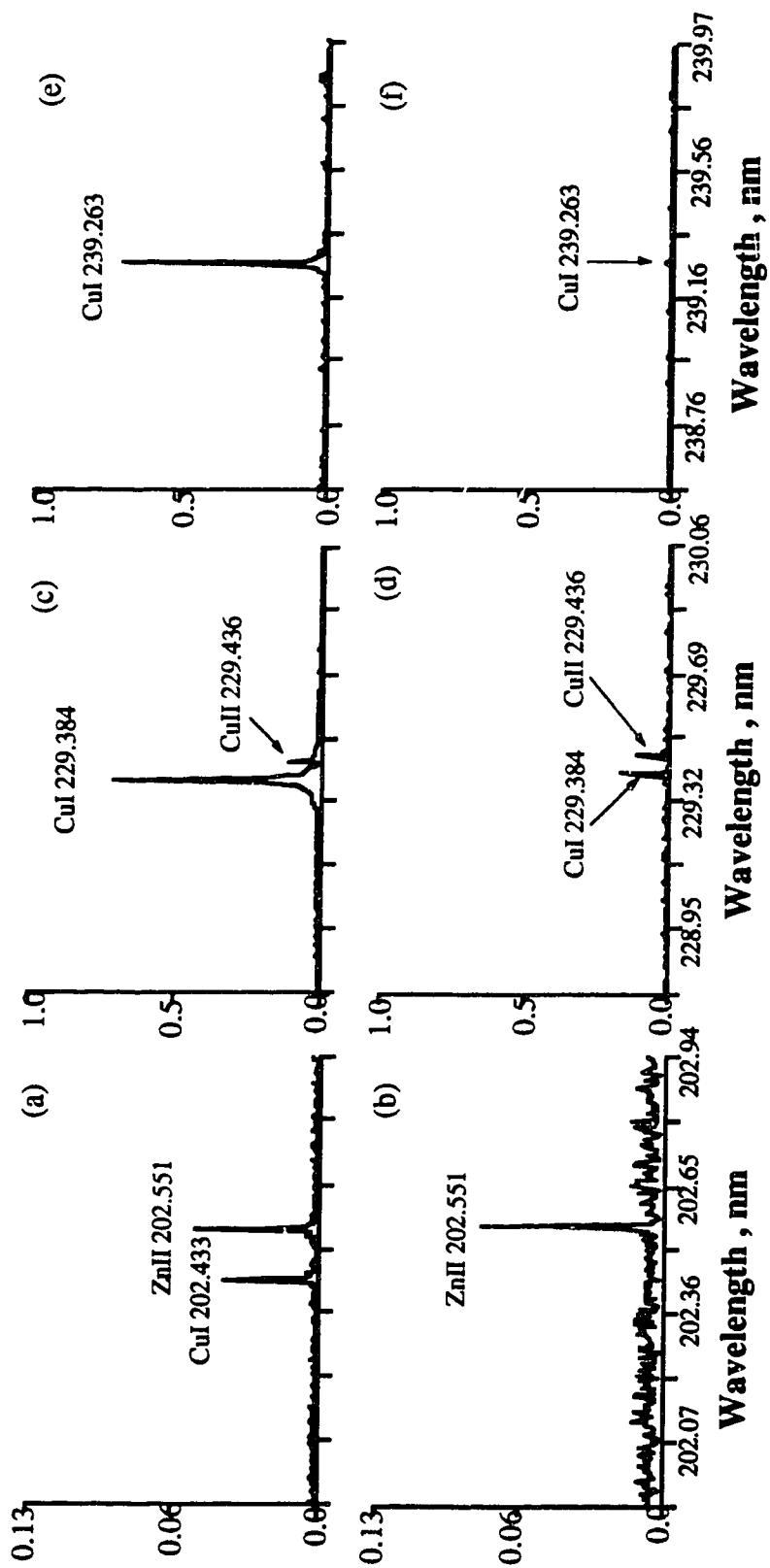


Fig. 5.17 Partial spectra showing the relative intensities of three lines in GD (a), (c), (e) and ICP (b), (d), (f).



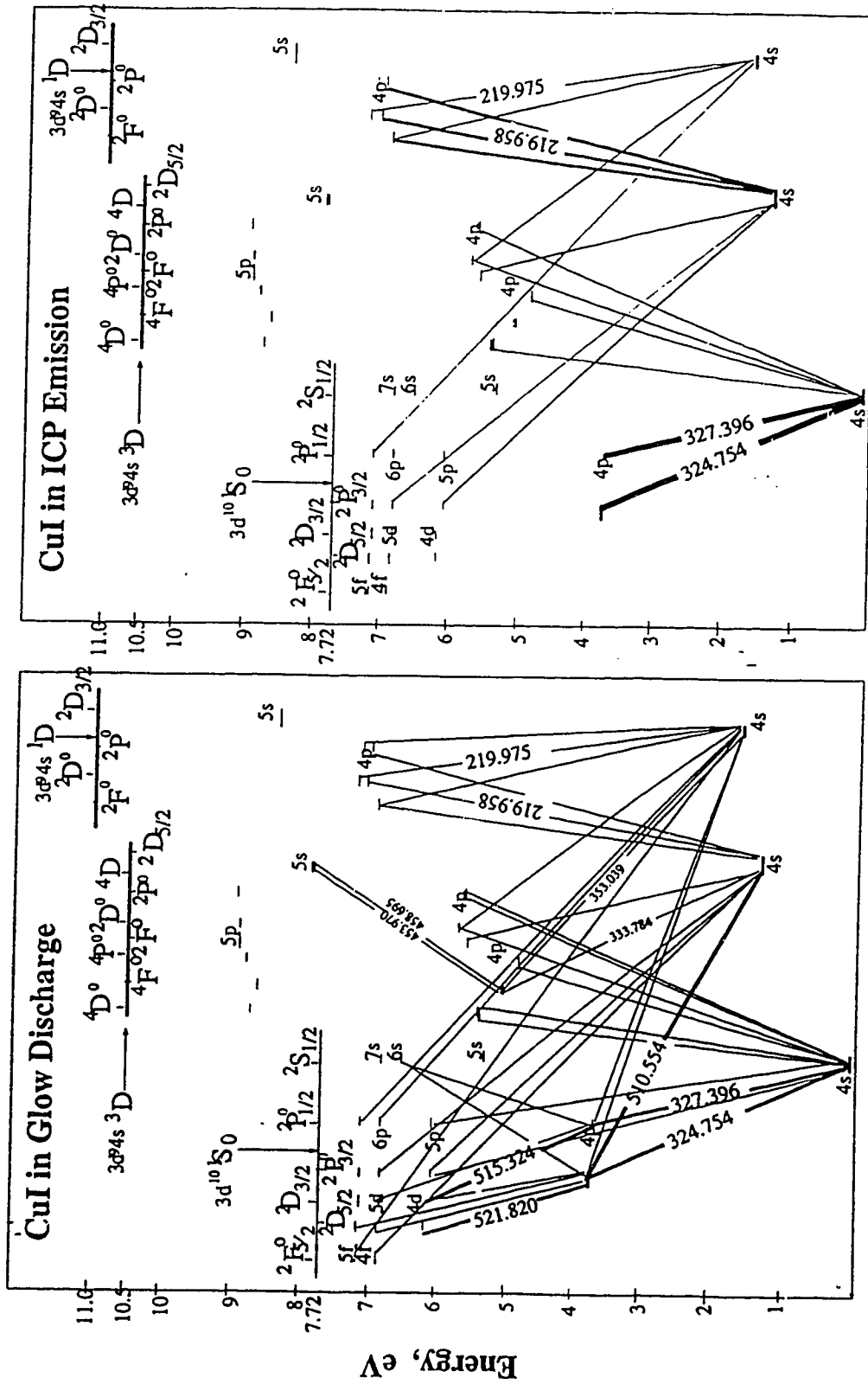


Fig. 5.18 Grotrian diagram showing the CuI transitions observed in ICP with the comparison to those in GD.

exclusive between these two sources and certainly some exceptions are found. But, the over all picture is quite consistent and, as will be seen in the next sections, the pictures fits Zn, Ag and Cd spectra as well.

#### 5.3.4 Zinc Neutral Atom Lines

Ar glow discharge and ICP ultraviolet spectra of the brass sample were shown earlier in Fig. 5.10. In the upper half (longer wavelength) of these spectra a number of lines are present that appear only in the glow discharge spectrum. Expanded scale spectra for this upper region are shown in Fig. 5.19. The line type, wavelength, energy and transition for the nine highlighted lines are given in Table 5.5. Three of the lines are CuI lines and six are ZnI lines. Two of the CuI lines (line 4 and 6) are the result of transitions from the  $3d^{10}5p$  level to the  $3d^94s^2$  and the third CuI line (line 9) involves a  $3d^94s4p$  to  $3d^94s^2$  transition. As discussed earlier, such lines are often strong lines in the GD spectrum and may be weakly excited in the ICP, behavior which is observed in this case.

The ZnI lines appear only in the GD spectrum. All the lines have relatively high excitation potentials (8.5 to 9.0 eV) and involve transitions from 7d, 6d and 5d levels to the 4p levels on the triplet side of the ZnI energy level diagram (See Fig. 5.20 and Table 5.5 [6,11]). It would take forbidden singlet-triplet transitions to populate these levels from the  $3d^{10}4s^2$  zinc ground state. Again, as with copper, these upper d states are likely populated from the top by a process such as ion-electron recombination.

A host of other lines were also observed for several other transitions among these levels. Most of these lines fall in the visible region of the spectrum. The full spectra of the brass sample for this region were shown

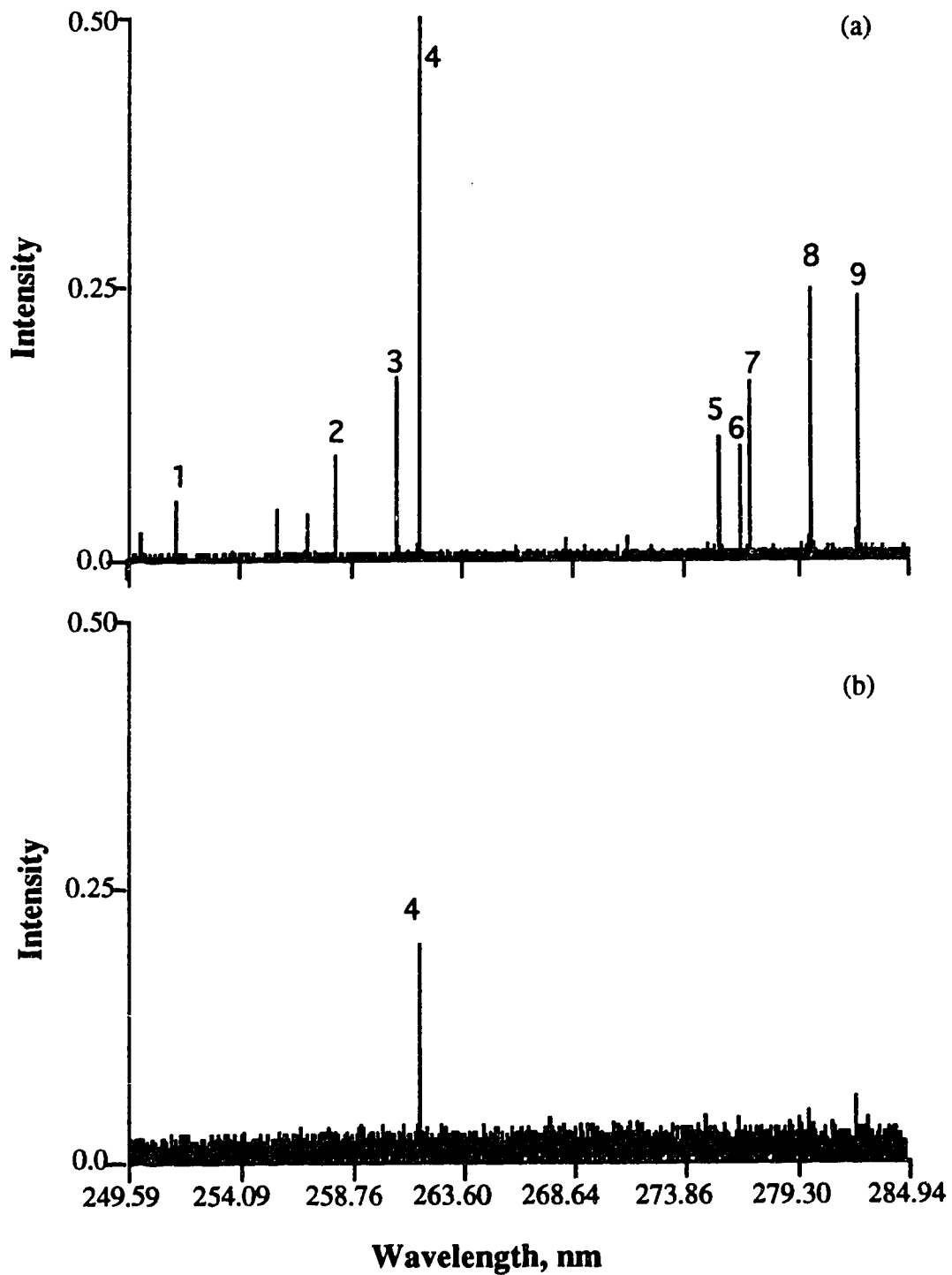


Fig. 5.19 A portion of brass spectra showing the zinc lines in GD (a) and ICP (b).

Table 5.5 Characteristics of lines highlighted in Fig. 5.19

No	Type	Wavelength, nm	Energy, eV	Transition [9,11]
1	ZnI	251.581	9.00	$3d^{10}4s7d - 3d^{10}4s4p$
2	ZnI	258.244	8.83	$3d^{10}4s6d - 3d^{10}4s4p$
3	ZnI	260.856	8.83	$3d^{10}4s6d - 3d^{10}4s4p$
4	CuI	261.837	6.12	$3d^{10}5p - 3d^9 4s^2$
5	ZnI	275.645	8.50	$3d^{10}4s5d - 3d^{10}4s4p$
6	CuI	276.637	6.12	$3d^{10}5p - 3d^9 4s^2$
7	ZnI	277.098 277.087	8.50	$3d^{10}4s5d - 3d^{10}4s4p$
8	ZnI	280.106 280.087	8.50	$3d^{10}4s5d - 3d^{10}4s4p$
9	CuI	282.437	5.78	$3d^9 4s4p - 3d^9 4s^2$



in Fig. 5.1 and 5.2. Expanded scale spectra highlighting the 5s to 4p and 4d to 4p spectral lines are shown in Fig. 5.21 and listed in Table 5.6 along with several other observed visible ZnI lines. The ZnI line at 334.502 nm is actually one of a triplet and this is illustrated in Fig. 5.22a. The scale expanded spectrum and insert show the three lines of the triplet. The 330 line is a doublet with lines at 330.259 and 330.294 nm as shown in Fig. 5.22b.

Two weak lines can be noted in Fig. 5.22b just to the left of the 330 nm lines. An interesting scale expanded plot of this spectrum is shown in Fig. 5.23a. and the lines are clear. At first, we had some difficulty identifying these peaks until it was realized that they were aliased into this spectral region from the UV. As noted in Chapter 2 and reference 12, the aliasing point for these spectra is 316.443 nm. Lines with wavelength shorter than this value will be folded into the upper part of the visible spectrum. Most of the potential confusion that could be generated from aliasing is eliminated by use of the 1P21 photomultiplier tube whose spectral response, as a result of having a glass envelope, stops at about 300 nm. However, the spectral response cut is not sharp and thus some aliased lines can often be seen in this lower region (short wavelength) of the visible spectrum.

For zinc, this is actually fortuitous. The program SpectroPlot [13] is designed to handle wavelength identification in multiple aliased regions and the spectral plot shown in Fig. 5.23a is labeled with the alternate aliased wavelength scale. These lines were thus ultimately identified as ZnI 303.578 nm and CuI 303.610 nm. This CuI line is one of the ubiquitous  $3d^94s4p$  to  $3d^94s^2$  transitions. This ZnI line is a result of one of the transitions possible between the 6s to 4p triplet levels. Another 6s to 4p line

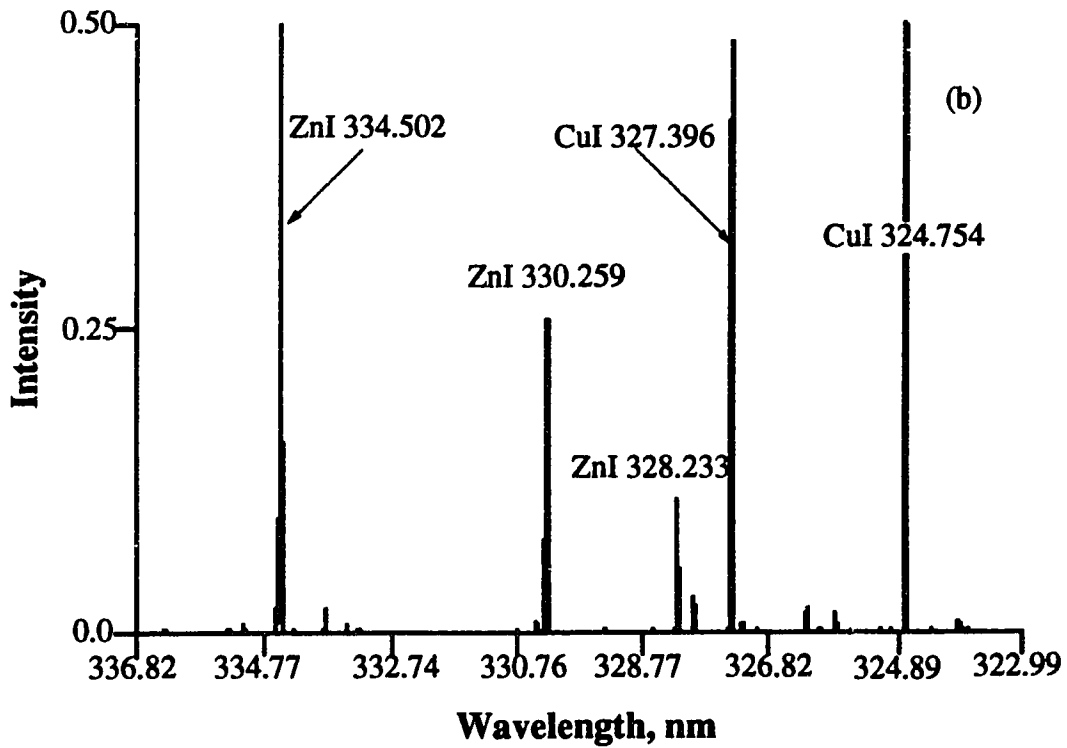
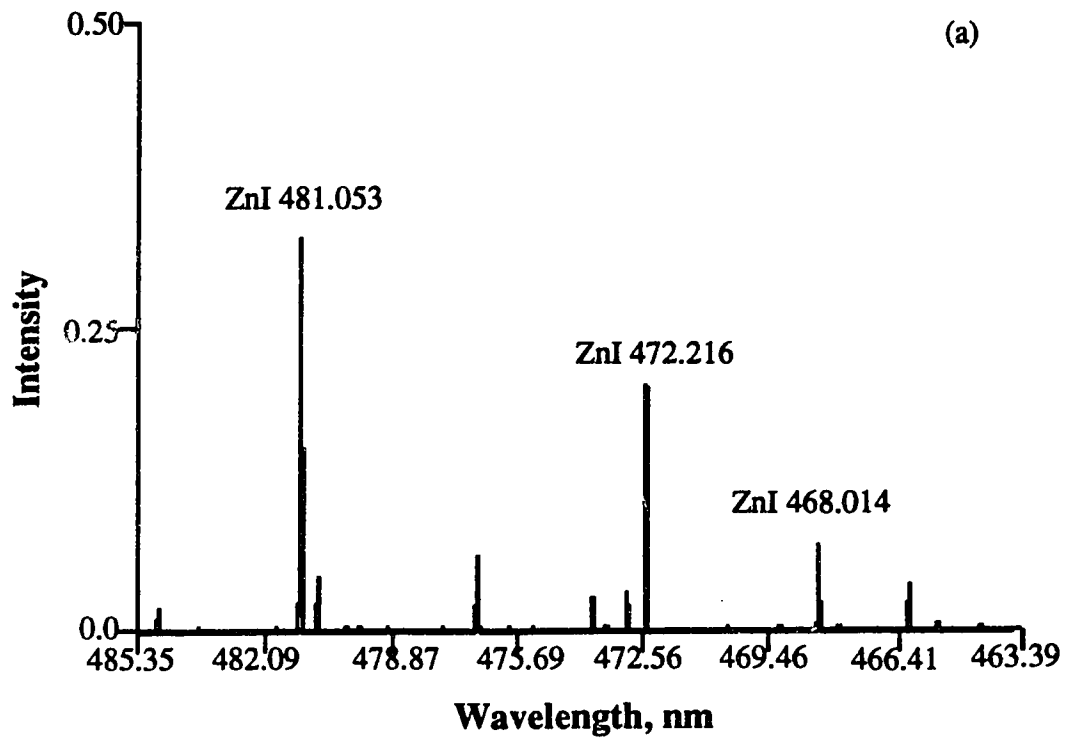


Fig. 5.21 Zn I lines generated from 5s to 4p and 4d to 4p transitions.

Table 5.6 Visible region ZnI lines

Type	Wavelength, nm	Energy, eV	Transition
ZnI	481.053	6.66	5s (triplet) to 4p (triplet)
ZnI	472.216	6.66	5s (triplet) to 4p (triplet)
ZnI	468.014	6.66	5s (triplet) to 4p (triplet)
ZnI	334.502	7.78	4d(triplet) to 4p (triplet)
ZnI	330.259	7.78	4d (triplet) to 4p (triplet)
ZnI	328.233	7.78	4d (triplet) to 4p (triplet)
ZnI	307.206	8.11	6s (triplet) to 4p (triplet)
ZnI	303.578	8.11	6s (triplet) to 4p (triplet)
ZnI	307.590	4.03	4p (triplet) to 4s (triplet)
ZnI	636.235	7.74	4d (singlet) to 4p (singlet)
ZnI	462.981	8.47	5d (singlet) to 4p (singlet)



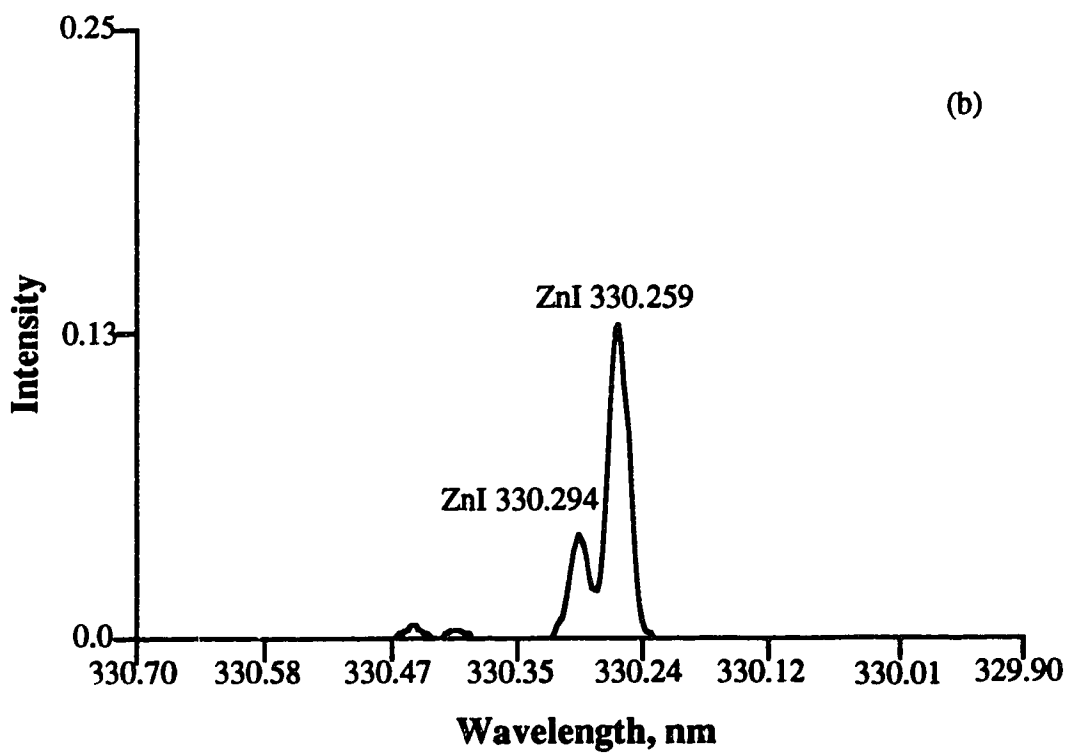
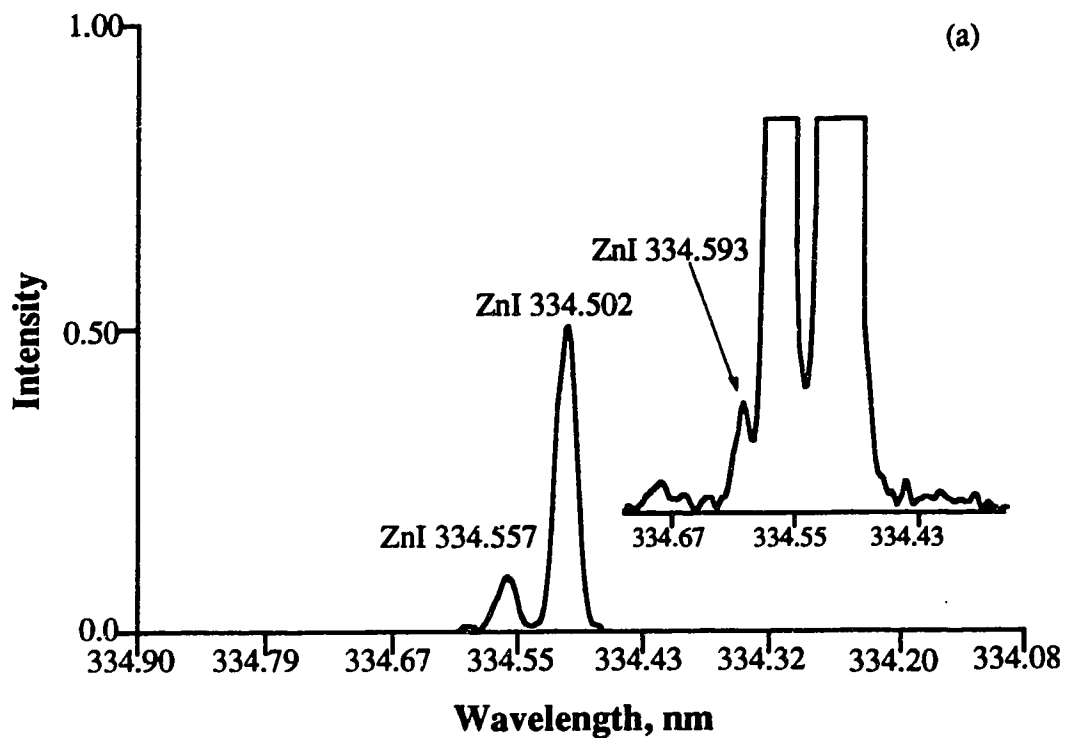


Fig.5.22 ZnI lines generated from 4d to 4p transitions observed in GD.

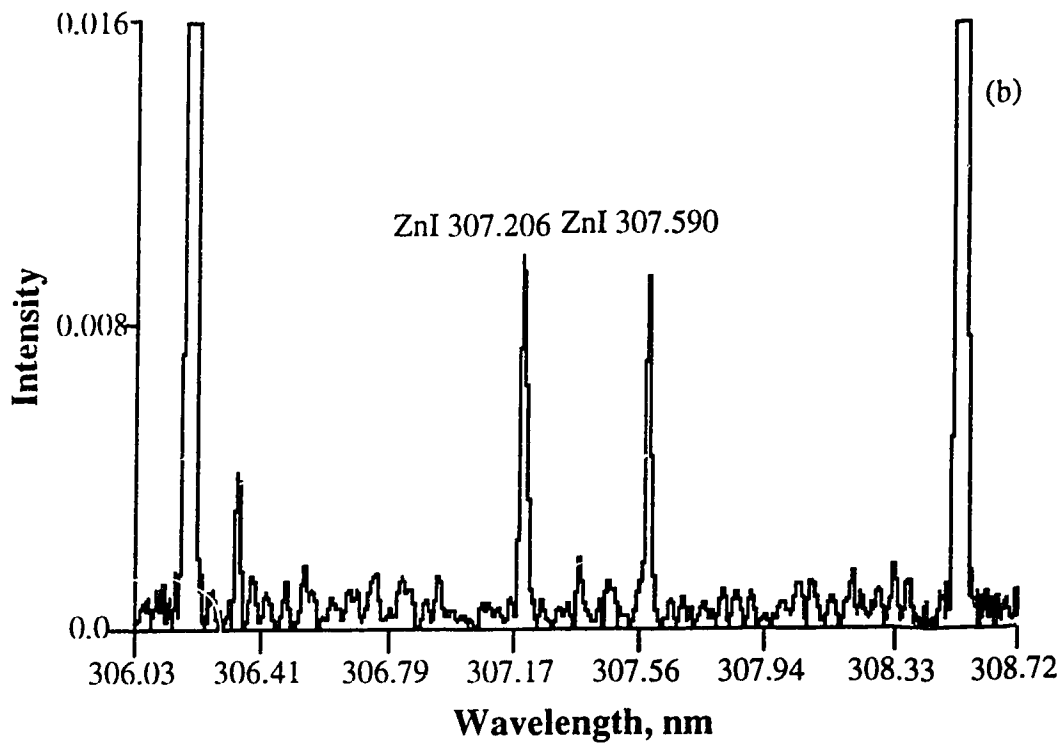
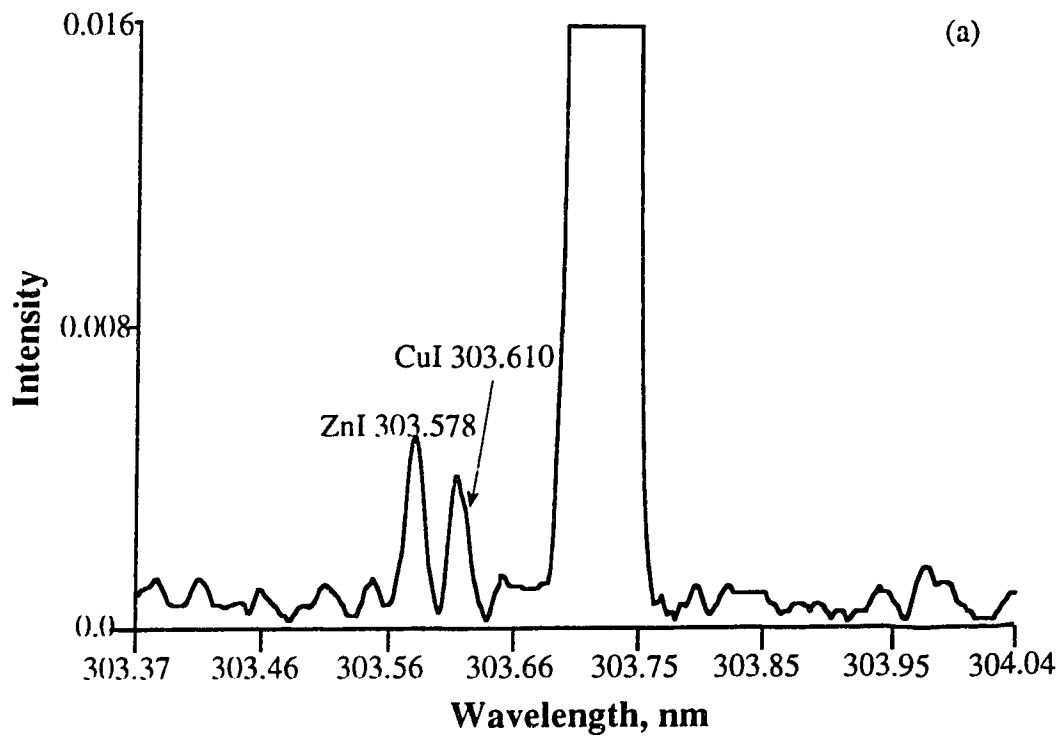


Fig. 5.23 UV lines fall into the visible region because of aliasing.

was found at 307.206 nm and it is shown in Fig 5.23b. This line is again, an aliased line and falls between the two CuI resonance lines (See Fig. 5.21).

This vast array of high energy triplet lines that is observed in the GD spectrum of ZnI clearly point to the "top-down" as the likely process leading to population of the upper states of these transitions. As well, we can clearly see the ZnI line at 307.590 nm. This line is a result of the "forbidden" transition from the 4p triplet to the 4s singlet ground state. The observation of this line is indicative of stepwise de-excitation in the triplet system. So many populated states are feeding the 4p triplet level that even this forbidden line is clearly observed.

Further evidence for stepwise de-excitation can be found on the singlet side of the ZnI energy level diagram. Lines for both the 4d to 4p (636.235 nm) and 5d to 4p (462.981 nm) singlet - singlet transitions are observed in the spectrum (See Fig. 5.24). The upper levels of these lines are likely populated by the same mechanism discussed in the CuI system.

All of these ZnI high excitation potential lines were either very weak or completely absent from the ICP spectrum of the brass sample. Basically, ZnI 213.856 nm was the only strong ZnI line observed in ICP. Energy level diagrams denoting major ZnI lines observed in the glow discharge and the ICP are shown in Fig. 5.25.

### 5.3.5 Silver Neutral Atom Lines

The visible region of the GD spectrum for Ag with He as the filler gas is shown in Fig. 5.26. The major visible lines observed for Ag are noted on the figure and they are also listed in Table 5.7. As noted earlier for copper, the resonance lines of Ag (338.289 and 328.068 nm) are, to

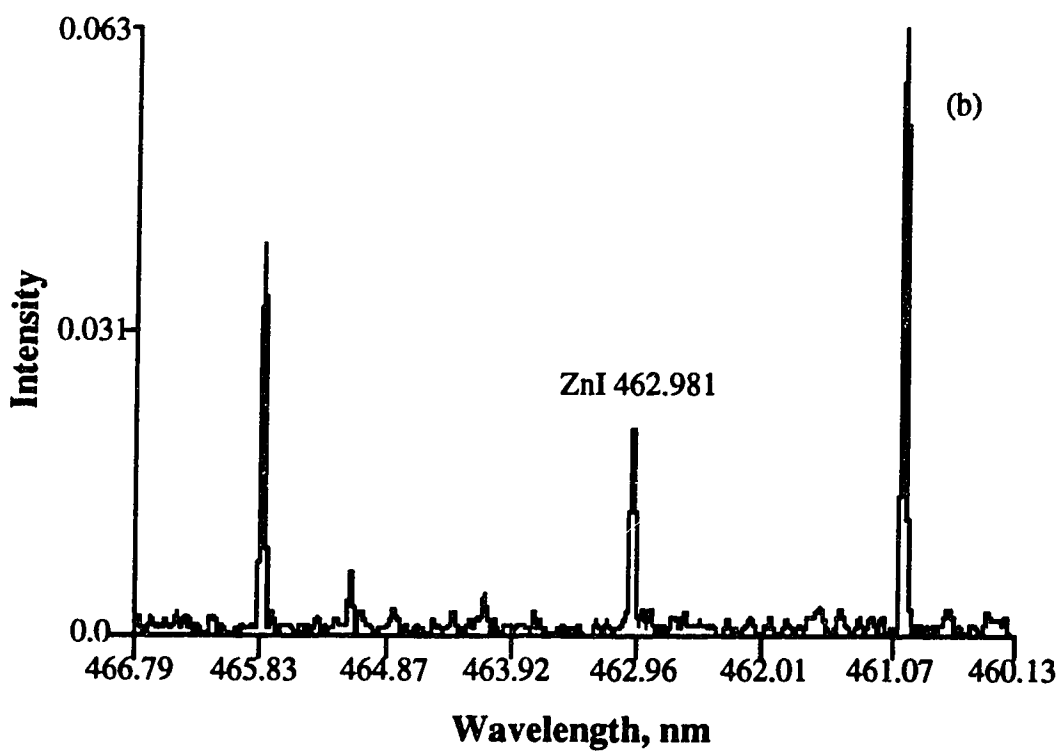
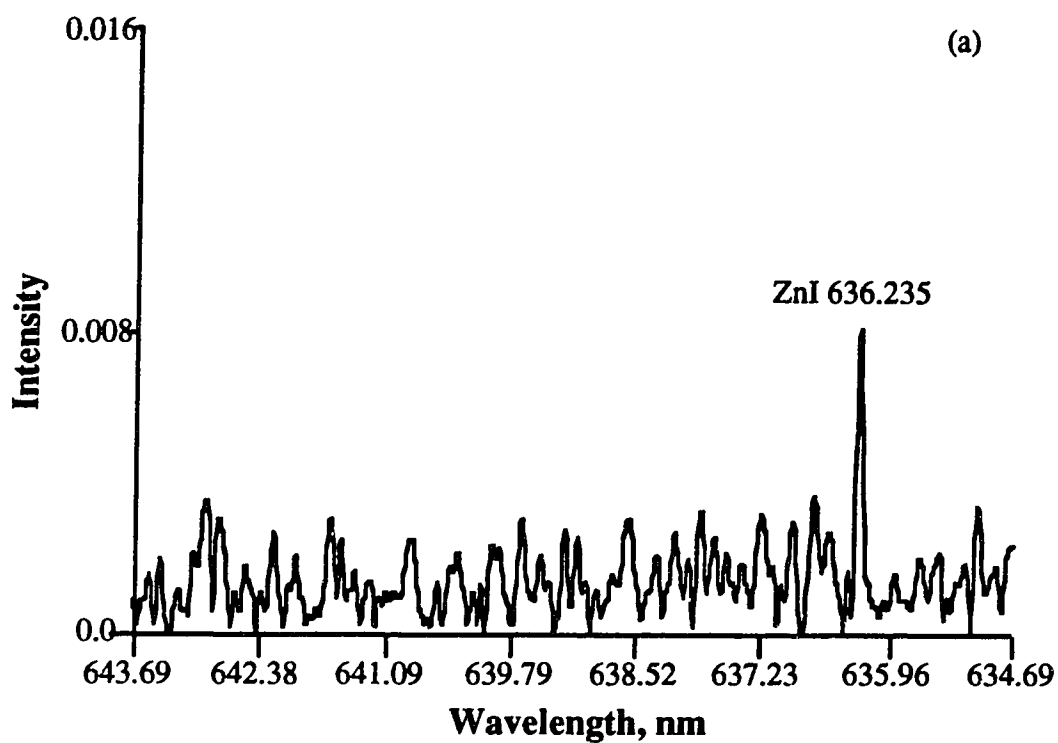


Fig. 5.24 Lines from transitions  $3d^{10}4s4d \rightarrow 3d^{10}4s4p$  (singlet) and  $3d^{10}4s5d \rightarrow 3d^{10}4s4p$  (singlet).

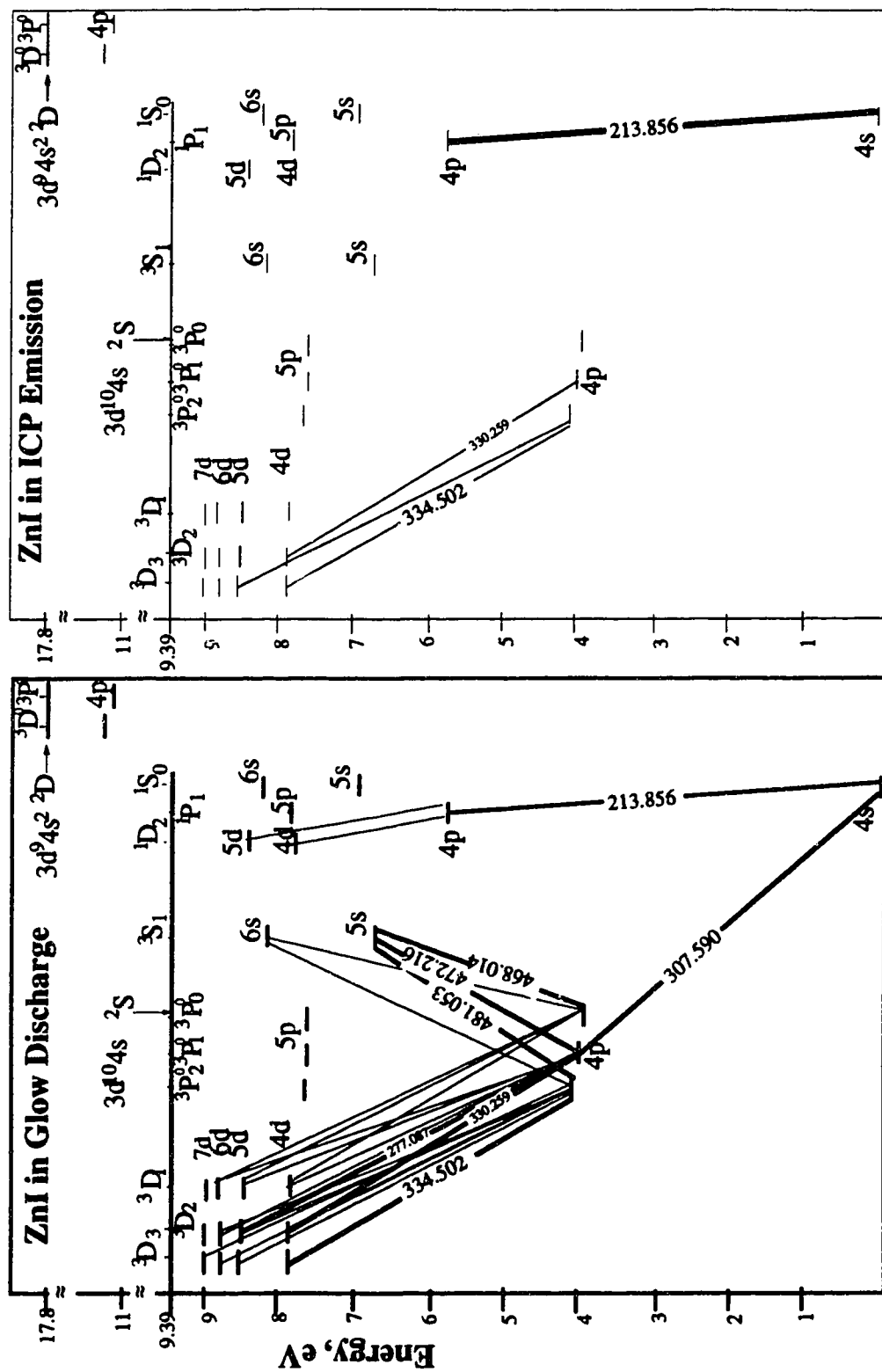


Fig. 5.25 Grotrian diagram showing the ZnI transitions observed in ICP with the comparison to those in GD.

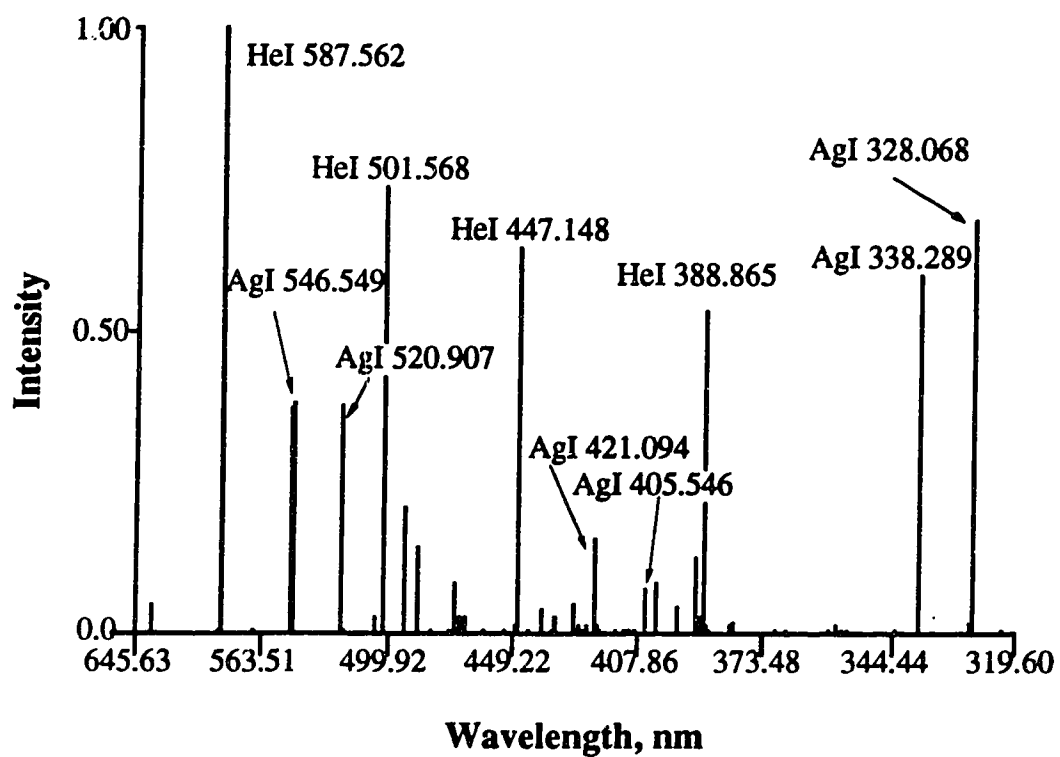


Fig. 5.26 Ag visible spectrum from a He based glow discharge.

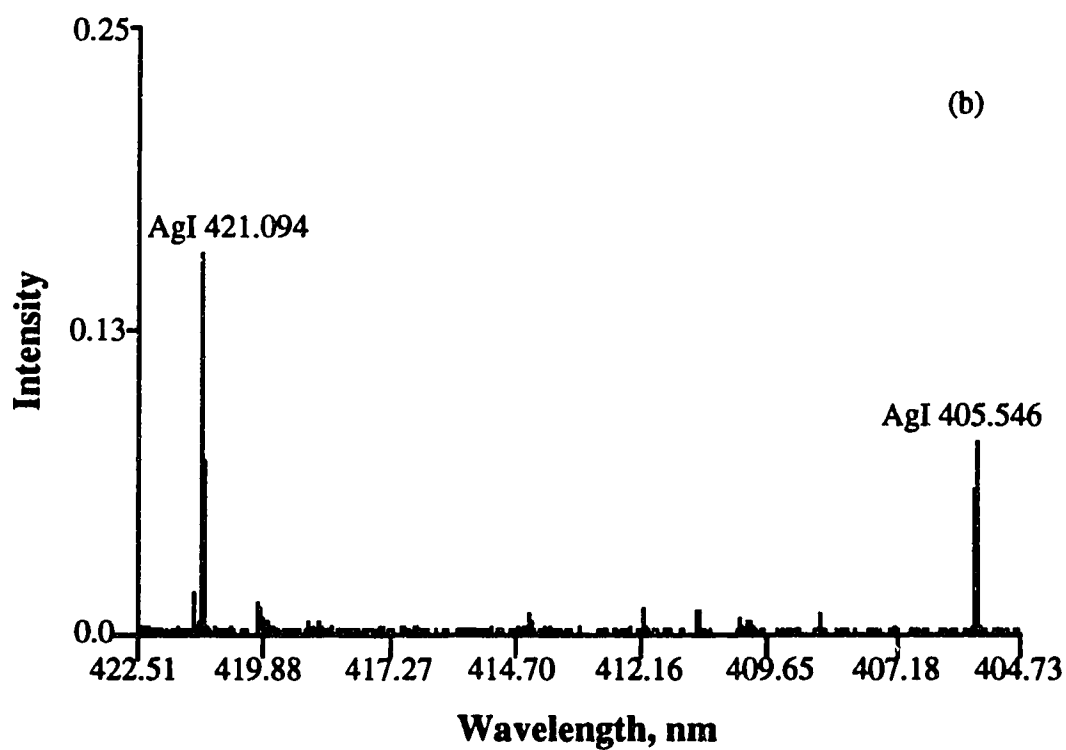
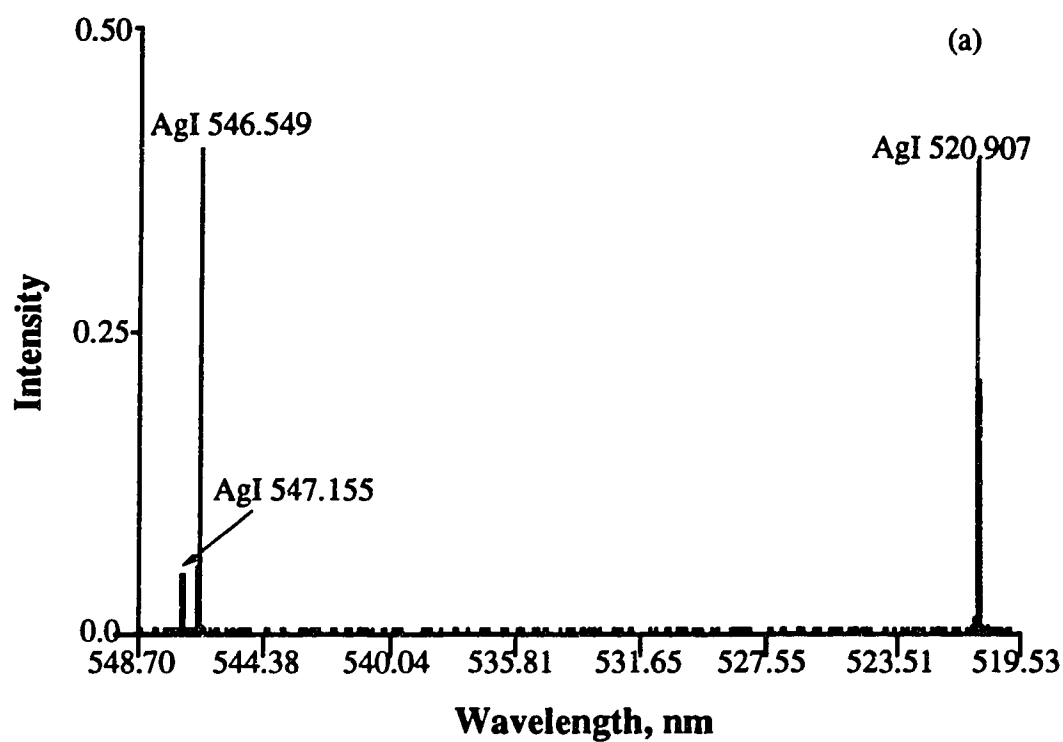


Fig. 5.27 Scale expanded spectrum showing AgI lines from 5d  $\rightarrow$  5p and 6d  $\rightarrow$  5p transitions.

Table 5.7 Characteristics of AgI lines

Type	Wavelength, nm	Energy, eV	Transition
AgI	328.068	3.66	5p to 5s
AgI	338.289	3.78	5p to 5s
AgI	546.549	6.04	5d to 5p
AgI	520.907	6.04	5d to 5p
AgI	421.094	6.72	6d to 5p
AgI	405.526	6.72	6d to 5p
AgI	466.848	6.44	7s to 5p
AgI	447.608	6.44	7s to 5p
AgI	381.086	7.02	7d to 5p
AgI	206.117	6.01	6p to 5s
AgI	206.983	5.98	6p to 5s



some extent, self absorbed.

In basic structure, the energy level diagram for AgI is analogous to that of for CuI [6,14]. The ground state is  $4d^{10}5s$  and the resonance doublet is a result of transitions from the  $4d^{10}5p$  levels to the  $4d^{10}5s$  ground state. Most of the other silver lines observed in the GD spectrum are a result of transitions from the upper levels on the  $4d^{10}$  side of the energy level diagram to the  $4d^{10}5p$  level. These include the 546.549 and 520.907 nm lines shown in Fig. 5.26 and 5.27 which are the result of  $5d$  to  $5p$  transitions and the 421.094 and 405.526 nm lines which are result of  $6d$  to  $5p$  transitions.

Additional transitions are shown in Figs. 5.28 and 5.29. The 466.848 and 447.608 nm line shown in Fig. 5.28 are from  $7s$  to  $5p$  transitions, and the 381.086 nm AgI line shown in Fig. 5.29a is from a  $7d$  to  $5p$  transition. Finally the 206.117 and 206.983 nm lines shown in Fig. 5.29b are a result of transitions from the  $6p$  level to the  $4d^{10}5s$  ground state.

Thus it seems that the upper states on the  $4d^{10}$  side of the energy level diagram are being populated, which could be driven by the same process as for the CuI system. However, in contrast to copper, we did not observe any lines that originated on the  $4d^95s^2$  side of the AgI energy level diagram. For example, we looked for but did not observe AgI 282.437 nm (8.13 eV). Most of the lines with the  $4d^95s^2$  pseudo ground state are, however, strongly autoionizing lines with their upper states well above the ionization potential of Ag (IP = 7.57 eV). The upper state of the autoionizing lines that were observed earlier for Cu (458.695 and 453.970 nm) are only 0.07 and 0.15 eV above the IP of Cu, while the upper state of the AgI 282.437 nm is 0.56 eV above the IP of Ag. Thus, if dielectric recombination does occur (Equation 5.3) the preferred route of

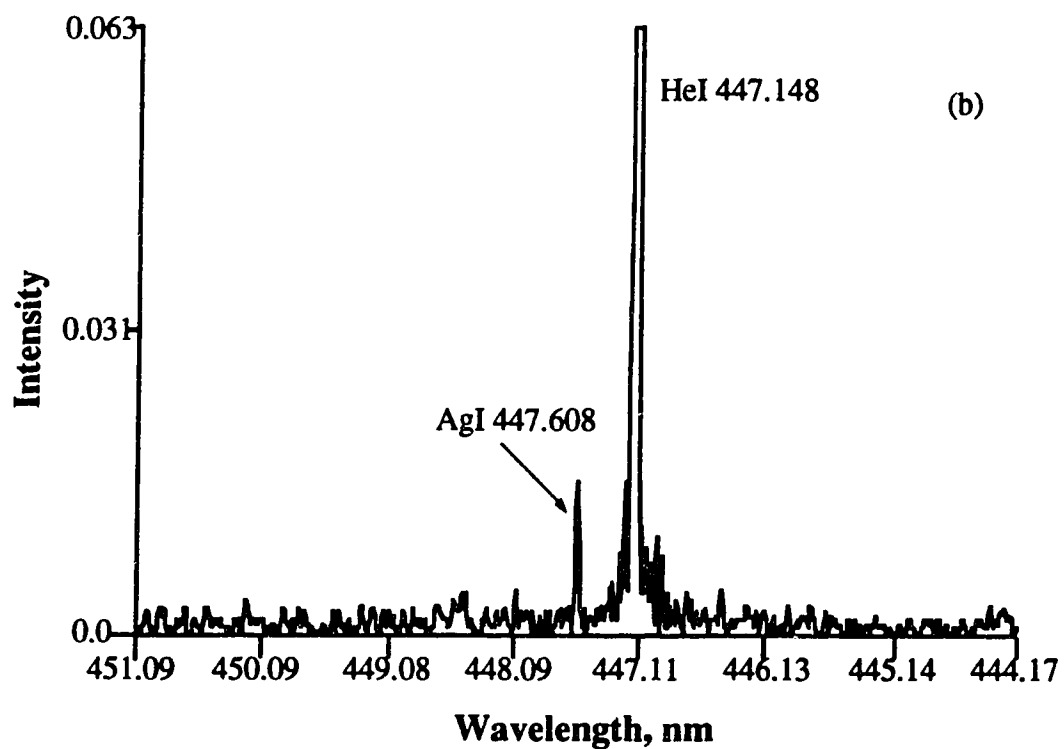
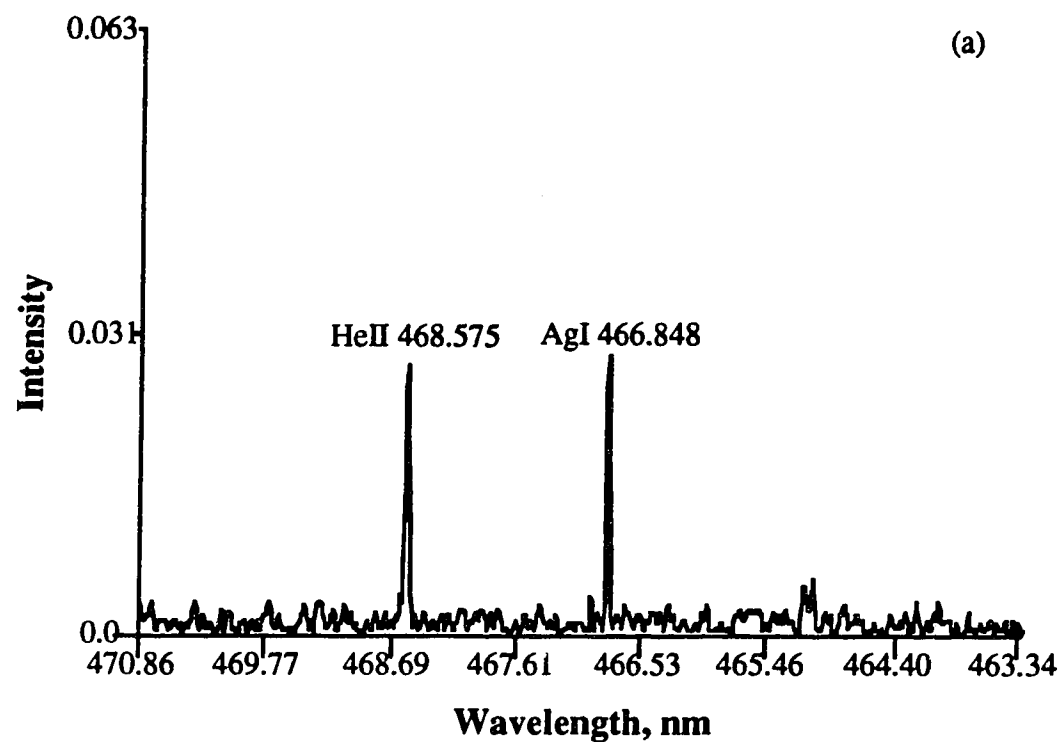


Fig. 5.28 Scale expanded spectrum showing AgI lines from  $7s \rightarrow 5p$  transitions.

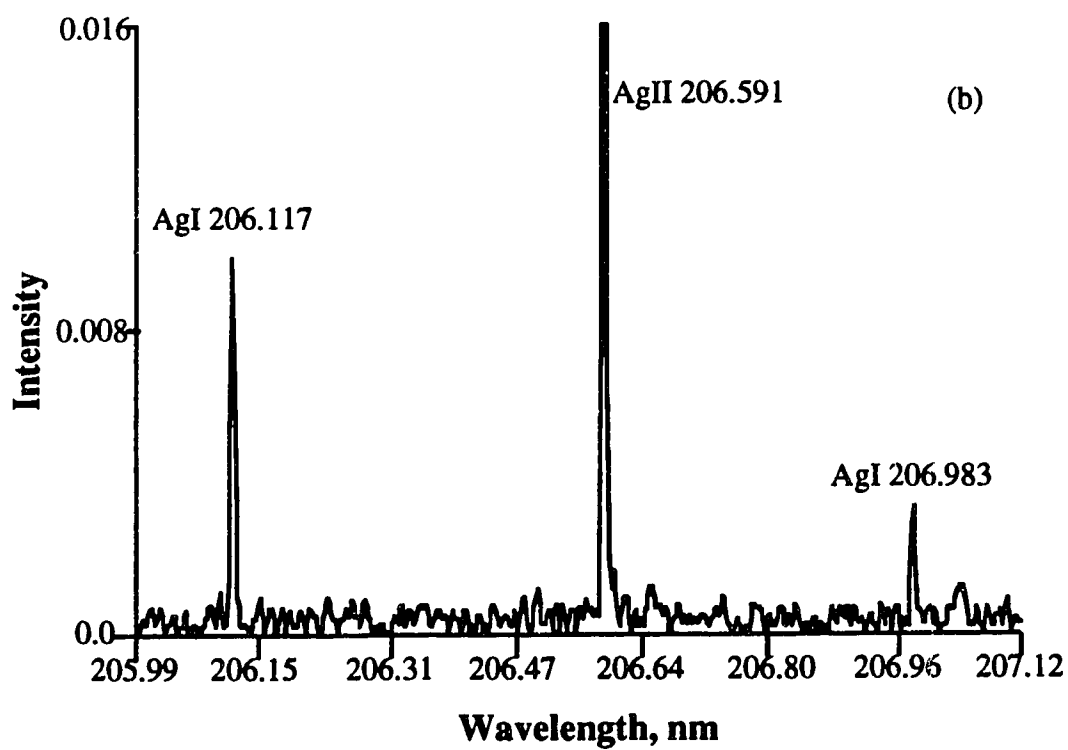
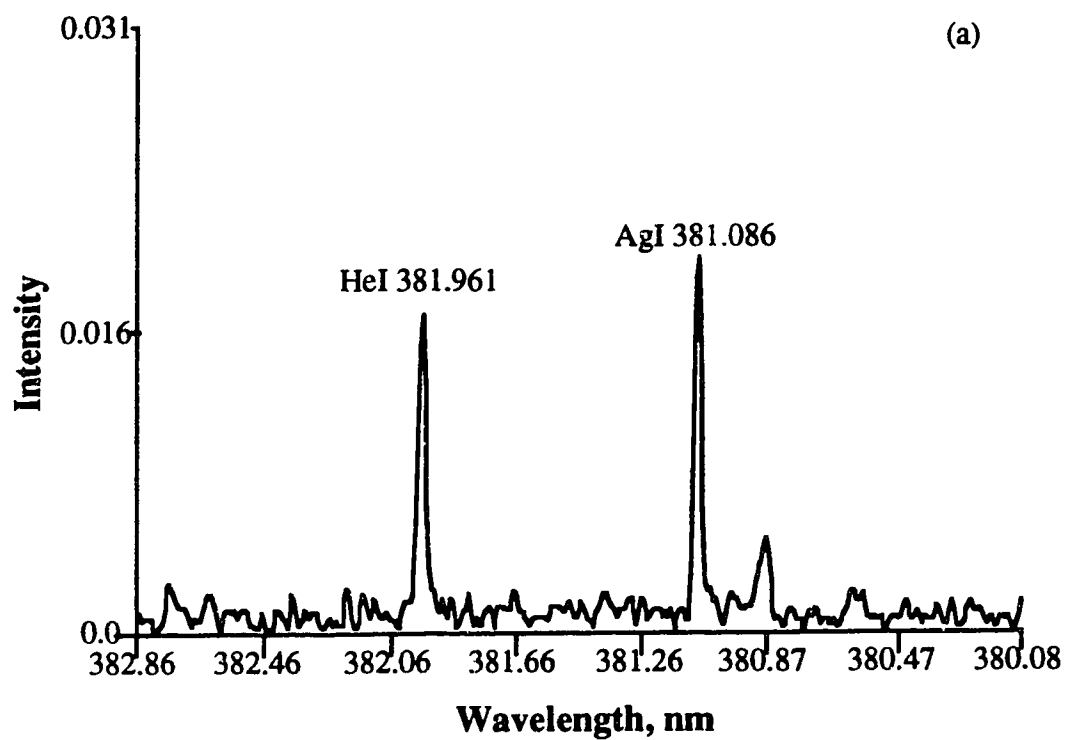


Fig. 5.29 Scale expanded spectrum showing AgI lines from  $7d \rightarrow 5p$  and  $6p \rightarrow 5s$  transitions.

de-excitation could be autoionization (Equation 5.5) rather than by radiative relaxation (Equation 5.4).

An interesting line that was observed in Fig. 5.28a should be noted. The line at 468.575 nm is a HeII line. The excitation potential is 51 eV from the ground state helium ion. The presence of this line indicates the extraordinary excitation capability of the glow discharge.

### 5.3.6 Cadmium Neutral Atom Lines

The visible glow discharge spectrum for Cd (Ar filler gas) is shown in Fig. 5.30a. The basic structure of the energy level diagram for CdI is analogous to that for ZnI [6,15]. The major lines observed in the visible spectral region are from upper level transitions among the triplet levels. For example the two lines shown in Fig. 5.30b are a result of transitions from the 6s (triplet) to the 5p (triplet) levels. The characteristics of these lines and the other CdI lines discussed in this section are presented in Table 5.8. It should be noted that the cadmium was placed in an aluminum holder in a Grimm type GD (See Chapter 2). Some sputtering of the aluminum holder occurred and is the source of the AlI 396.152 nm line noted in Fig. 5.30a.

Several lines resulting from 5d (triplet) to 5p (triplet) transitions are shown in Figs 5.31 and 5.32a, and one line (CdI 325.252 nm) indicative of a 7s (triplet) to 5p (triplet) transition is shown in Fig. 5.32b. Finally, the line at 326.105 nm is a result of the "forbidden" transition from the 5p (triplet) to the 5s (singlet).

In the ultraviolet cadmium spectrum, weak spectral evidence was found for excitation of the 6d and 7d levels of the triplet system. A line was observed at 288.077 nm (Fig. 5.33a) which is the result of a 6d to 5p

Table 5.8 Characteristics of the CdI lines

Type	Wavelength, nm	Energy, eV	Transition
CdI	508.582	6.39	6s (triplet) to 5p (triplet)
CdI	479.992	6.39	6s (triplet) to 5p (triplet)
CdI	361.445	7.37	5d (triplet) to 5p (triplet)
CdI	361.287	7.37	5d (triplet) to 5p (triplet)
CdI	361.051	7.37	5d (triplet) to 5p (triplet)
CdI	346.765	7.37	5d (triplet) to 5p (triplet)
CdI	346.620	7.37	5d (triplet) to 5p (triplet)
CdI	340.365	7.37	5d (triplet) to 5p (triplet)
CdI	325.252	7.76	7s (triplet) to 5p (triplet)
CdI	326.105	3.80	5p (triplet) to 5s (singlet)
CdI	288.077	8.10	6d (triplet) to 5p (triplet)
CdI	267.754	8.44	7d (triplet) to 5p (triplet)
CdI	276.389	8.44	7d (triplet) to 5p (triplet)

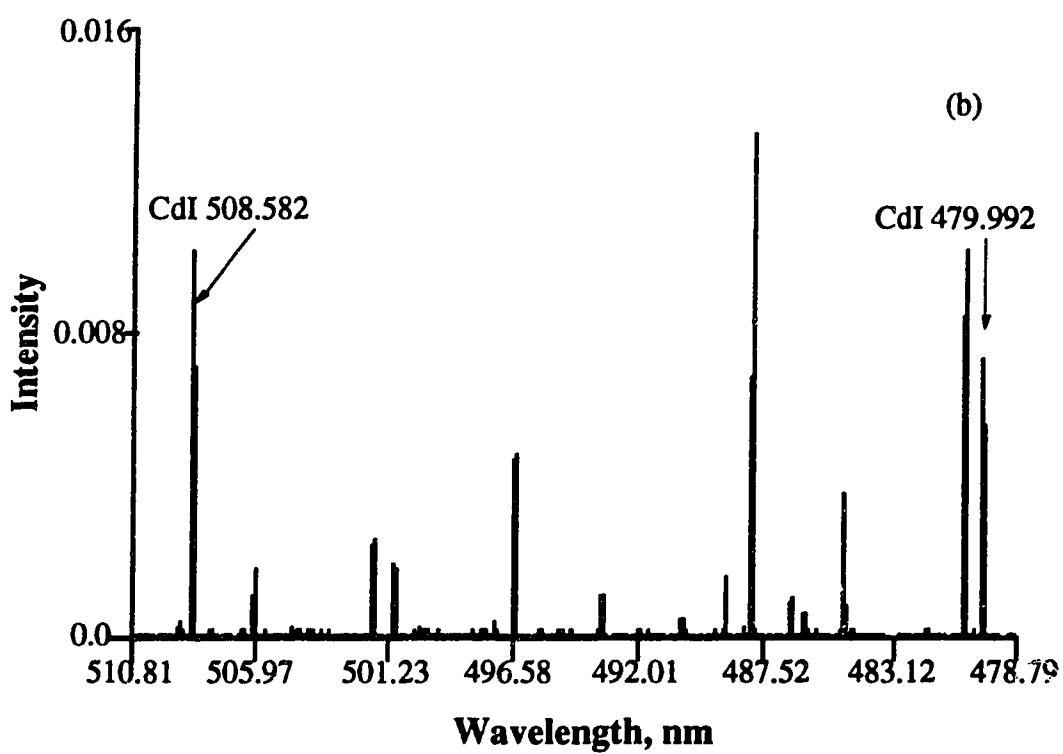
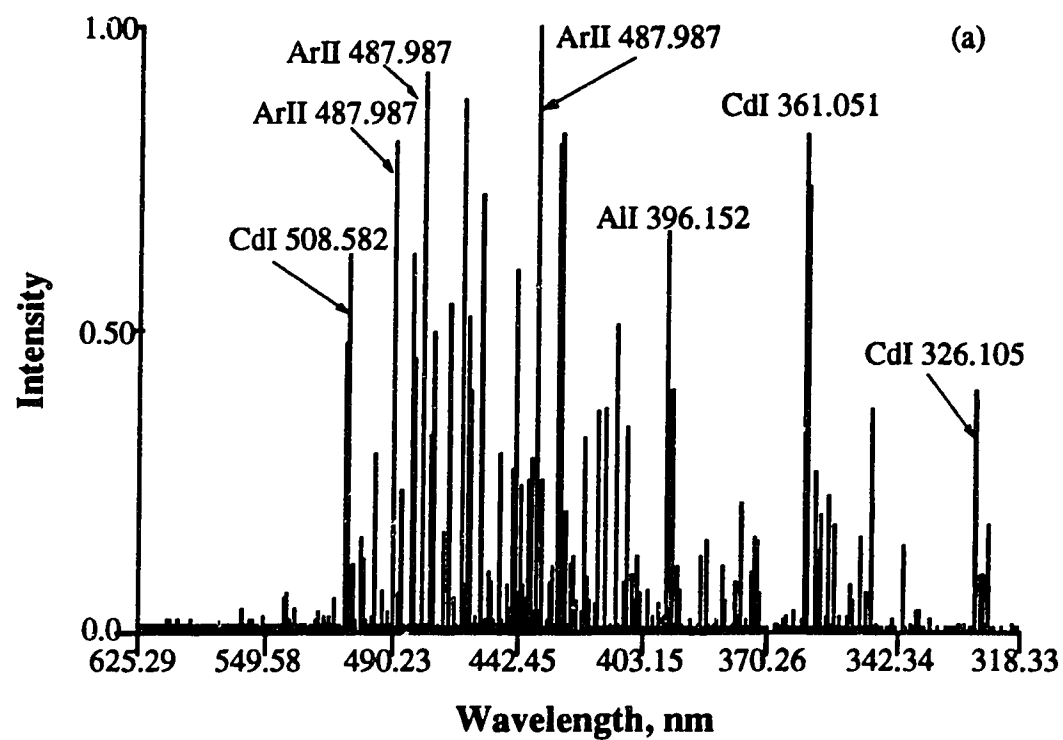


Fig. 5.30 Cd visible spectrum from a He based glow discharge.

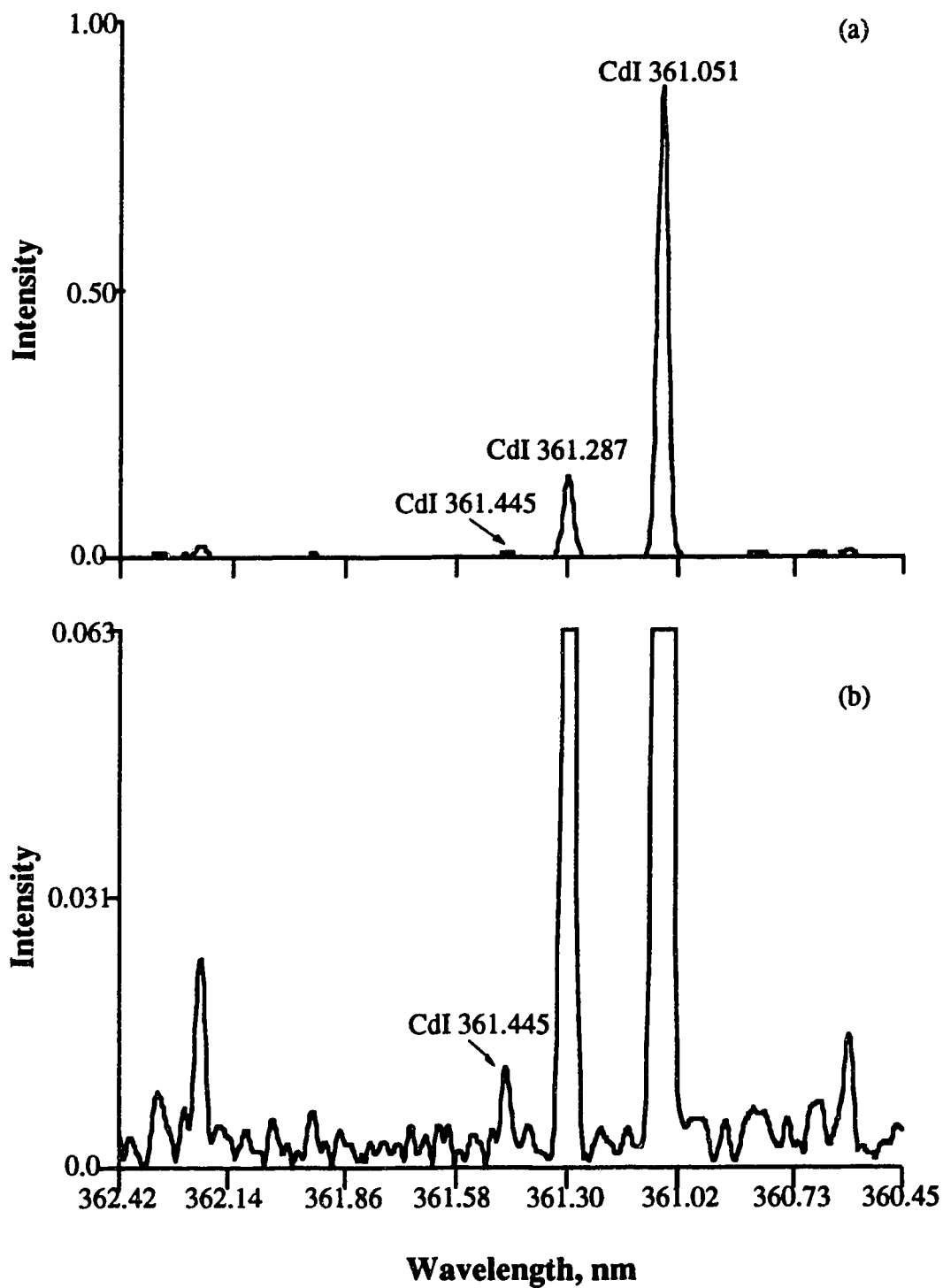


Fig. 5.31 CdI lines from transitions 5d (triplet) to 5p (triplet).

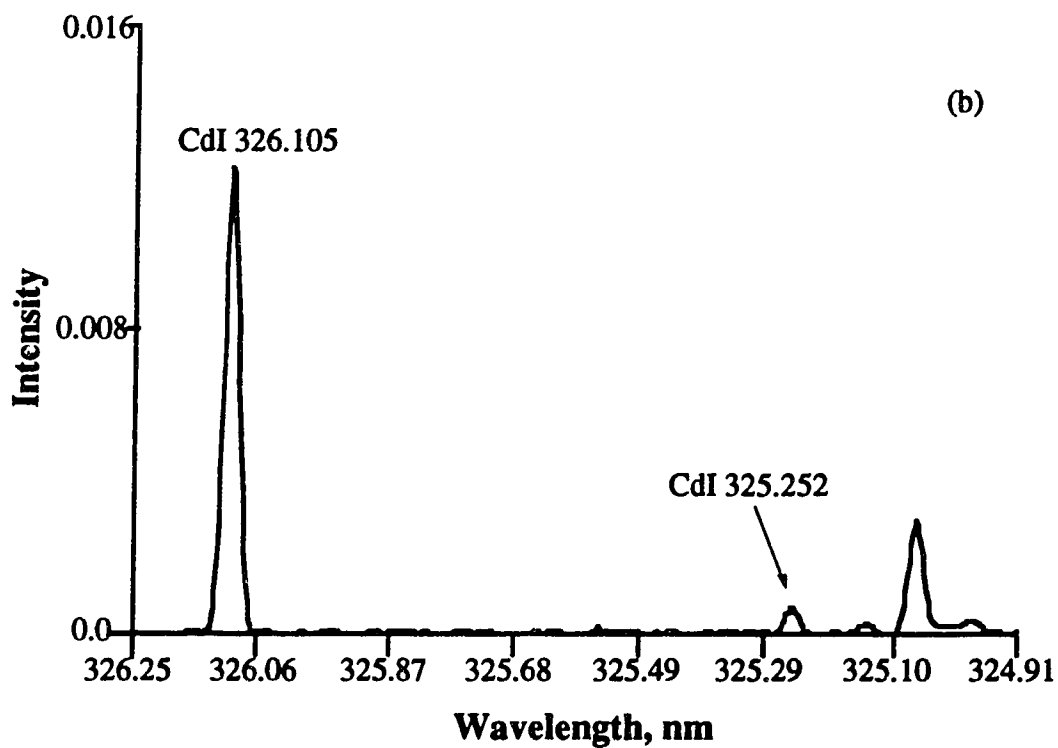
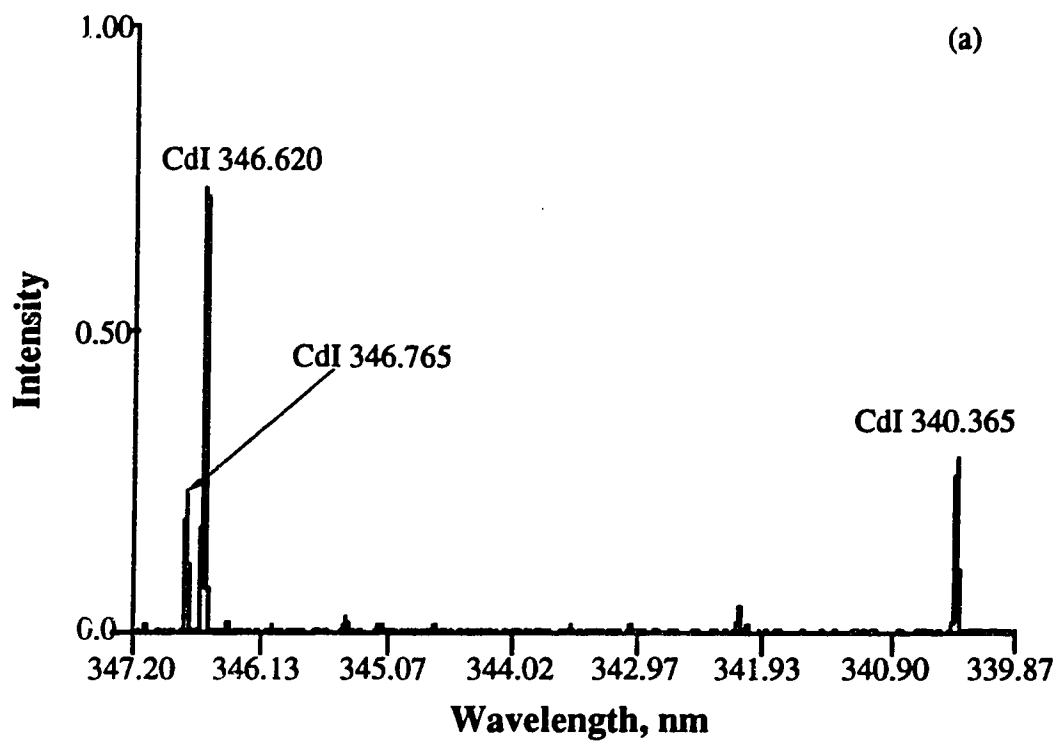


Fig. 5.32 Some CdI lines from transitions 5d (triplet) to 5p (triplet) and 7s to 5p.



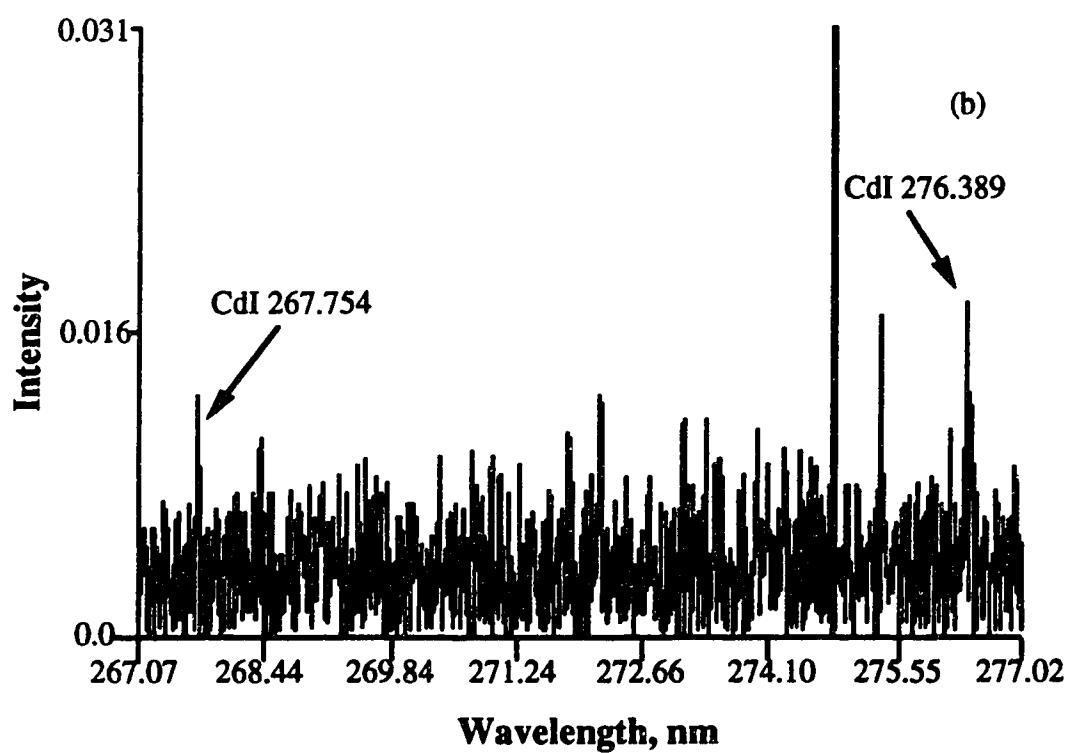
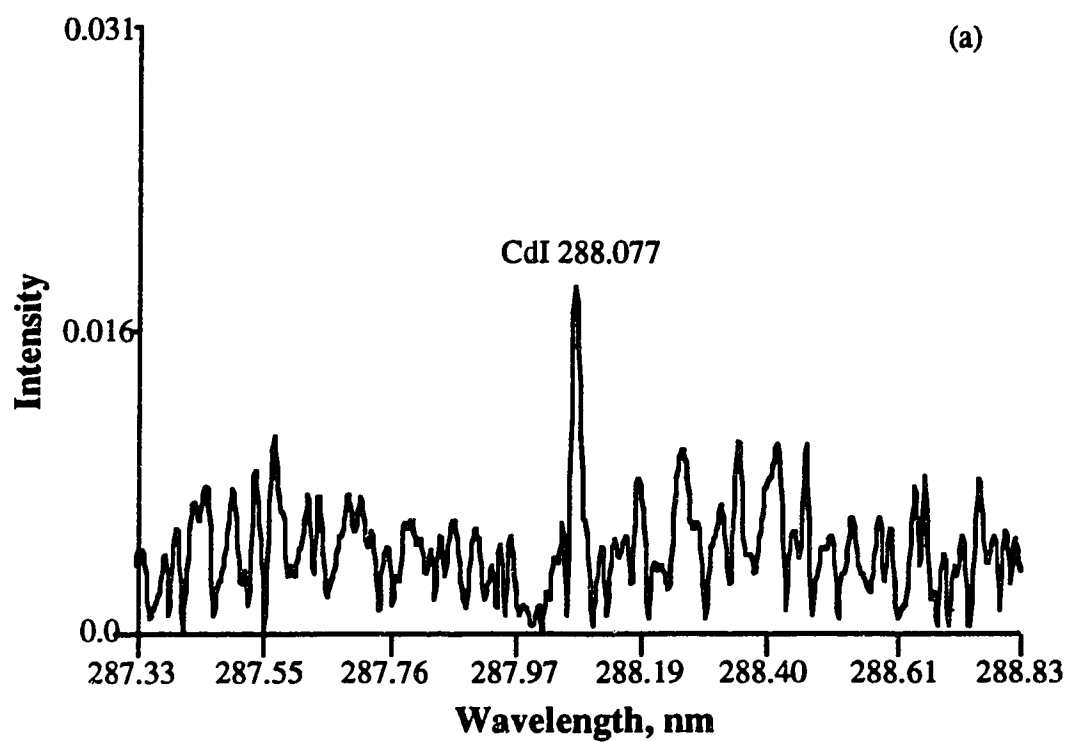


Fig. 5.33 Some CdI lines from transitions 6d (triplet) to 5p (triplet) and 7d to 5p.

transition and two very weak lines were observed at 267.754 and 276.389 nm (Fig. 5.33b) which are the result of 7d to 5p transitions. Perhaps these levels are populated by a process such as ion-electron recombination and relax non-radiatively to the 5d level resulting in the strong emission observed from these levels in the visible region. Overall, the CdI spectral results are similar to those from zinc and tend to point towards the "top-down" process as a mechanism for populating these triplet transitions.

### 5.3.7 Ion-electron Recombination and the Filler Gas Ion Lines

All the evidence studied so far point to one conclusion - in a glow discharge, there is a specific process that populates the high level excited states of the neutral atoms, followed by stepwise de-excitation. Among all the possibilities, ion-electron recombination is the most likely candidate for this process. This process, generally speaking, involves a ground state ion and a slow electron. The energy difference involved in the process is released as continuous background radiation [16]. The recombination product is an excited atom with a potential energy close to its ionization potential, which quickly relaxed down-ward by collisions until it reaches a large energy gap [17]. Then it emits a photon at a wavelength determined by the specific transition. This mechanism is another version of saying "a top-down process". It can explain very well the spectral evidence we discussed in the previous sections. Recall the different response of the high level transition signals with the variation of discharge current observed in Chapter 3 [Fig 3.8]. It can be qualitatively explained by ion-electron recombination. At constant pressure while increasing the voltage, the signals increase with the current due to the increasing population of both the atoms and the electrons. However, there is a maximum in the process.

Beyond this point, the signal intensity decreases with a further increase in the voltage. This may be attributed to the high electron energy and high temperature brought about by the high voltage. At this point, ion-electron recombination becomes less effective. On the other hand, when the voltage is kept constant and the pressure is increased, the signal from the high level transitions increased, and increased faster at higher current. With a relatively low voltage (800 V in this case), increasing the pressure will decrease the thickness of the cathode dark space and lower the average electron energy (*i.e.* more frequent collisions). The population of ground state ions and electrons will increase as well. This makes a good environment for the process of ion-electron recombination. As a consequence, the signal will rapidly increase. It has been indicated that the recombination loss of ions and electrons is proportional to the current [10], and our signal profile is close to that proportion at the high end. This may be direct evidence for the occurrence of ion-electron recombination. Other evidence also supports this assumption, as will be seen in the following section.

A rather striking difference exists between the Ar glow discharge spectrum and that for the Ar ICP. All the Ar emission lines in the ICP are ArI lines, while in the glow discharge, both ArI and ArII lines are observed. As well the ArII lines are very strong, in most cases considerably stronger than the ArI lines. An expanded scale spectrum of the Ar based glow discharge is shown in Fig. 5.34a. All six lines observed in this region are ArII and they are listed in Table 5.9 along with their excitation potentials. These values are from the ground state of the ion which is 15.76 eV, so total excitation energies in the range of 35 eV are

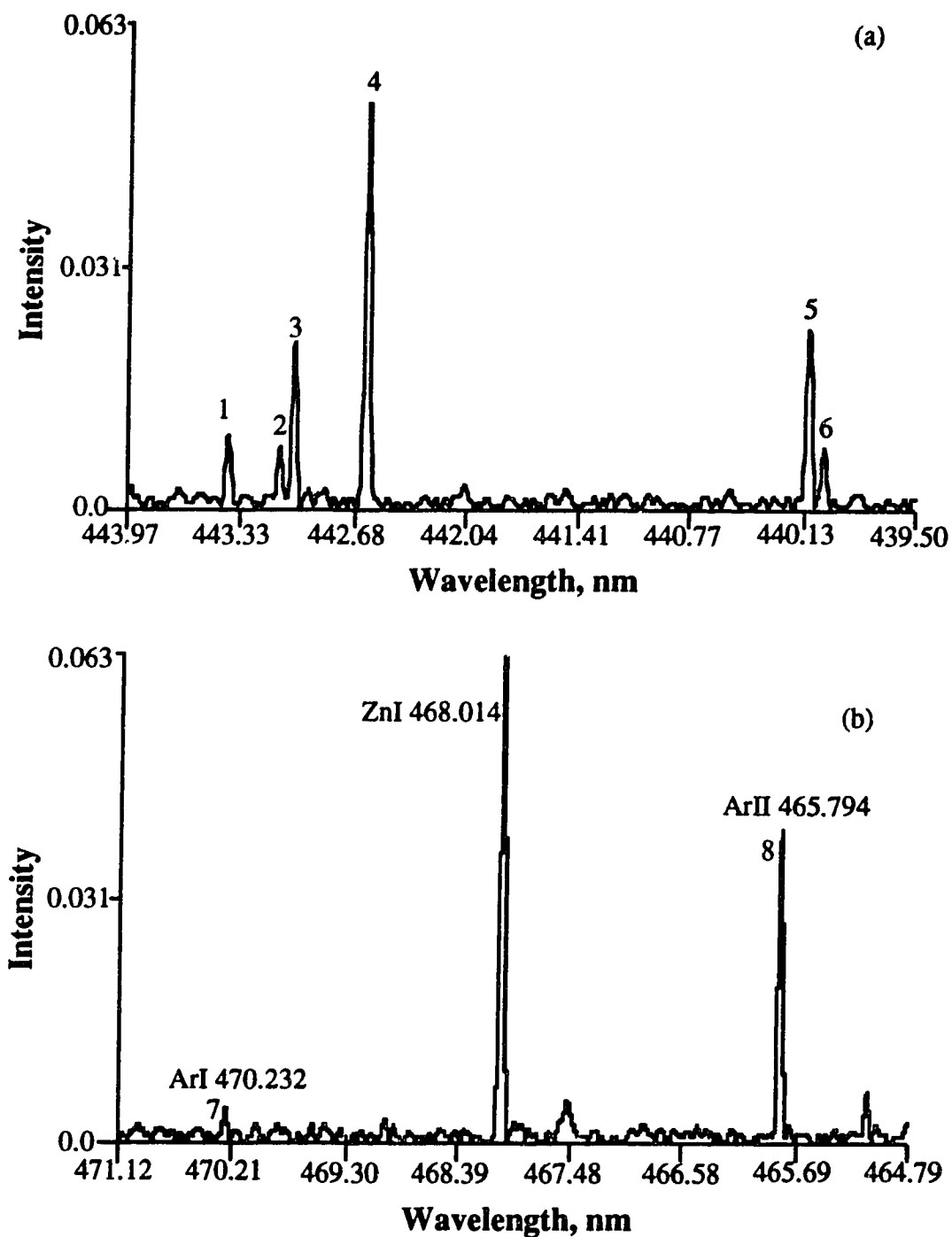


Fig. 5.34 ArII lines observed in the visible region in glow discharge.

Table 5.9 Argon lines noted in Fig. 5.34

Line	Type	Wavelength, nm	Energy, eV
1	ArII	443.384	24.16
2	ArII	443.100	19.22
3	ArII	443.019	19.61
4	ArII	442.601	19.54
5	ArII	440.099	19.22
6	ArII	440.010	19.26
7	ArI	470.232	14.46
8	ArII	465.794	19.80

required to excite those ion lines. Not one of these lines shown in Fig. 5.34a were observed in the ICP spectrum.

A second spectral region is shown in Fig. 5.34b. Within this region both an Ar neutral atom and an ion line can be observed. This neutral atom line is listed as a strong line in spectral tables [7] but, in the GD, it is clearly weak relative to the ArII line at 465.794 nm.

A group of argon lines emitted in the GD is shown in Fig. 5.35 along with the corresponding spectral segment from an ICP spectrum. The lines are identified in Table 5.10. Line 3, 4 and 5 (ArI lines) appear in both spectra, but the ion lines (lines 1, 2, 6 and 7) appear only in the GD spectrum.

Certainly it is well known that Ar ions are present in both discharges. It is also clear from the above spectral data, that the ions are not excited to emitting states in the ICP, but are in the glow discharge. One possible explanation for this is that the excited states of the argon ion are generated by ion-electron recombination from Ar<sup>2+</sup>:



It turns out that one very distinct difference between these two discharges is the presence of Ar<sup>2+</sup> species in the mass spectra of an Ar based glow discharge, a species that is not found in the background mass spectrum of an Ar ICP [18]. We have adapted the same glow discharge device used for these emission studies for use in GD-MS [19]. A portion of the background mass spectrum for this device with Ar as the filler gas and Al as the sample is shown in Fig. 5.36. Note that the Ar<sup>2+</sup> signal is quite strong ( $m/z = 20$ ), almost as large as that for <sup>27</sup>Al<sup>+</sup>. Thus the Ar<sup>2+</sup> species are certainly present in the discharge. A high electric potential and a low kinetic energy

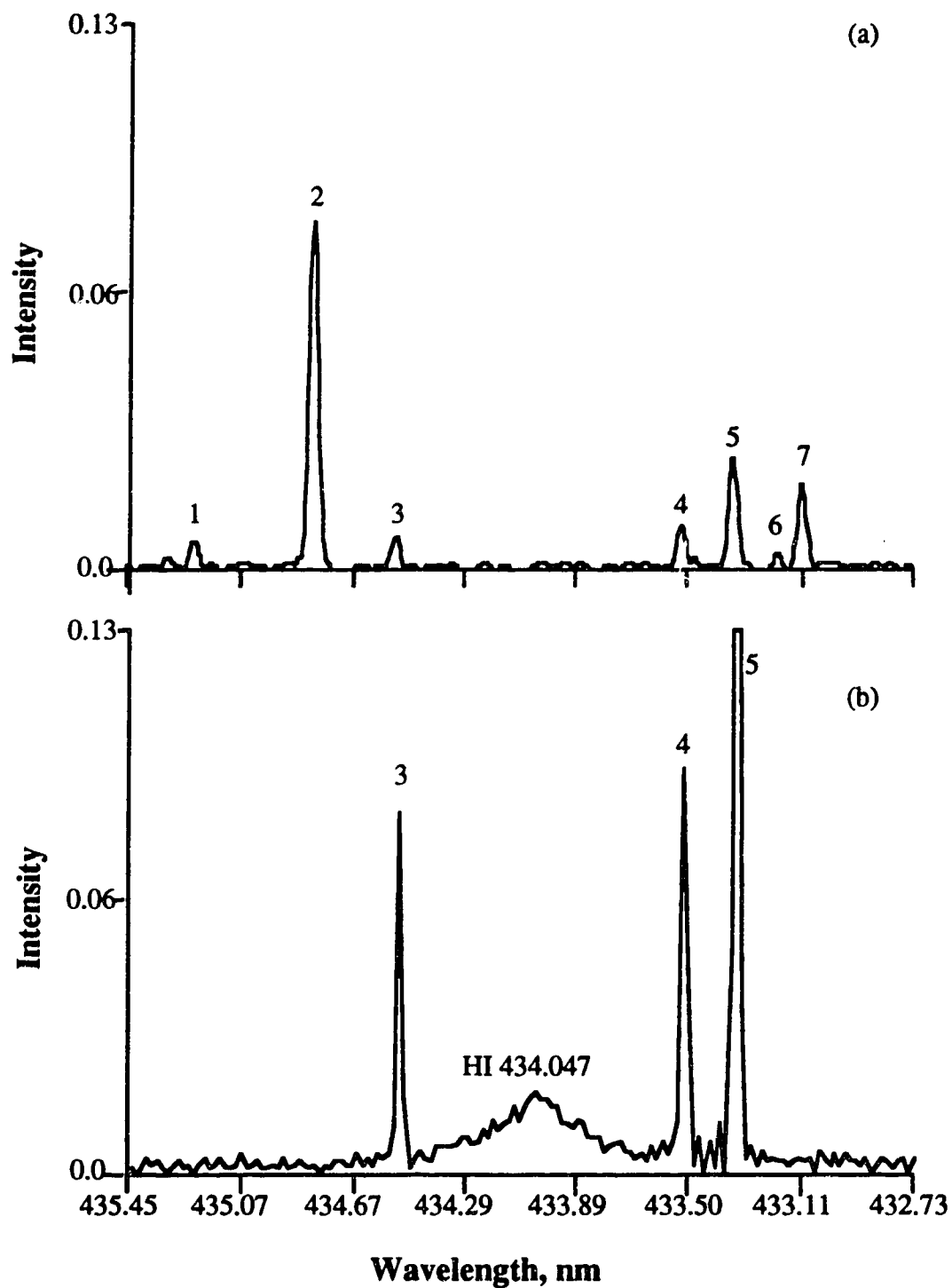


Fig. 5.35 Comparison of some Ar lines between GD (a) and ICP (b).

Table 5.10 Ar lines noted in Fig. 5.35

Line	Type	Wavelength, nm	Energy, eV
1	ArII	435.220	19.30
2	ArII	434.806	19.49
3	ArI	434.517	14.68
4	ArI	433.534	14.68
5	ArI	433.359	14.68
6	ArII	433.203	19.30
7	ArII	433.120	19.61



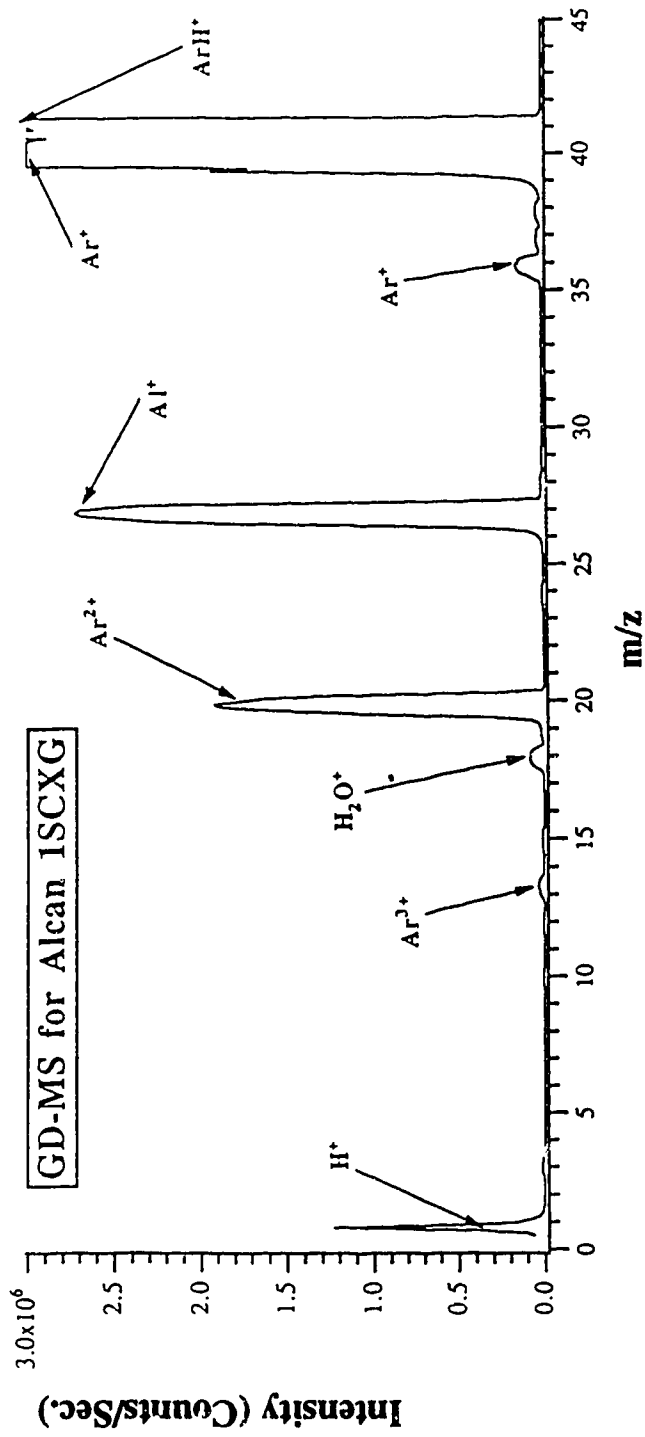


Fig. 5.36 A portion of an argon based GD-MS spectrum showing the existence of  $Ar^{2+}$  ions.

of this ion make it readily capture a low energy electron. This situation makes ion-electron recombination a distinct possibility as a mechanism for the generation of excited argon ions and hence the ArII lines.

It is also interesting to point out that NeII lines exist in the background spectrum of a Ne based glow discharge. Expanded scale spectra of the Ne based glow discharge spectrum (Fig. 5.1b) are shown in Fig. 5.37. The NeII lines shown have excitation potentials of about 31 eV while that for the NeI line is about 20 eV. Ne<sup>2+</sup> has also been observed in Ne filler gas based GD mass spectrometry [20] and, perhaps, ion-electron recombination is also possible for the generation of neon ion line emission signals. In the last section, it was found that a HeII line existed in the background of the He glow discharge spectrum. The second IP of He is 54.4 eV. In GD-MS we have observed Ar<sup>4+</sup> species in the background spectrum. The fourth IP of Ar is 59.8 eV, so it is possible that He<sup>2+</sup> could be generated in the glow discharge and the line could also be produced in the ion-electron recombination.

It does appear that ion-electron recombination contributes little to the spectral character of the ICP, or perhaps, better stated, that radiative stepwise de-excitation is not operative in the ICP. There are several reasons behind this phenomenon. Firstly, ion-electron recombination needs both low energy electrons and ions, or the relative velocity of the ions and the electron should be as low as possible, to be effective. It is well known that the gas temperature and the average electron temperature is much higher in an ICP than in a GD. That means a high kinetic energy in the ICP for both partners of the recombination. Thus, recombination efficiency will be lower in the ICP than in the glow discharge. Secondly, in a glow discharge, this process mainly happens in the negative glow and surrounding area. As

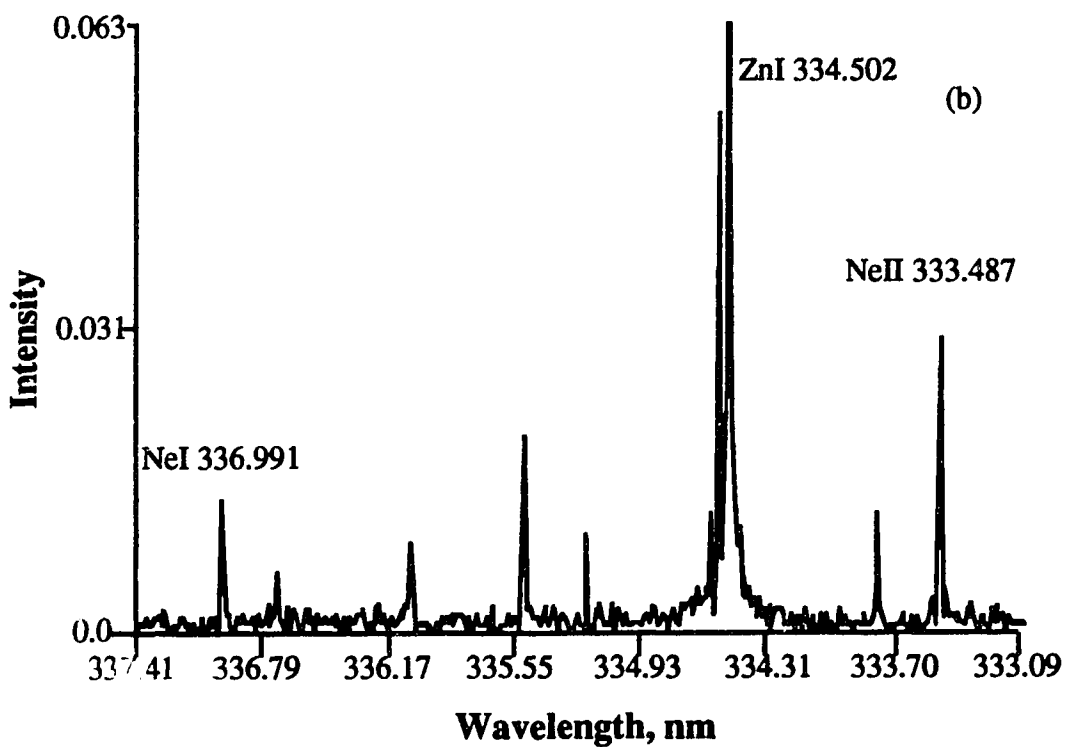
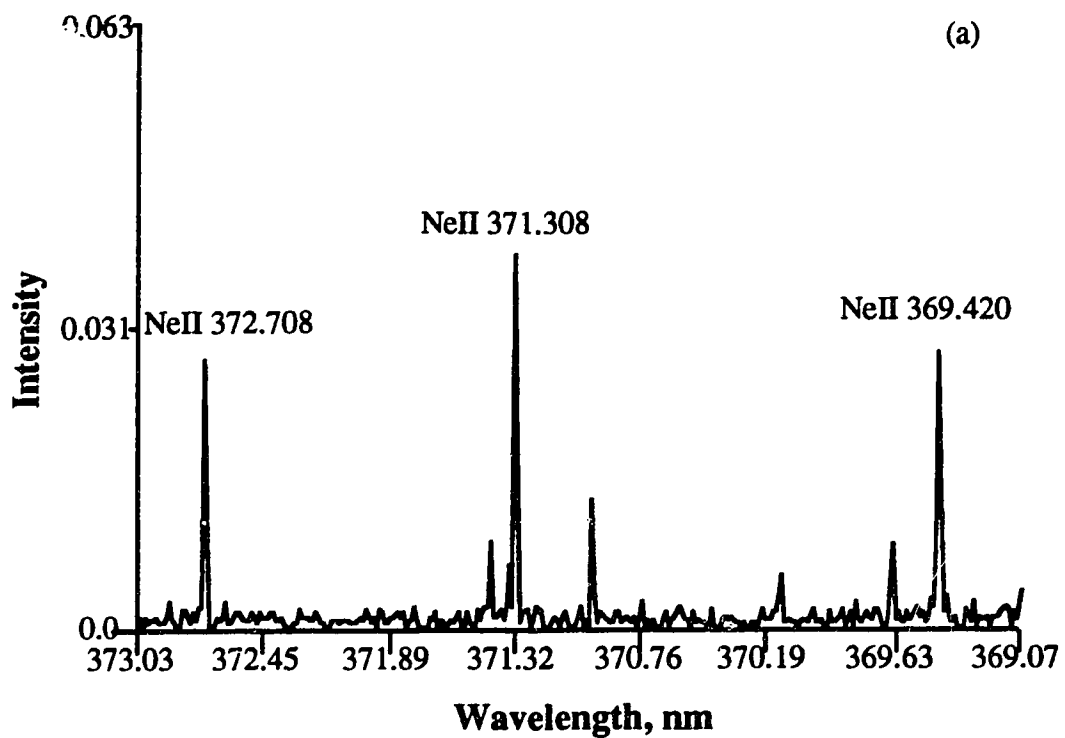


Fig. 5.37 A portion of a spectrum obtained from a Neon based GD.

discussed in Chapter 3, this is a region where the electric field strength is close to zero. The movement of both ions and electrons (slow electrons) is basically by diffusion. The Coulombic force between the ions and the electrons which are close to each other increase the chances of recombination. In the ICP, on the other hand, there is a strong alternating electric field. At any moment, the ions and the electrons are accelerated in opposite directions. In other words, their relative velocities are always high. This makes the ion-electron recombination very difficult. Studies of the r.f. boosted [21] and the microwave boosted [5] hollow cathode glow discharge demonstrated depression of the high energy level transitions and enhancement of resonance line emission. This is consistent with recombination being decreasing at high strength field. Thirdly, the ICP operates at a much higher gas pressure than the glow discharge. The high pressure and high temperature make the collision frequency of species high in the ICP plasma. This provides a very effective path for non-radiative de-excitation. The average life time of the excited state of the upper levels would be significantly shortened by the collision process. Should ion-electron recombination occur in the ICP, the resulting excited atom is likely quickly collisionally deactivated without the emission of radiation. However, an interesting dichotomy does exist with respect to the ICP emission spectrum. Note in Fig. 5.5 that the 324.754 nm resonance line of copper (a strong emission in the ICP spectrum) has exactly the same upper state as the 510.554 nm line. However, while the 510.554 nm line is a strong line in the GD spectrum, it could not be observed in the ICP spectrum.

### 5.3.8 Formation of Ground State Ions

If the assumption is right, *i.e.* ion-electron recombination is the major source of the excitation of neutral atom lines, a following question is "how are the ions generated in the glow discharge?". Three processes are considered as the major sources for the production of the analyte ground state ions. The first one is direct electron impact ionization. The electrons could have a kinetic energy of few hundred eV up to the applied potential, especially in the cathode dark space. Effective electron impact mainly happens in the cathode dark space and the interface between the cathode dark space and the negative glow. At these regions, the neutral sample atoms have the highest concentration and the electron beam has the largest number flux and energy flux. However, due to the great potential fall between the cathode and the negative glow, most of the ions formed here will be accelerated towards the cathode. Their contribution to the ion-electron recombination might not be very important.

The second source of the ions is the Penning process (Equation 4.1, Chapter 4). Data obtained from GD-MS measurement [22] indicated that Penning processes play a significant role in the production of both gas ions and the analyte ions. In our case, the contribution of this mechanism can also be significant.

The third source of analyte ions is the process we discussed in Chapter 4, charge transfer (Equation 4.2, Chapter 4). From the discussion in Chapter 4, it is clear that the charge transfer process is responsible for the emission of many ion lines. The ions relax to ground state after the emissions. These ions may also be a source of ions to contribute to ion-electron recombination.

## 5.4 Conclusion

From the discussion above, the following brief conclusions can be made: first, the emission character of the spectra in an argon based glow discharge is strikingly different from that of the same gas based ICP. The ArII lines in the glow discharge make most of the difference in the background emission, while the analyte high energy level transitions make the most difference in the analyte spectra. The excitation of the neutral atom lines in the glow discharge is most likely caused by ion-electron recombination followed by stepwise de-excitation.

## References

1. R.K. Marcus, Ed. *Glow Discharge Spectroscopies*, Plenum Press, New York, 1993.
2. P.W.J.M. Boumans, J. Broekaert and R.K. Marcus, *Spectrochim. Acta* **46B** 111 (1991).
3. P.R.Banks and M.W. Blades, *Spectrochim. Acta* **47B** 1287 (1992).
4. D. Fang and R.K. Marcus, "Fundamental Plasma Processes" in *Glow Discharge Spectroscopies*, R.K. Marcus, Ed. Plenum Press, New York, 1993, p44.
5. E.B.M. Steers and F. Leis, *J. Anal. At. Spectrom.* **4** 199 (1989).
6. C. Candler, *Atomic Spectra and the Vector Model*, 2nd ed. Hilger and Watts, London 1964.
7. A.N. Zaidel', V.K. Prokofev, S.M. Raiskii, V.A. Slavnyi and E. Ya. Shreider, *Table of Spectral Lines*, Plenum, New York, 1970.
8. G.R. Harrison, Ed. *MIT Wavelength Tables*, The MIT Press, Cambridge, Mass. 1969.
9. A.G. Shenstone, *Philo. Trans. Roy. Soc. (London)*, [A] **241** 37 (1948).
10. F. Llewellyn-Jones, *The Glow Discharge and an Introduction to Plasma Physics*, Methuen, London, 1966.
11. C.E. Moore, Ed. *Atomic Energy Levels*, Vol. II, National Bureau of Standards, Washington D. C. 1952.
12. G.B. King, B.R.Todd and G. Horlick, *Spectrochim. Acta* **47B** E333 (1992).
13. G.B. King and G. Horlick, *Spectrochim. Acta* **47B** E353 (1992).
14. A.G. Shenstone, *Phys. Rev.* **57** 894 (1940).

15. C.E. Moore, Ed. *Atomic Energy Levels*, Vol. III, National Bureau of Standards, Washington D. C. 1958.
16. G. Herzberg, *Atomic Spectra and Atomic Structure*, Dover Publications, New York, 1944.
17. W.T. Silfvast, L. H. Szeto and O.R. Wood, II, *Appl. Phys. Lett.* **36** 615 (1980).
18. X. Feng and G. Horlick, *J. Anal At. Spectrom.* **9** 823 (1994).
19. Y. Shao and G. Horlick, *Spectrochim. Acta* **46B** 165 (1991).
20. N. Jackubowski and D. Stuewer, *Fresenius Z. Anal. Chem.* **335** 680 (1989).
21. P.B. Farnsworth and J.P. Walters, *Spectrochim. Acta* **37B** 773 (1982).
22. W. Vieth and J.C. Huneke, *Spectrochim. Acta* **45B** 941 (1990).



## Chapter 6 Summary and Future Work

### 6.1 Summary

Glow discharge devices are simple in their physical design, but the plasma in the glow discharge is very complicated. The discharge potential and the relatively low gas pressure establishes a non-uniform electric field between the cathode and the anode. Under the bombardment of positive ions and neutral atoms, the cathode emits secondary electrons. These electrons are accelerated towards the anode by the electric field. The filler gas and analyte atoms can be ionized by the electrons which results in more ions available for the bombardment of the cathode. The discharge is sustained by this process. At the same time, analyte material is sputtered away from the bulk sample (cathode) and transported into the plasma. Where it is excited and/or ionized.

Glow discharges produce a so-called cold plasma. The gas temperature in the discharge chamber is not higher than 1500 K, which is fairly low compared to that of the inductively coupled plasma (ICP). As a result, self-absorption of the resonance lines of the analyte neutral atoms is observed. However, the glow discharge shows great power in the excitation and ionization of analyte and discharge gases. In the UV and visible region, the analyte lines dominate the spectra. The characteristics of their emission spectra depend on the identity of discharge gas. A spectral feature strongly displayed in one discharge gas is often completely absent from another. In

these spectra, the analyte ion lines are the most distinctive (CuII lines, for example). Some ion lines are strongly enhanced by a specific discharge gas. When the energy level of an ion matches the ionization potential or the metastable energy of the discharge gas, the transitions from this level are selectively enhanced. This leads to the conclusion that charge transfer and Penning processes play a significant role in the excitation of analyte ions.

In contrast to the ion lines, neutral atom line emission characteristics are similar for different discharge gases. However, the spectra of glow discharge emission is dramatically different from that of the ICP. In a detailed comparison between the spectra from a glow discharge and an ICP, it was found that the glow discharge favors the high energy transitions of neutral atoms. Strong emission often comes from transitions which originate from excited states which have an excitation energy close to the ionization potential. It is believed that the excited states of analyte atoms are formed at high energy levels and followed by stepwise de-excitation. A "top-down" scheme was clearly displayed in the Grotrian diagram. The profile of signal variation as a function of the discharge current indicates that ion-electron recombination is the major source of these highly excited atoms. The observation of diffuse lines (which originate from the auto-ionizing states) in the copper system from the brass argon discharge is a clear indication of recombination processes [1].

The selective excitation of some ion lines and high energy neutral atom lines in the glow discharge provides a good explanation to the phenomenon that the Boltzmann' plot could not be applied to the glow discharge plasma to measure the excitation temperature. As briefly mentioned in Chapter 3, the excitation temperature for iron atoms

determined in this way was very different from that for ions. The phenomenon is not difficult to understand because the excitation of the ions is not a thermal process. Some ion lines used for the construction of the Boltzmann plot may be selectively enhanced by charge transfer and/or Penning processes. For example, if copper ion lines are used to construct a Boltzmann plot, the result could be totally different for Ar and Ne gases if some of the enhanced lines are used. Just imagine using the CuII 224.700 nm line and other lines from the 5s - 4p transitions, it would result a very low excitation temperature for the argon discharge due to the strong emission at 224.700 nm and extremely weak emission from the others. On the contrast, the neon discharge would show a very high "excitation temperature" due to the selective enhancement on the 5s - 4p transitions by neon-Cu charge transfer. This is schematically shown in Fig. 6.1. Unfortunately, the transition probability data are not available to generate an actual graph. However, based on equation (3.9),

$$\ln(I_{pq}\lambda_{pq}/g_pA_{pq}) = \ln (IN_0hc/4\pi Z(T)) + (-E_p/kT(\text{exc}))$$

a different plot could show the difference in the "excitation temperature". If the systems are in local thermal equilibrium, the plot will show the difference in the real excitation temperature. Otherwise, it will show the difference in the apparent "excitation temperature". The argument is the following, taking the Ne-Cu and Ar-Cu discharge systems as examples:

For the Ne-Cu system, we assign the line intensity as  $I_{Ne}$  and the "excitation temperature" as  $T_{Ne}$ , then we have:

$$\ln(I_{Ne}\lambda_{pq}/g_pA_{pq}) = \ln (IN_0hc/4\pi Z(T)) + (-E_p/kT_{Ne}) \quad (6.1)$$

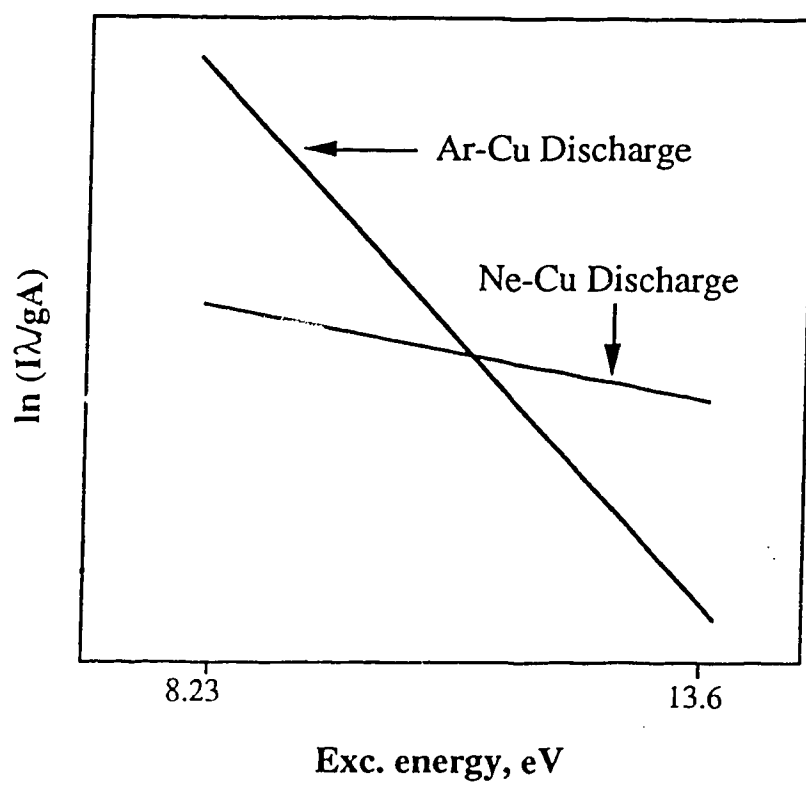


Fig. 6.1 A schematic illustration of two Boltzmann plots.

In the Ar-Cu system, similarly, we assign the line intensity as  $I_{Ar}$  and the "excitation temperature" as  $T_{Ar}$ , then we have:

$$\ln(I_{Ar}\lambda_{pq}/g_pA_{pq}) = \ln(N_0hc/4\pi Z(T)) + (-E_p/kT_{Ar}) \quad (6.2)$$

Subtract equation (6.2) from equation (6.1), we get:

$$\ln(I_{Ne}/I_{Ar}) = (-E_p/kT_{Ne}) - (-E_p/kT_{Ar})$$

i.e.

$$\ln \frac{I_{Ne}}{I_{Ar}} = \frac{E_p}{k} \left( \frac{1}{T_{Ar}} - \frac{1}{T_{Ne}} \right) \quad (6.3)$$

A plot of  $\log(I_{Ne}/I_{Ar})$  against  $E_p$  will be a straight line with the slope being  $\frac{1}{k} \left( \frac{1}{T_{Ar}} - \frac{1}{T_{Ne}} \right)$ .

From the slope value of the line, the difference between  $T_{Ar}$  and  $T_{Ne}$  can be evaluated. Let the slope be  $s$  and  $T_{Ne}$  be  $n$  times of  $T_{Ar}$ , then we have

$$n = \frac{1}{1 - skT_{Ar}} \quad (6.4)$$

The disadvantage of this type of plot is that all the lines used in the plot must be the same set and all have a measurable intensity in both systems. However, we do not need to know the transition probability and for the same measuring system, the response factor of the detector does not need to be corrected. If a well established reference emission source is

available, the "excitation temperature" in another emission source can be calculated.

Fig. 6.2 is a rough representation of this kind of plot because the line relative intensities are not very reliable. From this graph, the slope of the line is 1.592 which generates a relationship between  $T_{Ar}$  and  $n$  as:

$$n = \frac{1}{1 - 0.00013719 T_{Ar}}$$

From this relationship,  $T_{Ar}$  must be smaller than 7290 K. Otherwise  $T_{Ne}$  would be infinity. If  $T_{Ar}$  is 3000 K, for example,  $n=1.6995$  and  $T_{Ne}$  will be 5100 K according to this equation. This tells us a different story from the one presented in Chapter 3. The reason is that different lines were chosen.

For neutral atom lines in a glow discharge, the Boltzmann plot can not generate a meaningful excitation temperature either. As discussed in Chapter 5, the excitation of some of the high level states is a result of ion-electron recombination, and compared to a Boltzmann distribution, these levels must be overpopulated. If lines from transitions originating from these levels are used with low energy lines to construct the Boltzmann plot, the result will be abnormally high. Fig. 6.3 is an example of Boltzmann plots using FeI lines. It is clear that in the low energy region the plot has a large slope which generates a low "excitation temperature"(2600 K). While in the higher energy region, the slope is much smaller which generate a high temperature (10500 K). Furthermore, with the same argument, the "excitation temperature" will depend heavily on the thermometric species. The higher the ionization potential of the species, the higher the "excitation

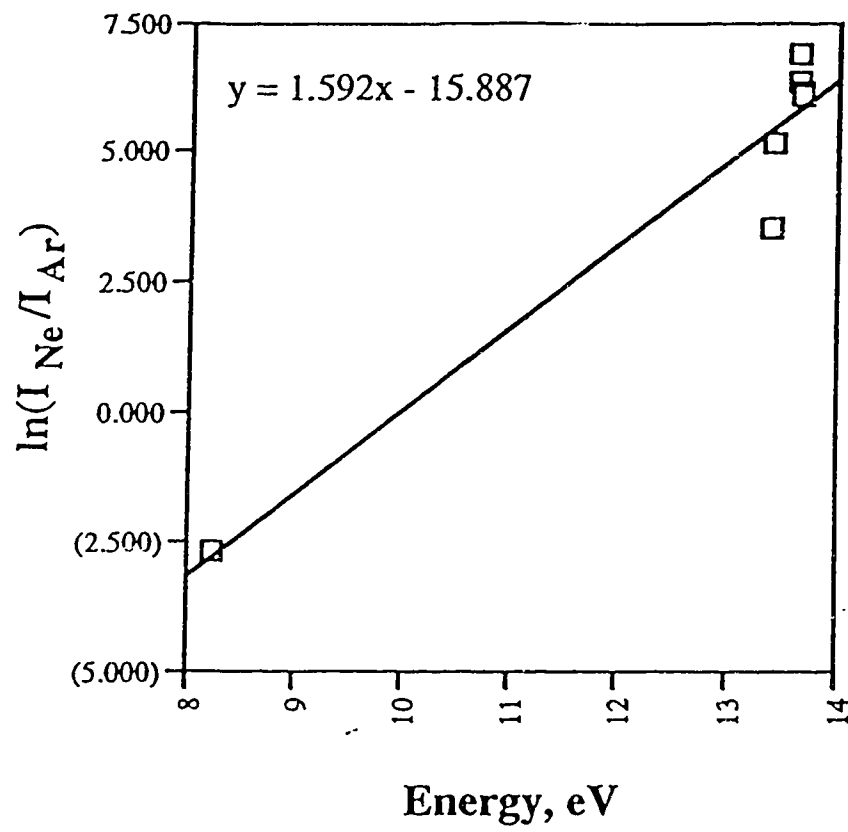


Fig. 6.2 A plot used for calculating  $T_{Ne}$  and  $T_{Ar}$ .

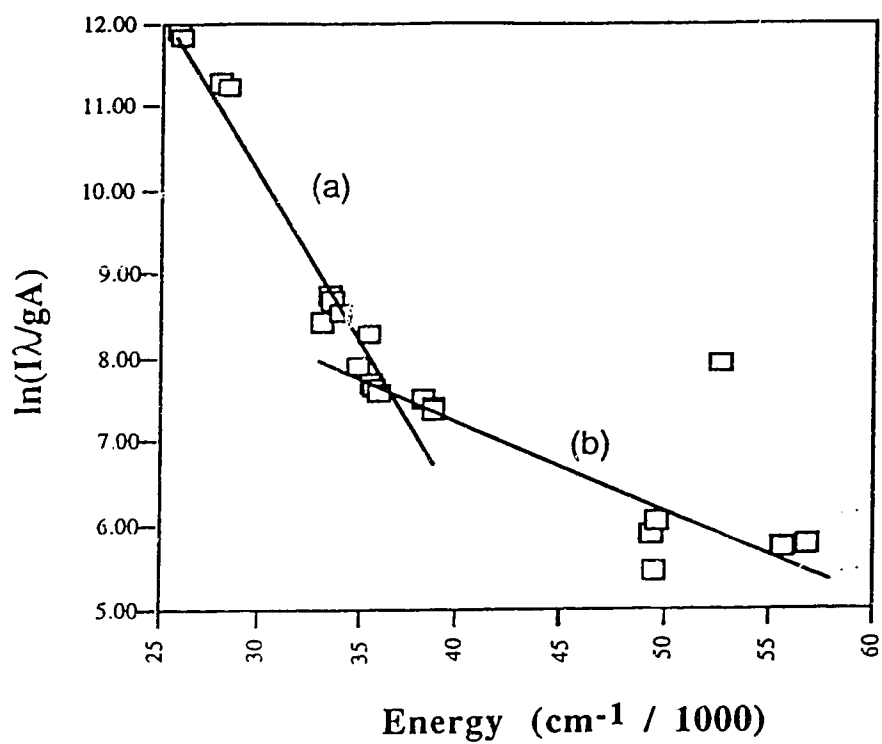


Fig. 6.3 Boltzmann plots for Fe-Ar discharge.



temperature" will be generated from the Boltzmann plot. Because ion-electron recombination generates excited states close to the ionization potential of the thermometric species, and these levels will be overpopulated. After all, "excitation temperature" in a glow discharge is not a clear concept. It may not reflect the actual distribution of the thermometric species in a non-thermal equilibrium system such as a glow discharge.

## 6.2 Future Work

So far, Cu, Zn, Fe, Ag and Cd have been studied. All the evidence leads to the same conclusions that charge transfer and Penning processes play an important role in the ionization-excitation of these elements. While ion-electron recombination populates the high energy levels of neutral atom excited states. Stepwise de-excitation from the high excited levels contributes the most to the majority of the emission lines. More studies of these processes by comparing the spectral characteristics of additional elements may supply further evidence for these processes. A clearer insight to excitation in the glow discharge, especially in the negative glow region will appear and a better understanding of the discharge processes will result from these studies. Glow discharge device modification and parameter control based on an understanding of the fundamental processes in the plasma will be beneficial to the application of this technique.

## Reference

1. J. D. Ingle, Jr. and S. R. Crouch, *Spectrochemical analysis*, Prentice Hall Inc. New Jersey. 1988, p207.

## Appendix

· Compact Disk containing the following information:

1. Computer program           - SpectroPlot
  
2. Data files  
Interferograms   - Ag, Al, Al-alloy, Brass, Cd, Cu, Fe and Zn;  
Spectra           - Ag, Al, Al-alloy, Brass, Cd, Cu, Fe and Zn.